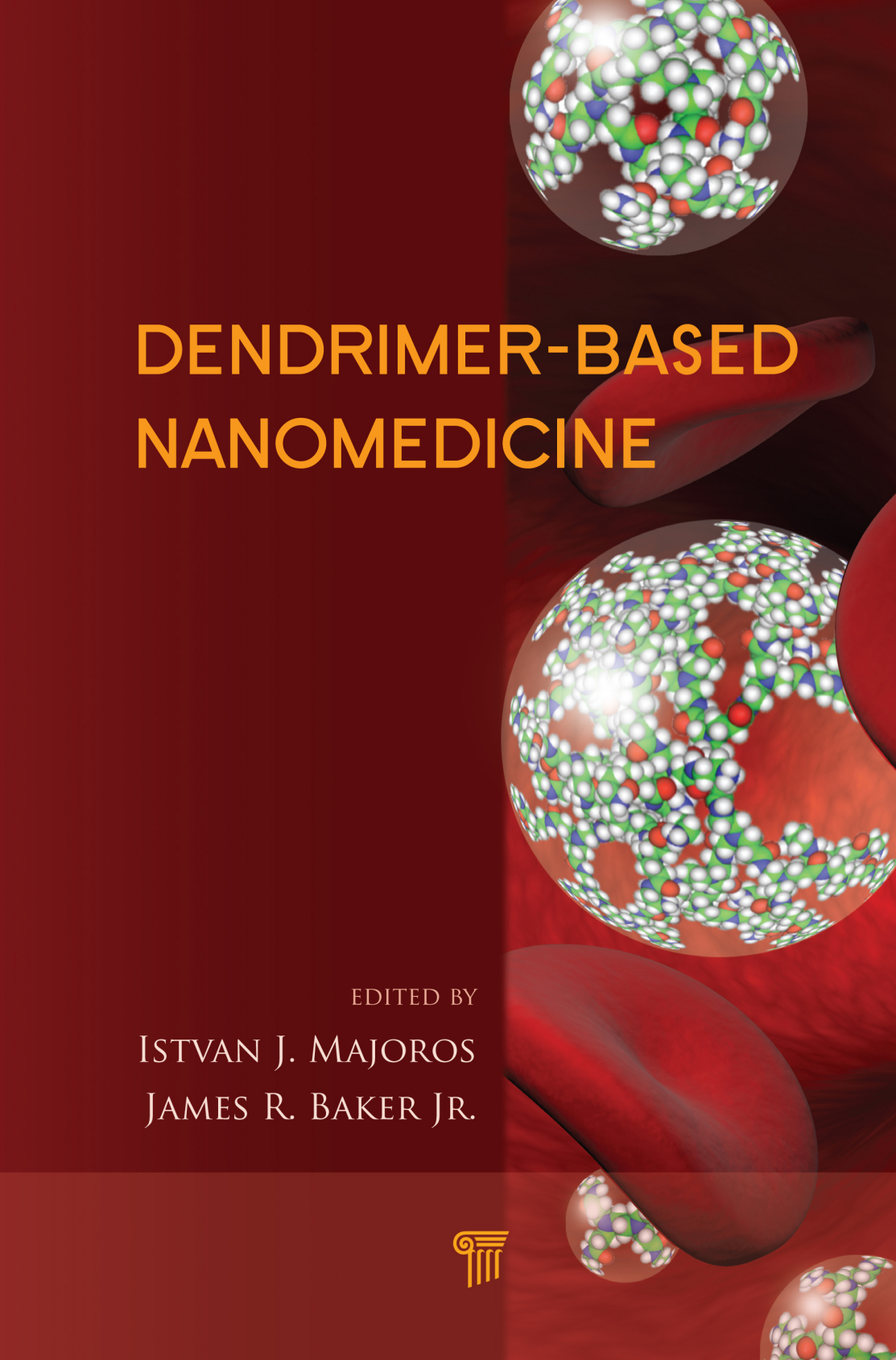
DENDRIMER-BASED
NANOMEDICINE
EDITED BY
Istvan J. Majoros
James R. Baker Jr.

DENDRIMER-BASED

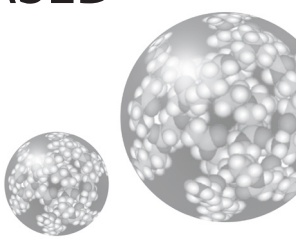

This page intentionally left blank

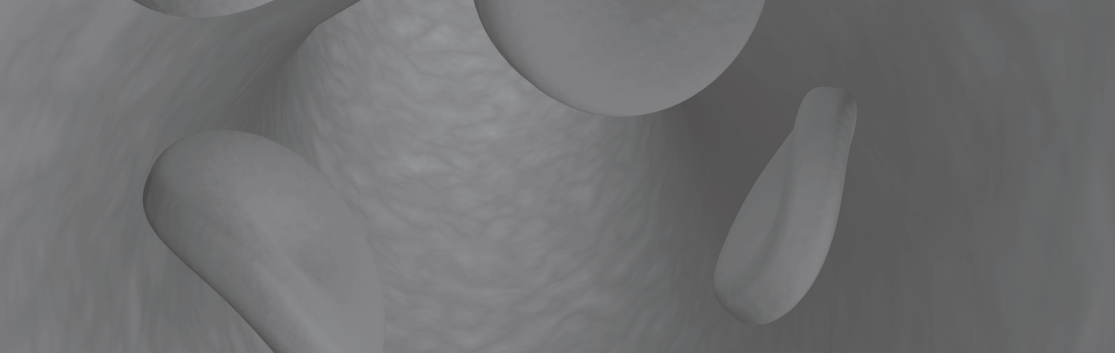

EDITED BY

Istvan J. Majoros

James R. Baker Jr.

University of Michigan, USA

DENDRIMER-BASED

Pan Stanford Publishing

Published by

Pan Stanford Publishing Pte. Ltd.
5 Toh Tuck Link
Singapore 596224

Distributed by

World Scientific Publishing Co. Pte. Ltd.

5 Toh Tuck Link, Singapore 596224

USA office: 27 Warren Street, Suite 401-402, Hackensack, NJ 07601

UK office: 57 Shelton Street, Covent Garden, London WC2H 9HE

British Library Cataloguing-in-Publication Data
A catalogue record for this book is available from the British Library.

DENDRIMER-BASED NANOMEDICINE

ISBN-13 978-981-4241-04-5
ISBN-10 981-4241-04-0

Typeset by Stallion Press
Email: enquiries@stallionpress.com

Printed in Singapore.

Preface

This book discusses in detail recent advances in nanomedicine, specifically dendrimer-based approaches to therapeutics. Nanomedicine is a new and dynamic field and is defined as the application of engineered materials of 100 nanometers or less in size for various medical uses. These structures come in many forms and are employed for different tasks, but are able to perform unique activities over conventional medical treatments due to their size. These materials approach the scale of biological materials, allowing them to interact with cells and other biological structures in new and unprecedented ways. This makes nanomaterials particularly effective in the monitoring, repair, assembly, and control of biological systems, molecules, and structures.

A wide variety of structures and materials are involved in nanomedicine: nanoparticles, nanofibers, nanoporous membranes, nanochips, nanotubes, nano-sensors, and many others. This book will focus on a class of nanostructures known as poly(amidoamine) (PAMAM) dendrimers and their use in medical applications. Dendrimers are a unique class of macromolecules having highly branched, three-dimensional architectures with low polydispersity and high functionality (Figure 1).[1,2] A typical dendrimer is built upon an initiator core, with several branching interior layers composed of repeating units and multiple active primary amine groups at its surface (Figure 2). This unique architecture and the functionality at this scale make dendrimers excellent carrier molecules for use in nanoscale medical applications[3] (for PAMAM dendrimers, the current possible range of

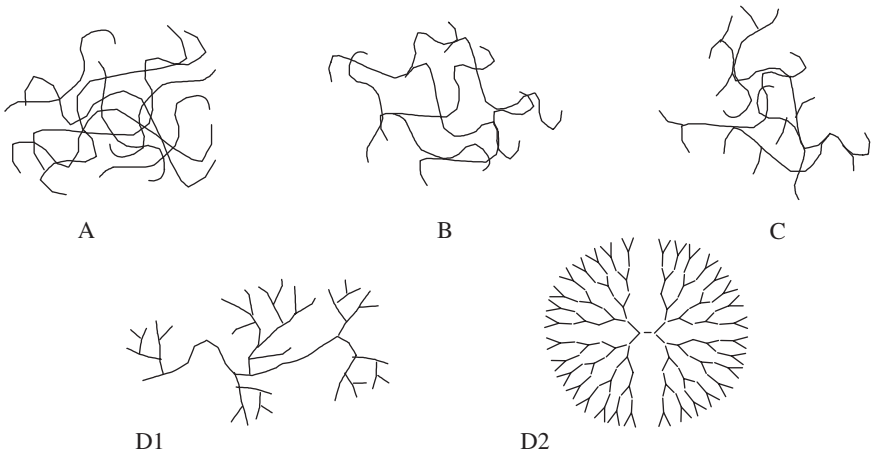

Figure 1: Simplified architecture of four major classes of polymers (A, linear; B, cross-linked; C, branched; D1, hyperbranched; D2, dendritic).

scale is a total diameter of between 1.5 and 14.5 nm). The branching architecture of PAMAM dendrimers resembles natural biomolecules (Figure 3). Of the several varieties of dendrimers, Starburst™ poly(amidoamine) (PAMAM) dendrimers have been commercialized by Dendritech (Midland, MI, USA), leading to its widespread investigation.

Dendrimers have been explored as light-harvesting agents,[4] chemical sensors,[5] catalysts[6] and cross-linking agents.[7] They also have been investigated in the biomedical field for drug delivery[8–10] and gene therapy[11,12] and as imaging contrast agents.[13] Several dendrimer-based products are under development for the treatment and diagnosis of a variety of diseases. VivaGel™ (Star-pharma) is a topical polylysindendrimer-based microbicide designed to prevent the transmission of HIV and other sexually transmitted diseases. SuperFect®, developed by Qiagen, is used for gene transfection in a broad range of cell lines. The US Army Research Laboratory developed

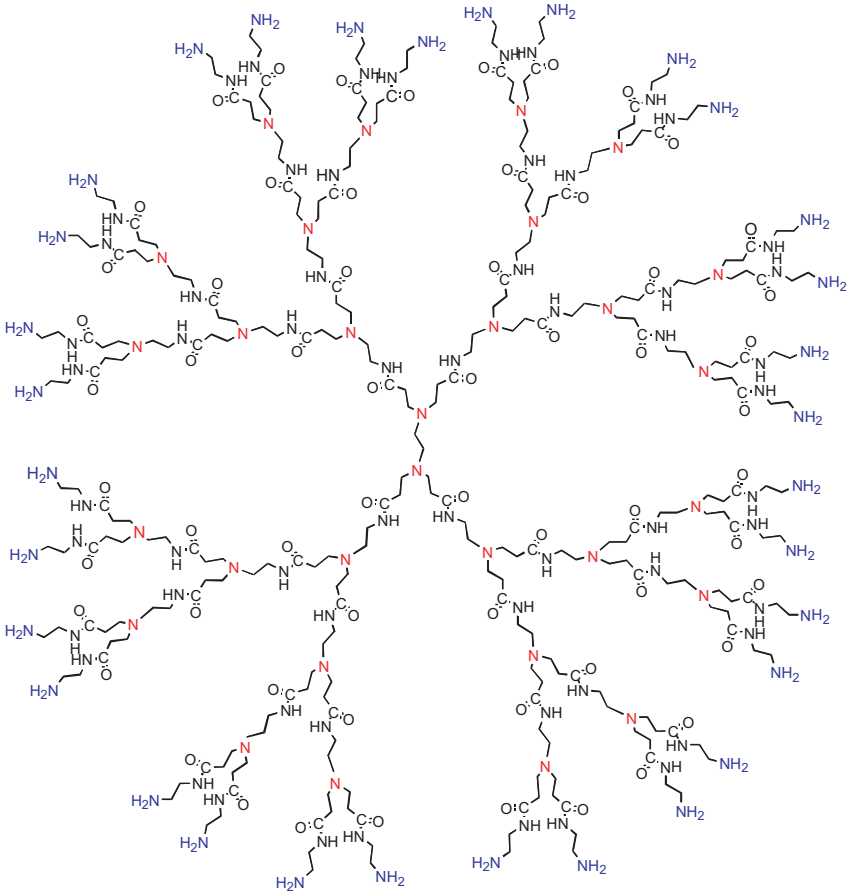

Figure 2: Schematic theoretic structure of a G3.0 PAMAM dendrimer molecule (generally, a commercial primary amine dendrimer).

Alert Ticket™ as a dendrimer-based diagnostic for anthrax detection. Stratus® CS, which is a system for the rapid diagnosis of heart attacks, has been commercialized by Dade Behring and is also based on dendrimers.

There have been over 1000 published patents relating to dendrimers since the first dendrimer patent was issued to D. A. Tomalia in 1984, and nearly 20 NIH-supported projects currently in progress involve dendrimers.

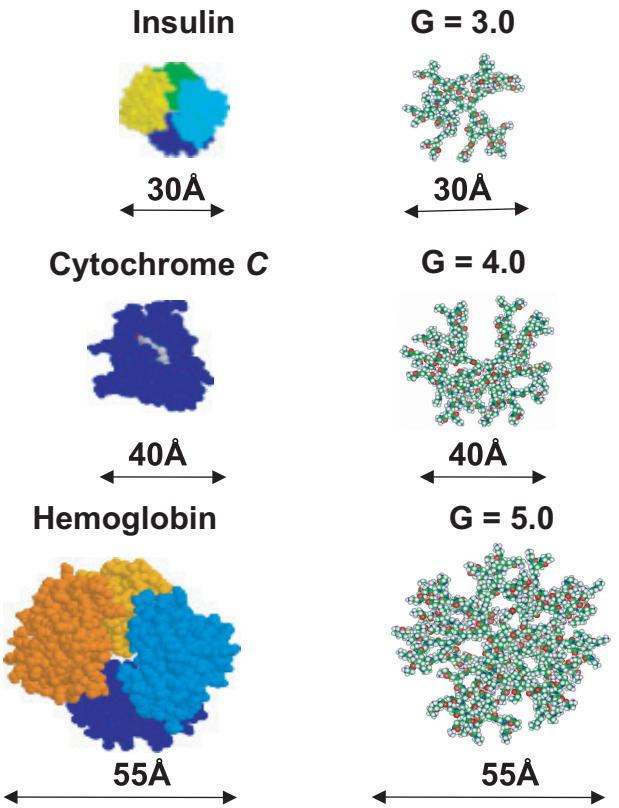

Figure 3: Dendrimer size can be controlled through molecular engineering to closely resemble antibodies, enzymes, and globular proteins in size. Poly(amidoamine) (PAMAM) ammonia core dendrimer generations 3, 4, and 5 closely match in size and shape insulin (30 Å), cytochrome C (40 Å), and hemoglobin (55 Å)[3] (Figure 4), respectively. Because of the close resemblance to these and other biomolecules, dendrimers are able to efficiently travel through the body.

The pharmaceutical and biomedical applications of dendrimers are of great interest and have been extensively reviewed.[2, 14–17, 19]

The major focus of this book is on the research and development of dendrimers, especially PAMAM dendrimers, as drug-delivery agents.

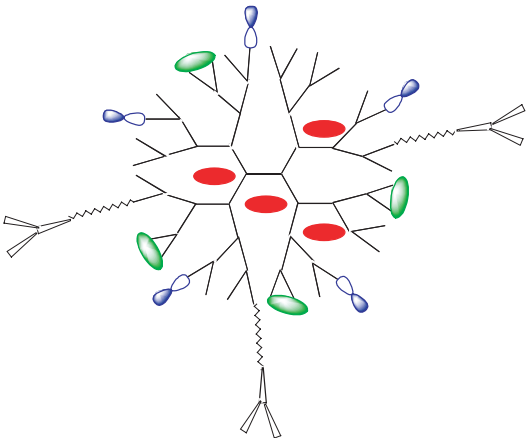

Figure 4. Scheme of a dendrimer-based multifunctional drug-delivery nanodevice, where ⩙⩙⩙⩙ are spacers, ⬭ are imaging units, ⩔ are targeting ligands, ⬭ are drug molecules, and ⬭ are apoptosis sensors.

The construction of a dendrimer-based nanodevice for the purpose of drug delivery often involves the addition of the specific drug or of therapeutic molecules to the surface of the polymer by a permanent/cleavable chemical bond. In many of the cases the drug may be encased within the structure of the dendrimer. The attachment of various moieties provides targeting, tracing, and/or other properties to the molecules (Figure 4). The final construct is an engineered nanoparticle, which has enhanced properties when compared to a free drug — ideally one which will deliver the drug to a specific biological site. According to Langer,[18] polymer drug-delivery systems are expected to continuously maintain drug levels in a therapeutically desirable range, to reduce harmful side effects, to decrease the amounts of a drug needed for therapy, to decrease the number of doses (and possibly allow for less invasive dosing and improve patient compliance with the prescribed drug regimen), and to facilitate drug

administration for pharmaceuticals with short *in vivo* half-lives (e.g., proteins and peptides).

In this book we present the use of PAMAM dendrimer-based nanoparticles for drug delivery through the focus of the many disciplines involved — chemistry, biology, engineering, and genetics — along with the associated *in vivo* and *in vitro* testing and computer modeling methods. We hope research in this area will continue to push the boundaries of science and develop new kinds of medical treatments for people in need and that this book will help disseminate information about this work to foster enthusiasm and further research for the benefit of all mankind.

References

1. D. A. Tomalia, H. Baker, J. Dewald, M. Hall, G. Kallos, S. Martin, J. Roeck, J. Ryder, and P. Smith, A new class of polymers: Starburst dendritic macromolecules, *Polym. J.*, **17**(1), 117–132, 1985.
2. R. Esfand and D. A. Tomalia, Poly(amidoamine) (PAMAM) dendrimers: From biomimicry to drug delivery and biomedical applications, *Drug Discovery Today*, **6**, 427–436, 2001.
3. R. Esfand and D. A. Tomalia, Poly(amidoamine) (PAMAM) dendrimers: From biomimicry to drug delivery and biomedical applications, *Research Focus, Reviews*, **6**(8), 427–436, 2001.
4. U. Hahn, M. Gorka, F. Vogtle, V. Vicinelli, P. Ceroni, M. Maestri, and V. Balzani, Light-harvesting dendrimers: Efficient intra- and intermolecular energy-transfer processes in a species containing 65 chromophoric groups of four different types, *Angew. Chem. Int. Ed.*, **41**, 3595, 2002.

5. M. Wells and R. M. Crooks, Interactions between organized, surface-confined monolayers and vapor-phase probe molecules 10. Preparation and properties of chemically sensitive dendrimer surfaces, *J. Am. Chem. Soc.*, **118**, 3988, 1996.
6. J. Bu, Z. M. A. Judeh, C. B. Ching, and S. Kawi, Epoxidation of olefins catalyzed by Mn(II) salen complex anchored on PAMAM-SiO2 dendrimer, *Catal. Lett.*, **85**, 183, 2003.
7. B. D. Viers, B. J. Bauer, Y. Akpalu, F. Grohn, D. Liu, and G. Kim, Hydrogels formed by end-linking peg to dendrimer cross-link agents, *Polym. Prepr.*, **41**, 728, 2000.
8. S. W. Poxon, P. M. Mitchell, E. Liang, and J. A. Hughes, Dendrimer delivery of oligonucleotides, *Drug Deliv.*, **3**, 255, 1996.
9. I. Majoros, T. Thomas, C. Mehta, and J. Baker Jr., PAMAM dendrimer-based multi-functional engineered nanodevice for cancer therapy. *Journal of Medicinal Chemistry*, **48**(19), 5892–5899, 2005.
10. I. Majoros, A. Myc, T. Thomas, C. Mehta, and J. Baker Jr., PAMAM dendrimer-based multi-functional engineered nano-device for cancer therapy II: Synthesis, characterization, and functionality, *Biomacromolecules*, **7**(2), 572–579, 2006.
11. J. D. Eichman, A. U. Bielinska, J. F. Kukowska-Latallo, and J. R. Baker, Jr., The use of PAMAM dendrimers in the efficient transfer of genetic material into cells, *Pharm. Sci. Technol. Today*, **3**, 232, 2000.
12. J. F. Kukowska-Latallo, A. Bielinska, J. Johnson, R. Spindler, D. A. Tomalia, and J. Baker Jr., Efficient transfer of genetic material into mammalian cells using Starburst polyamidoamine dendrimers, *Proc. Natl. Acad. Sci.,* **93**, 4897–4902, 1996.

13. H. Kobayashi, S. Kawamoto, T. Saga, N. Sato, A. Hiraga, T. Ishimori, Y. Akita, M. H. Mamede, J. Konishi, K. Togashi, and M. W. Brechbiel, Novel liver macro-molecular MR contrast agent with a polypropylenimine diaminobutyl dendrimer core: Comparison to the vascular MR contrast agent with the polyamidoamine dendrimer core, *Magn. Reson. Med*., **46**, 795, 2001.
14. Y. Kim and S. C. Zimmerman, Applications of dendrimers in bio-organic chemistry, *Curr. Opin. Chem. Biol.*, **2**, 733, 1998.
15. R. Duncan, Dendrimers: Novel carriers for oral and parenteral drug delivery, *Polym. Mater. Sci. Eng*., **84**, 214, 2001.
16. M. Liu and J. M. J. Frechet, Designing dendrimers for drug delivery, *Pharm. Sci. Technol. Today*, **2**, 393, 1999.
17. U. Boas and P. M. H. Heegaard, Dendrimers in drug research, *Chem. Soc. Rev.*, **33**, 43, 2004.
18. R. Langer, Drug delivery and targeting, *Nature* **392**, 5, 1998.
19. *Handbook of Theoretical and Computational Nanotechnology* Edited by M. Rieth and W. Schommers Vol 6: István Majoros, Thommey Thomas, and James R. Baker, Jr., *Molecular Engineering in Nanotechnology: Engineered Drug Delivery*, pp. 673–717, 2006.

István J. Majoros
James R. Baker, Jr.
University of Michigan, USA

Contributors

Preface

István J. Majoros* and James R. Baker Jr.†

* University of Michigan, Nanotechnology Institute for Medicine and Biological Science, Internal Medicine — Allergy Research, Macromolecular Science and Engineering, Ann Arbor, MI 48109

† Nanotechnology Institute for Medicine and Biological Science, Internal Medicine, University of Michigan, Ann Arbor, MI 48109

Chapter 1

Brent B. Ward* and James R. Baker Jr.†

* Oral and Maxillofacial Surgery, University of Michigan Hospitals, 1500 E. Medical Center Drive, Ann Arbor, MI 48109-0018

† Nanotechnology Institute for Medicine and Biological Science, Internal Medicine, University of Michigan, Ann Arbor, MI 48109

Chapter 2

Thomas H. Dunham*, Brent B. Ward*, and James R. Baker Jr.†

* Oral and Maxillofacial Surgery, University of Michigan Hospitals, 1500 E. Medical Center Drive, Ann Arbor, MI 48109-0018

† Nanotechnology Institute for Medicine and Biological Science, Internal Medicine, University of Michigan, Ann Arbor, MI 48109

Chapter 3

István J. Majoros and Daniel E. Carter

University of Michigan, Nanotechnology Institute for Medicine and Biological Science, Internal Medicine — Allergy Research, Macromolecular Science and Engineering, Ann Arbor, MI 48109

Chapter 4

Jing Yong Ye and Theodore B. Norris

Department of Electrical Engineering and Computer Science, Center for Ultrafast Optical Science, Michigan Nanotechnology Institute for Medicine and Biological Sciences University of Michigan, 2200 Bonisteel Blvd., Ann Arbor, MI 48109-2099

Chapter 5

István J. Majoros*, Andrew Becker*, Thommey Thomas†, Rameshwer Shukla† and Xiangyang Shi†

*University of Michigan, Nanotechnology Institute for Medicine and Biological Science, Internal Medicine — Allergy Research, Macromolecular Science and Engineering

†Michigan Nanotechnology Institute for Medicine and Biological Sciences, University of Michigan, Ann Arbor, MI 48109

Chapter 6

Thommey P. Thomas and Jolanta F. Kukowska-Latallo

Michigan Nanotechnology Institute for Medicine and Biological Sciences, University of Michigan, Ann Arbor, MI 48109

Chapter 7

Andrzej Myc*, Chandan B. Mehta* and István J. Majoros†

* Michigan Nanotechnology Institute for Medicine and Biological Sciences, University of Michigan, Ann Arbor, MI 48109

† University of Michigan, Nanotechnology Institute for Medicine and Biological Science, Internal Medicine — Allergy Research, Macromolecular Science and Engineering, Ann Arbor, MI 48109

Chapter 8

Scott D. Swanson* and Christopher R. Williams†

* Michigan Nanotechnology Institute for Medicine and Biological Sciences, Department of Radiology, University of Michigan, Ann Arbor, MI 48109-0553

† University of Michigan, Biomedical Engineering, Ann Arbor, MI 48109-2099

Chapter 9

Seungpyo Hong*,† Almut Mecke*,‡, Pascale Leroueil*,§, Mark M. Banaszak Holl*,†,§,¶ Bradford G. Orr †,¶

* Michigan Nanotechnology Institute for Medicine and Biological Sciences The University of Michigan, Ann Arbor MI 48109,

† Program in Macromolecular Science and Engineering, ‡ Department of Physics, § Department of Chemistry, ¶ Applied Physics Program, Ann Arbor, MI 48109

Chapter 10

Senthil K. Kandasamy, Hwankyu Lee and Ronald G. Larson

Department of Chemical Engineering, The University of Michigan Ann Arbor, MI 48109

Chapter 11

Xiangyang Shi and Su He Wang

Michigan Nanotechnology Institute for Medicine and Biological Sciences, University of Michigan, Ann Arbor, MI 48109

Contents

Chapter 1

Targeted Drug Delivery in General, New Technology in Medicine

Brent B. Ward & James R. Baker Jr.

Outline

1.1 Introduction

The term "silver bullet" originates from folklore in which a silver bullet was the only type of bullet for firearms effective against a number of mystical foes. In modern vocabulary its use refers to a simple fix for a complex or intractable problem. In search of such solutions, the attention of investigators to pharmacologics which specifically target disease while leaving the host otherwise untouched has evolved.

A medline search of "targeted therapy" or "targeted drug delivery" reveals two articles from 1902–1978 with the first mention attributed to the use of propanolol for essential hypertension by Lauro *et al.*[1] In the 1980's 53 articles were published with the concept of targeted approaches which blossomed in the 1990's to 261. Since that time significant expansion in this field has occurred with 1429 articles for targeted approaches from 2000 to 2006. While these references refer to a wide variety of diseases the preponderance deals with potential solutions for the treatment of cancers. This explosion of information in targeting is likely attributable to our increasing knowledge of disease, in particular cellular mechanisms and receptors, as well as the technological advances in vehicles for drug delivery.

The purpose of this chapter is to provide the reader with a historical context of the fields of research which have contributed to this revolution while leaving the in depth discussion of devices, methodologies, and current approaches to other chapters which specifically deal with these subjects.

1.2 Historical Perspective

The current state of targeted therapy technology takes root in collaborative efforts from a number of physical, biological and medical disciplines under the broad umbrella of nanotechnology. The birth of nanotechnology is usually attributed to a talk given by physicist Richard Feynman in 1959, "There's Plenty of Room at the Bottom" at the American Physical Society. He suggested concepts such as small robots building smaller robots resulting in the creation of billions of tiny factories and a reduction in print type size to permit the Encyclopedia Britannica to be fit to the size of a pin head. The term nanotechnology was actually coined in 1974 by Professor Noro Taniguchi of the Tokyo Science University. By strict definition, nanotechnology refers to molecular devices smaller than 1 micron and therefore on the "nano" scale. One nanometer is one billionth or 10^{-9} of a meter.

Soon after mechanical and electrical approaches became feasible, biologists began to explore opportunities for advancement. In 1996 the first scientific conference entitled, "Biological Approaches and Novel Applications for Molecular Nanotechnology" was held. The resulting concept of nanomedicine has emerged as an offshoot of nanotechnology referring to highly specific medical intervention at the molecular scale for curing disease or repairing damaged tissues, such as bone, muscle, or nerve.[2] It combines the expertise of individuals in medicine, biology, math, chemistry, engineering, and computer science for the creation of devices to meet these needs. Institutes for nanomedicine sponsored by the national institutes of health, universities, and the private sector have arisen as an outcome of this direction.

1.3 Targeted Drug Delivery

While all advances associated with targeted drug therapy are not strictly bound to nanomedicine, most of the current progress is within this realm and is the focus of this text. It should be recognized that targeted therapies are different from "passive targeting". Examples of passive targeting included technologies such as "enhanced permeability and retention (EPR)" and the products created by the Alza Corporation which seeks to overcome the body's natural barriers to drug entry and extend the time in which drugs remain at their site of action. Nanomedicine targeted approaches attempt to interact with the cell in a number of complex ways to offer advantage over untargeted approaches which treat all cells the same. It is important to recognize that for targeting to occur, some selective process must take place whereby normal host tissues are not affected in similar ways to the tissues in which the desired effect is to take place. While this introduction can in no form be exhaustive, some global approaches to this problem have included:

1. Systemic delivery of agents with a selective advantage to cells which abnormally express or overexpress a surface or intracellular receptor that is targeted.
2. Delivery of agents which replace disease rendering defective biochemical processes with competent alternatives (gene therapy).
3. Delivery of agents or devices which inhibit specific cellular pathways in targeted cells.
4. Immune boosting for direct destruction of desired cells (immunotherapy).

Given the confines of this chapter as an overview and the fact that the majority of targeted approaches are directed toward tumor biology, the examples given will come from this realm. It is important for the reader to realize that these concepts have been globalized to many other disease processes. Also of importance is that few examples will be offered in each realm which is representative of a large body of pre-clinical and clinical evidence for which volumes could be dedicated to each individual subject.

1.4 Systemic Delivery of Agents with a Selective Advantage to Cells which Abnormally Express or Overexpress a Surface Receptor that is Targeted

Advances in cancer research have resulted in significant understanding of the cellular and molecular changes leading to malignancy. The concepts of tumor progression were elaborated by Foulds in the 1950's[3] which was shortly followed by evidence from cytogenetics in the 1960's. Molecular techniques evolved and revealed that tumorogenesis results from a single altered cell.[4] Ultimately a multi-step model with acquisition of various cellular abnormalities was proposed.[5] While all of the steps involved at present remain unknown, our understanding of the cancer cell and of the role of the surrounding network of tissues is increasing.[6] Markers of pre-malignancy and malignancy have been identified in some cases and targeted approaches are being made to utilize these markers in treatment strategies. In addition, other nontransforming markers which are overexpressed for a variety of reasons may be targeted to offer some selective advantages in treatment.

A preclinical example of this process has evolved though the creation of targeted dendrimer therapy. Dendritic macromolecules, or dendrimers, are uniformed spherical nano-structures ranging from 10 to 200 Angstroms in diameter. Dendrimers have been used as a backbone for the attachment of several types of biological materials including folate. These molecules can direct the dendrimers to locations where receptors are expressed on tumor cell surfaces. Dendrimers can also be conjugated to therapeutic molecules, such as methotrexate, allowing for efficacious delivery and a higher dose load to tumor cells avoiding the systemic toxicity of current therapeutic strategies.[7]

Dendrimers with folate and methotrexate have been shown to bind to KB cells expressing high levels of folate binding protein. In animal model studies targeted chemotherapy with dendrimers showed ten times the efficacy and decreased toxicity compared to standard chemotherapy with free drug.[8] Phase I clinical trials for this therapy are planned.

Using this technology one can envision a multitude of devices whereby both the targeted agent and the chemotherapeutic agent utilized could be specifically modified to meet the need of the receptor characteristics and physiological properties of an individual tumor. In support of this concept, additional dendrimers which target epidermal growth factor receptor (EGFR), prostate specific membrane antigen (PSMA), and RGD peptides have been fabricated and tested as well as conjugates with Taxol as the therapeutic arm. In this scenario, patient tumors could be screened for their cell surface receptor levels in order to make decisions regarding which therapeutic would have greatest potential.

Another targeting approach for cellular receptors comes from the work with monoclonal antibodies for targeting of receptors. EGFR which is presently being targeted in colorectal cancer as well as head and neck cancer (HNSCC) with a number of other tumors currently under study. EGFR is a very desirable target in HNSCC with mRNA overexpression present in approximately 92% of specimens studied.[9] EGFR overexpression in HNSCC is the result of both decreased receptor down regulation and increased mRNA synthesis.[10] Following ligand binding, EGFR is internalized and found in the intracellular compartment and ultimately the nucleus. Targeted approaches for EGFR have been studied in clinical trails where antibodies directed to EGFR have shown promise as an adjunct to radiation therapy. Bonner *et al.* studied in a randomized prospective multinational trial the effect of cetuximab (monoclonal antibody to EGFR) and radiation vs. radiation alone. With cetuximab, median survival, progression free survival and local regional control of disease were all increased.[11] Based in large part on these results, the FDA in 2006 approved cetuximab as the first new treatment in 45 years for head and neck cancer.

1.5 Delivery of Agents which Replace Disease Rendering Defective Biochemical Processes with Competent Alternatives (Gene Therapy)

Our understanding of cellular processes associated with disease has made possible the creation of therapeutics which has potential to enter all cells but replace missing components in defective cells such that they only exhibit their effect in this environment. An example of such a strategy

includes the use of gene therapy in which viral and nonviral vectors transfer genetic material to diseased cells.

Attempts at gene therapy have resulted in some success and many challenges in need of further exploration to create an effective treatment. Despite its current clinical limitations, a number of solid tumors including pancreatic, breast, colon, lung, prostate and head and neck cancer have been successfully treated in mouse models.[12–14]

In clinical practice a recombinant adenovirus has been used to deliver competent p53 (TP53 gene) to cells which are p53 deficient. p53 is a tumor suppressor gene which monitors DNA damage, inducing cell cycle arrest for repair or apoptosis when necessary.[15] p53 inactivation has been demonstrated in up to 50% of all human cancers.

Gene therapy has been attempted for cells with mutated p53 with the use of an adenoviral vector containing wild-type p53.[16] In clinical study, 33 patients had injection of Adenovirus-p53 (Ad-p53) intratumorally without any evidence of toxicity. Seventeen non resectable patients could be evaluated for clinical efficacy. Two patients demonstrated greater than 50% response and an additional six had stable disease for up to 3.5 months. Nine patients had unabated progression of disease. An additional six patients showed stable disease for up to 3.5 months. Nine patients had unabated progression of disease.

Another growing area related to viral gene therapy includes the use of oncolytic vectors for cancer cell destruction while leaving the normal cells in the body unaffected. A number of different viruses have been studied for this purpose including vaccinia, adenovirus and herpes simplex

virus. A number of animal trials using this technology have shown promising results.[17,18]

HSV-1 has been used with the production of two vectors G207 and NV1020 in phase I and II clinical trials after success *in vivo* and animal models.[19,20] ONYX-015, an adenovirus which can only replicate in cells lacking functional p53. Khuri and Nemunaitis *et al*.[21] reported on a non-randomized phase II trial of 37 patients with multiple recurrent tumors who received ONYX-015. Thirty patients could be evaluated for disease response. Treatment with ONYX-015 caused tumors to shrink in 25 of the 30 cases with greater than 50% response in 63% of the patients. There were 8 complete and 11 partial responses and in some patients with tumors as large as 10 cm in diameter complete regression was noted. At six months none of the responding tumors had progressed.

1.6 Delivery of Agents or Devices which Inhibit Specific Cellular Pathways Present in Targeted Cells

Molecular targeted therapeutics in this category includes nucleic acid drugs (antisense oligonucleotides and small inhibitory RNA) and small molecule inhibitors. Antisense oligonucleotides are single stranded DNA or RNA of approximately 20 nucleotides in length. RNA antisense oligonucleotides are EXON regions of the desired mRNA to block ribosomal translation and therefore protein production.[22] DNA antisense oligonucleotides bind to complementary RNA creating a DNA/RNA hybrid which is subsequently degraded. Both pathways have the potential for gene silencing.

Small interfering RNA's (siRNA's) are double stranded RNA molecules which also have the potential to block protein production. They can be directly introduced into cells via virus or experimental manipulation. Double stranded RNA in the cell is cleaved by the Dicer enzyme into 21–28 nucleotide sequences which form RNA-induced silencing complexes through their association with DSRNA-binding protein R2D2.[23]

In pre-clinical models siRNA targets have been tested in a number of cancers including breast, liver, esophagus, and melanoma.[24] As a recent technology, reports of human clinical trials for this therapy have not yet emerged.

Another example of pathway targeting comes from the Philadelphia Chromosome in chronic myelogenous leukemia which was discovered in the 1960's. This chromosomal translocation between chromosomes 9 and 22 leads to a fusion protein bcr-abl which becomes a continuously active tyrosine kinase associated with the disease. Imatinib (Gleevec®, Novartis) takes its mechanism of action by binding to bcr-abl at the ATP binding site thereby inhibiting the activity of the protein. While the abl tyrosine kinase is also inhibited in other cells its effect is more profound in CML due to its dependence on high levels of the abnormal protein. Although eradication of CML is not achievable, Imatinib limits the growth of the tumorogenic cells and decreases the risk of blastic crisis.

1.7 Immune Boosting for Direct Destruction of Desired Cells

Immunotherapy in general involves approaches to expand and activate the immune system to target cancer cells for tumor control. To date,

CD8+ cytolytic T lymphocytes (CTL) appear to play the key role in tumor response which is supported by the CD4+ T helper cells. Both cells receive information from antigen presenting cells for activation against potential immunogenic peptides for tumor control. Augmenting this system through exogenous antigen presentation and the boosting of cellular signals for increased activation has been studied extensively and continues to show promise in clinical application.

Current body sites for clinical trials for cancer immunotherapy include prostate, pancreas, melanoma, and kidney. In melanoma, MDX-010 anti-CTLA-4 and IL-2 are used to augment and prolong T-cell antitumor response in preclinical and clinical phase I/II studies.[25] An additional approach has been combination therapy with anti-CTLA-4 and vaccine therapy.[26]

Treatment for renal cell cancer highlights a number of approaches. Greater than 20 years experience with high dose Interleukin-2 (IL-2) as an immunomodulator has been conclusively shown to give complete regression in 5–7% of candidates for therapy.[27] Additional areas of research in this arena include T-Cell transfer whereby T-cells for *ex vivo* expansion are harvested from and later delivered to the patient. Combination of this approach with cloning of cells which recognize p53, NY-ESO-1, and other antigens has shown promise.[28]

1.8 Conclusion and Future Direction in Research and Technology

Advances in targeted drug delivery are likely to continue to change treatment approaches in the near- and long-term future. As our understanding

of the complex processes involved in the diseased cell increases, new opportunities for targeting will emerge. Targets at present come from a variety of sources including both normal and abnormal cellular receptors and biochemical processes. When normal cellular processes are involved, selective advantage is offered by an upregulation of these processes in the tumor cell compared to normal tissue. This allows tumor cells to be more highly affected than their normal counterparts. Abnormal receptors and processes also offer an opportunity for targeting in that they do not have counterparts within normal tissue.

Development of new and the expansion of currently available strategies hold great promise in cancer and all diseases. Approaches for targeting will continue to expand both as our knowledge of potential targets increases and as our ability to create targeted therapeutics continues to expand. With accelerating speed it is likely that the trend towards increasingly specific treatment will remain a desirable outcome long into the future of nanomedicine. The limited number of strategies reviewed here has provided only a small number of examples of an ever growing field of science in targeted therapeutics for drug delivery.

1.9 References

1. R. Lauro, A. Platania, C. Liberatore, G. Reda, and C. Spinelli, Biochemical profile of essential arterial hypertension. Indications for a targeted therapy: Experience with propranolol, *Clinica Terapeutica*, **85**(1), 19–25, 1978.
2. NIH Roadmap for Medical research, http://nihroadmap.nih.gov/nanomedicine/

3. L. Foulds, Tumor progression, *Cancer Research*, **17**, 355–356, 1957.
4. P. C. Nowell, The clonal evolution of tumor cell populations, *Science*, **194**, 23–28, 1976.
5. B. Vogelstein and K. W. Kinzler, The multistep nature of cancer, *Trends Genet*., **9**, 138–141, 1993.
6. D. Hanahan and R. A. Weinberg, The hallmarks of cancer, *Cell*, **100**, 57–70, 2000.
7. A. Quintana, E. Raczka, L. Piehler, I. Lee, A. Myc, I. Majoros, A. Patri, T. Thomas, J. Mulé, and J. R. Baker Jr., Design and function of a dendrimer-based therapeutic nanodevice targeted to tumor cells through the folat receptor, *Pharmaceutical Research*, **19**, 1310–1316, 2002.
8. J. Kukowska-Latallo, K. A. Candido, Z. Cao, S. S. Nigavekar, I. J. Majoros, T. P. Thomas, L. P. Balogh, M. K. Khan, and J. R. Baker Jr., Nanoparticle targeting of anticancer drug improves therapeutic response in animal model of human epithelial cancer, *Cancer Research*, **65**, 5317–5324, 2005.
9. J. R. Grandis and D. J. Tweardy, Elevated level of transforming growth factor alpha and epidermal growth factor receptor messenger RNA are early markers of carcinogenesis in head and neck cancer, *Cancer Research*, **53**, 3579–3584, 1993.
10. J. R. Grandis, Q. Zeng, S. D. Drenning, and D. J. Tweardy, Normalization of EGFR mRNA levels following restoration of wild-type p53 in a head and neck squamous cell carcinoma cell line, *Int. J. Oncol*., **13**, 375–378, 1998.
11. J. A. Bonner, P. M. Harari, J. Giralt, N. Azarnia, D. M. Shin, R. B. Cohen, C. U. Jones, R. Sur, D. Raben, J. Jassem, R. Ove, M. S. Kies,

J. Baselga, H. Youssoufian, N. Amellal, E. K. Rowinsky, and K. K. Ang, Radiotherapy plus cetuximab for squamous-cell carcinoma of the head and neck, *N. Engl. J. Med.*, **354**, 567–578, 2006.

12. J. F. Tseng and R. C. Mulligan, Gene therapy for pancreatic cancer, *Surg. Oncol. Clin. N. Am.*, **11**, 537–569, 2002.
13. J. W. Rocco, D. Li, W. H. Liggett Jr., L. Duan, J. K. Saunders Jr., D. Sidransky, and B. W. O'Malley Jr., p16INK4A adenovirus-mediated gene therapy for human head and neck squamous cell cancer, *Clin. Cancer Res*, **4**, 1697–1704, 2004.
14. S. Varghese and S. D. Rabkin, Oncolytic herpes simplex virus vectors for cancer virotherapy, *Cancer Gene Ther.*, **9**, 967–978, 2002.
15. B. J. Baum, M. Kok, S. Tran, and S. Yamano, The impact of gene therapy on dentistry a revisiting after six years, *JADA*, **133**, 35–44. 2002.
16. G. L. Clayman, A. K. el-Naggar, S. M. Lippman, Y. C. Henderson, M. Frederick, J. A. Merritt, L. A. Zumstein, T. M. Timmons, T. J. Liu, L. Ginsberg, J. A. Roth, W. K. Hong, P. Bruso, and H. Goepfert, Adenovirus-mediated p53 gene transfer in patients with advanced recurrent head and neck squamous cell carcinoma, *J. Clin. Oncol.*, **16**, 2221–2232, 1998.
17. A. Hemminki, A. Kanerva, E. J. Kremer, G. J. Bauerschmitz, B. F. Smith, B. Liu, M. Wang, R. A. Desmond, A. Keriel, B. Barnett, H. J. Baker, G. P. Siegal, and D. T. Curiel, A canine conditionally replicating adenovirus for evaluating oncolytic virotherapy in a syngeneic animal model, *Mol. Ther.*, **7**, 163–173, 2003.
18. P. J. Cozzi, S. Malhotra, P. McAuliffe, D. A. Kooby, H. J. Federoff, B. Huryk, P. Johnson, P. T. Scardino, W. D. Heston, and Y. Fong,

Intravesical oncolytic viral therapy using attenuated, replication-competent herpes simplex viruses G207 and Nv1020 is effective in the treatment of bladder cancer in an orthotopic syngeneic Model, *FASEB J*., **15**, 1306–1308, 2001.

19. R. Liu, S. Varghese, and S. D. Rabkin, Oncolytic herpes simplex virus vector therapy of breast cancer in C3(1)/SV40 T-antigen transgenic mice, *Cancer Research*, **65**, 1532–1540, 2005.
20. J. J. Bennett, K. A. Delman, B. M. Burt, A. Mariotti, S. Malhotra, J. Zager, H. Petrowsky, S. Mastorides, H. Federoff, and Y. Fong, Comparison of safety, delivery, and efficacy of two oncolytic herpes viruses (G207 and NV1020) for peritoneal cancer, *Cancer Gene Ther*., **9**, 935–945, 2002.
21. F. R. Khuri, J. Nemunaitis, I. Ganly, J. Arseneau, I. F. Tannock, L. Romel, M. Gore, J. Ironside, R. H. MacDougall, C. Heise, B. Randlev, A. M. Gillenwater, P. Bruso, S. B. Kaye, W. K. Hong, and D. H. Kirn, A controlled trial of intratumoral ONYX-015, a selectively replicating adenovirus, in combination with cisplatin and 5-fluorouracil in patients with recurrent head and neck cancer, *Nat. Med*., **6**(8), 879–885, 2000.
22. H. Wang, G. Prasad, J. K. Buolamwini, and R. Zhang, Antisense anticancer oligonucleotide therapeutics, *Curr. Cancer Drug Targets*, **1**, 177–196, 2001.
23. Y. Dorsett and T. Tuschl, siRNAS: Applications in function genomics and potential as therapeutics, *Nat. Rev. Drug Discovery*, **3**, 318–329, 2004.
24. M. Izquierdo, Short interfering RNAs as a tool for cancer gene therapy, *Cancer Gene Ther*., **12**, 217–227, 2004.

25. A. V. Maker, G. Q. Phan, P. Attia, and J. C. Yang *et al*., Tumor regression and autoimmunity in patients treated with cytotoxic T-lymphocyte-associated antigen 4 blockade and interleukin 2: A phase I-II study, *Ann. Surg. Oncol*. **12**(12), 1005–1016, 2005.

26. A. van Elsas, R. P. Sutmuller, A. A. Hurwitz, J. Ziskin, J. Villasenor, J. P. Medema, W. W. Overwijk, N. P. Restifo, C. J. Melief, R. Offringa, and J. P. Allison, Elucidating the autoimmune and anti-tumor effector mechanisms of a treatment based on cytotoxic T lymphocyte antigen-4 blockade in combination with a B16 melanoma vaccine: Comparison of prophylaxis and therapy, *J. Exp. Med*., **194**, 481–489, 2001.

27. S. A. Rosenberg, J. C. Yang, D. E. White, and S. M. Steinberg, Durability of complete responses in patients with metastatic cancer treated with high-dose interleukin-2: Identification of antigens mediating response, *Ann. Surg*., **228**, 307–319, 1998.

28. C. J. Cohen, Z. Zheng, R. Bray, Y. Zhao, L. A. Sherman, S. A. Rosenberg and R. A. Morgan, Recognition of fresh human tumor by human peripheral blood lymphocytes transduced with a bicistronic retroviral vector encoding a murine anti-p53 TCR. *J. Immunol*., **175**, 5799–5808, 2005.

Chapter 2

General Carriers for Drug Delivery

Thomas H. Dunham, Brent B. Ward &
James R. Baker Jr.

Outline

2.1 Introduction: The Trojan Horse

Drug carriers offer the promise to modern pharmaceuticals that the Trojan Horse held out to the ancient Greeks: the hope that a smarter attack will succeed where protracted brute force had previously failed. For the ancient Greeks the Trojan Horse was a method for breaching the insurmountable perimeter defenses of Troy; for modern pharmaceuticals the drug carrier seeks to improve delivery of a drug and/or enhance its effectiveness as a therapeutic. To this end, drug carriers perform three major tasks that provide a method to alter the therapeutic index of drugs by (1) prolonging and improving the therapeutic activity, (2) decreasing drug metabolism, and (3) reducing systemic toxicity. Drug carriers also serve the important role of providing specificity, which is the focus of another chapter in this book. The central point in understanding drug carrier function is a recognition that the treatment of disease does not happen in a vacuum and that the complexity of biological systems presents remarkable challenges to a therapeutic approach. The ideal drug carrier imparts an "intelligence" to the therapeutic compound that organic chemistry and biology alone cannot provide. To again evoke the Trojan Horse analogy, the modern drug carrier is, in a sense, an admission of our therapeutic failures akin to that of the ancient Greeks, who sat for a decade on the beach ineffectively fighting the deadly and efficient fortress of Troy. It was only when they plotted a smarter toxic approach that they succeeded:

"Which like a steed of monstrous height appear'd:
The sides were plank'd with pine; they feign'd it made
For their return, and this the vow they paid.

Thus they pretend, but in the hollow side
Selected numbers of their soldiers hide:
With inward arms the dire machine they load,
And iron bowels stuff the dark abode."

Virgil, *The Aeneid*, *Book 2*

This chapter seeks to provide a general introduction to polymer drug carriers, their derivatives, and respective formats. It should be recognized that this chapter cannot be all-inclusive, and that a number of carrier systems using proteins and liposomes are not described here but are in development.

2.2 Polymers Introduction

Polymer chemistry is partly responsible for the introduction of the term of art, "nano-device". To some people, the term "nano-device" elicits images of tiny robots that are controlled remotely; at present this is a reality of science fiction alone. Science *fact* offers a radically less sophisticated "device": small (5–100 nm) polymer nano-devices are polymer backbones with other useful molecules attached to them, such as a therapeutic, a contrast agent, and/or a targeting moiety. The composition of the polymer carrier, or polymer nano-device, depends on the utility that the polymer carrier is meant to serve and is therefore modular in its approach and varied in its definition.

Polymer chemistry as a methodology for carrying drugs is historically recognized as being born in 1955,[1,2] when researchers first used the water-soluble polymer PVP (polyvinyl pyrrolidone) as a drug depot for the

biologically active primary amine mescaline. Since then, the field has expanded dramatically beyond the depot effects; researchers have harnessed the power of conjugating multiple molecular subunits and have examined a wide array of polymers, ligands and therapeutics which are designed to enhance drug delivery and or effectiveness.

Polymers used as drug carriers have a dominant property of water solubility, which is an obvious requirement for use in the aqueous environment of living cells. The configuration of a polymer is crucial to its function. Polymers may be linear, branched, or micelle in structure and, given the current technologies available, include such structures as multivalent polymers, branched polymers, block copolymers, stars, dendrimers, dendronized polymers, and hybrid glycol and peptide derivatives.[1] Given this complexity, a general classification has been devised for a description of the polymeric drug carriers (Figure 1).

Based on this classification, there are several forms of polymer-based drug carriers defined by their primary function.

a) *Sequestrants* Polymer sequestrants act to isolate compounds systemically within an organism. An elegant example of the sequestrants is the cholesterol-lowering bile acid sequestrant (BAS) drug Colesevelam HCl or WelChol® (Daiichi Sankyo Inc., Parsippany NJ). This macro-molecule is an orally administered compound with a polymer backbone and hydrophobic side-arms that have a high avidity for glyocholic acid bile salts. The action of binding the bile salts in the gastrointestinal tract and their ultimate excretion causes the liver in turn to create more bile salts

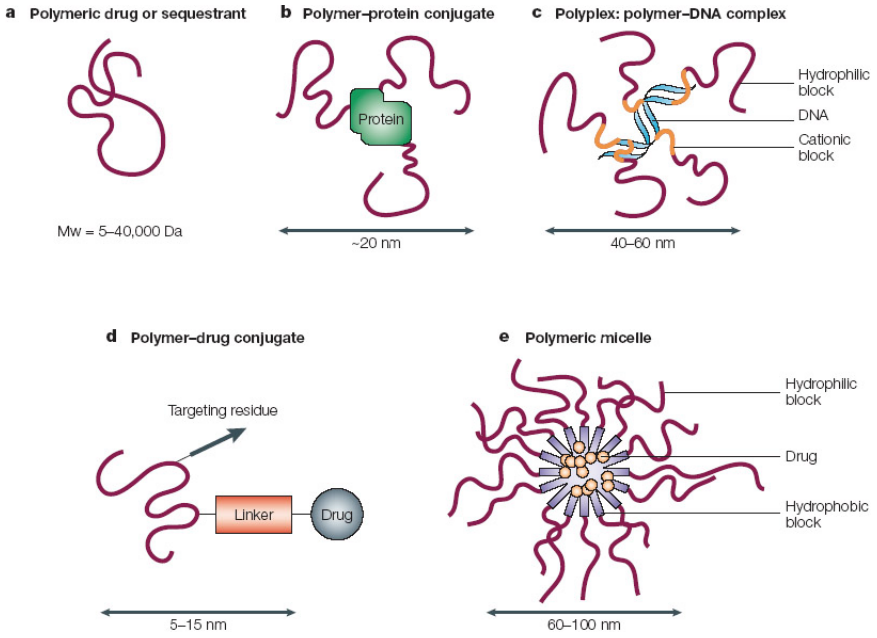

Figure 1: Schematic representation of polymer therapeutics now in — or progressing toward — clinical development. (Used with permission: R. Duncan, The dawning era of polymer therapeutics, *Nature Rev. Drug Disc.*, **2**, 347–360, 2003.)

requiring more cholesterol, which it derives from LDL-cholesterol that circulates in the bloodstream.[3]

b) *Polymer-protein Conjugates* The proteins in this category include peptides, antibodies, and proteins. The rationale for attaching proteins to polymers in order to stabilize them from metabolism in the blood stream, via the elicitation of an immune response, leads to very low stability in the presence of plasma and low pharmacological half-lives due to the biological degradation of the kidney and liver. Polymer-protein conjugation is optimized when three conditions are met: (1) the polymer to which the protein will

be linked has only one functionalized end group so as to mitigate the problem of protein cross-linking during conjugation; (2) the stable and relevant linking chemistry between the protein and polymer is itself biocompatible and does not illicit detrimental immunogenic recognition; (3) an approach to the protein synthesis that allows for reproducibility with regard to site-specific protein modification.[2]

c) *Polyplex/Polymer-DNA Conjugates* This type of polymer is designed to compete with its viral counterpart, the adenovirus vectors, as an efficient method of carrying not only DNA but also dsRNA, also known as siRNA or RNAi. Polyplexes are formed through electrostatic interactions between nucleic acid compounds (DNA and RNA) and polymers. While adenovirus vectors do an excellent job of delivering nucleic acids into cells, they offer less-than-ideal protective features parenterally and limited specificity with regard to cell types. Polyplexes, on the other hand, can be engineered for specificity and possess excellent biocompatibility.

d) *Polymer-Drug Conjugates* The polymer-drug conjugate is a most elegant example of a "multifunctional" nano-device. In the schematic representation above, there are four functions being served by four discrete subunits: the drug acts as the therapeutic; the linker reduces steric hindrance and acts as the bridge between the drug and the polymer; the polymer provides biocompatibility and a mechanism of entrée into the cell — or perhaps a time release function; and the targeting moiety provides specificity

that may either reduce systemic toxicity or increase local concentration — or both. Thus, the polymer-drug conjugate is termed a multifunctional device. The individual subunits used in polymer-drug conjugates vary widely but have general limitations parallel to those of polymer-protein conjugates.

e) *Polymeric Micelles* The polymeric micelle is a polymeric analog of the liposome and carries its drug payload on the "inside" of its hydrophobic-cored micelle. The micelle is formed spontaneously when block polymers, so called because of their discrete amphipathic ends, self-assemble to form micelles in the presence of a solvent containing the drug to be encapsulated. Thus, polymeric micelles act as mechanisms to deliver poorly water-soluble drugs. Additionally, polymeric micelles can be targeted as carriers for clinical use.

An important characteristic of a polymer-based drug carrier generally is the net electronic charge of the macro-molecule. The charge of a carrier is measured in units called the zeta potential and, in the simplest of terms, is a measurement of the combined effect of the molecular polarity and ionic charge in an electric field. The modulation of a polymeric charge can result in an altered compartmentalization profile of the carrier from the cellular level with regard to passive or active macro-molecular uptake or systemically, via a parenteral administration, with regard to organ and tissue concentrations. Therefore, carrier specificity — and, conversely, non-specificity — can be influenced by changing the charge of both polymeric molecules and liposomes.

2.2.1 Synthetic polymers

A large number of synthetic polymers have been developed for drug delivery, including polyethylene glycol (PEG), polyvinylpyrrolidone (PVP), polyethylenimine (PEI), PLGC, dendrons, and dendrimers, to name only a few. Representative examples of this group are provided as a non-exhaustive list of this ever-expanding field.

2.2.1.1 Polyethylene glycol (PEG)

PEG is a polymer of repeating subunits of identical structure [(H(OCH_2 CH_2)$_n$-OH (n > 3)]. PEGylation is the covalent coupling of a PEG structure to another molecule and is a process which can be used for enhanced drug characteristics. Examples of current pegylated drugs include Pegfilgrastim for chemotherapy-induced neutropenia, and pegylated doxorubicin or peginterferon alpha-2a for cancer therapy. Pegylation decreases renal clearance, enzymatic degredation, and immune detection, which increases drug half-life.[4] These characteristics allow less frequent and more patient convenient dosing schedules in a number of therapeutics. In clinical practice, a once-weekly dosage of peginterferon alpha-2a was tested in a randomized prospective trial with a dosage of interferon alpha-2a three times per week. In a study population of 531 patients, peginterferon alpha-2a was more effective as a single weekly dose than the standard tri-weekly therapy with interferon alpha-2a.

2.2.1.2 Polyvinylpyrrolidone (PVP)

PVP is a polymer made from the carcinogenic monomer N-vinyl pyrrolidone. The polymer has a track record for safety that extends to the first half

of the 20th century, when it was used as a volume expander for trauma patients. PVP has been used as a pure polymer and in combination with a number of other combined polymers, including poly(vinyl alcohol) (PVA) and chitosan. An interesting application of this technology is the reported creation of a potential magnetic delivery-based system with PVP and PVA hydrogels combined with iron oxide. Bleomycin crosslinked to this magnetic PVP demonstrated sustained release *in vivo* through passive drug release.[5] Other applications for PVP and PVP-combined polymers have included delivery of nitric oxide,[6] pingyangmycin,[7] and Celecoxib, to name only a few.[8]

2.2.1.3 Dendrimers

Dendrimers are repeatedly branched molecules first described by a number of authors in the late 1970s and early 1980s. Due to their unique architecture and potential for drug delivery, the great amount of interest in dendrimers has resulted in over 5000 scientific papers written on the subject by the end of 2005. A dendrimer is a uniform, spherical nanostructure ranging from 10 to 200 Angstroms in diameter. The surface of a dendrimer is characterized by the presence of functional groups that together can be utilized as a backbone for the attachment of several types of biological materials. One advantage of a dendrimer is that a number of different molecules can be conjugated to its surface through these functional groups, and nanodevices for both drug delivery and diagnostic purposes can be conjugated to a single carrier device. Functional attachments have included iron oxide for targeted imaging; a phiphiluxG1D2 apoptosis sensor for monitoring; drugs, including methotrexate and

Taxol chemotherapeutics; and folic acid, RGD peptides, and antibody fragments for targeting. The exact structure, connection, and numbers of targeting molecules and drugs are crucial to the function of these molecules, thus the need for nanotechnology synthesis and analysis tools is great.

Dealing only with drug delivery and using a cell line which overexpresses the high-affinity folate receptor, *in vitro* and *in vivo* xenograft mouse tumor models for targeted chemotherapy using methotrexate have suggested that the increase in efficacy is 10- to 50-fold. In addition, given the targeted nature of this approach, a decrease in systemic toxicity has been demonstrated when compared to the use of a free drug.[9,10] Phase I clinical trials for this therapy are planned.

Expanding on this technology, it will be possible to create a multitude of devices whereby both the targeted agent and the chemotherapeutic agent utilized could be specifically modified, based on the receptor characteristics and physiological properties of an individual tumor. To date, additional targeting dendrimers have been fabricated, including targeting to the epidermal growth factor receptor (EGFR), to RGD peptides, and to prostate specific membrane antigen (PSMA).[11] Utilizing this treatment modality, a patient's tumor could be screened for its cell surface receptor levels in order to make decisions regarding which targeting agent would have the greatest potential for success.

Outside of cancer therapy, dendrimers have been utilized for a number of potential medical applications, including drug delivery of glitazones for diabetes, ketoprofen for pain control, and DNA, as well as delivery of proteins for transfection and transduction.

2.2.2 Naturally occurring polymers

2.2.2.1 Chitosans

Chitosans are linear polysaccharides composed of randomly distributed β-(1-4)-linked D-glucosamine and N-acetyl-D-glucosamine. Chitosan is produced commercially by deacetylation of chitin from the exoskeleton of crustaceans. From a drug delivery standpoint, chitosan is an avid binder of negatively charged surfaces, including mucosal membranes, and can serve as a transport device for polar drugs and in viral gene delivery.

Chitosan microparticles that encapsulate the pigment epithelium-derived factor (PEDF), a potent anti-angiogenic factor, have been studied in a preclinical osteosarcoma model *in vitro* and *in vivo* using cell lines and a nude mouse orthotopic model. In the results, both tumor volumes and tumor weights were decreased by the therapy, and lesser evidence of bone degredation and distant metastasis was observed.[12] In another preclinical study, chitosan was attached to paclitaxel for intraperitoneal delivery, using a mouse xenograft model for ovarian cancer. The drug conjugate increased the maximally tolerated dose, decreased toxicity, and improved the therapeutic index, in comparison to results obtained using commercial paclitaxel.[13] In non-cancer applications, chitosan has been studied for transmucosal delivery of calcitonin, pituitary adenylate cyclase-activating polypeptide, insulin, cefadroxil, and vaccines.[14]

2.2.2.2 Alginates

Alginates are linear, unbranched block polymers consisting of two monomeric units, guluronic acid and manuronic acid, in a variety of

configurations. Alginate microparticles have been studied as carriers for the controlled release of drugs because of their biocompatibility and the low cost of producing them. Alginates have excellent bioadhesive properties, especially in combination with chitosans. Alginate microparticles have been investigated for drug delivery as well as DNA and proteins.

Alginate beads loaded with metronidazole have been shown to deliver slow-release, systemic drug delivery using *in vivo* models.[15] Oral administration for specific treatment of peptic ulcer disease has been studied in an attempt to eradicate Helicobacter pylori bacteria colonization of the stomach. In one study, chitosan-treated alginate beads with metronidazole were used in a mouse model. H. pylori clearance was noted as 100% with a dose of 15 mg/kg in the treatment arm, while doses of metronidazole in suspension delivered at 20 mg/kg gave only 33.33% clearance.[16]

2.2.3 Combination therapeutics

As demonstrated by some of the examples above, the harnessing of multiple platforms into single combination devices may pose possibilities to enhance potential and limit toxicity. An additional preclinical example of such an endeavor is the combination of chitosan chloride and PEG into a thermosensitive hydrogel, which is under study as a potential nasal drug delivery system. In this model the liquid at room temperature transitions to a non-flowing hydrogel at 37°C. Using this model, insulin was entrapped and delivered to rats, and blood glucose levels demonstrated effective delivery in a slow-release system for over four hours after administration.[17] Other similar endeavors include combination of alginate/PEG[18] and dendrimer/PEG.[19]

2.3 Delivery of Drug Carriers

The mechanism for the delivery of drug carriers is dependent upon the characteristics of the delivery vehicle and the desired compartment of the body for application of the pharmacologic. Methods for delivery include any mucosal surface of the body (primarily nasal, oral, vaginal, rectal), intralesional injection, intramuscular or IV administration, and subcutaneous or intralesional implantation. Depending upon the application, specific carrier characteristics become more or less desirable for the optimal solution. For example, in mucosal membrane administration, chitosan avidity to mucosal surfaces enhances the applicability of this technology. For implantation strategies desiring the slow release of a drug, slowly biodegradable polymers like PLGA with drug implantation serve as a model. For targeted systemic therapy, dendrimers have the capacity to localize to receptor-laden regions, including to a tumor, for drug delivery.[20]

2.4 Future Directions and Conclusions

The future for drug delivery in a specific and sustained fashion holds great promise for the treatment of disease. The continued development of this technology will greatly enhance both the quantity and quality of life for patients with acute and chronic illness. The prospect of daily, weekly, monthly, or longer administration of a medication for the patient who now doses medications three times per day will limit the incapacitation of a disease. In addition, the possibilities for painless mucosal administration of medications which at present require injection seem imminent.

It is likely that our knowledge of drug delivery agents and the number of possible candidates will continue to progress in dramatic fashion. In addition, our understanding of underlying disease processes will continue to grow. Recognition of each delivery method's strengths and weaknesses, combined with comprehension of the pathophysiology of the disease process, allows for the optimal in drug delivery design. It is the integration of this knowledge with the ever-increasing availability of potential drug carriers that will add to our ability to fight disease.

A variety of delivery methods have been described in this chapter, which are available in various stages of development from basic science to clinical application. These examples only serve to highlight the vast array of carriers, techniques, and the global knowledge now available on this subject.

2.5 References

1. R. Duncan, The dawning era of polymer therapeutics, *Nature Reviews*: *Drug Discovery*, **2**, 347–360, 2003.
2. H. Jatzkewitz, Peptamin (glycyl-L-leucyl-mescaline) bound to blood plasma expander (polyvinylpyrrolidone) as a new depot form of a biologically active primary mine (mescaline). *Z. Naturforsch*, **10**, 27–31, 1955.
3. J. M. McKenney, Pharmacologic options for aggressive low-density lipoprotein cholesterol lowering: Benefits versus risks, [Review] [28 refs.] [Journal Article. Review] *American Journal of Cardiology*, **96**(4A), 60E–66E, 2005.

11. R. Shukla, T. P. Thomas, J. Peters, A. Kotlyar, A. Myc, and J. R. Baker Jr., Tumor angiogenic vasculature targeting with PAMAM dendrimer-RGD conjugates, [Journal Article. Research Support, N.I.H., Extramural] *Chemical Communications*, **46**, 5739–5741, 2005.

12. C. R. Dass, K. G. Contreras, D. E. Dunstan, and P. F. Choong, Chitosan microparticles encapsulating PEDF plasmid demonstrate efficacy in an orthotopic metastatic model of osteosarcoma, **28**(19), 3026–3033, 2007.

13. V. Vassileva, J. Grant, R. De Souza, C. Allen, and M. Piquette-Miller, Novel biocompatible intraperitoneal drug delivery system increases tolerability and therapeutic efficacy of paclitaxel in a human ovarian cancer xenograft model, *Cancer Chemother. Pharmacol*., (Mar 21 Epub) 2007.

14. F. Zheng, X. W. Shi, G. F. Yang, L. L. Gong, H. Y. Yuan, Y. J. Cui, Y. Wang, Y. M. Du, and Y. Li, Chitosan nanoparticle as gene therapy vector via gastrointestinal mucosa administration: results of an *in vitro* and *in vivo* study, *Life Sci*. (Epub 2006) **80**(4), 388–396, 2006.

15. Y. Murata, N. Sasaki, E. Miyamoto, and S. Kawashima, Use of floating alginate gel beads for stomach-specific drug delivery, *Eur. J. Pharm. Biopharm*., **50**(2), 221–226, 2000.

16. R. A. Ishak, G. A. Awad, N. D. Mortada, and S. A. Nour, Preparation, *in vitro* and *in vivo* evaluation of stomach-specific metronidazole-loaded alginate beads as local anti-Helicobacter pylori therapy, *J. Control Release* (Mar 1 Epub) 2007.

17. J. Wu, W. Wei, L. Y. Wang, Z. G. Su, and G. H. Ma, A thermosensitive hydrogel based on quaternized chitosan and poly(ethylene glycol) for nasal drug delivery system, *Biomaterials*, **28**(13), 2220–2232, 2007.

18. Q. Wang, N. Zhang, X. Hu, J. Yang, Y. Du, Alginate/polyethylene glycol blend fibers and their properties for drug controlled release, *J. Biomed. Mater Res. A* (Jan, Epub) 2007.

19. D. Chandrasekar, R. Sistla, F. J. Ahmad, R. K. Khar, and P. V. Diwan, Folate coupled poly(ethyleneglycol) conjugates of anionic poly(amidoamine) dendrimer for inflammatory tissue specific drug delivery, *J. Biomed. Mater Res. A* (Jan 31 Epub) 2007.

20. C. Berkland, E. Pollauf, C. Raman, R. Silverman, K. (Kevin) Kim, and D. W. Pack, Macromolecule release from monodisperse PLG microspheres: Control of release rates and investigation of release mechanism, *Journal of Pharmaceutical Sciences*, **96**(5), 1176–1191, 2007.

4. G. Molineux, Pegylation: Engineering improved pharmaceuticals for enhanced therapy, *Cancer Treat. Rev*., **28**, 13–16, 2002.
5. D. Guowei, K. Adriane, X. Chen, C. Jie, and L.Yinfeng, PVP magnetic nanospheres: Biocompatibility, *in vitro* and *in vivo* bleomycin release, *Int. J. Pharm*., **1**, 78–85, 2007.
6. A. B. Seabra and M. G. De Oliveira, Poly(vinyl alcohol) and poly(vinyl pyrrolidone) blended films for local nitric oxide release, *Biomaterials*, **17**, 3773–3782, 2004.
7. K. Adraine, J. Huang, G. Ding, J. Chen, and Y. Liu, Self assembled magnetic PVP/PVA hydrogel microspheres; magnetic drug targeting of VX@ auricular tumors using pingyamgmycin, *J. Drug Target*, **14**(4), 243–253, 2006.
8. P. Gupta and A. K. Banasal, Modeling of drug release from celecoxib-PVP-meglumine amorphous systems. *PDA J. Pharm. Sci. Technol*., **59**(6), 346–354, 2005.
9. A. Quintana, E. Raczka, L. Piehler, I. Lee, A. Myc, I. Majoros, A. K. Patri, T. Thomas, J. Mulé, and J. R. Baker Jr., Design and function of a dendrimer-based therapeutic nanodevice targeted to tumor cells through the folate receptor, *Pharmaceutical Research*, **19**, 1310–1316, 2002.
10. J. F. Kukowska-Latallo, K. A. Candido, Z. Cao, S. S. Nigavekar, I. J. Majoros, T. P. Thomas, L. P. Balogh, M. K. Khan, and J. R. Baker Jr., Nanoparticle targeting of anticancer drug improves therapeutic response in animal model of human epithelial cancer, *Cancer Research*, **65**, 5317–5324, 2005.

This page intentionally left blank

Chapter 3

Poly(amidoamine) Dendrimer Synthesis and Characterization

István J. Majoros & Daniel E. Carter

Outline

3.1 Introduction

Drug delivery by way of nanoparticles is a rapidly progressing area of research which unites researchers from the fields of chemistry, chemical engineering, biology, and medicine. Traditional drug therapies are often hindered by the natural processes of biochemical regulation within the body. The goal of nano-scale drug carriers is to mimic naturally occurring biological molecules in order to limit such

interferences as well as to enhance the productivity of therapeutic drug treatments.

There are four main areas of concern when considering a drug carrier for use in a biological system: (1) drug resistance due to physiological barriers, (2) cellular-level drug resistance, (3) distribution and possible modification of the drug within the body, and (4) excretion of the drug from the body.[1] Compared to traditional therapies, controlled drug delivery is usually a more effective, patient-friendly means of treatment.

Polymers are becoming the frontrunners in the race to find the ideal carrier because of their versatility and their capabilities as both the carrier and the controlled dispenser of drugs. As a result, many polymeric materials have been synthesized solely for this purpose. Table 1 classifies many of the polymers currently being researched as drug carriers. The first major separation is between natural and synthetic polymers. Natural polymers are not engineered and are, therefore, difficult to adapt to multiple applications. Synthetic polymers may be engineered for a very specific use or for a broad range of applications. They can be further broken down into biodegradable and non-biodegradable synthetic polymers. The most promising of these synthetic polymers are the dendrimers.

The divergent growth strategy, now widely used for dendrimer synthesis, was discovered independently by Vögtle and by Tomalia in 1978–1979. The divergent methodology based on acrylate monomers was discovered in 1979 and was developed in the Dow Chemical Laboratories from 1979 to 1984. It was first reported at the 1st International Conference, Japan Society of Polymer Science, in Kyoto (1984) and was published in

Tab. 1. Polymer carriers commonly used for drug delivery today.

Polymer types	*Examples*
Natural	
Protein-based	Collagen, albumin, gelatin
Polysaccharides	Agarose, alginate, cyclodextrins, polysaccharide hydrogel
Synthetic	
Biodegradable	
Polyanhydrides	Poly(sebacic acid), poly(adipic acid) poly(terephthalic acid)
Polyesters	Poly(lactic acid), poly(glycolic acid), poly(hydroxy butyrate), poly(dioxanones)
Polyamides	Polyamino acids, poly(imino carbonates)
Non Biodegradable	
Acrylic polymers	Polymethacrylates, poly(methyl methacrylate), poly(hydroxyethyl methacrylate)
Silicones	Polydimethylsiloxane, colloidal silica
Cellulose derivatives	Cellulose acetate, hydroxypropyl methyl cellulose, carboxymethyl cellulose, ethyl cellulose
Others	Polyvinyl pyrrolidone, ethyl vinyl acetate
Dendrimers	Poly(amidoamine), poly(propyleneimine), aromatic ester & ether-type dendrimers

1985.[2] This approach provided a high yield of poly(amidoamine) (PAMAM) dendrimers with molecular weights ranging from several hundred to over one million Daltons (i.e., Generations 1–12) and is presently

the preferred commercial route to synthesizing Starburst® PAMAM dendrimers. Several significant advantages offered by the divergent method include the following:

1. Allows direct dendritic growth of dendrons from a wide variety of atomic, molecular, and polymeric as well as physical objects as cores. Does not require a second core anchoring step, which is sterically limited via the convergent method.
2. Adaptable to large-volume scale-up (e.g., PAMAM is produced in multi-kilogram quantities).
3. Low-cost, readily available commodity monomers (i.e., methyl acrylates and ethylenediamine) may be used for synthesis.
4. May be used to prepared high generation (i.e., G = 0–12) dendrimers that precede and exceed the "de Gennes dense packed" state.

The procedures described are based on improved modifications from the original publications.[2–6] They focus on the divergent "excess reagent" syntheses of poly(amidoamines) using various alkylenediamine cores.

Many of these dendrimeric nanostructures have shown commercial promise for gene transfection and as drug delivery agents, immunodiagnostics reagents, nanocatalysts, magnetic resonance imaging contrast agents, nanoreactors, and nanocalibrators. Dendrimers are expected to play a significant role in the systematic development of nanoscale chemistry architecture and properties, both in the biological as well as the abiotic areas of interest.

3.2 Dendrimers as Unique Macromolecules

In the last 25 years, dendrimers have exploded onto the scientific scene. They have made their way from being highly unknown, underappreciated nanoparticles into becoming a medical wonder having immense possibilities in the minds of researchers around the world. The increase in the knowledge about and understanding of dendrimers is evidenced in the dramatic increase in patent literature regarding dendrimers since 1981. From 1981 to 1985, two patents were granted. Fifty-one were granted from 1991 to 1995, and over 1000 were granted from 2001 to 2005.[7] With increased publicity about them, dendrimers are now becoming more widely known outside of the scientific community as well.

However, as with many scientific advancements, it is important that we do not ask too much of dendrimers. This could easily be done as they possess many advantages over the nanoparticles described in earlier literature. One tremendous advantage is that the chemical structure of dendrimers is almost limitless. Also, dendrimers have been synthesized with incredible uniformity, which is quite unique in the production of nanoparticles. The true nano-scale size of these molecules lends itself to great precision among their many uses. However, their size also poses some limitations among uses (as drug carriers, for example). Examples of current dendrimer use include VivaGelk, created by Starpharma, which is an intra-vaginal product used against HIV and other sexually transmitted diseases. The dendrimer used here is an intrinsically active substance.[8] Another use can be found in the therapeutic application of dendrimers,[9] such as the anionic, poly(amidoamine) conjugates of d(+)-glucosamine

and (d)(+)-glucosamine-6-sulfate with immunomodulatory and antiangiogenic properties.[10]

Part of the bright future foreseen for dendrimers rises from the incredible systematic control of many of their properties. The control over certain dendrimer characteristics such as size, shape, branch length/density, and surface functionality allows for their customization for use in many fields.[11] The control over the size of dendrimers leads to a wide range of uses as MRI contrast agents. Small changes in the size of these contrast agents can result in differences in their pharmacokinetics, such as their permeability and excretion. Dendrimers of differing sizes have been found to be potential renal, blood pool, liver, lymphatic, and tumor contrast agents.[12] The defined architecture and the high multivalent surface moieties-to-volume ratio of the dendrimers make them intriguing candidates for synthetic vectors for therapeutic nucleic acids. Development of these vectors would require a link between the structures of dendrimers and the respective nucleic acid complexes as well as the biological viability would require of such systems.[13] The ability to specify the size of dendrimers allows for their use in the creation of multiple secondary structures like vesicles, tubules, fibers, and micellular structures. The creation of secondary dendrimer structures broadens the range of dendrimer use for drug and gene delivery. However, there first needs to be a better understanding of the mechanisms for the creation of such structures as well as increased concentration on the method of synthesis for dendrimers associated with more complex structures.[14] The future of dendrimers relies on such novel uses as well as on continued research on dendrimer activity within a biological environment.[15]

One of the most intriguing applications for dendrimers currently under study is using them as a means of transport in the body for drugs, genes or vaccines. The use of dendrimers through complexation with drugs ranges from targeted drug delivery to controlled release of drugs within the body.[16] Drug delivery through dendrimers may be accomplished two different ways: by complexation of a drug within the hydrophobic interior of the dendrimer or by way of covalently coupling the drug to the dendrimer's surface. Complexation of a hydrophobic drug allows it to become water soluble yet still maintain its natural properties once released. Targeted drug delivery can be achieved through covalent conjugation of both a targeting agent (like folic acid in the case of cancer cells) and the desired drug.[17]

Before there can be extensive use of dendrimers, however, a greater understanding of their activity and possible safety hazards must be achieved. Specifically, there is a pressing need to analyze the safety of nanoparticles in a biological system. Current usage of nanoparticles can provide a guide for the safe production and use of dendrimers. However, safety designations will have to be applied to each specific application, not to dendrimers as a whole. As of yet, this cannot be adequately accomplished because there is a lack of clinical experience with dendrimers.[18] Some basic knowledge concerning these topics may be ascertained from other areas. Dendrimers, of course, may be studied using molecular chemistry analytical techniques. However, because of their intrinsic polymeric nature, analytical techniques already in use in the field of polymers may give further insight into the biological activity and toxicity of dendrimers.[19]

3.3 Dendrimer Synthesis

The two main methods of synthesis for dendrimers are the divergent and convergent methods. The work done by Tomalia[2] and Newkome[20] in the early 1980s was built around the divergent method of synthesis.[2,20] For example, in an ethylene diamine (EDA)-cored PAMAM dendrimer, an EDA core is alkylated with methyl acrylate through Michael addition. This step results in a half-generation molecule with ester terminal groups. This is followed by amidation of the resultant ester terminal groups with excess EDA to create a full-generation, amine-terminated molecule. This reaction sequence is shown in Figure 1.

The drawback to the divergent method is that many reactions are required to occur simultaneously as one reaches higher-generation dendrimers. This results in imperfect samples and side reactions which make

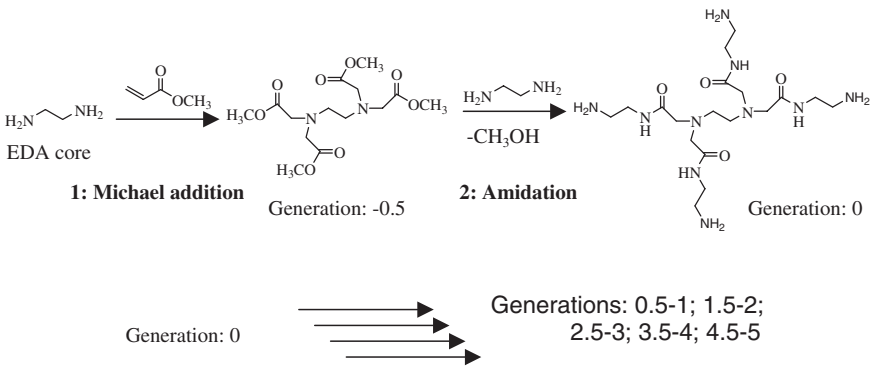

Figure 1: PAMAM dendrimer synthesis: D. A. Tomalia and I. Majoros: Supramolecular polymers; dendrimeric supramolecular and supramacromolecular assemblies, in *Supramolecular Chemistry*, ed. Alberto Ciferri, Marcel Dekker, Inc. New York, 2000.

purification of these dendrimers quite difficult. As a result, the convergent method was created in order to minimize this problem during dendrimer synthesis. This method, developed by Frechet,[21] is somewhat similar except that the separate dendron arms are created and then added to the desired core. This reduces the number of simultaneous reactions needed and allows for intermediate purification, resulting in a near-perfect dendrimer structure. The divergent method and convergent method are compared in Figure 2 and Figure 3.

No matter which type of synthesis is used, purification is a crucial part of the process. Excess methyl acrylate must be removed from half-generation PAMAM dendrimer solutions after Michael addition in order to prevent the creation of lower-generation dendrimers during the following amidation step. This may be done using a rotary evaporator and through the bubbling of dry nitrogen through a neat dendrimer solution. Also, after the synthesis of full generation dendrimers, the large

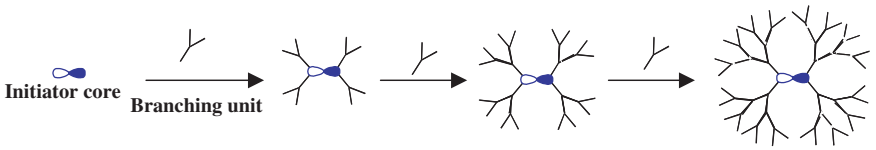

Figure 2: EDA core-based divergent method for the synthesis of dendrimers.

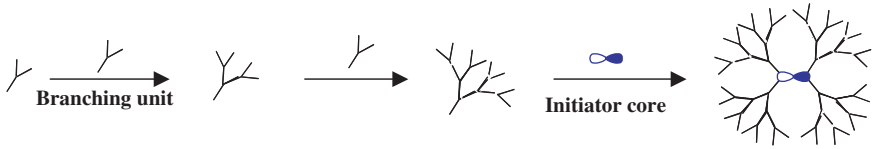

Figure 3: Convergent method for the synthesis of tetra dendron arm star macromolecule (called dendrimers).

excess of EDA must be removed in order to prevent the creation of lower-generation dendrimers during the next Michael addition step. This may be done using a rotary evaporator, wiped film still, and/or tangential flow ultrafiltration.

Various dendrimer structures may be obtained by altering the initiator core, repeat units, and the surface groups. The method of synthesis can also be altered, as many new methods have been developed in order to obtain a high yield and reduce the number of purification steps needed. Although many factors of the synthesis or structure may be varied, the de Gennes dense-packing effect will be a factor. As the generation is increased, the surface groups will become more densely packed and will eventually reach an upper limit.[22] In the case of EDA-cored PAMAM dendrimers, this upper limit is generation 10.

3.4 Mathematical Description of Theoretical Dendrimer Structure

As described earlier, dendrimer synthesis is a reiterative process which adds to the structure through reaction at the end groups. Because of the branched nature of their structure, dendrimers are often compared to tree-like electro-mechanical circuits[23] (Figure 4). Through each cycle of the reaction sequence, new generations are formed in a highly controlled manner. As a result, there is also great control over the molecular weights of dendrimers, providing a narrow molecular weight distribution.

For any polymer, the molecular weight can be described as the molecular weight of the repeating units multiplied by the degree of

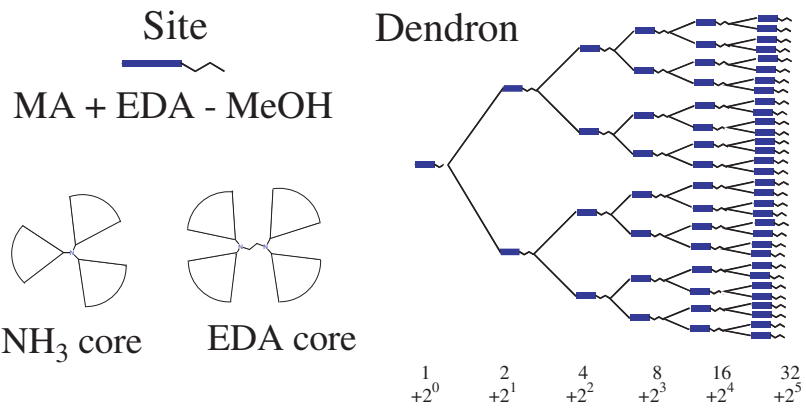

Figure 4: Dendron as a tree-circuit analog and dendrimer as dendron-arm star macromolecules (for ammonia and EDA cores). (Reprinted with permission from I. J. Majoros, C. B. Mehta, and J. R. Baker Jr., *J. Comput. Theor. Nanosci*., **1**, 193–198 (2004). Copyright © American Scientific Publishers.)

polymerization (the number of repeating units making up the polymer). In the case of dendrimers, the molecular weight of the core must also be added on. The degree of a dendrimer is given by[5]:

$$F_c \cdot \left(\frac{F_r^{g+1} - 1}{F_r - 1} \right) \tag{1}$$

where F_c is the core functionality (4 for EDA cores and 3 for NH_3 cores), F_r is the multiplicity of the repeating units, and g is the generation number. Using this equation, the general notation for the molecular weight of dendrimers is given by[5]:

$$MW = MW_{\text{core}} + (\text{Molecular weight of monometers})\, F_c \cdot \left(\frac{F_r^{g+1} - 1}{F_r - 1} \right) \tag{2}$$

When evaluating the molecular weight for a PAMAM dendrimer with an EDA core and repeating units of methyl acrylate (MA) and EDA, one must remember that methanol is a side product of the amidation reaction in PAMAM synthesis. The molecular weight is then given by[23]:

$$MW = EDA + (MA + EDA - MeOH) * 2^2 \left(\frac{2^{g+1} - 1}{2 - 1} \right) \tag{3}$$

where EDA, MA, and MeOH are the molecular weights of EDA, MA, and methanol, respectively. Note that the molecular weights of EDA and MA used must be those of their original forms, not their reacted forms in the dendrimer structure.

The number of terminal groups can also be determined using the equation[5,23]:

$$\text{Number of terminal groups: } Z = F_c \cdot F_r^g \tag{4}$$

The number of tertiary amines of a dendrimer structure can also be determined using the equation[23]:

$$\text{Number of tertiary amines: } T_c + F_c \left(\frac{F_r^g - 1}{F_r - 1} \right) \tag{5}$$

where T_c is the number of tertiary amines in the core (EDA core has two tertiary amines). The equations given provide the theoretical structure of dendrimers. It must be noted that there are many deviations from the theoretical values which will be discussed further in the following section.

3.5 Structural Deviations in Poly(amidoamine) Dendrimers

The synthesis of poly(amidoamine) (PAMAM) dendrimers is quite a precise process, as described earlier, especially when compared to other polymer synthesis. However, it is by no means a perfect process. PAMAM dendrimer synthesis always results in structural defects.[24] The major structural defects include incomplete Michael addition, fragmentation, and intramolecular cyclization.[25]

The primary cause of PAMAM dendrimer structural deviations is incomplete Michael addition, resulting in asymmetrical dendrimer structures (Figure 5(a)). This is a result of the natural tendency of reactions not to go all the way to completion. Incomplete Michael addition is minimized by using an excess of methyl acrylate.

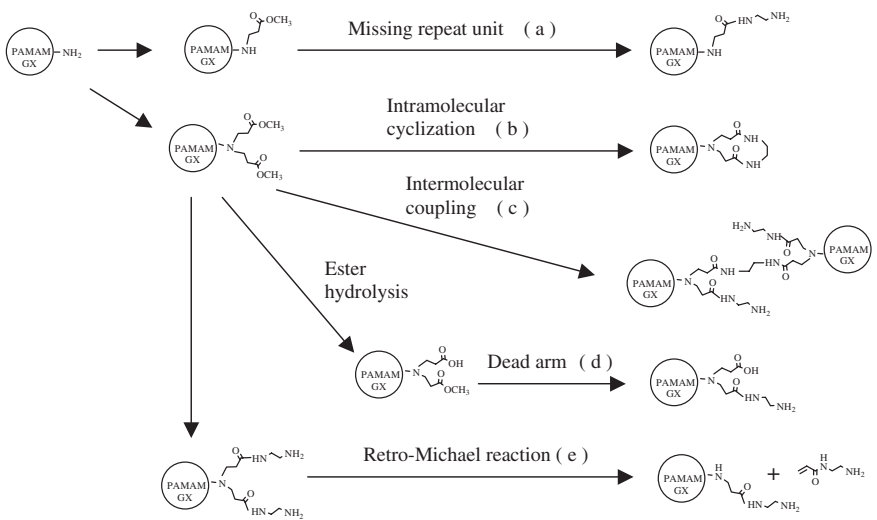

Figure 5: Concurrent reactions in PAMAM dendrimer synthesis.[25]

Fragmentation of dendrimers is caused by the retro-Michael side reaction. Fragmentation creates asymmetrical structures similar to those created by incomplete Michael addition (Figure 5(e)). These defects are a product of the existence of an equilibrium between the Michael reaction and retro-Michael reaction. This side reaction is especially relevant at higher temperatures as the equilibrium is greatly shifted towards the retro-Michael reaction, but even at room temperature significant effects have been noticed.[26] This emphasizes the need for temperature control during dendrimer synthesis.

Other defects can be caused by interactions within dendrimers as well as among dendrimers. Intramolecular dendrimer reaction resulting in cyclization can occur during the amidation step of dendrimer synthesis (Figure 5(b)). A wide variety of cyclic products may be formed in higher generations as a result of the many identical esters on the surface of the half-generations.[26] Also during amidation, intermolecular interactions resulting in intermolecular coupling are possible[27] (Figure 5(c)). The best way to prevent this defect is to ensure that a great enough excess of EDA is used during this step of the synthesis. In order to achieve a 95% monodisperse dendrimeric product (with an ammonia core), the excess needed ranges from 15–234 molar excess for generations 1–5, respectively.[2] Intramolecular cyclization and intermolecular coupling can be minimized if a methanol solution of the half-generation dendrimer is added to this large excess of EDA under dry nitrogen and proper stirring. These defects, again, are more prominent with higher temperatures.

Another key to preventing structural defects is avoiding dendrimer contact with water. Half-generation ester-terminated dendrimers readily undergo hydrolysis in the presence of water to form carboxylic acid groups.[2] These carboxylic acid groups will not amidate under normal reaction conditions, creating a "dead" arm (Figure 5(d)).

3.6 Characterization

The most widely used methods of characterization for dendrimers are most likely proton and carbon NMR.[19] NMR provides a relatively simple method for the structural analysis of dendrimers. Routine spectra taken during the synthesis of dendrimers can reveal the chemical transformations occurring at the terminal groups. This is an incredibly useful method of monitoring the purity of dendrimer production, even at high generations. NMR may also be used to identify possible structural defects in the dendrimer. Other types of spectroscopy, though not as widely used, may also be used for these purposes, including IR,[28] UV-vis,[29] and fluorescence[30] spectroscopy.

Another method of characterizing a highly purified dendrimer structure, mainly its terminal group functionality, is potentiometric titration. This is crucial to designing any type of further reactions using the dendrimer. Titration of PAMAM dendrimers using HCl followed by back-titration using NaOH can be used to determine the number of primary and tertiary amines, as shown in Figure 6.

The molecular weight of the dendrimer is often characterized using Size Exclusion Chromatography (SEC) (Gel Permeation Chromatography,

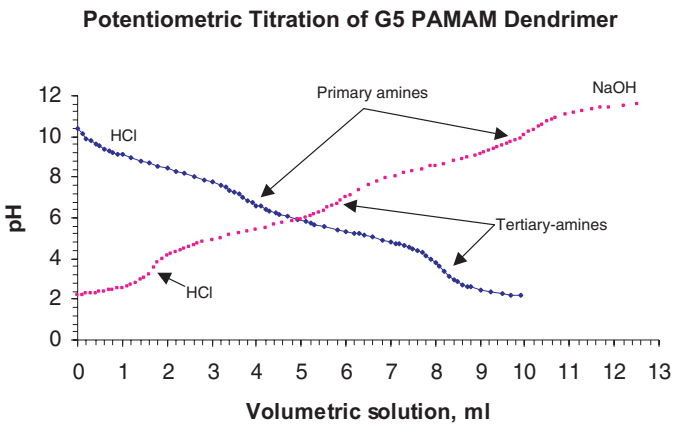

Figure 6: Potentiometric titration of a single PAMAM G5 dendrimer batch in 0.1 M NaCl solution (# of primary amines: 110; # of tertiary amines: 108 were calculated).

GPC). This, again, is crucial for designing further reactions using the dendrimer and requires a highly purified sample. The SEC is commonly used to determine the molecular weight, molecular weight distribution, and root mean square radius. Molecular weight analysis by GPC and supported by MALDI-TOF MS for the same G5 dendrimer batch as above is shown in Figure 7. The retention times found in SEC can also be utilized to quantify the structural defects which were described earlier.[4] Polyacrylamide gel electrophoresis (PAGE) can be used to check the purity and homogeneity of PAMAM dendrimers.[31] PAGE separates molecules based on their charge-mass ratio. Therefore, if the synthesis produced a monodisperse dendrimer product with respect to molecular weight and structure, the PAGE analysis should show only a single band. The resultant band(s) can also be compared to standards as another method of determining the size of the dendrimer molecules.

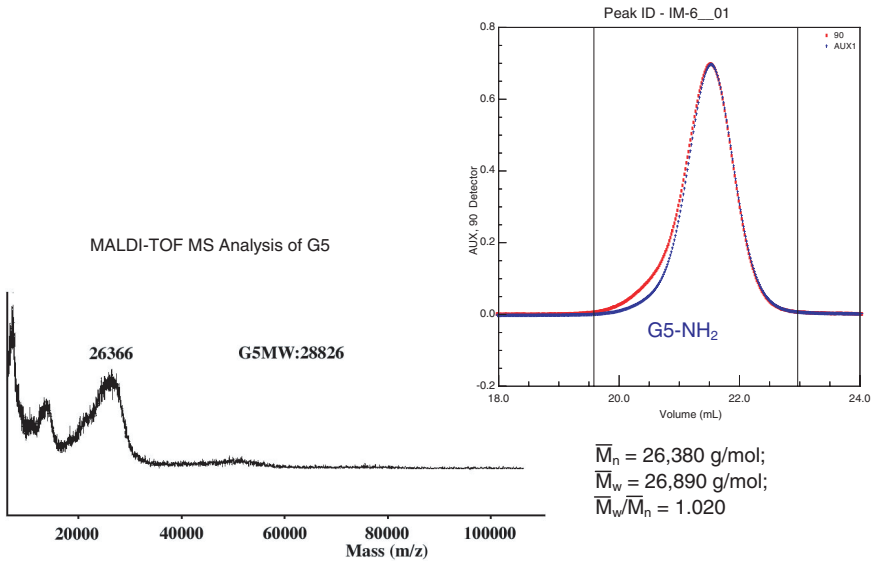

Figure 7: Determination of molecular weight by MALDI-TOF MS and GPC.

HPLC analysis is used to determine the purity of a dendrimer sample as well as some of its structural characteristics. A narrow peak is desired, as this suggests uniformity of the dendrimer. A wider peak is a result of structural inhomogeneity created by structural defects. When compared to the elution graphs of known standards, HPLC can also be used to determine the functional groups present in a dendrimer solution.[32]

There are two main types of microscopy used for visual analysis of dendrimers, atomic force microscopy (AFM)[29] and near-field scanning optical microscopy (NSOM).[33] These types of microscopy give a measured topography which can be used to find particle volume. Knowing the volumes of individual species can then tell you the species composition. Once this information is known, it is then possible to determine the number of dendrimers in a cluster.

3.7 Physicochemical Properties

Following synthesis, dendrimers can be isolated as pale amorphous syrups which can be dissolved using most organic solvents. One distinct property of the half-generation dendrimers as compared to the full-generation dendrimers is the display of surface active properties shown in water, which creates a foamy solution. Also, the half-generation dendrimers show a lower intrinsic viscosity than the corresponding full-generation dendrimers (Figure 8). This difference in viscosity is a result of increased aggregation of the amine-terminated full-generation dendrimers by way of intermolecular hydrogen bonding.[2]

An important property of PAMAM dendrimers is their tendency to form cationic structures under physiologic conditions (pH = 7.4). Under these conditions, the primary amines on the surface of the dendrimer readily protonate. This creates a polycationic dendrimer with ammonium terminal groups, which leads to a more basic solution.[34]

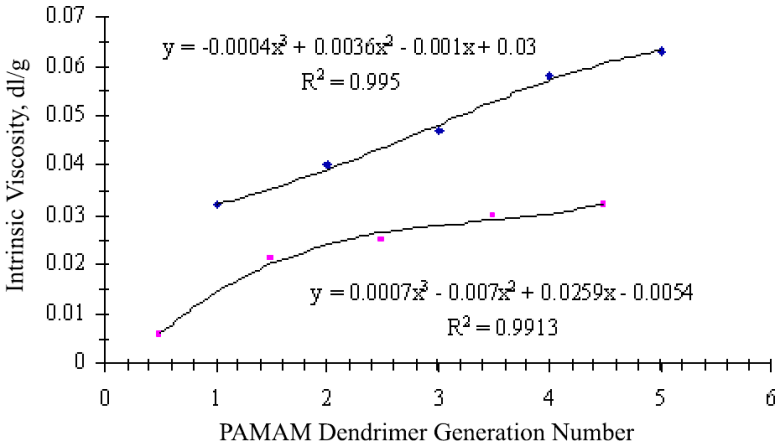

Figure 8: Intrinsic viscosity of PAMAM dendrimers.

The absorbance spectrum of the dendrimers is often used to determine properties such as dendrimer concentration in solution. The predominant factor of the spectrum of a PAMAM dendrimer is the lack of UV absorbance above a wavelength of 210 nm.

3.8 References

1. I. Brigger, C. Dubernet, and P. Couvreur, Nanoparticles in cancer therapy and diagnosis, *Advance Drug Delivery Review*, **54**, 631–651, 2002.
2. D. A. Tomalia, H. Baker, J. Dewald, M. Hall, G. Kallos, S. Martin, J. Roeck, J. Ryder, and P. Smith, A new class of polymers: Starburst dendritic macromolecules, *Polymer Journal*, **17**(1), 117–132, 1985.
3. D. A. Tomalia, H. Baker, J. Dewald, M. Hall, G. Kallos, S. Martin, J. Roeck, J. Ryder, and P. Smith, Dendritic macromolecules: Synthesis of starburst dendrimers, *Macromolecules*, **19**, 2466–2468, 1986.
4. P. Smith, S. Martin, M. J. Hall, and D. A. Tomalia, A characterization of the structure and synthetic reactions of polyamidoamine Starburst® polymers III-D, 357–385, In *Applied Polymer Analysis and Characterization*, Ed. J. Mitchell Jr., Hanser, New York, 1987.
5. D. A. Tomalia, A. M. Naylor, and W. A. Goddard III, Starburst dendrimers: Molecular-level control of size, shape, surface chemistry, topology, and flexibility from atoms to macroscopic matter, *Angewandte Chemie International Edition*, **29**, 138–175, 1990.
6. A. B. Padias, H. K. Hall Jr., D. A. Tomalia, and J. R. McConnell, Starburst polyether dendrimers, *Journal of Organic Chemistry*, **52**, 5305–5312, 1987.

7. J. S. Rutt, Dendrimers and nanotechnology: A patent explosion, Foley and Larner Paper presented at the National Nanotechnology Initiative Conference, Washington DC, April 29, 2002. http://www.foley.com
8. N. Bourne, L. R. Stanbury, E. R. Kern, G. Holan, B. Matthews, and D. I. Bernstein, Dendrimers, a new class of candidate topical microbiocides with activity against herpes simplex virus infection. *Antimicrobial Agents and Chemotherapy*, **44**(9), 2471–2474, 2000.
9. M. Witvrouw, V. Fikkert, W. Pluymers, B. Matthews, K. Mardel, D. Schols, J. Raff, Z. Debyser, E. De Clercq, G. Holan, and C. Pannecouque, Polyanionic (i.e. polysulfonate) dendrimers can inhibit the replication of human immunodeficiency virus (HIV) by interfering with both virus absorption and later steps (reverse transcriptase/integrase) in the virus replication cycle, *Molecular Pharmacology*, **58**(5), 1100–1108, 2000.
10. S. Shaunak, S. Thomas, E. Gianasi, A. Godwin, E. Jones, I. Teo, K. Mireskandari, P. Luthert, R. Duncan, S. Patterson, P. Khaw, and S. Brocchini, Polyvalent dendrimer glucosamine conjugates prevent scar tissue formation. *Nature Biotechnology*, **22**(8), 977–984, 2004.
11. S. Svenson and D. A. Tomalia, Commentary; Dendrimers in biomedical applications — reflections on the field, *Advanced Drug Delivery Reviews*, **57**, 2106–2129, 2005.
12. H. Kobayashi and Martin W. Brechbiel, Nano-sized MRI contrast agents with dendrimer cores, *Advanced Drug Delivery Reviews*, **57**, 2271–2286, 2005.

13. C. Dufès, I. F. Uchegbu, and A. G. Schätzlein, Dendrimers in gene delivery B, *Advanced Drug Delivery Reviews*, **57**, 2177–2202, 2005.
14. K. T. Al-Jamal, C. Ramaswamy, and A. T. Florence, Supramolecular structures from dendrons and dendrimers, *Advanced Drug Delivery Reviews*, **57**, 2238–2270, 2005.
15. W. H. Hunt, Nanomaterials: Nomenclature, novelty and necessity, *JOM*, **56**, 13, 2004.
16. A. D'Emanuele and D. Attwood, Dendrimer–drug interactions, *Advanced Drug Delivery Reviews*, **57**, 2147–2162, 2005.
17. A. K. Patri, J. F. Kukowska-Latallo, and J. R. Baker Jr., Targeted drug delivery with dendrimers: Comparison of the release kinetics of covalently conjugated drug and non-covalent drug inclusion complex, *Advanced Drug Delivery Reviews*, **57**, 2203–2214, 2005.
18. R. Duncan and L. Izzo, Dendrimer biocompatibility and toxicity, *Advanced Drug Delivery Reviews*, **57**, 2215–2237, 2005.
19. A. M. Caminade, R. Laurent, and J. P. Majoral, Characterization of dendrimers, *Advanced Drug Delivery Reviews*, **57**, 2130–2146, 2005.
20. G. R. Newkome, Z. Yao, G. R. Baker and V. K. Gupta, Micelles. Part 1. Cascade molecules: A new approach to micelles, A [27]-arborol, *Journal of Organic Chemistry*, **50**, 2003–2004, 1985.
21. C. Hawker and M. J. Frechet, A new convergent approach to monodisperse dendritic macromolecules, *Journal of the Chemical Society-Chemical Communications*, **15**, 1010–1013, 1990.
22. P. G. De Gennes and H. Hervet, Statistics of "Starburst" polymers, *Journal de Physique Lettres*, **44**, 351–360, 1983.

23. I. J. Majoros, C. B. Mehta, and J. R. Baker Jr., Mathematical description of dendrimer structure, *Journal of Computational and Theoretical Nanoscience*, **1**, 193–198, 2004.

24. J. Peterson, A. Ebber, V, Allikmaa, and M. Lopp, Synthesis and CZE analysis of PAMAM dendrimers with an ethylenediamine core, *Proceedings of the Estonian Academy of Sciences: Chemistry*, **50**, 156–166, 2001.

25. J. Peterson, V. Allikmaa, J. Subbi, T. Pehk, and M. Lopp, Structural deviations in poly(amidoamine) dendrimers: A MALDI-TOF MS analysis, *European Polymer Journal*, **39**, 33–42, 2003.

26. J. Peterson, V, Allikmaa, T. Pehk, and M. Lopp, Fragmentaion of PAMAM dendrimers in methanol, *Proceedings of the Estonian Academy of Sciences: Chemistry*, **50**, 167–172, 2001.

27. X. Shi, I. Bányai, M. T. Islam, W. Lesniak, D. Z. Davis, J. R. Baker Jr., and L. P. Balogh, Generational, skeletal and substitutional diversities in generation one poly(amidoamine) dendrimers, *Polymer*, **46**, 3022–3034, 2005.

28. V. L. Furer, V. I. Kovalenko, A. E. Vandyukov, J. P. Majoral, and A. M. Caminade, Calculation of IR spectra of elementoorganic dendrimers, *Spectrochimica Acta Part A: Molecular and Biomolecular Spectroscopy*, **58**, 2905–2912, 2002.

29. S. Achar and R. J. Puddephatt, Organoplatinum dendrimers formed by oxidative addition, *Angewandte Chemie International Edition in English*, **33**, 847–849, 1994.

30. G. R. Newkome, C. D. Weis, C. N. Moorefield, and I. Weis, Detection and functionalization of dendrimers possessing free carboxylic acid moieties, *Macromolecules*, **30**, 2300–2304, 1997.

31. H. M. Brothers II, L. T. Piehler and D. A. Tomalia, Slab-gel and capillary electrophoretic characterization of polyamidoamine dendrimers, *Journal of Chromatography A*, **814**, 233–246, 1998.

32. M. T. Islam, I. J. Majoros and J. R. Baker Jr., HPLC analysis of PAMAM dendrimer based multifunctional devices, *Journal of Chromatography B*., **822**, 21–26, 2005.

33. J. A. Veerman, S. A. Levi, F. C. J. M. van Veggel, D. N. Reinhoudt and N. F. van Hulst, Near-field scanning optical microscopy of single fluorescent dendritic molecules, *The Journal of Physical Chemistry A*, **103**, 11264–11270, 1999.

34. S. E. Stiriba, H. Frey, and R. Haag, Dendritic polymers in biomedical applications: From potential to clinical use in diagnostics and therapy, *Angewandte Chemie International Edition in English*, **41**, 1329–1334, 2002.

This page intentionally left blank

Chapter 4

Optical and Biophotonic Applications of Dendrimer Conjugate

Jing Yong Ye & Theodore B. Norris

Outline

4.1 Introduction

Dendrimers have attracted much attention recently owing to their unique molecular architectures. In contrast to linear organic polymers, dendrimers are a novel class of macromolecules possessing a highly branched three-dimensional architecture, and well-controlled size and shape. The large number of end groups of a dendrimer can be chemically modified to associate different functionalities with them. In addition, dendrimers generally have a size on the order of a few nanometers, allowing some critical applications that require a compact multifunctional device on the nanometer scale. For example (Figure 1), a dendrimer-based multifunctional nano-device has been developed for targeted drug delivery to a specific tumor site, which has a targeting agent for specific binding to cancer cells, a fluorescent biomarker for monitoring the drug uptake, and anticancer drugs to cause apoptosis.[1] This nano-device has been tested for its ability to target cancer cells *in vitro* and *in vivo*. The experimental binding characteristics were in conformance with predictions from molecular modeling. It has been demonstrated that it is essential to have the multifunctional conjugates on the nanometer scale for controllable cellular internalization. This dendrimer-based drug delivery system shows enhanced therapeutic effects as compared to free drugs, while having reduced side effects.[2,3]

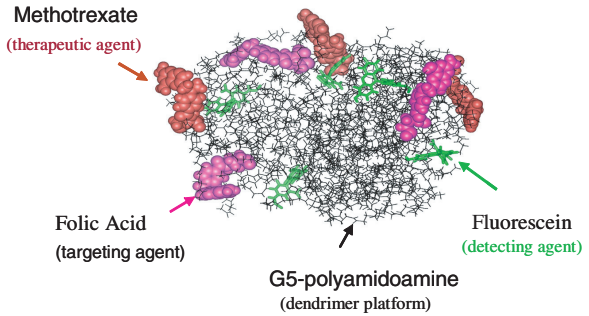

Figure 1: 3-D model of G5-dendrimer nano-device conjugated with fluorescein and folic acid through amide linkage, and methotrexate through ester-linkage. The model was generated using Molecular Dynamics simulations that would allow prediction of branch aggregation and 3-D locations of the functional groups. The derived model predicts surface exposure of all the three added functions.[1] (Reprinted with permission from *J. Med. Chem.*, **48**(11), 3729–3735, 2006. Copyright (2006) American Chemical Society.)

In addition to targeted drug delivery, the unique physical and chemical properties of dendrimers also result in many other applications, including tissue repair,[4–6] biosensing,[7–9] and photonic devices.[10–12] While much effort has been devoted to synthesizing a variety of dendrimers with various functionalities, as discussed in the other chapters of this book, we focus on several optical properties and biomedical applications of dendrimer conjugates in this chapter.

4.2 Linear Optical Properties of Dendrimers and Their Conjugates

Dendrimers have unique linear and nonlinear optical properties depending on their molecular architectures. Here we will discuss both the linear and

nonlinear optical response of dendrimers and their conjugates, and will illustrate several novel applications of dendrimer-based materials. Applications based on dendrimer's linear optical response have been reported for light-emitting diodes, light harvesters, and fluorescent biomarkers, etc.

4.2.1 Dendrimer light-harvesters and light-emitting diodes

Dendrimers have been recently investigated by several groups for applications as light-harvesting systems, owing to their unique molecular architectures that mimic a natural light-harvesting system.[12–16] In natural photosynthetic systems, a large array of chlorophyll molecules surrounds a single reaction center.[16] The intricate chlorophyll assembly acts as an efficient light-harvesting antenna that captures photons from the sun and transfers their energy rapidly to the reaction center where it is utilized to form ATP.[17] Similarly, the synthetic dendrimer has a highly branched structure that radiates out from a central core and is well suited to efficiently funnel energy to its center point. In addition, the high density of sites at the periphery can be functionalized with chromophore groups, acting as an efficient light-absorbing molecular antenna. The absorbed energy at the periphery rapidly transfers from the dendritic branches to the core, resulting in a light-harvesting action.

Fréchet and co-workers used a flexible poly(arylether) dendrimer that is functionalized with dye molecules at the periphery as a molecular antenna, while the core is functionalized with a suitable dye molecule that serves as the energy acceptor.[12,18] The energy absorbed at the periphery is funneled to a central fluorescent core primarily by a through-space

Förster-type mechanism, and energy transfer quantum yields greater than 90% have been measured for dendrimer sizes up to the fourth generation. In addition, instead of varying the chemical nature of dendrimer subunits and linker groups for efficient energy transfer, it has been reported that energy gradients can be formed in dendrimers to funnel the energy from periphery to the core more efficiently.[17,18] In this case, the entire dendrimer framework serves both as the light-absorbing antenna and as an energy transport medium. The energy gradient in phenylacetylene (PA) monodendrons leads to rapid and directional energy transport, and results in an energy transfer quantum yield that approaches unity.[12]

As dendrimers are being used more and more widely as new building materials for photonic devices, an understanding of the fundamental physics and chemistry behind the novel dendritic macromolecular architectures is helpful to improve the design for fabricating new dendrimer-based optical devices with high efficiency. Kopelman and colleagues discovered that the localization of excitation energy can be markedly different in different types of dendrimers.[19] For compact dendrimers, excitations are localized at the nodes of the Cayley trees of the molecular structure and the energy of lowest transition was not affected by an increase in dendrimer generation. In contrast, in extended dendrimers the excitations become less localized, with a hierarchy of localization lengths. The excitation energy transfer between dendrimer subunits has also been investigated extensively to understand the mechanism of this process and to help one improve the efficiency of using dendrimers as an artificially synthesized light-harvester.[20–22] For example, it has been discovered that energy can be funneled to the dendrimer core more efficiently for molecular structures with

designed energy gradients.[15,23,24] Several mechanisms for the excitation energy transfer from the dendrons to the core have been proposed.[25–28] It was demonstrated that the energy transfer can be attributed to the Coulombic dipole–dipole interactions in several organic dendrimer systems.[12,23,29] The dynamics of the energy transfer process in a carbonyl-terminated phenylacetylene dendrimer has been studied using both steady-state and time-resolved optical spectroscopy.[13] The intersite energy transfer time was calculated to be 6 ps, consistent with the experimentally measured value of 5–17 ps. It was also observed that the overall light-harvesting efficiency depends on the dendrimer size. The overall dendrimer quenching rate was found to decrease exponentially with dendrimer size over the first four generations.

Recently dendrimers have also attracted considerable attention as novel materials for organic light-emitting diodes (OLEDs).[10,11,30–32] OLEDs are of great interest for making less expensive full-color flat-pannel displays. Polymer based OLEDs can be fabricated through a solution process, such as spin-coating and inkjet printing, which has a much lower cost than high vacuum deposition process. Dendrimer is a solution-processible photoactive and electroactive material with the desired solubility and electronic and luminescence properties. The large dendrons surrounding the luminescent core of a dendrimer prevent concentration quenching by isolating the core, thus increasing the luminous efficiency of an OLED. Markhan *et al*. observed very high-efficiency green phosphorescence from a single-layer dendrimer organic light-emitting diode formed by spin-coating.[30] A first generation fac-tris(2-phenylpyridine) iridium cored dendrimer doped into a wide-gap 4,4-bis(N-carbazole) biphenyl host displayed a peak

external quantum efficiency of 8.1%. This exceptionally high quantum efficiency for a single-layer device was attributed to the excellent film forming properties and high photoluminescence quantum yield of the dendrimer blend and efficient injection of charge into the emissive layer. In addition, wide range tunability of the emission spectrum of an OLED is required in many applications. It has been recently demonstrated that color tuning from green to red can be obtained by adjusting the relative amounts of red and green emitting dendrimers in a blend.[33] With a simple two-layer structure this solution-processed OLED has achieved very high efficiencies across the whole color tuning range.

4.2.2 Real-time biosensing with dendrimer fluorescent biomarkers

The development of analytical methods for *in vivo* measurements to identify cancer signatures, monitor drug delivery and evaluate drug-induced effects in tumors has been a goal for enhancing cancer treatment.[34] As an important approach for *in vivo* tumor analysis, the use of fluorescent probes[35] has the advantage of being more biocompatible than radiation or chemical analysis, and builds on the wide base of technology developed for *in vitro* analysis using flow cytometry and histochemical staining. Dendrimers offer an ideal platform for integration of fluorescent markers, drugs, and targeting agents on a nanometer scale. The synthesis of multifunctional dendrimer-based nano-devices, with covalently linked tumor-targeting molecules such as folic acid (FA) or HER2-antibody, a sensing fluorescent molecule, and a chemotherapeutic drug such as methotrexate or taxol, has been recently reported.[1,8] It has been shown that this new

material can be purified to a very high degree and the final product is free of individual starting components, and has a well controlled 3D architecture with mono-dispersed stoichiometric numbers of added components. This multifunctional nano-device has been tested for its ability to target cancer cells *in vitro* and *in vivo* monitored by fluorescence measurements.

Our group performed initial demonstrations of the targeting capability to tumors using KB cell line (a sub-line derived from the cervical carcinoma HeLa cell line) as a model system. The binding of G5-FI-FA [poly(amidoamine) dendrimers generation-5 (PAMAM, G5) conjugated with fluorescein isothiocyanate (FI) and folic acid (FA)], and control G5-FI dendrimer to KB cells was investigated.[7] The details about the synthesis of this dendrimer conjugate can be found in Ref. 36. The FA enables the dendrimers to be selectively taken up by FA-receptor-positive KB cells. Confocal microscopic analysis provided evidence of cellular internalization *ex vivo* (Figure 2).

The challenge for characterizing targeting in live animal models, and ultimately people, is considerable. Fluorescent probes for tumor analysis *in vivo* is promising, but faces a number of hurdles. The most notable issue is due to the nature of tissues, which are highly light scattering and absorbing, thus making it difficult to perform non-invasive fluorescence analysis.[37–39] A two-photon optical fiber fluorescence probe (TPOFF) has been developed recently to quantitatively characterize the local concentration of biomarkers *in vivo*,[7,8] which bypasses the tissue scattering and absorption. Basically, in a TPOFF system femtosecond laser pulses are delivered through a single-mode optical fiber, and the two-photon excited fluorescence from samples is collected back through the same fiber.

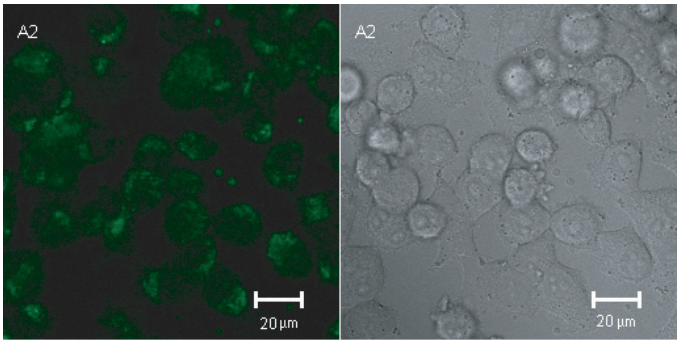

(a)

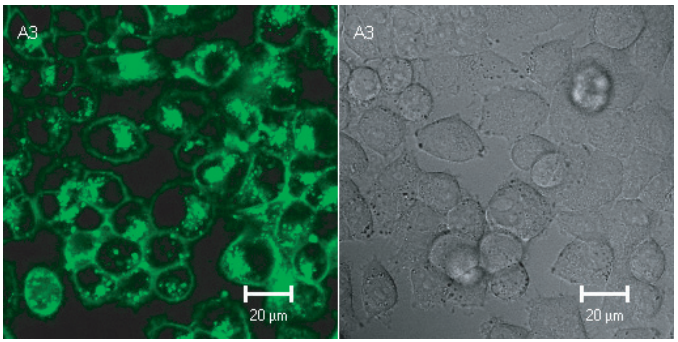

(b)

Figure 2: Confocal microscopic evidence of the uptake of fluorescent dendrimers in KB cells. KB cells were incubated with 250 nM of the non-targeted control dendrimer G5-FI (a) or the targeted dendrimer G5-FI-FA (b) for 48 hours at 37°C, and confocal images were taken in a Carl Zeiss microscope using an argon laser excitation beam. The left and right panels represent fluorescent and light images of the same observation field.[1] (Reprinted with permission from *J. Med. Chem.*, **48**, 3729–3735, 2005. Copyright (2005) American Chemical Society.)

In contrast to normal right angle fluorescence detection configuration, the use of a single optical fiber for both fluorescence excitation and collection allows one to construct a practical system for *in vivo* biosensing. The fluorescence signal collected through the fiber is separated from the excitation

beam with a dichroic mirror, and further filtered with a short-pass filter and a spectrometer, then detected with a photon-counting photomultiplier tube. The excitation volume is localized due to the nonlinearity of the two-photon absorption, ensuring the measurement of a specific site with small excitation volume in close proximity to the fiber tip. Since the wavelength of the emitted fluorescence light is significantly shorter than the excitation wavelength, the emission can be easily filtered and separated from the excitation light to obtain a high signal-to-noise ratio. In addition, the TPOFF probe employs near-IR light for excitation, which minimizes tissue damage, absorption, and photobleaching. Finally, this TPOFF method also allows one to use a single laser source to excite a wide variety of fluorophores owing to the wide two-photon excitation spectrum.

The uptake of the FA-targeted dendrimer nano-device in the KB cell tumor model has been measured *in vitro* and *in vivo* using the TPOFF method. The two-photon fluorescence (TPF) intensity from standard solutions of G5-FI and G5-FI-FA with concentrations ranging from 10 nanomolar to 100 micromolar is shown in Figure 3.

Although the TPF signals from both samples have a linear concentration dependence, the signal from G5-FI-FA is slightly lower than that from G5-FI. Since the absorption spectra of these two solutions are similar, the difference in the fluorescence signal indicates there is a small quenching effect due to adding the FA to the dendrimer conjugate. Cultured KB cell pellets treated with different concentrations of the dendrimer conjugates were then measured with the TPOFF probe. The KB cells treated with the targeted nano-device G5-FI-FA were found to give significantly higher fluorescence than those treated with the control G5-FI

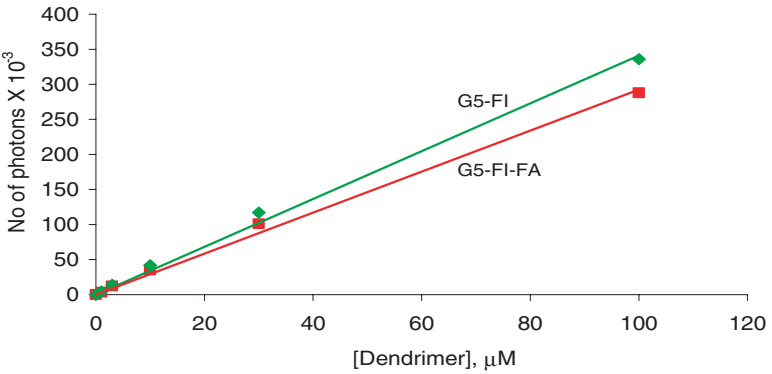

Figure 3: TPF power as functions of the concentrations of G5-FI and G5-FI-FA. The fluorescence quantum yield of G5-FI-FA is slightly lower due to partially quenching effect by FA.[3] (Reprinted with permission from "Engineered particles," *OE Magazine, SPIE*, 2003.)

(Figure 4(a)). This finding indicated that the dendrimer conjugated with a targeting agent can be used to enhance the binding affinity to cancer cells. The saturation of G5-FI-FA binding was observed, which confirmed that the targeting is through specific binding to the high affinity folate receptors. At saturation, the level of G5-FI-FA bound was calculated to be 2 pmols per10^6 cells, which is in agreement with the flow cytometry result, as shown in Figure 4(b).

Other fluorophores have also been conjugated to dendrimers for fluorescence detection of drug delivery *ex vivo* and *in vivo*. 6-carboxytetramethylrhodamine succinimidyl ester (6T) was used to synthesize dendrimer conjugates with fluorescence emission wavelength different from fluorescein dendrimer conjugates and for better photostability.[8] G5 dendrimer in a buffer solution was mixed with 6T, and the mixture was dialyzed in PBS and water, ultrafiltered and lyophilized to obtain the

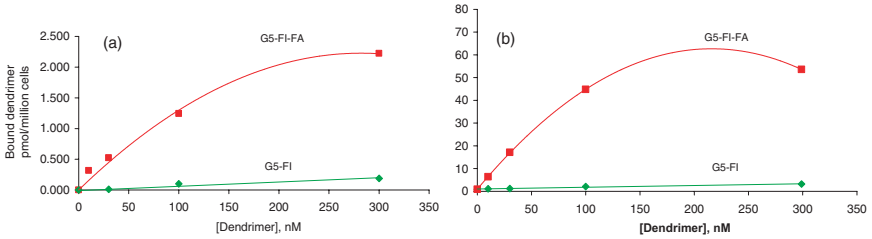

Figure 4: Dose-response curves for the binding of G5-FI and G5-FI-FA on KB cells determined respectively by TPF (a) and flow cytometry (b).[3] (Reprinted with permission from "Engineered particles," *OE Magazine, SPIE*, 2003.)

product of G5-6T. To conjugate the targeting agent FA with G5-6T, FA was initially activated and mixed with the G5-6T, then dialyzed. The remaining surface NH_2 groups of G5-6T and G5-6T-FA were acetylated by reacting in one reaction step with acetic anhydride in the presence of triethylamine. The product was analyzed by ^{1}H-NMR and UV-visible spectroscopy and the results indicated that the respective numbers of 6T and FA molecules per dendrimer were 3 and 4, respectively. Two-photon fluorescence emissions from both the dendrimer conjugates G5-6T and G5-6T-FA showed a maximum emission at 560 nm, similar to free 6T.

In vivo studies further demonstrated that the targeted delivery of G5-6T-FA can be achieved in a live animal. KB cell tumors in SCID mice were selected as a model system, which over express the high affinity FA-receptor (FAR).[8] Control tumors were developed by using the MCA207 cell line, because *in vitro* binding studies showed that MCA207 cells have little binding with FA-conjugated dendrimers. G5-6T-FA and G5-6T were injected into the tail veins of mice bearing KB-cell and MCA207 xenograft tumors. A TPOFF probe was used to analyze the

binding of the dendrimer conjugates in these two kinds of tumors. Significant enhancement of targeted delivery of FA-conjugated dendrimers to KB cell tumors was observed. Figure 5 shows there was a 6-fold increase in TPOFF readings in KB cell tumors of mice receiving G5-6T-FA as compared to the non-targeted G5-6T dendrimer. There was a 3-fold increase in the fluorescence of G5-6T-FA dendrimers in FAR-positive KB cell tumors as compared to the FAR-negative MCA207 tumors. In the FAR-positive KB cells, the concentration of G5-6T-FA reached average levels of about 2 μM. Because there are 3 to 4 FA per dendrimer, the result indicates that the average intracellular FA equivalent is 6–8 μM. This value is in good agreement with that obtained from radioactive FA binding studies. These studies demonstrate that dendrimers

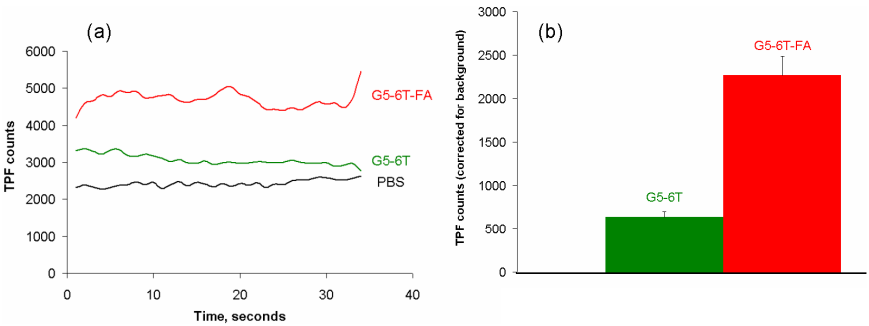

Figure 5: TPF measurement in KB cell tumors in mice injected with G5-6T or G5-6T-FA. Five million KB cells were injected subcutaneously into mice to form tumors that were allowed to grow for two weeks. The mice were injected with the dendrimers, and after 14 h, the tumors were surgically removed and TPF counts were taken. (a) The traces represent mean of two different tumors from two different mice taken in five different internal regions of each tumor. (b) The mean value of all counts corrected for the PBS background fluorescence.

can be functionalized for targeted drug delivery and for sensitive *in vivo* fluorescence biosensing.

4.2.3 Multicolor two-photon flow cytometry using targeted dendrimer conjugates

Besides using dendrimer conjugates as biomarkers for single color fluorescence detections, targeted dendrimer conjugates can further allow ratiometric measurements based on multi-color correlated fluorescence detection. Multicolor fluorescence detection is often preferred, because information of different processes in a biological system may be revealed all at once by using multiple biomarkers. In some particular situations, correlation of fluorescence from multiple biomarkers is required for ratiometric measurements in order to sensitively monitor some biological changes in a complicated system. As demonstrated in the following two-photon flow cytometry measurement, dendrimer fluorescent conjugates act well as multicolor biomarkers owing to their unique molecular architecture.[40]

In a conventional (one-photon excitation) flow cytometer, single cell detection is achieved by injecting a cell sample into the center of a sheath flow, which hydrodynamically focuses the cell and delivers cells one by one to the point of excitation with an accuracy of ±1 μm or better.[41] On the other hand, two-photon flow cytometry utilizes the nonlinear property of multi-photon excitation process to selectively detect single cells.[40] One major advantage of two-photon flow cytometry over conventional flow cytometry is that it allows analyzing circulating cells *in vivo*, where there is no controlled sheath flow. However, it is challenging to obtain

quantitative results in two-photon flow cytometry, because the two-photon excitation volume is small and the cells flow through the excitation region in random positions with different velocities and paths, thus being excited unevenly. Figure 6(a) shows the two-photon excited fluorescence signal versus time (bin number) from stained cells. Due to the uneven excitation in the system, the intensity distribution of the fluorescent peaks (Figure 6(b)) spreads out from just above background to its maximum possible signal level, which corresponds to cells that flow directly through the center of the excitation volume and have the highest fluorophore concentration. Thus, the fluorescence signal level alone cannot be used as a parameter to differentiate cell populations, unlike that in the conventional flow cytometry.

In order to realize quantitative measurements in two-photon flow cytometry, multiple fluorescence-collecting channels at different wavelengths have been used. The ratio of fluorescence signals in these channels was used as a parameter to reflect the biological properties of the cells.

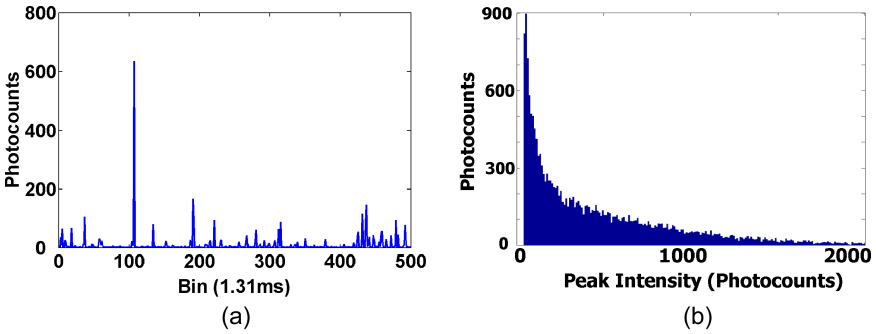

Figure 6: (a) Typical single channel raw data from two-photon flow cytometry; each peak corresponds to a labeled cell passing through the laser focus; (b) Histogram of the intensity distribution of peaks in a single channel.

However, normal fluorescence dye staining may not provide correlated fluorescence emissions as needed in the two-photon flow cytometry and a well defined fluorescence ratio cannot be obtained. As an example, mouse peripheral mononuclear blood cells (PMBC) stained with two dyes: CFSE and DeepRed, were investigated. CFSE is a biocompatible dye used here as a "trigger", i.e., as an indicator to count cells passing through the excitation volume. DeepRed, serving as a "reporter" dye, is a cell-permeating probe that binds to the outer membrane of mitochondria. The ratio of reporter over trigger fluorescence signal would indicate the viability of a cell. However, a wide distribution in a two-channel dot plot of the trigger versus reporter fluorescence photocounts was observed, as shown in Figure 7(a). The wide distribution indicates the signals in the two fluorescence channels are not correlated and rendered it difficult to distinguish

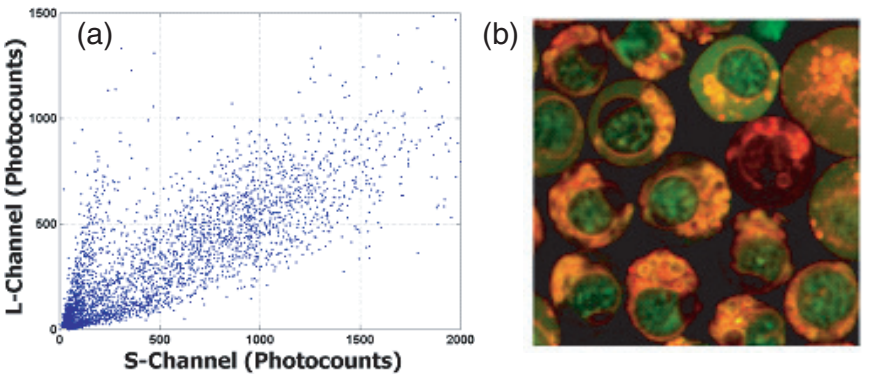

Figure 7: (a) Two-channel dot plot of mouse peripheral mononuclear blood cells (PMBC) stained with CFSE and DeepRed. The two-photon excited fluorescent signals from CFSE and DeepRed go to S-channel and L-channel, respectively. (b) Confocal microscopy image of mouse peripheral mononuclear blood cells (PMBC) stained with CFSE (green) and DeepRed (red).

viable from non-viable cells. The reason why correlated fluorescence signals were not obtained was attributed to the different spatial distributions of the two dyes within each cell. Because two-photon fluorescence has a small localized excitation volume, the fluorescence intensity reflects the local concentration of different fluorescence biomarkers within a cell. Confocal microscopy image (Figure 7(b)) shows that CFSE is distributed within the nuclei of the cells, while DeepRed stains only the outer cytoplasm surrounding the nucleus. This confirms the inhomogeneous localization of these two dyes in a cell. In order to make ratiometric measurements, it is essential to have the fluorescence intensity of the trigger and reporter biomarkers correlated in order to obtain a well defined parameter to sensitively reflect biological changes in cells.

Targeted dendrimer fluorescent conjugates were used as biomarkers in order to correlate the signals from the trigger and reporter dyes.[40] Two different dyes were conjugated to dendrimers having the same targeting agent, respectively. By competing for binding to the same receptors on a cell, the concentrations of the two conjugates in the cell become correlated. KB cells were treated with the dendrimer-FITC-folic acid conjugate (G5-FI-FA) and dendrimer-DeepRed-folic acid conjugate (G5-DR-FA) at different concentrations (Table 1). As the ratio of the concentrations of the dendrimer conjugates varies, the fluorescence signals from the KB cell samples measured in the two-photon flow cytometer are in well separated clusters in a two-parameter (S-channel vs. L-channel) dot plot (Figures 8(a), (c), (e), (g)). The angular distributions of the ratio of the fluorescence intensity in the S- and L-channels peak at different values (Figures 8(b), (d), (f), (h)). The average angular distribution of these samples (samples 1 to 8 in

Tab. 1. Concentration of dendrimer dye conjugates used to incubate KB cell samples and their mean channel fluorescence measured with a conventional single photon flow cytometer.

Sample No.	*G5-FI-FA (nM)*	*G5-DR-FA (nM)*	*G5-FI (nM)*	*G5-DR (nM)*	*Mean Channel Fluorescence*	
					FITU (a.u.)	*DeepRed (a.u.)*
1	200	0	0	0	95.8	5.3
2	180	20	0	0	77.8	352.2
3	150	50	0	0	60.8	837.8
4	120	80	0	0	44.7	1138.3
5	80	120	0	0	42.7	2518.3
6	50	150	0	0	20.4	2141.3
7	20	180	0	0	9.7	2372.3
8	0	200	0	0	3.5	2365.8
9	0	0	0	0	2.86	5.86
10	0	0	200	0	3.4	5.1
11	0	0	0	200	2.9	12.2

Table 1) increases as the concentration ratio of G5-FI-FA to G5-DR-FA decreases. For unstained KB cell sample (sample 9) or KB cell samples stained with non-targeted dendrimer-dye conjugates (samples 10 and 11), the number of cells detected is three orders of magnitude lower compared to KB cell samples stained with dendrimer-dye-folic acid conjugates, and their angular distribution is random. This demonstrated that dendrimer dye conjugates can be used as biomarkers for multi-color correlated fluorescence detection, owing to the specific targeting capability of the dendrimer conjugates.

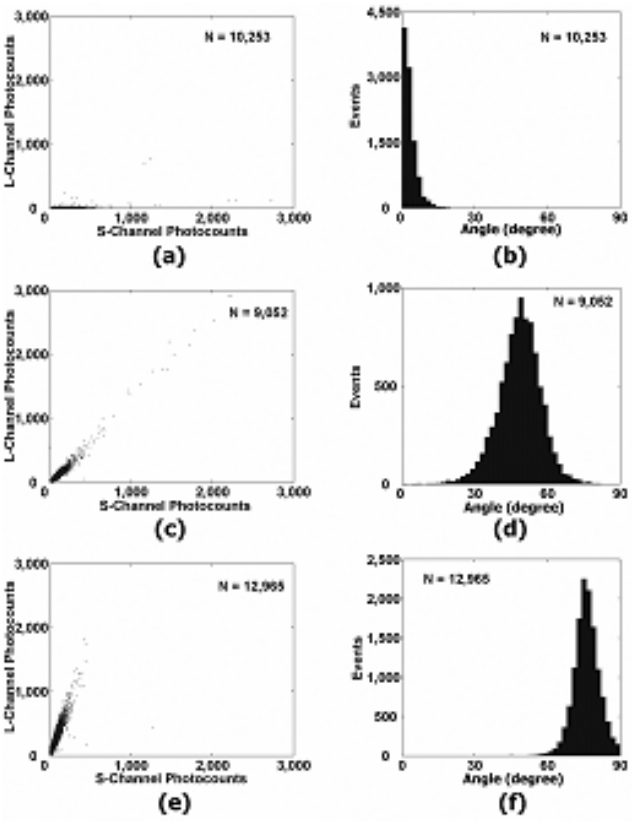

Figure 8: Two-channel dot plot and angular distribution of KB cell samples stained with G5-FI-FA and G5-DR-FA at different concentrations. (a) and (b) are the two-channel dot plot and angular distribution histogram from sample 1; (c) and (d) are from sample 2; (e) and (f) are from sample 3; (g) and (h) are from sample 8; (i) and (j) are from the mixture of sample 1 and sample 8 at volume ratio of 1:1; The average angle of KB cells stained with G5-FI-FA and G5-DR-FA at certain concentration ratio fits linear to the ideal average angle of free G5-FI-FA and G5-DR-FA solutions used to incubate the KB cells.[48] The concentration of dye conjugates used to incubate the KB cell samples are listed in Table 1. (Reprinted with permission from "Two-photon flow cytometry," *Proceedings of the SPIE*, Vol. **5700**, 78–79, 2005.)

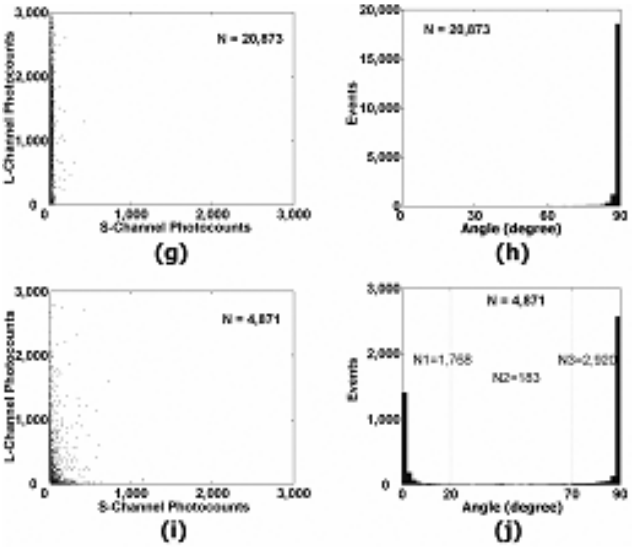

Figure 8: (*Continued*).

4.3 Nonlinear Optical Properties of Dendrimers and Their Conjugates

4.3.1 Dendrimer-based nonlinear electro-optical devices

Besides the linear optical response of dendrimers, nonlinear optical properties of dendrimers have also been investigated recently by several research groups. It was found that dendrimers containing multi-chromophores can be used to enhance nonlinear optical effects. Nonlinear optical chromophores having large quadratic hyperpolarizability are commonly incorporated into optically transparent polymers in order to develop organic electro-optical (E-O) devices with large high order E-O response. However, in a linear polymer host, the intermolecular interactions between densely doped chromophores tend to form aggregation, which limits the nonlinear

E-O effects.[42] In contrast to linear-chain polymers, dendrimers having three-dimensional architecture can effectively reduce the intermolecular interactions and prevent the aggregation formation, thus enhancing the non-linear E-O response. Yokoyama *et al*. demonstrated that using a rod-shaped chromophore as the branching unit enabled dendrons to be assembled into Langmuir-Blodgett monolayer films, which exhibited a large second-order susceptibility.[43,44] They also found that an asymmetric dendrimer with 15 nonlinear azobenzenes noncentrosymmetrically arranged along the molecule axis can be used to coherently enhance the second-order NLO effect.[44] Drobizhev *et al*. observed that dendrimers comprising 29 repeat units of 4,4'-bis(diphenylamino)stilbene chromophore have enhanced two-photon absorption cross section compared to its linear analog. The cross section has been measured for three consecutive dendrimer generations, and the result showed that the cross section increases faster than the total number of stilbene chromophores, suggesting that even larger cross sections can be obtained in higher generations of this type of dendrimer.[45]

4.3.2 Characterization of Dendrimer metal Nanoparticle Composite (DNC) enhanced Laser-Induced Optical Breakdown (LIOB) using Third Harmonic Generation (THG) measurements

In addition to enhancing nonlinear E-O response by taking advantage of the unique molecular structure of a dendrimer, dendrimers have also been used as an excellent template to form hybrid nanocomposites based on their 3D architecture and controllable size and shape. Dendrimer metal nanoparticle composites (DNC) display unique physical and chemical

properties as a consequence of the atomic/molecular level dispersion of the inorganic guest(s) with respect to the organic dendrimer host.[46–48]

Laser-induced optical breakdown (LIOB) in DNCs has been investigated recently in our group. LIOB has attracted much attention recently because it has been proven to be a unique technology that can be used in many fields including laser surgery, micromachining, three-dimensional optical data storage, etc.[49–51] In order to realize those applications, it is important to obtain an in-depth understanding of the breakdown mechanism and find an approach to achieve LIOB in a controllable way. Many attempts to control LIOB have been focused on selecting different laser parameters.[52–55] The breakdown threshold, on the other hand, is also determined by the nature of the material itself. It has been demonstrated that one can notably alter the LIOB threshold of a material by incorporating metal nanoparticles, which significantly enhance the electric field localized at their immediate surroundings.[56] The significant threshold reduction achieved with DNC particles opens up the possibility for a range of applications that take advantage of low threshold breakdown.[57–59]

A model system, a gold/dendrimer nanocomposite (DNC), was chosen for femtosecond laser-induced breakdown experiments to demonstrate the possibility to reduce the LIOB threshold by encapsulated metal nano-domains.[56] A generation-5 poly(amidoamine) (PAMAM) with ethylenediamine (EDA) core was used as a template to form a hybrid nanocomposite. A 4.0×10^{-4} M methanol solution of $\{Au(0)_{14}$-PAMAM_E5.$NH_2\}$, which denotes a DNC composed of 14 zero-valent gold atoms per an ethylenediamine core generation-5 PAMAM dendrimer, was held in a quartz cuvette. Figure 9 shows the absorption spectra of the pure PAMAM

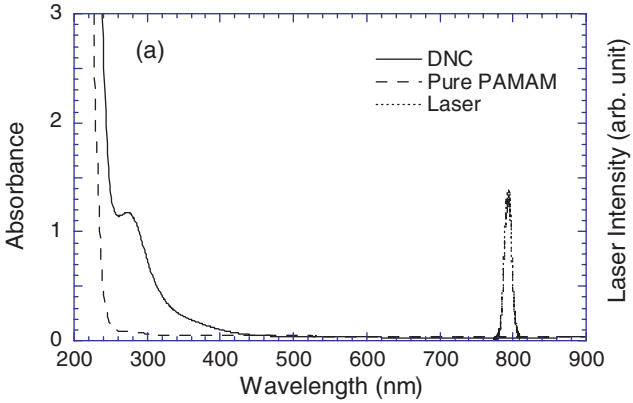

Figure 9: Absorption spectra of pure PAMAM and DNC in methanol together with laser spectrum.[56] (Reprinted with permission from J. Y. Ye, L. Balogh and T. B. Norris, "Enhancement of laser-induced optical breakdown using metal/dendrimer nanocomposites," *Applied Physics Letters*, **80**(10), 1713–1715, 2002. Copyright (2002) American Institute of Physics.)

dendrimer and DNC methanol solutions. In contrast to the pure PAMAM dendrimer, the DNC has an absorption maximum around 272 nm, which results from the plasmon resonance of the incorporated gold nanodomains. Third-harmonic generation (THG) measurements have been employed as a sensitive way for monitoring the LIOB *in situ* and in real time. The laser used for the THG is from a regeneratively amplified Ti: Sapphire laser with pulse duration of 100 fs and wavelength of 793 nm. The laser spectrum is shown in Figure 9. It can be seen that the DNC absorption peak is close to the one third of the laser wavelength, while there is no absorption in the wavelength regime of fundamental laser light.

The laser beam was focused using an f:1 off-axis (60°) parabola at the front interface between the quartz cuvette and the DNC solution

rather than the rear interface in order to avoid the complications of spatial and temporal distortion of the laser pulses caused by some nonlinear optical effects. The THG from the DNC and quartz interface was directed to a Brewster quartz prism to spatially separate it from the fundamental transmitted laser light, then further filtered with two UV interference band pass filters with center wavelength of 265 nm before detected with a photon counting system. The experimental setup is shown in Figure 10.

The intensity of the THG from the interface of DNC methanol solution and quartz surface follows a cubic power dependence before LIOB occurs. However, when the laser power was above a certain level, a sudden drop of the THG signal was observed. This change in THG signal results from the LIOB in the DNC solution. Because the intensity of THG is related to the material properties, i.e., the difference of the refractive index or third-order nonlinear susceptibility of the materials on both sides of a laser focus spot at an interface, the measurement of THG signal provided a sensitive way to monitor the LIOB *in situ* and in real time.[60,61]

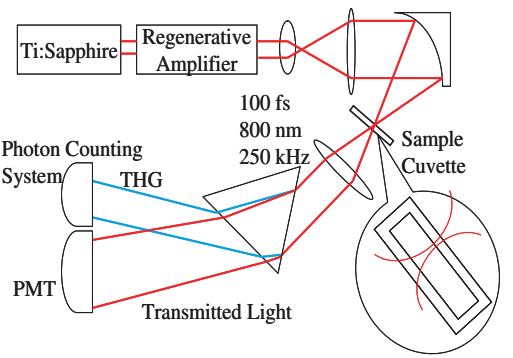

Figure 10: Experimental setup of using THG measurements to characterize the LIOB in DNC solution.

In addition, because THG is generated only from an interface, one could focus the study on the DNCs adsorbed on or in the vicinity of a surface. Since gold/PAMAM nanocomposites bind to a quartz surface effectively,[62] this system may also serve as a model for DNCs bound to a cell.

Figure 11(a) shows several examples of the breakdown events under irradiation power of 9 mW in the DNC solution. The rise of the THG signal occurs when a shutter in the laser beam is opened, while the sudden drop of THG indicates the breakdown. In contrast, the THG signal from the interface of the quartz and the pure template PAMAM dendrimer remains unchanged even under much higher irradiation power (Figure 11(b)). The breakdown threshold of the DNC was determined to be as low as 0.9 mW (9.5 mJ/cm^2), which is 113-fold lower than that of the pure dendrimer sample. The breakdown threshold of the DNC is also two orders of magnitude lower than the typical breakdown threshold of a tissue.[55] The LIOB in the DNCs was due to the high peak power of ultrashort laser pulses, which causes nonlinear multiphoton ionization in the sample. This is why the LIOB occurred even though there is no linear absorption at the laser wavelength (Figure 9).

The remarkable reduction of breakdown threshold of DNC compared with that of pure PAMAM dendrimer was attributed to the enhancement of the local electric field by the gold nanodomains in the DNCs due to strong optical extinction by resonantly driven electron plasma oscillations.[63–65] Local field enhancement by the encapsulated metal nanoparticles has also been observed by measuring the third-order nonlinear optical response in DNCs and DNCs incorporated thin films.[66]

A long waiting time for the breakdown in DNCs was observed, although it becomes shorter with increasing the laser power, as shown in

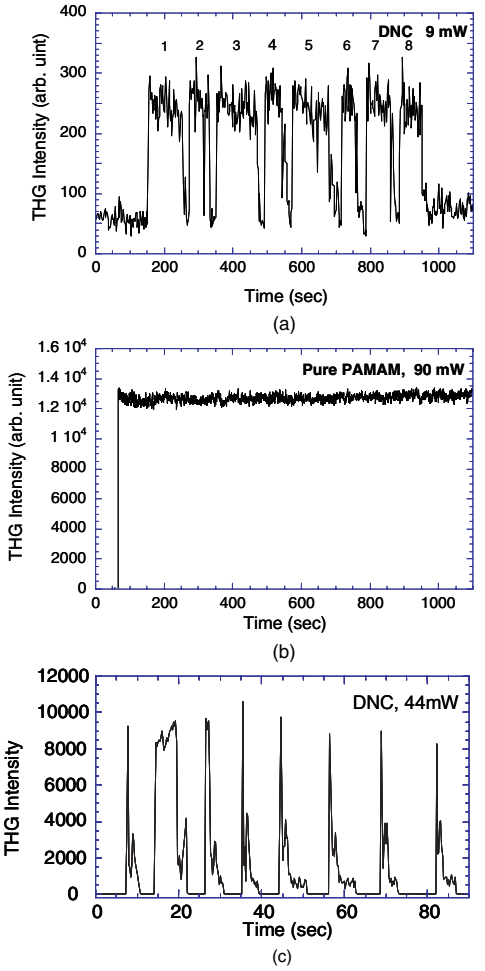

Figure 11: (a) The change of THG signals during LIOB in DNCs for eight events under laser irradiation of 9 mW.[56] (b) The THG signal from the pure PAMAM-quartz under irradiation of 90 mW. There is no LIOB observed. (c) Eight LIOB events in DNCs under laser irradiation of 44 mW. The waiting time is shorter comparing with that under irradiation power of 9 mW as shown in (a). (Reprinted with permission from J. Y. Ye, L. Balogh and T. B. Norris, "Enhancement of laser-induced optical breakdown using metal/dendrimer nanocomposites," *Applied Physics Letters*, **80**(10), 1713–1715, 2002. Copyright (2002) American Institute of Physics.)

Figure 11(c). Such long waiting time (on the order of seconds) suggests that large intermolecular interactions occurred before the breakdown happened. It has been proposed that a laser-driven aggregation of the DNCs occurred, which causes cluster formation and shifts the plasmon resonance to the laser frequency.[46,56] In addition, the waiting time was found to fluctuate in a wide range even under the same irradiation conditions. This statistical behavior of the waiting time and their average values are shown as functions of laser power and fluence in Figures 12(a) and (b), respectively. The fluctuation of the waiting time reflects the statistical behavior of the aggregation process.

A number of potential application taking the advantage of the unique features of the DNCs have been suggested,[56] including optically triggering release of encapsulated therapeutics in DNCs while avoiding unwanted damage to surrounding tissues due to the local reduction of threshold by DNCs, photo therapeutics through the highly enhanced local field in DNCs, and high-density optical data storage.

4.3.3 Dendrimer metal Nanoparticle Composite (DNC) enhanced microbubble generation for ultrasound imaging

In addition to the third harmonic generation from DNC solutions, other nonlinear optical properties of DNCs have also been investigated by several groups. For example, a large optical limiting effect in external type silver nanocomposites has been obtained, while a saturation absorption behavior was observed in internal Ag nanocomposites.[67] The optical limiting was assumed to be due to the formation of microbubbles by the LIOB in the aqueous solution upon absorbing energy from the irradiating laser. It is

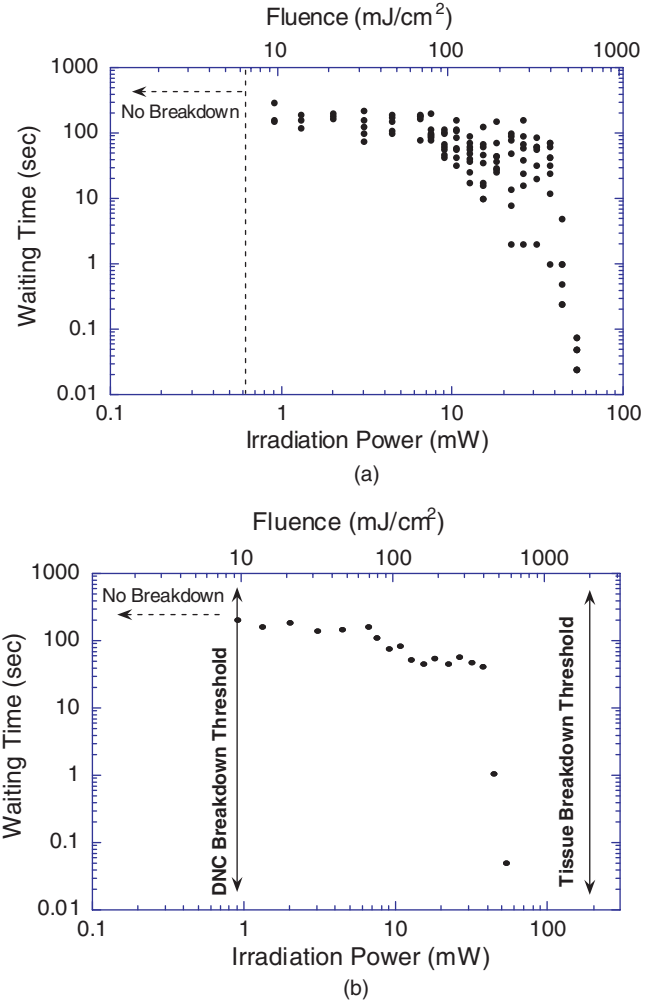

Figure 12: The laser power and fluence dependence of the waiting time for breakdown of DNC, (a) statistical behavior of the waiting time, and (b) average waiting time. The breakdown thresholds for DNCs and tissues are marked by solid arrows.[56] (Reprinted with permission from J. Y. Ye, L. Balogh and T. B. Norris, "Enhancement of laser-induced optical breakdown using metal/dendrimer nanocomposites," *Applied Physics Letters*, **80**(10), 1713–1715, 2002. Copyright (2002) American Institute of Physics.)

of great interest to study the dynamics of the microbubble generation in LIOB utilizing ultrasonic detection,[57] because a bubble is an excellent ultrasonic reflector and can be sensitively detected with high-frequency ultrasound.[59] A unique approach may be developed for targeted therapy and high resolution ultrasound imaging by taking advantage of the precise photodisruption and molecular therapeutics caused by ultrafast laser-induced DNC-enhanced optical breakdown in combination with high-frequency ultrasonic detections.

LIOB with focused femtosecond laser pulses has been widely utilized in medical and biological systems to produce highly refined cell and tissue effects while minimizing thermal and mechanical damage to surrounding materials.[68–72] Unlike thermal damage, optical breakdown with ultrafast laser occurs in transparent materials, i.e., materials that do not absorb low intensity light at a particular wavelength. However, when the laser intensity exceeds a critical value at the same wavelength, nonlinear absorption becomes strong enough in linearly transparent media, which causes optical breakdown in the material, i.e., photodisruption. During photodisruption a microbubble forms, resulting in a high velocity shockwave that propagates spherically outward from the effective point source. After traveling a few wavelengths from the source, this wave can be considered a broadband pressure wave, i.e., an acoustic emission, which can be detected with an ultrasound transducer. On the other hand, as discussed previously dendrimers have proven to exhibit specific molecular targeting.[73,74] Recent studies using metal-dendrimer nanocomposites have demonstrated the potential for biochemically targeted photodisruption to locally manipulate LIOB threshold fluences in specific tissues and

cells.[56,57] The microbubbles created in the LIOB process are controllable by carefully selecting a set of different laser parameters relevant to a particular medium.[58] Subsequent laser pulses of variable number, intensity, and repetition period may be varied to modify bubble size and lifetime by controlling a dynamic environment, due to gas and thermal diffusion and the generation of additional microbubbles, which helps to stabilize the LIOB bubble, regardless of its size. Consequently, the controllable LIOB increases the utility of microbubbles for site-activated ultrasound contrast agents of selectable size, lifetime, destructive capability, and dissolution dynamics.[59]

Figure 13 shows an integrated setup of a real-time acoustic detection of microbubbles generated from LIOB in DNC solutions.[57] Femtosecond laser pulses from a 250-kHz regeneratively amplified Ti: Sapphire laser ($\lambda = 793$ nm), were focused at the bottom of a small cylindrical tank with DNC solution. The focus of a single-element ultrasonic transducer (center frequency 50 MHz, 4.1 mm focal depth, 3 mm diameter) was aligned axially and laterally with the laser focal point. Ultrasonic pulses were launched to probe the microbubble formation and its dynamic evolution in the vicinity of the laser focus. When a bubble forms, the ultrasonic pulse echo signal has a component reflected from the top surface of the bubble in addition to a pulse from the tank bottom. By viewing acoustic shifts in consecutive pulse-echoes (i.e., wave-field plots), bubble formation and subsequent behavior can be visualized.

Aqueous solutions of a carboxyl terminated, ethylenediamine core, generation five poly(amidoamine) (PAMAM) dendrimer were

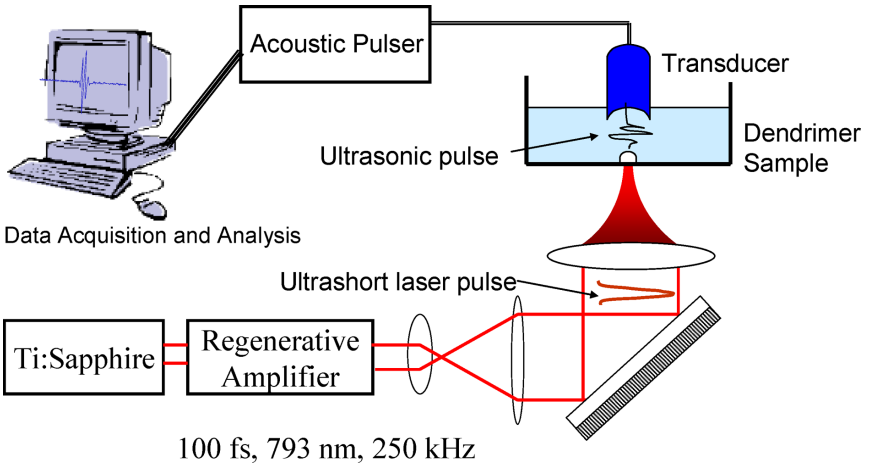

Figure 13: Schematic of integrated optical and acoustic experimental set-up for the detection of microbubble generation in DNC samples.

measured in comparison to a silver dendrimer nanocomposite, {Ag(0)97-PAMAM_E5.5COOH}, ({Ag(0)}E: for short).[75] Wave-field plots of consecutive pulse-echo recordings were recorded, which illustrated the LIOB bubble formation and behavior directly.

Figure 14(a) is a wave-field plot illustrating a bubble's formation in the pure dendrimer solution, while Figure 14(b) shows the result for {Ag(0)}E. A range of laser powers was tested for each aqueous solution. The optical threshold at which significant acoustic power is reflected from a microbubble was found to be 50 mW (260 mJ/cm^2 per pulse) for the pure dendrimer aqueous solution. In contrast, the LIOB threshold determined acoustically for the {Ag(0)}E solution is 4 mW (21 mJ/cm^2 per pulse), over an order of magnitude lower than the threshold of the pure dendrimer solution.

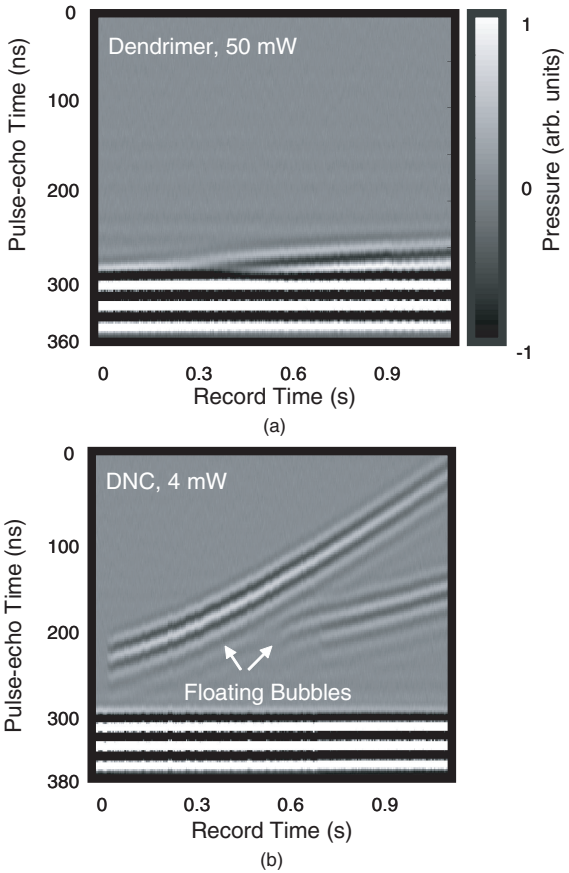

Figure 14: (a) Wave-field plot of dendrimer solution irradiated with 50 mW laser pulses (260 mJ/cm^2 per pulse). When the laser is unblocked (time origin approximates shutter opening), a bubble forms, adheres to the tank bottom, and grows. (b) Wave-field plot of $\{Ag(0)\}_E$ solution irradiated with 4 mW laser pulses (21 mJ/cm^2 per pulse). When the laser is unblocked, a bubble forms and floats upward toward the transducer. Around 0.6 seconds, a second bubble forms and also travels upward.[57] (Reprinted with permission from S. M. Milas *et al*., "Acoustic detection of microbubble formation induced by enhanced optical breakdown of silver/dendrimer nanocomposites," *Applied Physics Letters*, **82**(6), 994–996, 2003. Copyright (2003) American Institute of Physics.)

This finding indicates that it is possible to manipulate LIOB threshold values based on the solution's molecular attributes. This opens up a wide range of potential applications. For instance, in biomedical systems, DNC particles can be biochemically targeted to sites where localized photodisruption can be induced, either releasing encapsulated therapeutics or ablating aberrant cells (such as cancer cells or tissue). In addition, bubbles resulting from photodisruption can be manipulated with either acoustic or optical sources for enhanced therapeutic effects,[76] and probed with high frequency ultrasound to validate therapeutic efficacy.

4.4 Conclusions

Owing to their unique molecular architectures, dendrimers possess many novel physical properties that are not available in linear organic polymers. Different functionalities have been associated with a variety of dendrimer conjugates, such as targeting capability for drug delivery, specific biomarkers for biomedical imaging and sensing, efficient energy transfer for light harvesting and tunable light emitting diodes, etc. In addition, using dendrimers as a template, hybrid organic and inorganic nanoparticle composites can be synthesized, which creates a new dimension to modify material properties and opens up a range of promising applications in optics and biophotonics.

4.5 References

1. T. P. Thomas, I. J. Majoros, A. Kotlyar, J. F. Kukowska-Latallo, A. Bielinska, A. Myc, and J. R. Baker, Jr., Targetting and inhibition of cell growth by an engineered dendritic nanodevice, *J. Med. Chem.*, **48**, 3729–3735, (2005).

2. A. Quintana, E. Raczka, L. Piehler, I. Lee, A. Myc, I. Majoros, A. Patri, T. Thomas, J. Mule, and J. Baker Jr., Design and function of a dendrimer-based therapeutic nanodevice targeted to tumor cells through the folate receptor, *Pharmaceutical Research*, **19** (1310–1316), 2002.
3. T. Thomas, I. Majoros, J. Baker, Jr., J. Y. Ye, M. T. Myaing, and T. Norris, Engineered nanoparticles, *OE Magazine-SPIE*, **3**, 30, 2003.
4. V. Rozhkov, D. Wilson, and S. Vinogradov, Phosphorescent Pd porphyrin-dendrimers: Tuning core accessibility by varying the hydrophobicity of the dendritic matrix, *Macromolecules*, **35**, 1991–1993, 2002.
5. I. Dunphy, S. A. Vinogradov, and D. F. Wilson, Oxyphor R2 and G2: Phosphors for measuring oxygen by oxygen-dependent quenching of phosphorescence, *Anal. Biochem*., **310**, 191–198, 2002.
6. M. W. Grinstaff, Biodendrimers: New polymeric biomaterials for tissue engineering. *Chemistry*, **8**, 2838–2846, 2002.
7. J. Y. Ye, M. T. Myaing, T. B. Norris, T. Thomas, and J. Baker Jr., Biosensing based on two-photon fluorescence measurements through optical fibers, *Opt. Lett*., **27**, 1412, 2002.
8. T. Thomas, M. T. Myaing, J. Y. Ye, K. Candido, A. Kotlyar, J. Beals, P. Cao, B. Keszler, A. Patri, T. B. Norris, and J. Baker, Jr., Detection and analysis of tumor fluorescence using a two-photon optical fiber probe, *Biophysics Journal*, **86**, 3959, 2004.
9. B. L. Ibey, H. T. Beier, R. M. Rounds, G. L. Coté, V. K. Yadavalli, and M. V. Pishko, Competitive binding assay for glucose based on

glycodendrimer-fluorophore conjugates, *Analytical Chemistry*, **77**, 7039–7046, 2005.

10. T. D. Anthopoulos, M. J. Frampton, E. B. Namdas, P. L. Burn, and I. D. W. Samuel, Solution-processable red phosphorescent dendrimers for light-emitting device applications, *Adv. Mater*., **16**, 557, 2004.
11. E. B. Namdas, A. Ruseckas, I. D. W. Samuel, S.-C. Lo, and P. L. Burn, Photophysics of fac-tris(2-Phenylpyridine) iridium(III) cored electroluminescent dendrimers in solution and films, *J. Phys. Chem*., *B*, **108**, 1570, 2004.
12. A. Adronov, S. L. Gilat, J. M. J. Fréchet, K. Ohta, F. V. R. Neuwahl, and G. R. J. Fleming, Light harvesting and energy transfer in laser-dye-labeled poly(aryl ether) dendrimers, *Am. Chem. Soc*., **122**, 1175, 2000.
13. T. S. Ahn, A. L. Thompson, P. Bharathi, A. Mueller, and C. J. Bardeen: Light-harvesting in carbonyl-terminated phenylacetylene dendrimers: The role of delocalized excited states and the scaling of light-harvesting efficiency with dendrimer size, *J. Phys. Chem. B*., **110**, 19810–19819, 2006.
14. A. R. H. J. Schenning, E. Peeters, and E. W. Meijer, Energy transfer in supramolecular assemblies of oligo(p-phenylene vinylene)s terminated poly(propylene imine) dendrimers, *J. Am. Chem. Soc*., **122**, 4489–4495, 2000.
15. J. S. Melinger, Y. Pan, V. D. Kleiman, Z. Peng, B. L. Davis, D. McMorrow, and M. Lu, Optical and photophysical properties of light-harvesting phenylacetylene monodendrons based on unsymmetrical branching, *J. Am. Chem. Soc*., **124**, 12002–12012, 2002.

16. G. McDermott, S. M. Prince, A. A. Freer, A. M. Hawthornthwaite-Lawless, M. Z. Papiz, R. J. Cogdell, and N. W. Isaacs, Crystal structure of an integral membrane light-harvesting complex from photosynthetic bacteria, *Nature*, **374**, 517–521, 1995.
17. A. N. Glazer, Light harvesting by phycobilisomes, *Annu. Rev. Biophys. Biophys. Chem.*, **14**, 47–77, 1985.
18. S. L. Gilat, A. Adronov, and J. M. Fréchet, Light harvesting and energy transfer in novel convergently constructed dendrimers, *J. Angew. Chem., Int. Ed.*, **38**, 1422, 1999.
19. R. Kopelman, M. Shortreed, Z.-Y. Shi, W. Tang, Z. Xu, J. Moore, A. Bar-Haim, and J. Klafter, Spectroscopic evidence for excitonic localization in fractal antenna supermolecules, *Phys. Rev. Lett.*, **78**, 1239, 1997.
20. A. Andronov and J. M. J. Frechet, Light-harvesting dendrimers, *Chem. Commun.*, 1701–1710, 2000.
21. V. Balzani, P. Ceroni, M. Maestri, and V. Vicinelli, Light-harvesting dendrimers, *Curr. Opin. Chem. Biol.*, **7**, 657–665, 2003.
22. D. Gust, T. A. Moore, and A. L. Moore, Mimicking photosynthetic solar energy transduction, *Acc. Chem. Res.*, **34**, 40–48, 2001.
23. C. Devadoss, P. Bharathi, and J. S. Moore, Energy transfer in dendritic macromolecules: Molecular size effects and the role of an energy gradient, *J. Am. Chem. Soc.*, **118**, 9635–9644, 1996.
24. J. M. Serin, D. W. Brousmiche, and J. M. J. Frechet, Cascade energy transfer in a conformationally mobile multichromophoric dendrimer, *Chem. Commun.*, 2605–2607, 2002.

25. D. L. Jiang and T. Aida, Morphology-dependent singlet energy transduction in aryl ether dendrimer porphyrins: Cooperation of dendron subunits, *J. Am. Chem. Soc*., **120**, 10895, 1998.
26. S. Tretiak, V. Chernyak, and S. Mukamel, Exction-scaling and optical excitations of self-similar phenylacetylene dendrimers, *J. Chem. Phys*., **110**, 8161, 1999.
27. T. Sato, D.-L. Jiang, and T. Aida, A blue-luminescent dendritic rod: Poly(phenyleneethynylene) within a light-harvesting dendritic envelope, *J. Am. Chem. Soc*., **121,** 10658, 1999.
28. O. Varnavski, I. D. W. Samuel, L. O. Palsson, R. Beavington, P. L. Burn, and T. Goodson III, Investigations of excitation energy transfer and intramolecular interactions in a nitrogen corded distrylbenzene dendrimer system, *J. Chem. Phys*., **116**, 8893, 2002.
29. J. P. J. Markham, S.-C. Lo, S. W. Magennis, P. L. Burn, and I. D. W. Samuel, *Appl. Phys. Lett*., **80**, 2645, 2002.
30. S.-C. Lo, Nigel, A. H. Male, J. P. J. Markham, S. W. Magennis, P. L. Burn, O. V. Salata, and I. D. W. Samuel, Green phosphorescent dendrimer for light-emitting diodes, *Adv. Mater*., **14**, 975, 2002.
31. T. D. Anthopoulos, J. P. J. Markham, E. B. Namdas, I. D. W. Samuel, S.-C. Lo, and P. L. Burn, Highly efficient single-layer dendrimer light-emitting diodes with balanced charge transport, *Appl. Phys. Lett*., **82**, 4824, 2003.
32. S.-C. Lo, E. B. Namdas, P. L. Burn, and I. D. W. Samuel, Synthesis and properties of highly efficient electroluminescent green phosphorescent iridium cored dendrimers, *Macromolecules*, **36**, 9721, 2003.

33. E. B. Namdas, T. D. Anthopoulos, I. D. W. Samuel, M. J. Frampton, S.-C. Lo, and P. L. Burn, Simple color tuning of phosphorescent dendrimer light emitting diodes, *Appl. Phys. Lett*., **86**, 161104, 2005.

34. C. A. Nicolette and G. A. Miller, The identification of clinically relevant markers and therapeutic targets. *Drug Discovery Today*, **8**, 31–38, 2003.

35. R. Weissleder and V. Ntziachristos, Shedding light onto live molecular targets. *Nature Medicine*, **9**, 123–128, 2003.

36. J. D. Eichman, A. U. Bielinska, J. F. Kukowska-Latallo, and J. R. Baker Jr., The use of PAMAM dendrimers for the efficient transfer of genetic material into cells, *Pharmaceutical Sci. and Tech. Today*, **3**, 232, 2000.

37. X. Li, B. Chance, and A. G. Yodh, Fluorescent heterogeneities in turbid media: Limits for detection, characterization, and comparison with absorption. *Appl. Optics*., **37**, 6833–6844, 1998.

38. X. Gan and M. Gu, Spatial distribution of single-photon and two-photon fluorescence light in scattering media: Monte Carlo simulation. *Appl. Optics*, **39**, 1575–1579, 2000.

39. A. Sefkow, M. Bree, and M.-A. Mycek, Method for measuring cellular optical absorption and scattering evaluated using dilute cell suspension phantoms. *Appl. Spectroscopy*, **55**, 1495–1501, 2001.

40. C. F. Zhong, J. Y. Ye, A. Myc, T. P. Thomas, A. U. Bielinska, J. R. Baker Jr., and T. B. Norris, Two-photon flow cytometry. *Proceedings of SPIE*, **5700**, 78–89, 2005.

41. M. G. Ormerod, *Flow Cytometry*, Springer-Verlag, New York, 1999.

42. D. A. Tomalia, Starburst/cascade dendrimers: Fundamental building blocks for a new nanoscopic chemistry set, *Adv. Mater*., **6**, 529, 1994.
43. S. Yokoyama, T. Nakahama, A. Otomo, and S. Mashiko, Preparation and assembled structure of dipolar dendrons based electron donor/acceptor azobenzene branching, *Chem. Lett*., **1137**, 1997.
44. S. Yokoyama, T. Nakahama, A. Otomo, and S. Mashiko, Intermolecular coupling enhancement of the molecular hyperpolarizability in multichromophoric dipolar dendrons, *J. Am. Chem. Soc*., **122**, 3174–3181, 2000.
45. M. Drobizhev, A. Karotki, A. Rebane, and C. W. Spangler, Dendrimer molecules with record large two-photon absorption cross section, *Opt. Lett*., **26**, 1081–1083, 2001.
46. L. Balogh, D. R. Swanson, R. Spindler, and D. A. Tomalia, Formation and characterzation of dendrimer-based water soluble inorganic nanocomposites, *Proceedings of ACS PMSE*, **77**, 118, 1997.
47. L. Balogh, R. Valluzzi, G. L. Hagnauer, K. S. Laverdure, S. P. Gido, and D. A. Tomalia, Formation of silver and gold dendrimer nanocomposites, *J. Nanoparticle Res*., **1**, 353, 1999.
48. L. Balogh, D. A. Tomalia, and G. L. Hagnauer, Revolution of nanoscale proportions, *Chem. Innovation*, **30**, 19, 2000.
49. A. Vogel, Nonlinear absorpation: Intraocular microsurgery and laser lithotripsy, *Phys. Med. Biol,* **42**, 895, 1997.
50. E. N. Glezer, M. Milosavljevic, L. Huang, R. J. Finlay, T.-H. Her, J. P. Callan, and E. Mazur, Three-dimensional optical storage inside transparent materials, *Opt. Lett*., **21**, 2023, 1996.

51. X. Liu, D. Du, and G. Mourou, Laser ablation and micromachining with ultrashort laser pulses, *IEEE J. Quantum Electron*, QE-**33**, 1706, 1997.

52. B. C. Stuart, M. D. Feit, S. Herman, A. M. Rubenchik, B. W. Shore, and M. D. Perry, Nanosecond-to-femtosecond laser-induced breakdown in dielectrics, *Phys. Rev. B*., **53**, 1749, 1996.

53. M. Lenzner, J. Kruger, S. Sartania, Z. Cheng, C. Spielmann, G. Mourou, W. Kautek, and F. Krausz, Femtosecond optical breakdown in dielectrics, *Phys. Rev. Lett*., **80**, 4076, 1998.

54. B. C. Stuart, M. D. Feit, A. M. Rubenchik, B. W. Shore, and M. D. Perry, Laser-induced damage in dielectrics with nanosecond to subpicosecond pulses, *Phys. Rev. Lett*., **74**, 2248, 1995.

55. F. H. Loesel, M. H. Niemz, J. F. Bille, and T. Juhasz, Laser-induced optical breakdown on hard and soft tissues and its dependence on the pulse duration: Experiment and model, *IEEE J. Quantum Electron*., QE-**32**, 1717, 1996.

56. J. Y. Ye, L. Balogh, and T. B. Norris, Enhancement of laser-induced breakdown using metal/dendrimer nanocomposites, *Appl. Phys. Lett*., **80**, 1713, 2002.

57. S. M. Milas, J. Y. Ye, T. B. Norris, L. P. Balogh, J. R. Baker, Jr., K. W. Hollman, S. Emelianov, and M. O'Donnell, Acoustic characterization of enhanced laser-induced optical breakdown using silver/dendrimer nanocomposites, *Appl. Phys. Lett,* **82**, 994, 2003.

58. C. Tse, M. Zohdy, J. Y. Ye, T. B. Norris, L. Balogh, K. Hollman, and M. O'Donnell, Acoustic detection of controlled LIOB bubble

creation in tissue-making gelatin phantoms, *Proceedings of the 2004 IEEE Ultrasonics Symposium*, 350–353, 2004.

59. C. Tse, M. J. Zohdy, J. Y. Ye, T. B. Norris, L. P. Balogh, K. W. Hollman, and M. O'Donnell, Acoustic detection of controlled laser-induced microbubble creation in gelatin, *IEEE Transactions on Ultrasonics, Ferroelectrics, and Frequency Control*, **52**, 1962–1969, 2005.
60. T. Y. F. Tsang, Optical third-harmonic generation at interfaces, *Phys. Rev*. *A*., **52**, 4116, 1995.
61. Y. Barad, H. Eisenberg, M. Horowitz, and Y. Silberberg, Nonlinear scanning laser microscopy by third harmonic generation, *Appl. Phys. Lett*., **70**, 922, 1996.
62. J. A. He, R. Valluzzi, K. Yang, T. Dolukhanyan, C. Sung, J. Kumar, S. K. Tripathy, L. Samuelson, L. Balogh, and D. A. Tomalia, Electrostatic multilayer deposition of a gold-dendrimer nanocomposite, *Chem. Mater*., **11**, 3268, 1999.
63. U. Kreibig and M. Vollmer, *Optical Properties of Metal Clusters*, Springer, Berlin, 1995.
64. B. Lamprecht, J. R. Krenn, A. Leitner, and F. R. Aussenegg, Resonant and off-resonant light-driven plasmons in metal nanoparticles studied by femtosecond-resolution third-harmonic generation, *Phys. Rev. Lett*., **83**, 4421, 1999.
65. M. A. El-Sayed, Some interesting properties of metals confined in time and nanometer space of different shapes, *Accounts of Chemical Research*, **34**, 257, 2001.

66. Y. Wang, X. Xie, and T. Goodson III, Enhanced third-order nonlinear optical properties in dendrimer-metal nanocomposites, *Nano Lett*., **5**, 2379–2384, 2005.

67. R. G. Ispasoiu, L. Balogh, O. P. Varnavski, D. A. Tomalia, and T. Goodson III, Large optical limiting from novel metal-dendrimer nanocomposite materials, *Journal of Am. Chem. Soc*., **122**, 11005, 2000.

68. T. Juhasz, F. H. Loesel, R. M. Kurtz, C. Horvath, J. F. Bille, and G. Mourou, Corneal refractive surgery with femtosecond lasers, *IEEE J. Quantum Electron*, **5**, 902–910, 1999.

69. K. König, I. Riemann, and W. Fritzsche, Nanodissection of human chromosomes with near-infrared femtosecond laser pulses, *Optics Letters*, **26**(11), 819–821, 2001.

70. F. H. Loesel, J. P. Fischer, M. H. Gotz, C. Horvath, T. Juhasz, F. Noack, N. Suhm, and J. F. Bille, Non-thermal ablation of neural tissue with femtosecond laser pulses, *Applied Physics B*., **66,** 121–128, 1998.

71. J. Serbin, T. Bauer, C. Fallnich, A. Kasenbacher, and W.H. Arnold, Femtosecond lasers as novel tool in dental surgery, *Applied Surface Science*, **197**, 737–740, 2002.

72. N. Shen, C. B. Schaffer, D. Datta, and E. Mazur, Photodisruption in biological tissues and single cells using femtosecond laser pulses, *Proc. Conference on Lasers and Electro-Optics*, 403–404, 2001.

73. A. K. Patri, T. Thomas, J. R. Baker Jr., and N. H. Bander, Antibody-dendrimer conjugates for targeted prostate cancer therapy, *Polymeric Materials: Science and Engineering*, **86**, 130, 2002.

74. E. C. Wiener, S. Konda, A. Shadron, M. Brechbiel, and O. Gansow, Targeting dendrimer-chelates to tumors and tumor cells expressing the high-affinity folate receptor, *Invest. Radiol.*, **32**(12), 748–754, 1997.

75. L. Balogh, D. R. Swanson, D. A. Tomalia, G. L. Hagnauer, and A. T. McManus, Dendrimer-silver complexes and nanocomposites as antimicrobial agents, *Nano Letters*, **1**(1) 18–21, 2001.

76. G. J. R. Spooner, A. R. Williams, D. L. Miller, and G. Marre, Optimization of parameters for photodisruptively nucleated ultrasonic cavitation in water and tissue models, *Proc. SPIE*, **3914**, 207, 2000.

This page intentionally left blank

Chapter 5

Dendrimer Conjugates for Cancer Treatment

István J. Majoros, Andrew Becker, Thommey Thomas, Rameshwer Shukla & Xiangyang Shi

---

Outline

5.0 Introduction

The field of chemotherapy is a special interface between chemistry and medicine, where improvement in treatment requires new innovation in chemistry. Current chemotherapy, now a term used almost exclusively to describe the treatment of cancer, involves the use of substances that target and destroy fast-growing cells. Cancer cells are killed by the treatment, but healthy cells of the body are destroyed along with them. This is a limiting factor for the efficacy of the treatment, as dosage must be cautious in order to avoid the severest side effects.

One long-standing idea for a way to improve the efficacy of chemotherapy in cancer treatment is to deliver the chemotherapeutic directly to the cancer cells, protecting healthy cells. This concept is known

as targeted delivery. A very promising method of targeted delivery under investigation involves the use of dendrimer conjugates.

An individual dendrimer conjugate begins with one dendrimer, having an approximately spherical shape, with many functional groups at its surface. Other molecules are then attached to these functional groups, and each molecule attached gives the conjugate new functionality. Generally a chemotherapeutic drug molecule is attached, along with some molecule which will help to target the specific cancer being treated (more on this later). Additionally, other molecules may be attached to give helpful functionality, such as a fluorescent tracer to help trace the path of the drug through the body.

The end result is something quite new, a drug which expands the idea of just what a drug is. It does many things, not just one. It is capable of destroying cancer cells while leaving healthy cells alone. Beyond that, it can be traced to prove that it has accumulated in the tumor under treatment. All of this is made possible by innovations in chemistry.

Molecular engineering on a nano-scale level has slowly become the wave of the future toward the realization of novel plateaus in a variety of scientific frontiers. The incorporation of nanotechnology into the design of novel materials has spread to encompass a host of disciplines, interrelating a diverse range of fields never previously thought to have the ability to work with one another. The emergence of this technology has come at a time when scientific knowledge has grown vast enough to at least allow us a slight glimpse into the capabilities nano-scale molecular engineering possesses. The recent research and development in the past decade regarding molecular engineering on the nano-scale level, specifically

within the field of drug delivery, has become of great importance to the disciplines of biomedical engineering, medicine, chemical engineering, and the like. A prime example of the importance of molecular engineering can be seen upon direct examination of the uses of synthetically fabricated macromolecules for application within biological systems. Engineered molecules such as these are under prominent investigation for use in chemotherapeutic drug design and delivery systems.

The use of nano-scale molecular engineering in the field of drug delivery has a number of advantages over the chemotherapeutic technologies currently used today. These advantages stem primarily from carrier composition and delivery and release methods, which in combination, allow for controlled drug release, resulting in fewer side effects and less toxicity to the body in comparison to conventional drug therapies. Secondary advantages of the use of this technology are the result of an increase in drug efficacy with the use of lower concentrations. With increased drug efficacy, industrial/pharmaceutical companies will synthesize smaller drug batches, which in turn produce less bio-hazardous chemical waste, therefore making this technology more environmentally friendly than commercial conventional drug syntheses.

Drug delivery techniques have undergone a vast expansion in research and methodology related to carrier systems and release methods. Over the past few decades we have been fortunate enough to undergo a great revision in the ideologies and in the research approaches related to drug carrier systems and their ability to be delivered or incorporated into biological systems. By revision and refinement of current working knowledge related to nano-scale molecular engineering,

scientists, engineers and medical researchers alike have been able to devise devices utilizing our technological capabilities to the fullest. By utilization of nano-scale molecular engineering techniques to produce and alter macromolecules which closely imitate the size and shape of biomolecules commonly found within human and animal systems, we possess the ability to engineer delivery of chemotherapeutic (as well as other) drugs into biological systems without the levels of toxicity and rejection by the body that result from the use of current cancer drug therapies on the market today.

The intentions of this chapter are to educate the reader on current strategies and methods used in the pursuit of the synthesis of an ideal chemotherapeutic drug delivery system. Each subtopic (imaging, targeting, and drug delivery) provides the synthesis, production, and characterization of our own multifunctional drug delivery devices. The chapter as an entirety provides an objective view of the application of nano-scale molecular engineering toward the production of a multifunctional drug delivery device jointly possessing all of the functions (imaging, targeting, and drug delivery/release) mentioned within. It also serves to express the complexity associated with device synthesis, quality control during production, and characterization. The culmination of this research has resulted in the synthesis of a well-defined device capable of fulfilling multiple functions simultaneously.

Nanotechnology in drug delivery represents one of the most rapidly advancing areas of interdisciplinary science in which the chemist, chemical engineer, biologist, and physician contribute to human health care. Because of the complexity of the biochemical events and homeostatic

regulation processes occurring within the cell, a variety of cellular mechanisms often prevent traditional drug therapies from working effectively. Many of these preventative mechanisms inhibit the activation or distribution of drug molecules to cancerous sites within the body. Nano-scale drug carriers, on the other hand, closely mimic the size and shape of biomolecules already present in the body and have the ability to suppress many of the preventative mechanisms activated during use of conventional cancer drug treatments.

There are basically three methods known for delivery of therapeutics:

1) The first is physical inclusion and delivery. Physical inclusion of bioactive agents, based on hydrophobic-hydrophilic interaction or coordination-chelation, in general does not alter the physicochemical properties of a drug. The vehicle for delivery in this case can be the use of a micro/nano emulsion or the use of appropriately chosen macromolecules. Simplicity is the advantage of this method. The disadvantages are a diffusion-controlled drug release and the formulation of the therapeutic delivery system itself.
2) The second method is one in which the vehicle (in our case, a macromolecule with primary amino groups on its surface) and the therapeutics (in our case, methotrexate and taxol) are covalently bonded. The result is a dendrimer-drug conjugate, which can be delivered into the cell, where the drug will be cleaved by enzyme catalyzed hydrolysis. This type of hydrolysis may take place if there is no significant steric hindrance and

if the appropriate enzyme is present. Simplicity is the advantage of this method also. The disadvantage is that the drug release is hydrolysis-controlled.

3) In the third method the vehicle (a dendritic macromolecule with primary amino groups on the outer part of the compound) and the drug are coupled through what is called a photocleavable linker. Simplicity and controlled drug release are the advantages of this method. The disadvantage is the formulation of the therapeutic delivery system itself.

Controlled drug delivery systems offer numerous advantages compared to conventional treatment forms, including improved efficacy, reduced toxicity (side effects), and improved patient compliance and convenience.

5.1 Dendrimer Conjugates for Cancer Treatment

Dendrimers are composed of polymer materials ranging in molecular weight and terminal reactive groups. The most commonly researched dendrimers for drug delivery are poly(amidoamine) (PAMAM), “starburst”, modified poly(propylene-imine) (POPAM), and aromatic ether-type dendrimers.

The use of molecular engineering techniques during the synthesis of a mono- or multifunctional dendritic drug carrier results in a product possessing a strikingly precise structure, a necessity for attachment of various secondary devices for visualization, cancer cell detection and targeting, and malignant cell destruction.

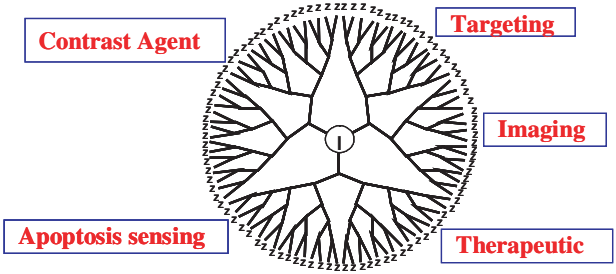

Figure 1: PAMAM dendrimer conjugated with various functions.

The reactive terminal groups can be used to attach chemotherapeutic drugs — targeting ligands that attach to over-expressed receptors present on the cancer cell surfaces and to fluorophores for visualization of the location of the dendrimer within a system, as demonstrated by Figure 1. Which terminal group is more likely to react is dependent on steric hindrance, hydrophobic interactions, and hydrogen bonding, as well as other factors. These carriers can be directed to cancer site locations if targeting agents are attached to the terminal groups of the dendrimer.

Other studies have also shown that dendrimer terminal groups can be conjugated to fluorochromes and enter cells, acting as an apparatus to sense physiological changes within the cell.[1] Enzymatic cleavage of the bond between the carrier and a fluorophore is also used to visualize carrier location and enzyme activation.

Dendrimers can be synthesized purely as drug carriers or as a variety of other single-function devices, which is discussed elsewhere in this chapter. In the past, researchers have conjugated each of these units to dendritic carriers separately, but much research is currently focusing on

developing a dendritic carrier with a therapeutic drug, a targeting unit, a fluorophore, and an apoptotic sensor attached. Conjugation of all of these units to one carrier creates a multifunctional device capable of simultaneously delivering medication to a patient in targeted locations, sensing the location of the device in the body, and dispersing and activating the drug that was delivered.[2–4,6–30] The fact that these dendrimers have the ability to be used for a variety of functions simultaneously sets these polymers apart from other carrier systems as one of the most complex drug delivery systems available for use today.

While the numerous benefits of using dendrimers as drug carriers far outweigh the negative aspects, it is necessary to note the concentration and sometimes generation-dependent (for PAMAM dendrimers) haemolysis present with use of dendrimers terminated with $-NH_2$ groups. Testing on cell lines *in vitro* has determined that dendrimers terminated by carboxyl, hydroxyl, and acetyl groups, however, do not exhibit haemolytic or cytotoxic properties.[29] Accumulation of dendrimers (generation-dependent) in areas of the body involved in excretion (the liver and kidneys) has also somewhat slowed clinical trials for these carriers. Areas in the body associated with filtration and excretory functions — more specifically, the kidneys and liver — are also affected by use of these carriers, as dendrimers can build up in either of these locations, depending on the generation (size) used. Continued research in this field will certainly speed the process toward the modification and approval of these carriers for clinical use in the near future.

Because of the tertiary amino groups present in the interior of the structure and the primary amino groups present on the surface,

PAMAM dendrimers are pH-responsive and have been used as non-specifically targeted controlled drug delivery systems triggered at low pH.[5,31,32] Partial acetylation, however, can be used to neutralize the dendrimer surface, preventing side reactions and nonspecific targeting from occurring during delivery while also increasing the solubility of the dendrimer in the specific reaction (Figure 2). The remaining nonacetylated primary amino groups can then be used for the attachment of various functional molecules including targeting agents, imaging agents, and therapeutic drugs.

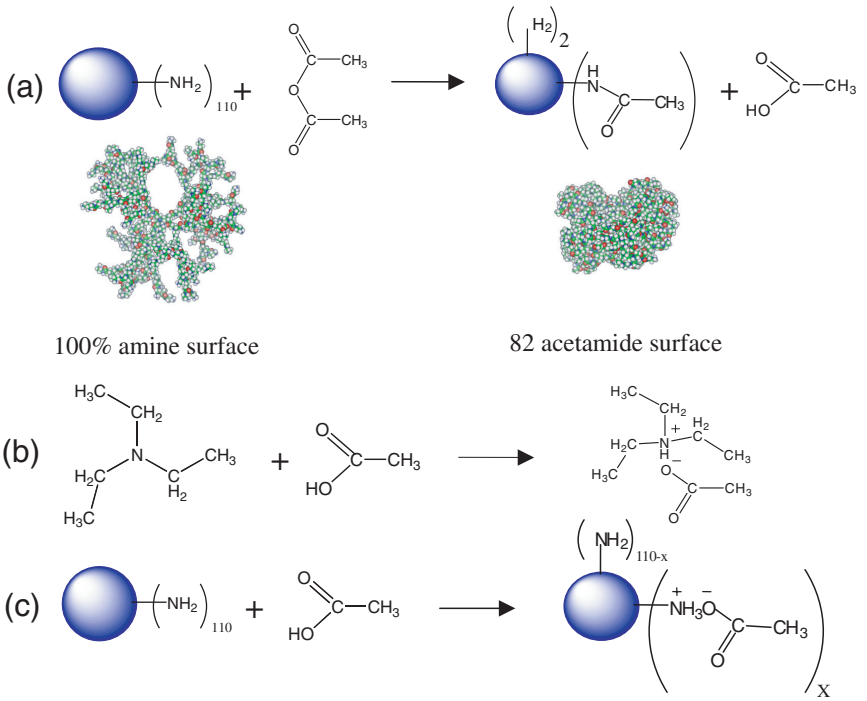

Figure 2: (a) The acetylation reaction (in MeOH in the presence of Et_3N, r.t. overnight), (b) the proton trap (salt formation), and (c) the competition reaction to (b). A computer model of non acetylated and 80% acetylated G5 dendrimer.

5.2 Partial Acetylation

Theoretically, G5 dendrimer has 128 primary amine groups on its surface. Potentiometric titration revealed 110 primary amines of the dendrimer (for the determined batch) used for acetyl derivatization. The measured molecular weight by GPC of the G5 dendrimer, 26,380 g/mol, is somewhat lower than the theoretical one, 28,826 g/mol. An example of this can be seen in Figure 3. Since these dendrimers are synthesized by batch technology, the number of actual primary and tertiary amines and the molecular weight vary slightly between batches. These results indicate a slight deviation from the theoretical structure. In an attempt to correlate the structure of the dendrimer for experimental data, a model can be assumed with 18 "missing arms," mostly from a fifth-generation level, corresponding to the 18 missing primary amine groups.

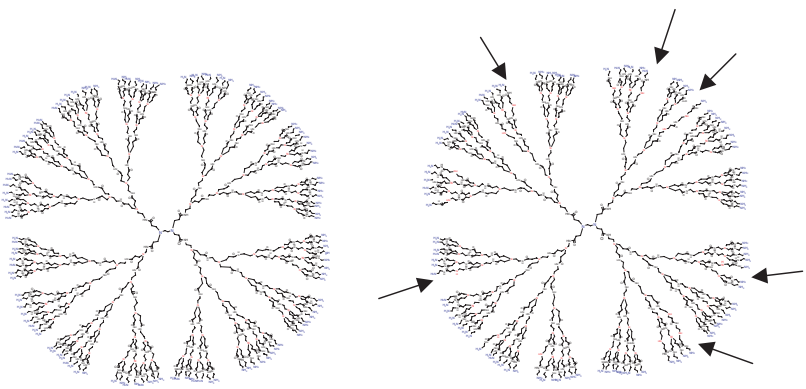

Figure 3: The theoretical (left) and defective (right) structure of G5 PAMAM dendrimer. Each is labeled with its respective generation, number of primary amine groups, and molecular weight (g/mol). The arrows represent missing arms.

The acetylation reactions are usually carried out in anhydrous methanol solution at room temperature for 24 hours. The volume of a dendrimer decreases with increasing molecular weight (an increasing degree of acetylation). (In the pH = 2.74 of the GPC mobile phase all primary and tertiary amines are protonated.) That is, the size of the acetylated dendrimers is smaller despite their increasing molecular weight (Figure 4). The GPC data indicate that the acetylated dendrimer molecules do not follow the behavior of the conventional polymer molecules, most probably because of their spherical shape, increasing hydrophobicity, and polycationic nature. Therefore, the conventional molecular weight determination method based on calibration cannot be used in such cases. Determination of molecular mass (absolute molecular mass) of such molecules can be established by GPC when the system is equipped with a concentration detector (such as a Refractive Index (RI) detector) and a Multi Angle Laser Light Scattering (MALLS). Additionally, this

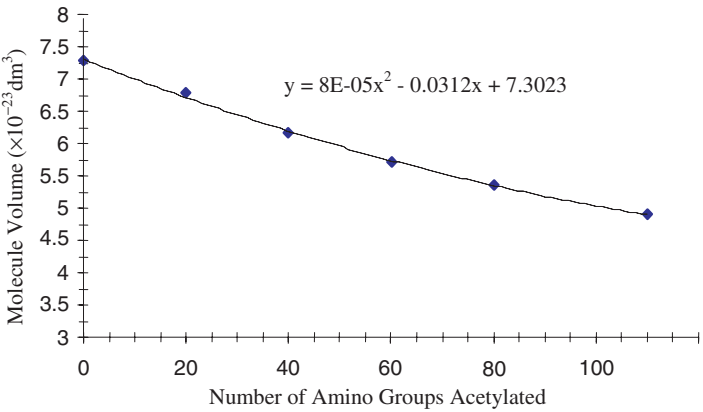

Figure 4: GPC data of acetylated G5 dendrimers: Relation of molecule volumes and number of acetylated amino groups.

setup allows determination of the molecular weight distribution and the root-mean square radius.

The GPC data of the acetylated dendrimers shown in Table 1 indicate that the molecular weight increases during acetylation. The molecular weight distribution (MWD) of all acetylated dendrimers remains very narrow, similar to the MWD of the nonacetylated dendrimer (Tab. 1). The calculated root-mean-square radius decreases during acetylation. The decreasing radius and the increasing elution volume with an increasing degree of acetylation indicate a more compact structure for the acetylated molecules. The increasingly compact structure is due to the decreasing number of available primary amines for protonation, resulting in less repulsion by charges, which expand the volume (size) of the dendrimer. ^{1}H NMR spectra of the acetyl-derivatized

Tab. 1. M_n, M_w/M_n, Root-Mean-Square Radius, and M_n, theoretically determined by GPC and calculated based on the result of potentiometric titration.

Sample	*Molecular Weight*		*MWD*	*rms radius,*[c] (Å)
	Theoretical[b]	*Measured*		
G5 0Ac[a]	27 914	27 250	1.037	25.3
G5 20Ac	28 754	28 530	1.032	24.7
G5 40Ac	29 594	29 470	1.035	24.4
G5 60Ac	30 434	30 360	1.041	23.4
G5 80Ac	31 274	31 030	1.038	22.9
G5 fully Ac	32 954	32 710	1.054	22.3

[a] Number stands for number of acetylated primary amines.
[b] Molecular weight was calculated assuming eight missing arms from generation 5 level.
[c] Root-mean-square radius.

dendrimers show the peak at 1.87 ppm is related to the -CH_3 protons of the acetyl group.[33]

The acetylation reaction product is a mixture of different partially acetylated dendrimers. The number of acetyl groups is represented by a mean value (or number-average number of acetyl groups) and can be calculated by the following formula.

$$\overline{N_a} = \frac{\sum n_i \cdot N_i}{\sum n_i}$$

(This formula is analogous to the formula of number-average molecular weight in polymer chemistry.)

The acetic acid, which is a side product of the acetylation, may also react with the amines (Et_3N and free -NH_2 compete in forming the alkylammonium acetate salt). The unexpected peak at 1.81 ppm in each spectrum is related to the protons of the -CH_3 group in the salt. In a model reaction, salt formation between the dendrimer and the acetic acid was simulated. The peak at 1.81 ppm in the ^1H NMR spectra was assigned to the protons of the methyl groups in the salt. On the other hand, the methyl proton peak of the acetic acid is at 2.1 ppm (from the NMR handbook of Aldrich). Thus, it can be safely stated that the peak at 1.81 ppm represents the methyl protons of the salt generated by the side reaction.[33] As experience shows, this salt can be removed by careful dialysis under appropriate conditions (or membrane filtration using PBS and DI water) (Figure 5(a)).

Converting all primary amines to acetyl derivatives alters the structure of the dendrimer. The peaks of the protons related to the two -CH_2- groups next to the primary amine at 3.16 and 2.63 ppm disappear.

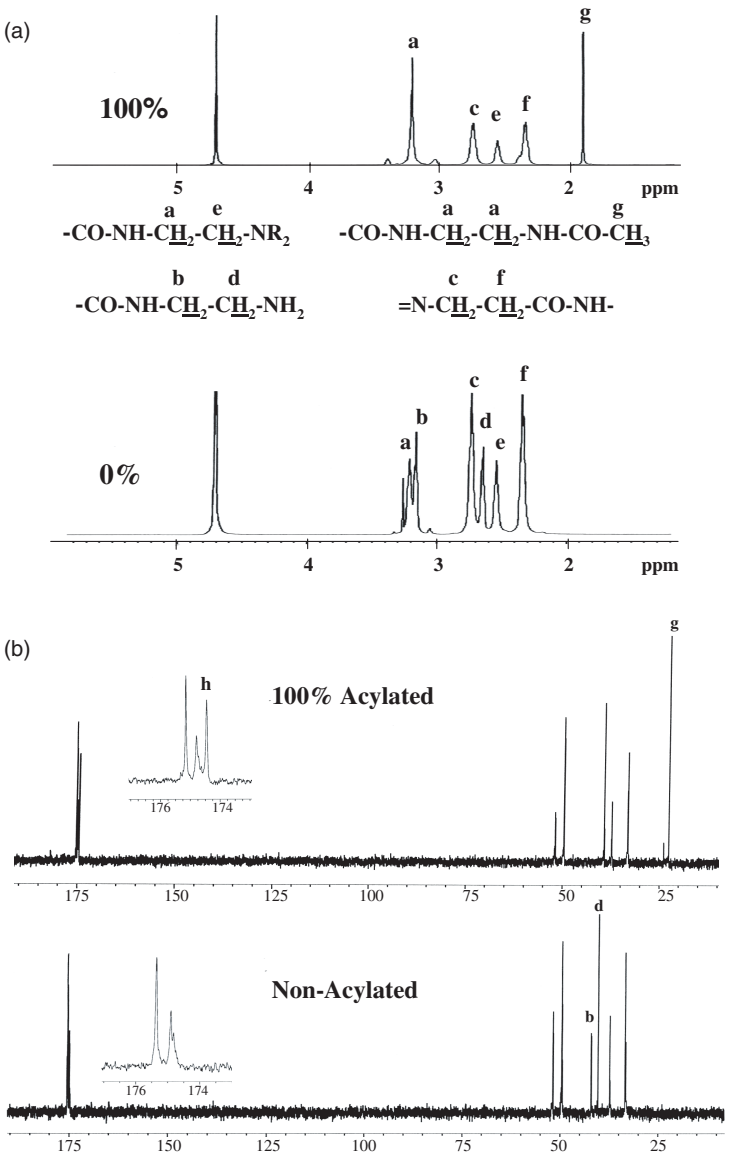

Figure 5: (a) ^{1}H NMR spectra of acetylated (after dialysis) and nonacetylated dendrimers. (b) ^{13}C NMR spectra of acetylated (after dialysis) and nonacetylated dendrimers. (Reprinted with permission form *Macromolecules* **36**, 5526–5529, 2003 Copyright (2003) American Chemical Society.)

On the other hand, there is an increase in the intensity of the peak due to the -CH_2- (the "a" type of proton in Figure 5(a)) adjacent to the amide group at 3.20 ppm.

The ^{13}C NMR spectra show that the peak at 22.4 ppm corresponds to the -CH_3 carbon of the acetyl group (Figure 5(b)). The ^{13}C NMR spectrum also shows a new peak at 174.4 ppm that is due to the dCO of the acetyl group.

The comparison of the intensity of the peak at 1.87 ppm, representing the protons of the -CH_3 of the acetyl groups to Σ(-CH_2-), may be used to determine the level of primary amino group acetylation of the dendrimer surface. The measured -CH_3/Σ(-CH_2-) ratios represent 21, 44, 66, 85, and 114 acetylated primary amino groups and are in good agreement with the calculated values for the acetylation of the 20, 40, 60, 80, and 120 (all) primary amine groups (Figure 6). During the acetylation, the acetic anhydride reacts with the primary amino groups; however, the generated acetic acid can also react in a competing side reaction with the amines, producing acetate salt.

The rate of amide formation is apparently lower than the rate of amine consumption because of the acetate salt formation in a competing reaction. The acetate formation also competes with the triethylamine acetate salt formation (a designed reaction to eliminate free acetic acid from the system).

5.3 Imaging

In vitro and *in vivo* imaging tools utilizing non-invasive techniques have been rapidly increasing in quality as the technology progresses. These

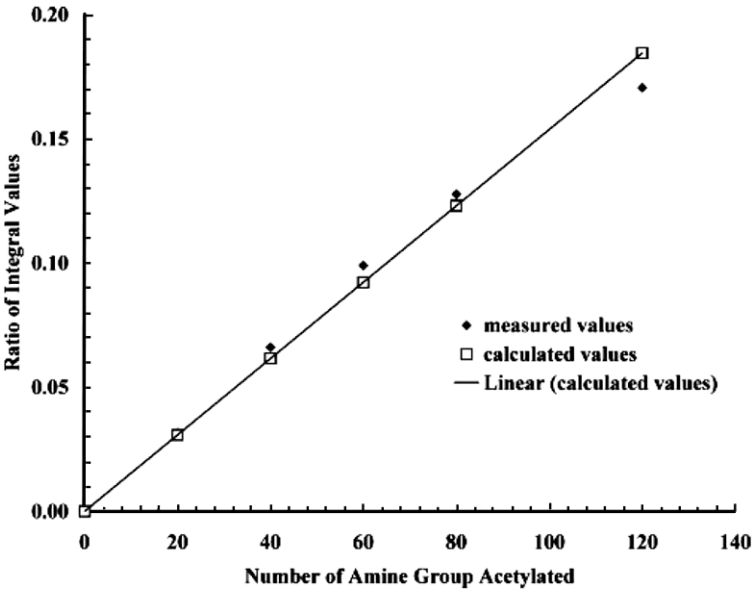

Figure 6: The number of the proton ratio of -CH_3 in the acetyl groups and all -CH_2- groups in the dendrimer structure vs. the number of primary amine groups acetylated: (□) the ratio of the number of protons in the methyl groups generated by acetylation (theoretical reaction) vs. the number of protons in the methylene groups in the interior of the dendrimer (-CH_3/-CH_2-); (◆) the ratio of the number of protons in the methyl groups generated by acetylation (actual reaction) vs. the number of protons in the methylene groups in the interior of the dendrimer (-CH_3/-CH_2-, calculated from NMR data). (Reprinted with permission form *Macromolecules* **36**, 5526–5529, 2003 Copyright (2003) American Chemical Society.)

tools can be used to detect and monitor tumor growth and other cancer-related physiological events. Imaging can also be used to detect molecular markers specific to the presence of tumors. The majority of imaging techniques rely on energy's interacting with tissues in the body.[34] Magnetic

resonance imaging (MRI, see Chapter 8) is one of these techniques. Other methods, however, rely on utilization of molecular probes for imaging. The strength of these chemical sensors lies in their minimal interference with the cells or sample in question.[35] The latest imaging techniques have included the use of dendrimer nanocomposites or nanoparticles as contrast agents (see Chapter 11).

5.3.1 Dye-based imaging

Optical imaging makes use of the variance in optical properties possessed by different tissues and fluids within the body. Optical imaging allows for physiological and molecular imaging of mounted/prepared cells and tissue samples and *in vivo* imaging of biological systems.

To optimally observe fluorescence through the use of optical imaging, fluorochromes in the near infrared range (NIR) of 650–900 nm must be used.[36] These wavelengths provide the best imaging capabilities because light in this range can cross through tissue very efficiently and absorption of these waves is very low in hemoglobin and water, therefore allowing for clear visualization of fluorophores in tissues. Little absorption of these wavelengths by hemoglobin and water also prevents background (auto) fluorescence.

5.3.2 Fluorescein isothiocyanate

Fluorescein isothiocyanate (FITC) is a commonly used marker for optical imaging. The conjugation of FITC to proteins is relatively easy and does not destroy the biological activity of the labeled substances.[37] FITC can be attached to the surface of a dendrimer to serve as a fluorescent marker for visualizing tumors.

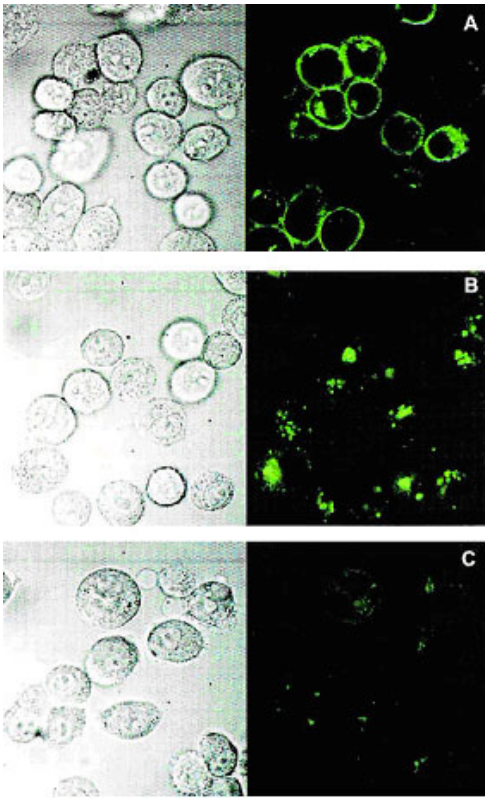

Figure 7: Confocal and fluorescence microscopic images of cells treated with G5-Ac-FITC-FA. Each panel shows corresponding light (left) and fluorescent (right) images of the same slide. The upper two panels demonstrate the binding and uptake of folic acid dendrimer conjugates into KB cells at (a) 30 minutes and (b) 24 hours. As a control, (c) KB cells were incubated with fluorescent G5-Ac-FITC not conjugated to folic acid. The top two panels clearly demonstrate the binding and internalization of the nanodevice over 24 hours.

The KB cell line is a human epidermoid carcinoma that over-expresses folate receptors. Using this imaging technique, it has been found that uptake of the acetamide and hydroxyl nanodevices occurs in these KB

cells, but no uptake occurs in cells that lack a FA receptor. The acetamide-capped G5-Ac-FITC-FA material appears to internalize over a period of 24 hours (Figure 7(b)). The control dendritic device (without FA) failed to bind to the cells (Figure 7(c)). The use of FITC and the resultant fluorescent images allow researchers to track the location of their nanodevice. FITC is attached to the dendrimer through a thiourea bond (Figure 8).

To synthesize G5-Ac-FITC, G5-Ac partially acetylated PAMAM dendrimer in absolute DMSO is allowed to react with FITC under nitrogen overnight. After intensive dialysis in DI water and lyophilization, the final

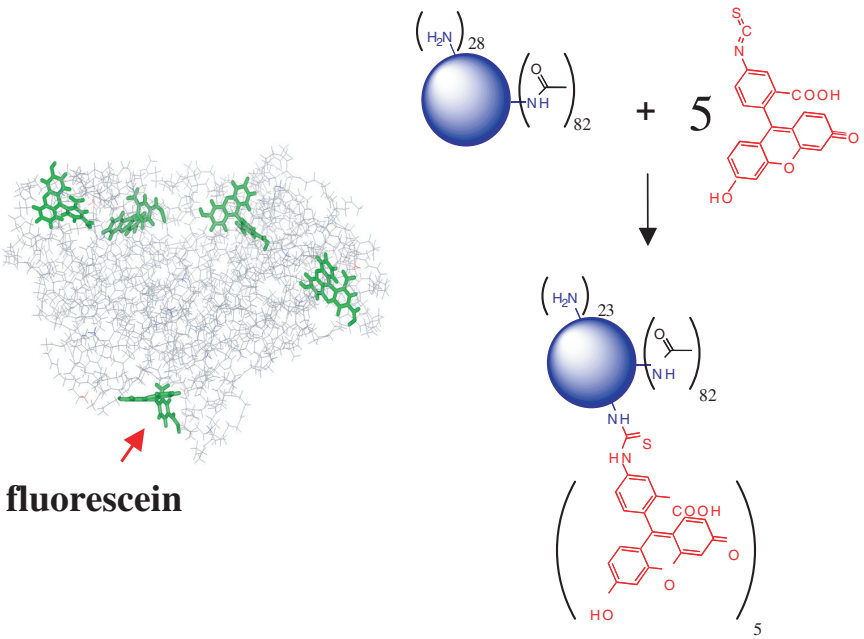

Figure 8: Synthesis of a mono-functional device (G5-Ac-FITC) in dimethyl sulfoxide overnight at room temperature. The 3D structures (left) represent the fluorescein molecules attached to the surface of the dendrimer.

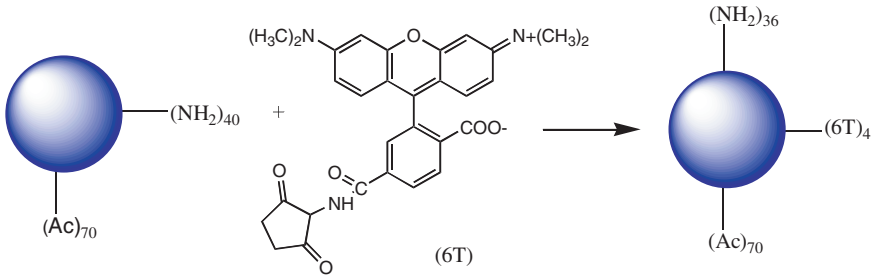

Figure 9: G5 dendrimer is reacted with 6-TAMRA (6T) to yield G5-Ac-6T.

product is isolated. Further purification can be achieved by membrane filtration, which uses PBS buffer and DI water.

5.3.3 6-TAMRA

Dendrimer nanoparticles targeted by folic acid using 6-TAMRA (6T) as a fluorescent probe have also been used to label KB cell tumors *in vivo*. An advantage of 6T is that, compared to FITC, it is less susceptible to photobleaching. Through a simple reaction (Figure 9), 6-TAMRA can be conjugated to G5 PAMAM dendrimers. G5 dendrimer is dissolved in DI water and 1M $NaHCO_3$ solution. A DMSO solution of 6T is slowly added to this solution at a reduced temperature, and the solution is stirred for 24 hours. Next, the mixture is dialyzed first in PBS then in water, is unfiltered, and is then lyophilized to obtain the product G5-Ac-6T.

5.3.4 AlexaFluor®

Alexa Fluor® 488 (AF488) is a green fluorescent dye that can be used similarly to FITC and 6T to label dendrimers and help visualize tumors. Figure 10

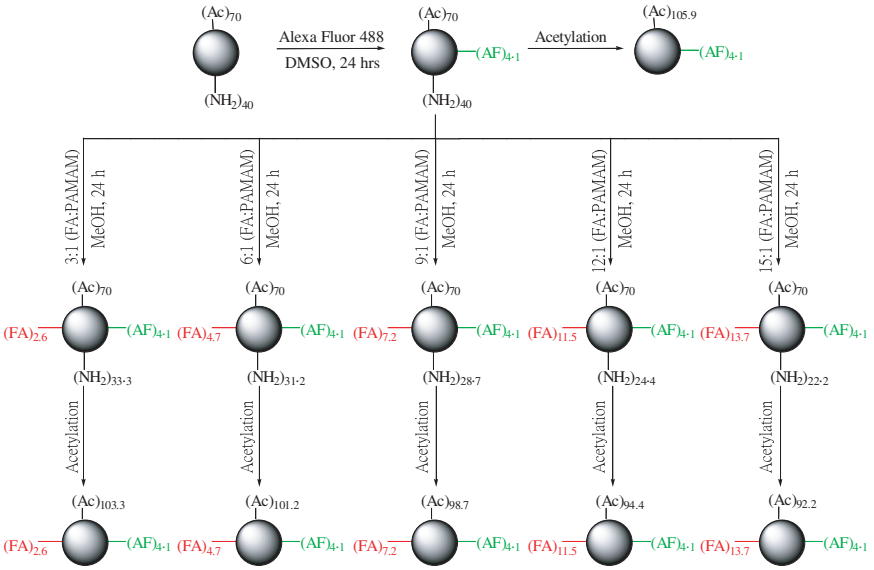

Figure 10: Synthetic scheme for G5 PAMAM dendrimer-based nanodevices with AF_{488} and different numbers of FA molecules (the device is fully acetylated).

shows how AF488 and FA are conjugated to the dendrimer and a complete nanodevice is synthesized.[38]

To fluorescently label the dendrimers, AF 488 dissolved in DMSO is added to the dendrimer/H_2O solution at a molar ratio of 5:1 (AF488:dendrimer) in the presence of 1M $NaHCO_3$ and the reaction mixture is stirred at room temperature for 48 hours. The resulting mixture of the dendrimer conjugate (G5-Ac_{70}-AF488) is then dialyzed in water for two days followed by 10 cycles of ultracentrifugation with water and PBS (w/ Ca^{2+} and Mg^{2+}), using a 10,000 molecular weight cut-off membrane at 21°C, 5000 rpm for 30 minutes each, and lyophilized for two days.[38]

5.3.5 Metal nanocomposite imaging. Dendrimer-assisted synthesis of inorganic nanoparticles for biomedical imaging

Dendrimers are a class of highly branched, monodispersed, synthetic macromolecules with well-defined composition and structure. The unique properties of dendrimers as well as their excellent biocompatibility and non-immunogenicity lead to the synthesis of various dendrimer/inorganic composite nanoparticles for a range of biomedical imaging applications. The major advantage of using dendrimers to synthesize nanoparticles is their tunable surface chemistry, providing many opportunities for the functionalization of nanoparticle surfaces. Dendrimers can be conjugated with both biological ligands (e.g., folic acid and proteins) and chelates for complexation with gadolinium to develop targeted magnetic resonance (MR) imaging contrast agents. Iron oxide nanoparticles can be synthesized and stabilized with the aid of poly(amidoamine) dendrimer carboxylates for both microscopic and MR imaging of biological systems *in vitro* and *in vivo*. Noble metal nanoparticles (e.g., Au and Ag) can be encapsulated within single dendrimer molecules or stabilized by multiple dendrimer molecules for cellular labeling and imaging studies (Figure 11). Detailed information can be found in the following respective Chapter 11.

5.4 Targeting

Drug targeting is critical for effective cancer chemotherapy. Targeted delivery enhances the chemotherapeutic effect and spares normal tissues from the toxic side effects of these powerful drugs.[39] Recent advances in

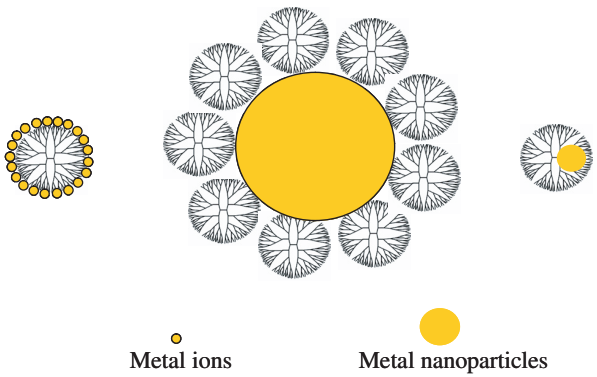

Figure 11: Schematic representation of hybrid metal/dendrimer nanocomposite particles for biomedical imaging. Left: dendrimer chelated with metal ions; middle: dendrimer-stabilized metal nanoparticles; right: dendrimer-entrapped metal nanoparticles.

the development of biocompatible polymers, combined with the identification of cancer-specific molecular targets, have allowed the application of polymers as agents for the specific targeting of cancer cells.[40–44] The targeting agent guides the polymer to the tumor site. The four following subsections (5.4.1–5.4.4) discuss targeting molecules that are being utilized for this application.

5.4.1 Folic Acid (FA) targeting

The vitamin folic acid (FA) serves as a one-carbon source for synthesis of several intermediary metabolites, most importantly for the synthesis of nucleotides required for DNA synthesis and cell growth. FA is taken up into a cell either through a low-affinity reduced folate carrier (RFC) or through a high affinity FA-receptor (FAR). The RFC is expressed ubiquitously in all cells and carries the naturally occurring reduced folates. FAR is expressed in low levels in normal cells and preferentially carries the

oxidized FA into cells. Because of its high affinity and cancer cell specificity, FA is a more suitable targeting agent than the reduced folates. There are three types of FAR — the α, β, and γ isoforms. The α and β isoforms are glycosylphosphatidylinositol (GPI)-anchored membrane proteins, and the γ isoform is a soluble protein. The α and β isoforms are membrane receptors respectively identified in epithelial and non-epithelial cells. The α isoform is over-expressed in several human carcinomas, even up to a hundred-fold[45–49] containing FA. This provides striking selectivity for targeting carcinomas using drug conjugates containing FA.

In addition to the tumor specificity of FAR-α in human carcinomas, there are other advantages for the selection of FA as a targeting agent. Expression of FAR in transformed epithelial cells is relatively enhanced on the basolateral surface ("blood side") of cancer cells, in comparison to the predominant apical ("tissue side") expression in normal cells, which complements the cancer cell specificity of FA.[50] The small molecular size of FA allows easy tumor penetration and favorable pharmacokinetics. FA is easily available and is inexpensive, and the chemical conjugation of FA to a polymer such as a dendrimer and the purification of the FA-conjugate complex is relatively simple. FA binds to its receptor with high affinity (K_d = 0.1 to 1 nM) and is largely non-immunogenic. The tumor cell density of FA receptors tends to be elevated during tumor progression, providing increased therapeutic potential during later stages of the cancer. Because of these advantages, FA has been widely studied for the targeting of bioactive agents such as protein toxins, oligonucleotides, plasmids, liposome-entrapped drugs, radiopharmaceutical agents, and MRI agents.[49,51–62]

FA is internalized into cells through the three-pronged process of the receptor-mediated endocytosis of the FA-FAR complex into endosomes, the trafficking and releasing of FA into the cytosolic compartments, and the recycling part of the endocytosed FAR back into the plasma membrane.[63–65] FA can be conjugated at its γ and α carboxyl group without losing the ability to bind to a FA receptor and to internalize into cells.[66] A variety of folate conjugates have been synthesized and shown to be endocytosed into FA-receptor expressing cells.[50,51,67–70] Although the trafficking pathway of FA has been investigated in multiple studies, a precise mechanism has not been elucidated. Trafficking through both clathrin-coated pits and caveolae has been reported. The trafficking mechanisms of any of the FA-drug conjugates and the releasing of folate and other moieties from the conjugates are not known. Nevertheless, FA-drug conjugates have been used for *in vivo* targeting.

Through conjugation of the functional molecule folic acid and partial or full acetylation of the dendrimer, *site-specific* targeted drug delivery by the dendritic device can be achieved.[71–73]

PAMAM dendrimers with well defined and highly branched structures contain multiple surface primary amino groups ideal for conjugation of several molecules of FA (Figure 12) and multiple other functions onto the surface amino groups of the dendrimer. FA-conjugated PAMAM dendrimers bind and internalize into FA-receptor-expressing KB cells. Competition assay with free FA shows that the PAMAM dendrimer device has a similar affinity for the folate receptor when compared to free FA. Therefore, the affinity of FA is not lost by conjugation with PAMAM dendrimer. The binding of the dendrimer device is relatively acid-resistant,

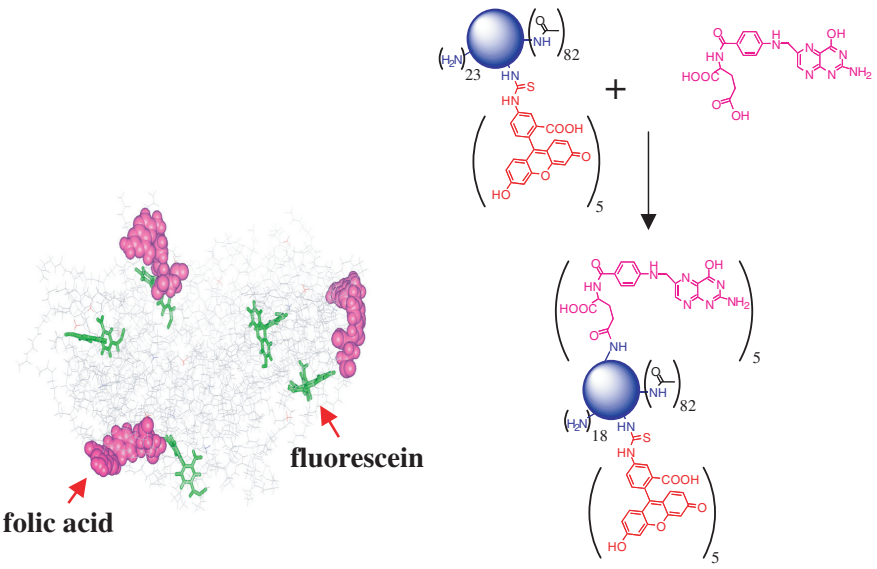

Figure 12: Synthesis of a bi-functional device (by using EDC in DMF/DMSO, one hour in DI water, two days). The 3D structure (left) represents the fluorescein and folic acid molecules attached to the surface of the dendrimer, respectively.

compared to the binding of free FA. This is probably due to the increased avidity caused by multiple anchoring of the device to two or more adjacent receptor binding sites. Multivalent interactions of FA moieties have also been demonstrated in FA linked to PEGylated cyanoacrylate nanoparticles.[59] Multiple anchoring does not seem to influence internalization of the dendrimer, as confocal microscopic analysis indicated it has cytosolic and nuclear localization.[60,104]

FA-mediated targeting systems have great clinical potential because of the overexpression of FAR in a multitude of human cancers, and FA-based nanoparticles serve as beneficial agents for diagnosis and treatment of cancer. Researchers can synthesize a variety of generation 5

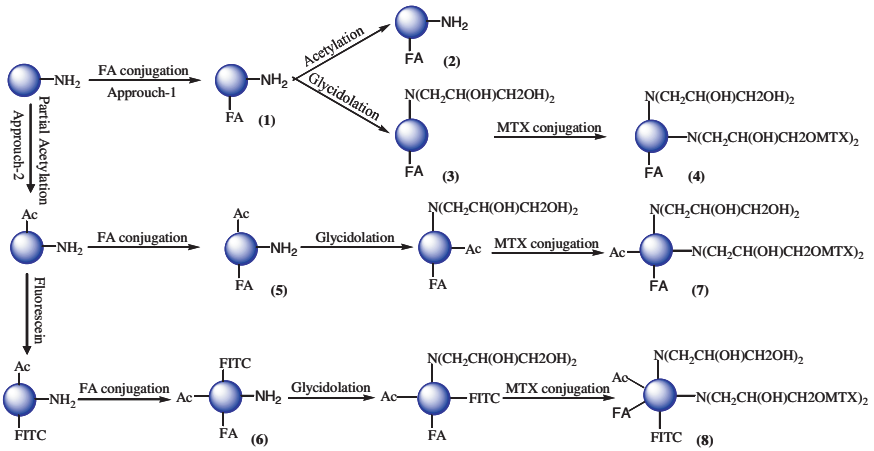

Figure 13: Schematic representation of the synthetic approaches used to synthesize mono- and multi-functional dendrimer nanodevices (FA: Folic Acid; MTX: Methotrexate; FITC: Fluorescein).

(G5) PAMAM dendrimer-based functional nanodevices using two synthetic approaches (Figure 13):

Approach 1

Synthesis from amine-terminated G5.NH_2 dendrimers. The synthesized materials include monofunctional G5-FA conjugates (terminated with amine, acetamide, and hydroxyl groups) and bifunctional G5-FA-OH-MTX (MTX denotes methotrexate) conjugates terminated with hydroxyl groups.

Approach 2

Synthesis from partially acetylated G5 dendrimers. The synthesized materials include a set of mono- and multi-functional G5-Ac-FA,

G5-Ac-FITC-FA, G5-Ac-FA-OH-MTX, and G5-Ac-FITC-FA-OH-MTX nanodevices (FITC denotes fluorescein isocyanate).

For Approach 2, the conjugation of glycidol to the acetylated bifunctional device is a necessary precursory step in order to attach MTX via an ester linkage and eliminate the remaining NH_2 groups to avoid any unwanted nonspecific targeting within the biological system. Conjugation of glycidol to the G5-Ac-FITC-FA converts all the remaining primary amino groups to alcohol groups, producing G5-Ac-FITC-FA-OH. SEC is often used to evaluate the molecular weights of these dendrimer nanodevices, while UV-Vis spectrometry is employed to detect the functional moieties upon dendrimer surface modification. NMR techniques are also utilized to confirm the dendrimer surface functionalization and to estimate the average number of surface functional moieties. In addition, CE is used to evaluate the molecular distribution and quality control of these dendrimer-based nanodevices, since the charge distribution and electrophoretic mobility often change upon dendrimer surface conjugation. CE analysis provides a unique way to evaluate the molecular distribution and heterogeneity of the dendrimer-based nanodevices for targeted cancer therapy.

It has been shown that the uptake of these nanodevices can be blocked by the simultaneous presence of free FA. The acetamide and the hydroxyl nanodevices have an approximately similar affinity for the folate receptor. However, the binding affinity of these nanodevices is greater than that of free FA, possibly because of the multiple binding sites on the nanodevices.

5.4.2 Arg–Gly–Asp (RGD) targeting

The identification of molecular markers that can differentiate newly formed capillaries from their mature counterparts can be utilized for targeted delivery of cytotoxic agents to the tumor vasculature.[74–76] The $\alpha_V\beta_3$ integrin is one of the most specific of such unique markers. The $\alpha_V\beta_3$ integrin is found on the luminal surface of the endothelial cells only during angiogenesis. Therefore, this marker can be recognized by targeting agents that are restricted to the vascular space during angiogenesis.[77,78] High-affinity $\alpha_V\beta_3$ selective ligands, Arg–Gly–Asp (RGD), have been identified by phage display studies.[79] The doubly cyclized peptide (RGD4C, containing two disulfide linkages via four cysteine residues) and a conformationally restrained RGD bind to $\alpha_V\beta_3$ more avidly than peptides with a single disulfide bridge or linear peptides. There has been growing interest in the synthesis of polymer-RGD conjugates for gene delivery,[80] tumor targeting[81] and imaging applications.[82]

The G5-Ac-AF-RGD conjugate is synthesized as shown in Figure 14. As discussed previously, amine terminated dendrimers are reported to bind to the cells in a non-specific manner, owing to positive charge on the surface. In order to improve targeting efficacy and reduce the non specific interactions, amine terminated G5 dendrimers are partially surface-modified with acetic anhydride (75% × molar excess) in the presence of triethylamine as the base.[33] The conjugate is purified by dialysis against PBS buffer initially and then against water. The use of a 75-molar excess of acetic anhydride leaves some amine groups for further modification and prevents problems arising out of aggregation, intermolecular interaction, and decreased solubility. For detection of conjugates by flow cytometry or confocal

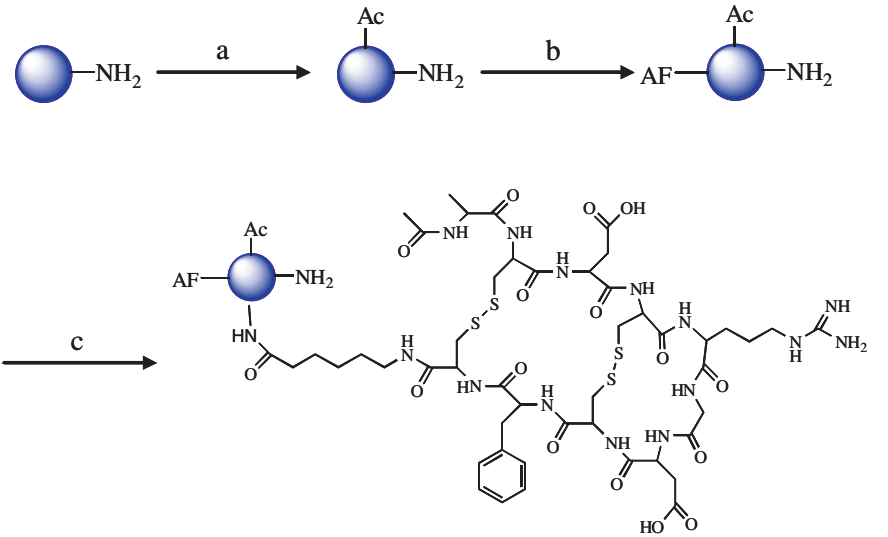

Figure 14: The synthesis of the G5-Ac-AF-RGD conjugate: (a) Ac_2O, Et_3N; (b) AF-NHS ester; (c) RGD4C, EDC, HOBt. (R. Shukla and T. P. Thomas *Chemical Communications*, **46**, 5739–5741, 2005. Reproduced by permission of The Royal Society of Chemistry.)

microscopy, a detectable fluorescent probe is needed. Alexa Fluor 488 (AF) has been used as a fluorescent label because it is significantly brighter than fluorescein conjugates and is also much more photostable. The partially acetylated dendrimer is reacted with a 5-molar excess of an Alexa Fluor-NHS ester dissolved in anhydrous DMSO to give the fluorescently labeled conjugate (G5-Ac-AF). This conjugate is purified by gel filtration and subsequent dialysis. The conjugate shows an absorption peak at λmax 498 nm.

In ^{1}H NMR spectroscopy, broad peaks belonging to aromatic protons can be seen. Integrating the total number of aromatic protons versus dendrimer peaks gives an average number of dye molecules attached to the dendrimer. The number of dye molecules is estimated to be about three

per dendrimer by ^{1}H NMR and UV-*vis* spectroscopy, as described in the manufacturer's protocol (Molecular Probes).

The RGD peptide used (RGD4C) has a conformationally restrained RGD sequence that binds specifically with high affinity to $\alpha_V\beta_3$. The RGD binding site in the heterodimeric $\alpha_V\beta_3$ integrin is located in a cleft between the two subunits. In order to keep the binding portion of the peptide exposed to the target site, an ε-Aca (acylhexanoic acid) spacer is used to conjugate the peptide to the dendrimer. A protonated NH_2 terminus of the RGD4C peptide is not essential for biological activity; therefore, the NH_2 terminus is partially capped with an acetyl group.[33] An active ester of the peptide is prepared by using EDC in a DMF/DMSO solvent mixture in the presence of HOBt, and then this is added dropwise to the aqueous solution of the G5-Ac-AF. The reaction times are 2 and 24 hours, respectively. The amidation occurs predominantly on the acylhexanoic acid linker carboxylate group. The partially acetylated PAMAM dendrimer conjugated with Alexa Fluor and RGD peptide, G5-Ac-AF-RGD, is purified by membrane filtration and dialysis. The ^{1}H NMR of the conjugate shows overlapping signals in the aromatic region for both the Alexa Fluor and the phenyl ring of the peptide, apart from the expected aliphatic signals for the dendrimer. The number of peptides is calculated to be 2–3 peptides per dendrimer, based on MALDI-TOF mass spectroscopy.

5.4.3 Drug delivery through the epidermal growth factor receptor

Several human carcinomas, including the cancers of the head and neck, breast, colon, ovary, lung, prostate and liver, overexpress the Epidermal

Growth Factor Receptor (EGFR).[83,84] Several cancer-specific biological end points such as tumor invasiveness, resistance to chemo- and radiation therapy and lower patient survival rate have all been well correlated with the degree of tumor EGFR expression.[83,85,86] Because of the potential role of abnormal EGF regulation in the tumor cell growth, several EGFR-targeted therapeutic strategies such as the delivery of apoptosis-inducing agents, tyrosine kinase inhibitors, antisense nucleotides, and siRNAS have been attempted.[87–95]

EGFR-targeting macromolecules have been synthesized in which a PAMAM dendrimer (G5) was used as the carrier molecule, mouse EGF was used as the targeting agent, and FITC was used as the fluorescence-detecting agent.[96] These G5-FI-EGF conjugates bind and internalize into the EGFR-expressing A431 epidermoid carcinoma cell line (Figure 15). The receptor-specific binding of the conjugates is demonstrated by the lack of binding of the control conjugate G5-FI and the blocking of the G5-FI-EGF binding by pre-incubation with excess free EGF (Figure 15). In addition to internalizing into the A431 cell line, the conjugates internalize into several cell lines of squamous cell carcinomas of the head and neck but not into the EGFR-negative MCF 7 cell line.[96] Dendrimer-based EGFR-targeting will be highly suitable for imaging and targeted drug delivery in several cancers.

5.4.4 Human epidermal growth factor receptor (HER-2) targeting

The human epidermal growth factor receptor (HER-2), a receptor tyrosine kinase, has been detected in several solid tumor malignancies.[94,97] The elevated levels of HER-2 detected in many breast tumors (up to 100-fold

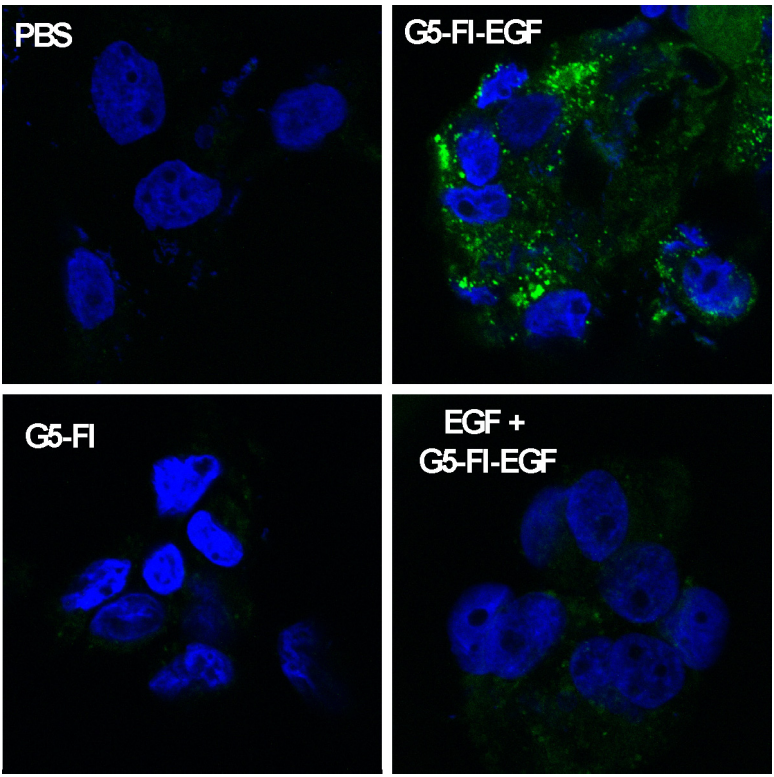

Figure 15: Internalization of G5-FI-EGF into A431 cells. The A431 cell line grown on coverslips was incubated with 300 nM each of G5-FI-EGF or the control conjugate G5-FI, at 37°C for 1 hour. Some cells were pre-incubated with 6 µM free EGF for 30 minutes prior to adding the conjugate (bottom right panel). The green and blue stains show FI-fluorescence and nuclei stained with DAPI, respectively.

higher than in normal mammary tissue) and the accessibility of the receptor from the extracellular space makes HER-2 a suitable candidate for the development of targeted therapies.[98] In order to target tumor cells *via* HER-2, Herceptin, the humanized recombinant monoclonal antibody against HER-2, is conjugated to the surface of a dendrimer-based nanodevice.

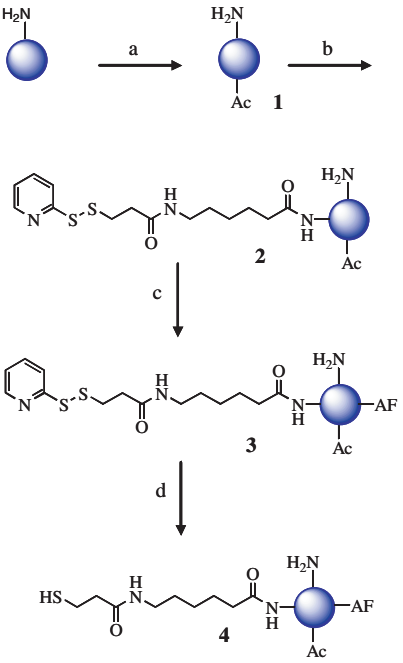

Figure 16: The modification of the dendrimer terminal group: (a) Ac_2O, Et_3N, MeOH, room temperature, 24 hours; (b) Sulfo-LC-SPDP, PBS, room temperature, 3 hours; (c) AF-NHS ester, DMSO/PBS, 24 hours; (d) DTT, PBS-EDTA, 2 hours. (Reprinted with permission from *Bioconjugate Chemistry*, Volume **17**(5), 1109–1115, 2006 Copyright (2006) American Chemical Society.)

The dendrimer terminal group modification is accomplished as shown in Figure 16. The partially acetylated G5 dendrimer (G5-Ac, **1**) is purified by repeated dialysis, initially using pH 7.4 PBS and subsequently using water. The purity of **Compound 1** and the extent of acetylation is measured and monitored by ^{1}H NMR. The degree of acetylation is measured by comparing the ratio of $NHCOCH_3$ protons with the sum of all methylene protons in the dendrimer to a calibration curve. In order to introduce a disulfide group on the dendrimer, the heterobifunctional

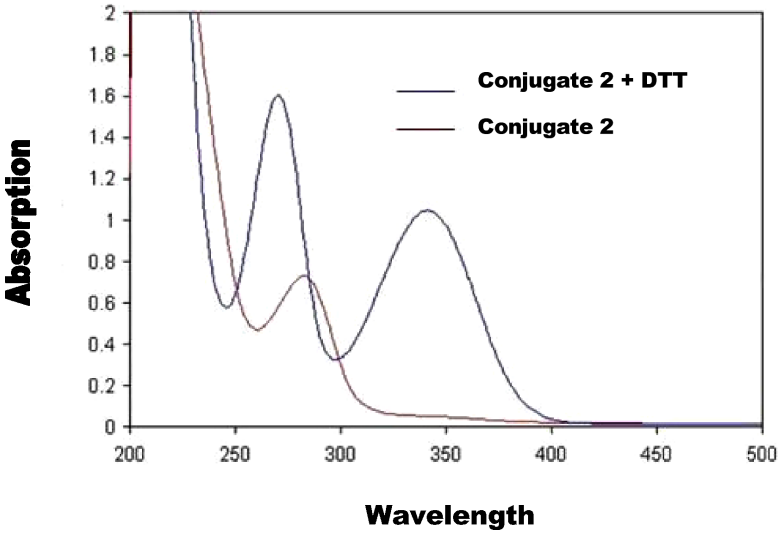

Figure 17: Pyridine 2-thione assay for determining the number of SPDP linkers on the dendrimer surface.

cross-linking agent sulfo-SPDP is conjugated to the partially acetylated dendrimer (G5-Ac, **1**) to provide a protected thiol in the form of a disulfide (G5-Ac-SPDP, **2**). The extent of disulfide modification can be monitored by UV spectroscopy, using the pyridine-2-thione assay (Figure 17). Briefly, DTT is added to a measured quantity of dendrimer and absorbance of the released 2-thiopyridine at 343 nm is recorded. On the basis of this measurement, an average of three disulfide groups per dendrimer in **Compound 2** were calculated, which is in agreement with values obtained by ^{1}H NMR by comparing the integral values of the heteroaromatic signals of the pyridine and the aliphatic signals of the dendrimer.

Compound 2 is reacted with a 5-molar excess of Alexa Fluor NHS ester to give Alexa Fluor-labeled **Conjugate 3**. The ^{1}H NMR of the conjugate shows overlapping signals in the aromatic region for both the

Alexa Fluor and the pyridine ring from the disulfide linker, apart from the expected aliphatic signals for the dendrimer.

The number of dye molecules is calculated to be about three, based on UV-*vis* spectroscopy. The reduction of disulfide bonds on dendrimer **Conjugate 3** can be carried out using dithiothreatol, DTT in PBS-EDTA buffer. The resultant dendrimer thiol, **Conjugate 4** (Figure 16), is carefully purified under an inert atmosphere in degassed PBS-EDTA buffer.

Herceptin is conjugated to thiol-modified dendrimer as shown in Figure 18. Briefly, a thiol reactive maleimide group is introduced on the antibody, **Conjugate 5**, with water-soluble sulfo-SMCC, using standard protocols, and the resulting **Conjugate 6** is purified by gel filtration. To minimize the free antibody, a 10-fold molar excess of dendrimer conjugate is used in the antibody-dendrimer coupling reaction; the un-reacted thiols are quenched with N-ethylmaleimide to minimize the dimer formation due to cross-linking

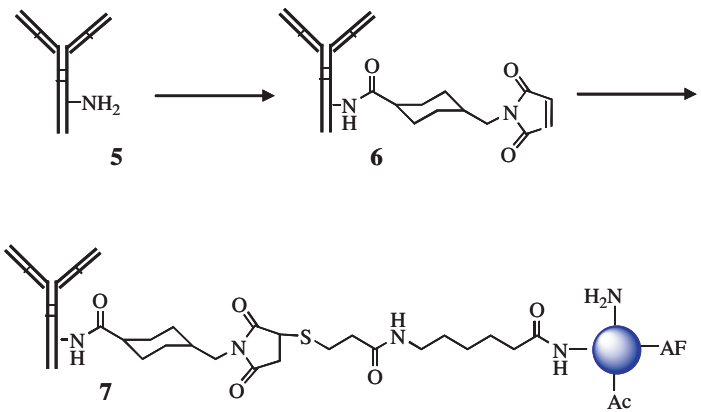

Figure 18: Herceptin is conjugated to thiol-modified dendrimer. (Reprinted with permission from *Bioconjugate Chemistry*, Volume **17**(5), 1109–1115, 2006 Copyright (2006) American Chemical Society.)

of dendrimer to dendrimer. Free un-reacted dendrimer is removed by filtration with a 100 K MWCO microcon. The resultant, **Conjugate 7**, is analyzed using PAGE, which shows a band above the antibody band that confirms the conjugation and an absence of a band for the free dendrimer. The fluorescence of the conjugates gives an indirect proof of conjugation, as the fluorescent label is attached to the dendrimer. From HPLC analysis the conjugate is shown to be very homogeneous. It is assumed that because of the steric hindrance posed by the relatively larger size of the antibody, there is negligible crosslinking under the reaction conditions.

5.5 Drugs

Current treatments for cancer include the administration of chemotherapeutic drugs which target fast-replicating cells, including hair, stomach lining, and bone marrow. Degeneration of these non-cancerous cells and tissues can be extremely harmful to the patient. Also, these drugs in the smallest dose that is able to kill cancer cells damage normal cells (non-fast-replicating cells). By conjugating these drugs to a dendrimer-based nanodevice, we are able to localize the effects of the drug to only cancer cells. Non-cancer cells, fast-replicating or not, are unharmed by this form of treatment. Therefore, the side effects of cancer treatment are eliminated. In addition, the amount of drug needed for these treatments will be a small fraction of the previous levels, resulting in less risk and decreased cost.

5.5.1 Methotrexate (MTX)

The FA analogue methotrexate (MTX) is a widely used chemotherapeutic drug for the treatment of a variety of malignancies.[99] Methotrexate inhibits

the cytosolic enzyme dihydrofolate reductase (DHFR), resulting in the depletion of the reduced folic acid that is required for nucleotide synthesis through one-carbon transfer, thus leading to the inhibition of DNA replication and subsequent cell death.[100]

In order to conjugate the drug methotrexate to the device, the remaining amino groups on the surface must be glycidylated, as previously mentioned. The partially acetylated G5-Ac-FITC-FA dendrimer conjugate in DI water is reacted with glycidol for 3 hours to yield G5-Ac-FITC-FA-OH. This reaction also helps prevent non-specific uptake into cells. MTX is reacted with EDC in a mixture of dry DMF and dry DMSO under nitrogen atmosphere for 1 hour. This organic reaction mixture is then added dropwise to the DI water solution containing the glycidylated dendrimer conjugate (Figure 19). The solution is vigorously stirred for three days to yield the final product, G5-Ac-FITC-FA-OH-MTX^{e} (superscript "e" denotes attachment *via* an ester bond).[101]

As the last step of the synthesis, the remaining terminal amine groups were fully acetylated to prevent non-specific electrostatic interactions.[38,102,103] This last step is particularly important because the remaining amine termini in the dendrimers protonate at physiological pH and cause non-specific binding and uptake *in vitro* and *in vivo.*

Unlike in conventional drug delivery, when using a drug-dendrimer nanodevice, the concentration gradient of the drug is undefined (Figure 20). Since the drug — in this case MTX — is conjugated to the surface of the dendrimer, the concentration in the space between nanodevices is zero. The concentration jumps from zero to a positive value every time a nanodevice is present, causing the concentration gradient to

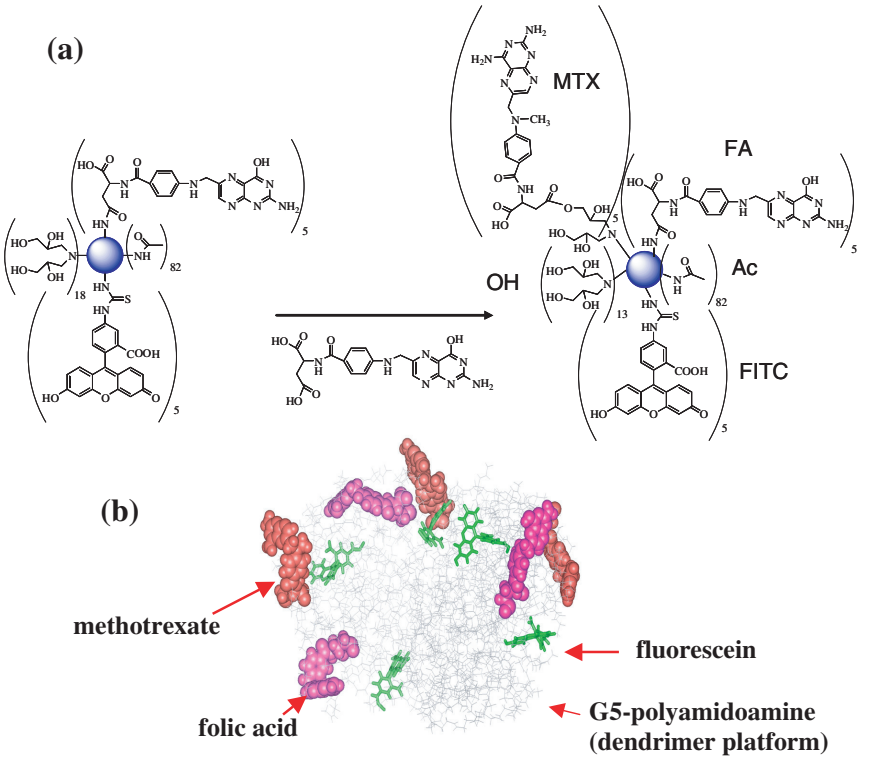

Figure 19: (a) The final step in the synthesis of a tri-functional nanodevice utilizing FITC (detecting agent), FA (targeting agent), and MTX (therapeutic agent) (by using EDC coupling chemistry in DMF/DMSO, one hour; DI water, three days, at room temperature). (b) Computer model of a trifunctional nanodevice (G5-Ac-FITC-FA-OH-MTX^{e}).

be undefined. This phenomenon has never before been encountered in drug delivery technology.

5.5.2 Paclitaxel (Taxol)

Paclitaxel (Taxol) is a novel anticancer drug which induces apoptosis by binding to microtubules within a dividing cell during mitosis, causing

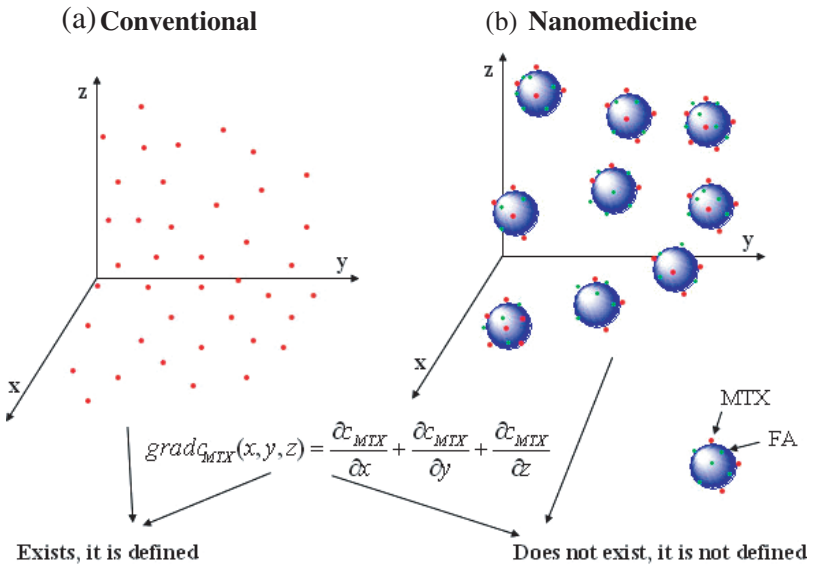

Figure 20: The difference in concentration profiles for (a) conventional and (b) nanomedicine drug delivery techniques.

kinetic stabilization and thereby preventing cell division through mitotic arrest.[104,105] Taxol inhibits microtubule depolymerization, thus encouraging tubulin assembly into stable aggregate structures.[105] So far, microtubule damage has been the only recognized means of cellular activity by Taxol that has currently been identified, and this is not specific for cancer cells. It has been indicated by other researchers, however, that there may be other methods of Taxol-induced apoptosis.[104] A variety of conjugates have been synthesized with the goal of increasing the specificity of Taxol to cancer cells. Multifunctional polymer-Taxol drug delivery systems are also being widely evaluated, as their ability to target overexpressed genes or receptors found on some cancerous cells helps greatly to lessen or eliminate undesirable side effects to the rest of the body.[105–108] The chemical structure of

G5 ⟶ G5-Ac ⟶ G5-Ac-FITC ⟶ G5-Ac-FITC-FA

⟶ G5-Ac-FITC-FA-OH ⟶ G5-Ac-FITC-FA-OH-Taxol

Figure 21: Synthetic strategy for production of functional dendrimer conjugates with imaging (FITC, fluorescein isothiocyanate), targeting (FA, folic acid), and cytotoxic drug (Taxol, paclitaxel) units [G5, poly(amidoamine) dendrimer generation 5; Ac, acetamide; OH, hydroxyl].

Taxol (Figure 22) shows the active 2' position -OH group (arrows) where attachment to the dendrimer is proposed to occur.

The synthetic strategy for production of dendrimer conjugates presented in Figure 21 details the method used for production of the multifunctional engineered dendrimer conjugate utilizing Taxol as the chemotherapeutic drug.[109]

The G5-Ac-FITC-FA-OH conjugates are synthesized similarly to those described previously in this chapter (5.4.1). However, unlike the conjugation of MTX to the dendrimers, the conjugation of Taxol to these dendrimers requires multiple steps.

First, Taxol-2'-hemisuccinate is synthesized by adding dry pyridine to a stirred solution of Taxol and succinic anhydride in CH_2Cl_2 at room temperature. The reaction mixture is stirred for 3 days at room temperature and then concentrated in vacuum. The residue is dissolved in CH_2Cl_2, and the Taxol-2'-hemisuccinate is purified on silica gel (and washed with hexane, followed with ethyl acetate) to give the final product.[110] Figure 22 presents the synthesis of Taxol-2'-hemisuccinate.

N-hydroxysuccinimido diphenyl phosphate was synthesized as described by Ogura *et al.* (Figure 23(a)).[111] The procedure for synthesis of

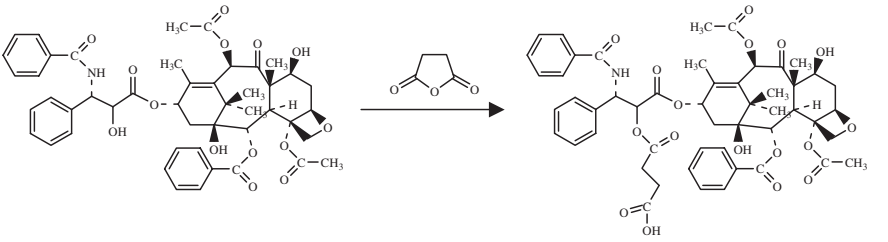

Figure 22: Synthesis of Taxol-2'-hemisuccinate (in CH_2Cl_2, in the presence of Pyridine, at room temperature for three days).

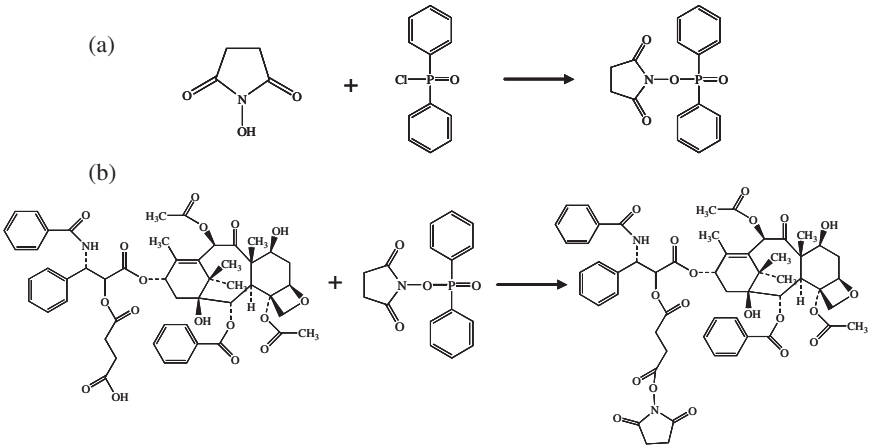

Figure 23: (a) N-Hydroxysuccinimido diphenyl phosphate formation. (Et_3N, CH_2Cl_2, room temperature, 30 minutes.) (b) Synthesis of the Taxol-hemisuccinate-N-succinimidyl ester (in acetonitrile, in the presence of Et_3N at room temperature for six hours). (Reprinted with permission from *Biomacromolecules*, **7**, 572–579, 2006 Copyright (2006) American Chemical Society.)

a Taxol-NHS ester was followed as described by Luo *et al.*[110] Triethylamine is added to a solution of Taxol-hemisuccinate and a 50% molar excess of SDPP in acetonitrile. The reaction is stirred for six hours at room temperature, than concentrated under vacuum. The residue is dissolved in ethyl

acetate and hexane and purified on silica gel. The purified Taxol-NHS ester is then dried for 24 hours in vacuum at room temperature to yield the final product. Figure 23(b) presents the synthesis of the Taxol-NHS ester.

The final reaction yields the dendrimer conjugate G5-Ac-FITC-FA-OH-Taxol[e]. In a DMF and DMSO solvent mixture, Taxol-NHS and 1–[3-(dimethylamino)-propyl]-3-ethylcarbodiimide hydrochloride (EDC) are dissolved, kept at room temperature, and stirred for two hours under nitrogen. This solution is added dropwise to a DI water solution containing the bifunctional dendritic carrier G5-Ac-FITC-FA-OH. This reaction mixture is stirred at room temperature for three days. After membrane filtration using PBS and DI water, and lyophilization, the trifunctional nanodevice is yielded. Figure 24 presents a graphical representation of this conjugation.

5.6 Characterization

Characterization and quality control of the G5 PAMAM dendrimer-based conjugates described above, including the molecular weight and number of primary amine groups, has been determined by multiple analytical methods such as high performance liquid chromatography (HPLC), gel permeation chromatography (GPC), UV spectroscopy, nuclear magnetic resonance spectroscopy (NMR), and capillary electrophoresis (CE). These methods of quality assurance will now be discussed in detail.

5.6.1 High-Performance Liquid Chromatography (HPLC)

High-performance liquid chromatography (HPLC) is a widely accepted method for the separation and purification of small molecules and is widely used in chemical laboratories. HPLC is often used to perform

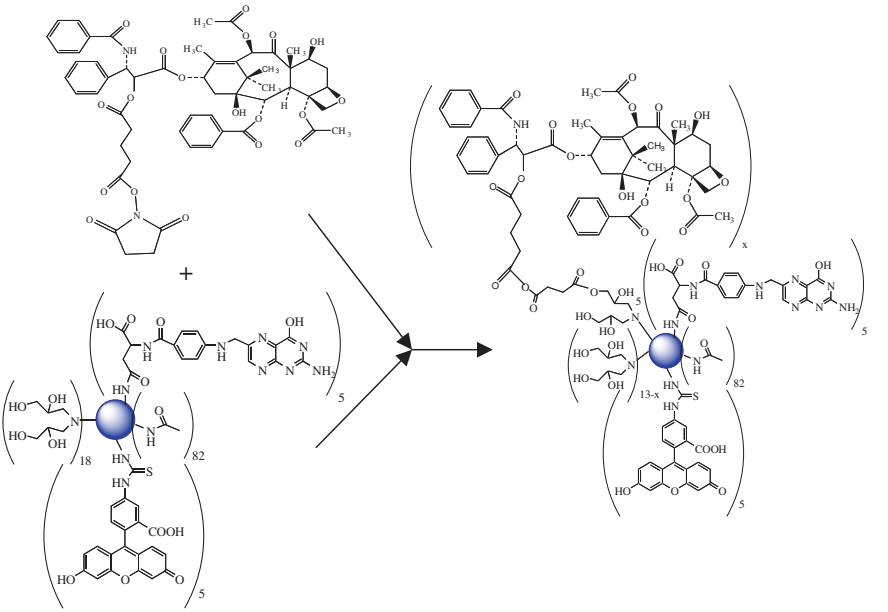

Figure 24: The final step in the synthesis of a tri-functional nanodevice utilizing FITC (detecting agent), FA (targeting agent), and Taxol (therapeutic agent) (by using EDC coupling chemistry in DMF/DMSO, 1 hour; DI water, three days, at room temperature) to produce (G5-Ac-FITC-FA-OH-Taxol[e]).

extensive characterization of FITC-, FA- and MTX-conjugated G5 dendrimers with various surface functionalities.[112] Methods have been developed to determine a common gradient that can be used to detect small functional molecules (FITC, FA and FITC) and all the mono-, bi- and tri-functional conjugates. The use of a common gradient allows researchers to determine the purity of the conjugates (i.e., whether any small molecular impurities are present), and additionally tells them about the stability of all compounds under experimental conditions. Since elution of analytes occurs as a result of counter-ion binding and surface

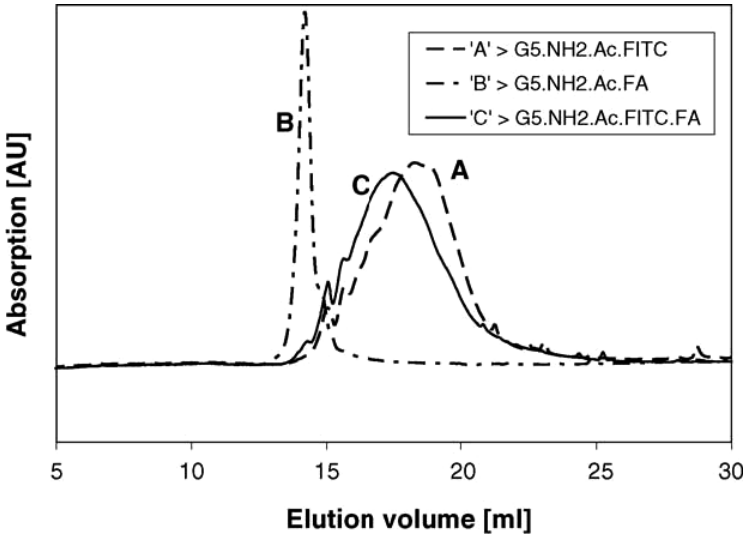

Figure 25: Elution profiles of FA- and FITC-conjugated dendrimers.

interaction between the conjugates and the stationary phase, a great deal of information regarding the surface properties of conjugates can be obtained.

It is evident from Figure 25 (as an example) that the FITC-conjugated G5-NH_2-Ac-FITC and G5-NH_2-Ac-FITC-FA devices exhibit broader elution profiles as opposed to the samples that do not contain any FITC molecules. This is due to the fact that FITC is most hydrophobic among the functional molecules. Out of a total number of 110 terminal groups of G5-NH_2-Ac, the functional molecules (FITC, FA, MTX) are attached to only three to five sites. Hence, it can be assumed that in terms of numbers and positions, the functional molecules are statistically distributed. However, in terms of attractions towards the stationary phase, the mismatch in properties between the host platform and the functional molecule is highest for FITC. Therefore, a nano-device bearing five FITC

molecules is expected to elute much later as opposed to another conjugate having two or three FITC molecules. Hence, statistical distributions of the number of FITC molecules would result in broader eluograms, as opposed to the distributions of less hydrophobic FA and MTX moieties.

5.6.2 Gel Permeation Chromatography (GPC)

The determination of the molecular weight of each conjugate structure is necessary in order to produce a well-defined multifunctional dendritic device. A gel permeation chromatography (GPC) instrument equipped with multiangle laser light scattering and a refraction index (RI) concentration detector can be utilized for this purpose. Table 2 presents the PAMAM dendrimer carrier and its mono-, bi-, and trifunctional conjugates with molecular weights and molecular weight distribution given for each.[101] The superscript numerals 2 and 3 (i.e., G5-Ac^2 and G5-Ac^3) indicate that these are two independent acetylation reactions. The GPC analytical data shows very high reproducibility.

The measured molecular weight ($\overline{M_n}$) of the G5 dendrimer of 26,380 g/mol is slightly lower than the theoretical one (28,826 g/mol). GPC data for each conjugate can be used in order to derive the precise number of each functional group attached to the carrier. The average number of each functional molecule can be calculated by subtracting the $\overline{M_n}$ value of the conjugate without the functional molecule in question from the $\overline{M_n}$ value of the conjugate containing the functional molecule and dividing by the molecular weight of the functional molecule. Figure 26 displays a sample GPC eluogram of a final product nanodevice.

Tab. 2: PAMAM dendrimer carrier and its mono-, bi-, and trifunctional conjugates with number and weight average molecular weights and molecular weight distribution.

	$\overline{M_n}$, *g/mol*	$\overline{M_w}$, *g/mol*	$\overline{M_w} / \overline{M_n}$
G5	26 380	26 890	1.020
G5-Ac[2]	29 830	30 710	1.030
G5-Ac[2]-FA	32 380	35 470	1.095
G5-Ac[2]-FA-OH	34 460	40 580	1.178
G5-Ac[2]-FA-OH-MTX[e]	36 730	36 960	1.006
G5-Ac[3]	29 880	30 760	1.030
G5-Ac[3]-FITC	32 150	32 460	1.100
G5-Ac[3]-FITC-OH	34 380	34 790	1.012
G5-Ac[3]-FITC-OH-MTX[e]	37 350	37 800	1.012
G5-Ac[3]-FITC-FA	34 710	35 050	1.010
G5-Ac[3]-FITC-FA-OH	36 820	37 390	1.016
G5-Ac[3]-FITC-FA-OH-MTX[e]	39 550	39 870	1.008

[a] $\overline{M_n}$ = number average molecular weight, $\overline{M_w}$ = weight average molecular weight calculated from GPC data, and $\overline{M_w} / \overline{M_n}$ = molecular weight distribution. (Reprinted with permission from the *Journal of Medicinal Chemistry* **48**, 5892–7899, 2005 Copyright (2005) American Chemical Society.)

5.6.3 Ultraviolet Spectroscopy (UV)

The combined UV spectra for free FA, MTX, and FITC (Figure 27(a)) are presented for comparison to Figure 27(b), the UV spectra of G5-Ac and mono-, bi-, and tri-functional dendritic devices. Figure 27(a) presents defining peaks for FA at precisely 281 and 349 nm; for MTX at 258, 304, and 374 nm; and for FITC at 493 nm. The distinguishing peaks for FA, FITC, and MTX visible in Figure 27(b) are dependent on the conjugation of each molecule to the dendrimer. Characterization of each dendritic

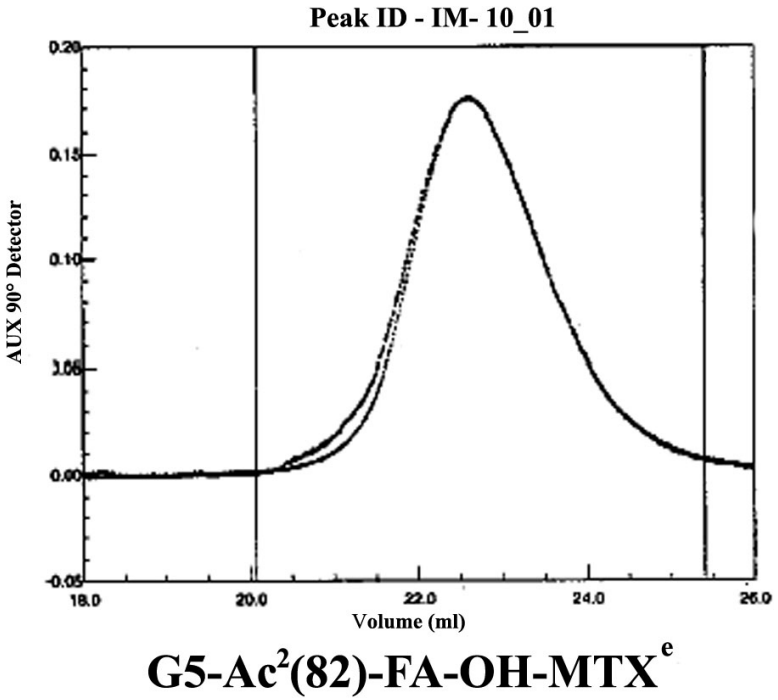

Figure 26: Illustrative GPC eluogram of a nanodevice with the RI signal and laser light scattering signal at 90° overlapping.

device by comparison of the UV spectra of free material and dendrimer-conjugated material is used to determine which function has been attached to the dendrimer. The theory that UV spectra possess additive properties is described in depth elsewhere.[113]

G5-Ac, the carrier dendrimer presented in Figure 27(b), demonstrates no characteristic peaks above 300 nm. With the attachment of FITC to the dendrimer, the monofunctional dendritic device G5-Ac-FITC is formed. The UV peak characteristic of FITC, as demonstrated by Figure 27(b), is present at 500 nm, a slight shift from the peak of 493 nm for free FITC. Building upon this same principle, the attachment of FA to form the

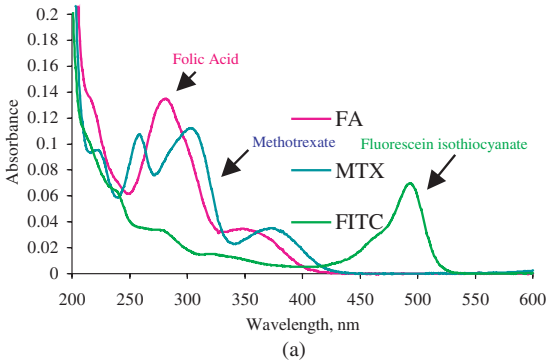

(a)

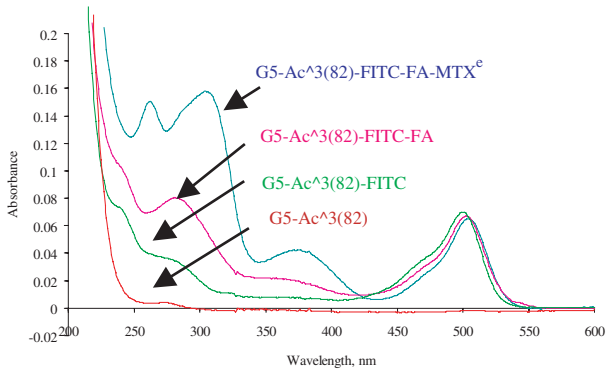

(b)

Figure 27: (a) UV spectra of free FA, MTX, and FITC. (b) UV spectra of G5-Ac and mono-, bi-, and trifunctional devices. (Reprinted with permission from the *Journal of Medicinal Chemistry* **48**, 5892–7899, 2005 Copyright (2005) American Chemical Society.)

bifunctional dendritic device G5-Ac-FITC-FA (as marked in Figure 27(b)) shifts the peak for FA to approximately 358 nm, as compared to 349 nm for free FA. The location of the other peak characteristic of free FA, 281 nm, remains unchanged in the conjugated device, and the peak for FITC (Figure 27(b)) is present at 502 nm. The trifunctional device G5-Ac-FITC-FA-MTX^e also has slightly shifted peaks. Peaks for MTX appear at 262

and 304 nm; peaks representing a combination of the MTX and FA converge at 372 nm, and a peak occurs at 505 nm for FITC. UV spectroscopy permits identification of what has been attached to the dendritic carrier through comparison of the characteristic absorption peaks of each functional group and the carrier after conjugation has occurred. UV spectroscopy also allows researchers to determine how the wavelength at which maximum absorption occurs for each attached function is affected by its conjugation to the dendrimer.

5.6.4 Nuclear Magnetic Resonance (NMR)

Nuclear magnetic resonance (NMR) can be used to determine if a conjugation reaction has occurred and for characterization of the prepared conjugate. It is an important tool for quality control in the nanodevice manufacturing process. The preparation process for a well characterized bifunctional G5-Ac-FA-OH-MTX nanodevice involves the following steps: (1) potentiometric titration of the dendrimer to determine the number of amine surface groups, (2) partial acytelation of the dendrimer, (3) determination of the number of acytelated amine groups via NMR and comparison to the calibration curve,[33] (4) conjugation with folic acid, (5) determination of the number of conjugated FA groups via NMR, (6) glycidolation of the remaining amino groups, (7) conjugation with methotrexate, and (8) determination of the number of conjugated methotrexate groups via NMR (Figure 28).

NMR analysis is required at several of the steps because of the additive or superimposing nature of the NMR peaks for folic acid and methotrexate, which are chemically similar. The first NMR spectrum is generated of the partially acytelated dendrimer and is compared with the calibration curve

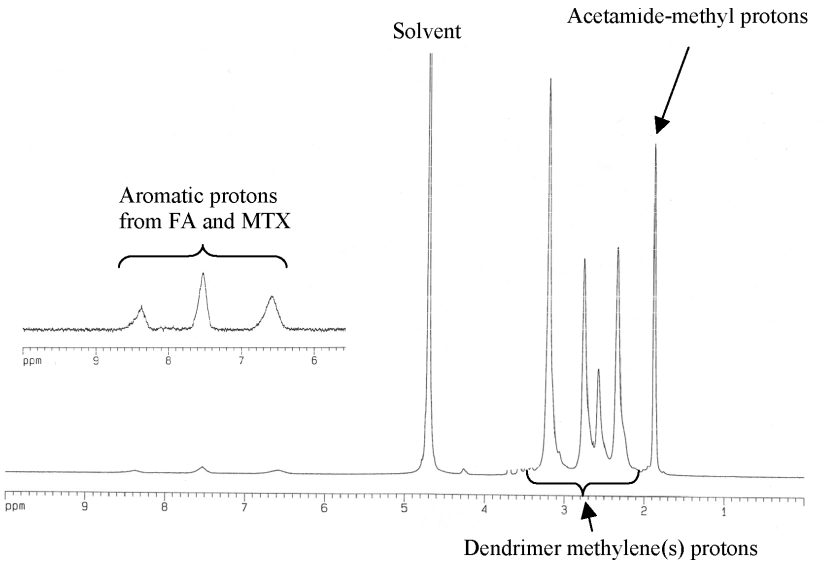

Figure 28: NMR spectra showing a G5-Ac-FA-OH-MTX PAMAM dendrimer conjugate. Note the short, broad peaks for aromatic protons, indicating covalent bonding between the methotrexate/folic acid and the dendrimer.

to determine the number of acytelated amine groups represented by the area under the acetamide-methyl proton peak. A second NMR spectrum is generated after conjugation with folic acid. In this spectrum several broad peaks appear corresponding to the aromatic protons of the conjugated folic acid. The integrated area under these curves can be compared with the integrated area under the acetamide-methyl proton curves (now known to correspond to a number of acytelated amine groups) in order to determine the number of conjugated folic acid groups. A last NMR spectrum is generated after conjugation with methotrexate; the broad peaks are now larger and represent both FA- and MTX-related aromatic protons. Comparison of the area under this

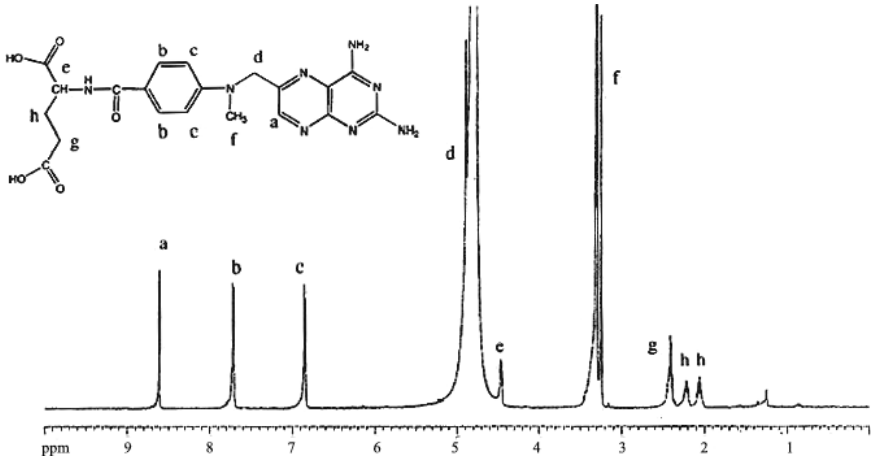

Figure 29: NMR spectra showing free methotrexate. Note the high and narrow aromatic proton peaks. (Reprinted with permission from the *Journal of Medicinal Chemistry* **48**, 5892–7899, 2005 Copyright (2005) American Chemical Society.)

curve and the area under the FA conjugated-only curve gives the number of conjugated methotrexate groups.

In the case of free MTX or FA in the product, whether due to incomplete conversion or to incomplete purification, both broad and narrow (Figure 29, corresponding to the free MTX, for example) aromatic proton peaks will appear in the NMR spectrum.

The result of the process is a well characterized nanodevice of known definition and quality, essential for medical applications.

5.6.5 Capillary Electrophoresis (CE)

Capillary electrophoresis (CE) is a powerful chromatographic method utilized in the analysis of biologic macromolecules such as DNA,[114]

proteins,[115] and peptides.[116] CE has high efficiency, high sensitivity, a short run time, and high automation capability, and it is suitable for the routine analysis of diverse dendrimer architectures, especially those that are carrying multiple charges.

CE is a fast and reliable practical analytical technique.[117] The separation of macromolecules is mainly based on the difference of their charge/mass ratios under practical conditions although some other factors may influence their separation, such as the hydrodynamic radius, counterion binding, and the adsorption/desorption of macromolecules onto the capillary surface. CE can provide data of theoretical interest as well as the molecular distribution for PAMAM dendrimers, the main question being how much charge the dendrimer molecules in fact carry in solution. For example, amineterminated PAMAM dendrimers may carry a large number of positive charges when protonated, and their high generations display particle-like characteristics. Fully modified PAMAM dendrimers contain interior tertiary amines, which are protonated under lower pH conditions and carry multiple positive charges.

Multifunctional PAMAM nanodevices bearing multiple surface ligands display significantly low charge/mass ratios. This is because of the multiple surface conjugations with functional moieties. Compared with other techniques (e.g., NMR, UV-vis spectrometry, HPLC) which generally reflect average molecular events, the variation and slight modification of PAMAM terminal groups can be magnified and sensitively detected using CE, mainly based on the change in charge/mass ratios. Figure 30 presents an example of a CE electropherogram. Further information on CE can be found in the literature.[118]

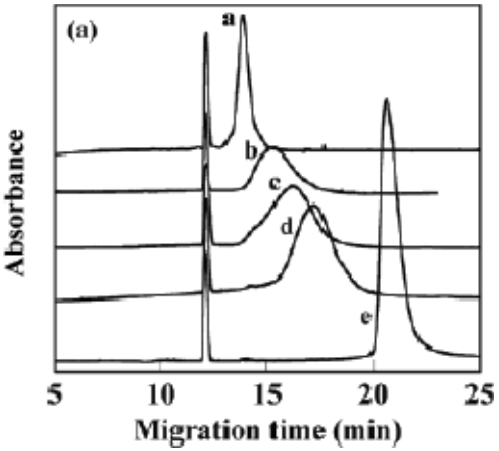

Figure 30: Normalized electropherograms of acetylated G5 PAMAMs with acetylation percentage of (a) 0%, (b) 25%, (c) 50%, (d) 75%, and (e) 100%.

5.7 Future Directions

Many exciting and untested possibilities exist for the exploitation of dendrimer-based nanodevices in medicine. Researchers around the world are exploring a wide range of novel applications. Anti-cancer research is ongoing, with efforts to adapt and refine the technology to target the many different cancers of the body individually, making it possible to provide treatment on a customized, even personalized patient-specific basis. The technology also holds great promise for use as a tool in cancer diagnosis as well as for treatment. Looking further, dendrimer-based technology will likely be adapted to provide targeted drug delivery in the treatment of a wide range of diseases other than cancer. If such efforts succeed, all can look forward to more effective, less invasive medicine in the future.

5.8 References

1. J. R. Baker Jr., A. Quintana, L. Piehler, M. Banaszak-Holl, D. A. Tomalia, and E. Raczka, The synthesis and testing of anti-cancer therapeutic nanodevices, *Biomedical Microdevices*, **3**(1), 61–69, 2001.
2. R. Esfand and D. A. Tomalia, Poly(amidoamine) (PAMAM) dendrimers: From biomimicry to drug delivery and biomedical applications, *Drug Discovery Today*, **6**(8), 427–436, 2001.
3. L. Balogh, A. Bielinska, J. D. Eichman, R. Valluzzi, I. Lee, J. R. Baker Jr., T. S. Lawrence, and M. K. Khan, Dendrimer nanocomposites in medicine, *Chimica Oggi/Chemistry Today*, **5**, 35–40, 2002.
4. K. Kono, M. Liu, and J. M. Fréchet, Design of dendritic macromolecules containing folate or methotrexate residues, *Bioconj. Chem.*, **10**, 1115–1121, 1999.
5. R. Esfand, D. A. Tomalia, A. E. Beezer, J. C. Mitchell, M. Hardy, and C. Orford, Dendripore and dendrilock concepts: New controlled-delivery strategies, *Polym. Prep.*, **41**(2), 1324–1325, 2000.
6. J. Li, D. Qin, J. R. Baker, and D. A. Tomalia, The characterization of poly(aminoamine) dendrimer. Packing by atomic force microscopy, *Polym. Prep.*, **41**(2), 1446–1447, 2000.
7. J. Li, D. R. Swanson, D. Qin, H. M. Brothers, L. T. Piehler, D. A. Tomalia, and D. J. Meier, Characterizations of core-shell tecto-(dendrimer) molecules by tapping mode atomic force microscopy, *Langmuir*, **15**, 7347–7350, 1999.
8. J. Li, L. T. Piehler, D. Qin, J. R. Baker Jr., D. A. Tomalia, and D. J. Meier, Visualization and characterization of poly(amidoamine)

dendrimers by atomic force microscopy, *Langmuir*, **16**, 5613–5616, 2000.

9. T. A. Betley, M. M. Banaszak-Holl, B. G. Orr, D. R. Swanson, D. A. Tomalia, and J. R. Baker Jr., Tapping mode atomic force microscopy investigation of poly(amidoamine) dendrimers: The effects of substrate and pH on dendrimer deformation, *Langmuir*, **17**, 2768–2773, 2001.
10. I. Lee, B. D. Athey, A. W. Wetzel, A. Kar, W. Meixner, and J. R. Baker Jr., Structural molecular dynamics studies on polyamidoamine dendrimers for a therapeutic application: Effects of pH and generation, *Macromol*., **35**(11), 4510–4520, 2002.
11. T. A. Betley, J. A. Hessler, A. Mecke, M. M. Banaszak-Holl, B. G. Orr, S. Uppuluri, D. A. Tomalia, and J. R. Baker Jr., Tapping mode atomic force microscopy investigation of poly(amidoamine) core-shell tecto(dendrimers) using carbon nanoprobes, *Langmuir*, **18**, 3127–3133, 2002.
12. A. W. Bosman, H. M. Janssen, and E. W. Meijer, About dendrimers: Structural, physical properties and application, *Chem. Rev*., **99**, 1665–1688, 1999.
13. A. Nourse, D. B. Millar, and A. P. Minton, Physiochemical characterization of generation 5 polyamidoamine dendrimers, *Biopolym*., **53**(4), 316–328, 2000.
14. G. Sui, M. Micic, Q. Huo, and R. M. Leblanc, Synthesis and surface chemistry study of a new amphiphilic PAMAM dendrimer, *Langmuir*, **16**, 7847–7851, 2000.

15. C. Kojima, K. Kono, K. Maruyama, and T. Takagishi, Synthesis of poly(amidoamine) dendrimers having poly(ethylene glycol) grafts and their ability to encapsulate anticancer drugs, *Bioconj. Chem*., **11**, 910–917, 2000.
16. S. C. Zimmerman, M. S. Wendland, N. A. Rakow, I. Zharov, and K. S. Suslick, Synthetic hosts by monomolecular imprinting inside dendrimers, *Nature*, **418**, 399–403, 2002.
17. P. Singh, Terminal groups in starburst dendrimers: Activation and reactions with proteins, *Bioconj. Chem*., **9**, 54–63, 1998.
18. D. A. Tomalia, D. M. Hedstrand, and L. R. Wilson, *Encyclopedia of Polymer Science and Engineering*, J. Wiley & Sons, Inc., **2**, 46–92, 1990.
19. D. A. Tomalia and P. R. Dvornic, *Polymeric Materials Encyclopedia*, CRC Press New York, **3**, 1814–1830, 1996.
20. G. Pistolis, A. Malliaris, C. M. Paleos, and D. Tsiourvas, Study of poly(amidoamine) starburst dendrimers by fluorescence probing, *Langmuir*, **13**, 5870–5875, 1997.
21. S. Uppuluri, S. E. Keinath, D. A. Tomalia, and P. R. Dvornic, Rheology of dendrimers. I. Newtonian flow behavior of medium and highly concentrated solutions of polyamidoamine (PAMAM) dendrimers in ethylenediamine (EDA) solvent, *Macromol*., **31**, 4498–4510, 1998.
22. G. Teobaldi and F. Zerbetto, Molecular dynamics of a dendrimer-dye guest-host system, *J. Am. Chem. Soc*., **125**(24), 7388–7393, 2003.

23. A. Schmitzer, E. Perez, I. Rico-Lattes, A. Lattes, and S. Rosca, First example of supramolecular assemblies in water of new amphiphilic glucose-persubstituted poly(amidoamine) dendrimers, *Langmuir*, **15**, 4397–4403, 1999.
24. J. Ruiz, G. Lafuente, S. Marcen, C. Omelas, S. Lazare, E. Cloutet, J. C. Blais, and D. Astruc, Construction of giant dendrimers using a tripodal building block, *J. Am. Chem. Soc*., **125**(24), 7250–7257, 2003.
25. D. A. Tomalia, H. Baker, J. Dewald, M. Hall, G. Kallos, S. Martin, J. Roeck, J. Ryder, and P. Smith, A new class of polymers: Starburst-dendritic macromolecules, *Polym. J*., **17**(1), 117–132, 1985.
26. D. A. Tomalia, A. M. Naylor, and W. A. Goddard III., Starburst dendrimers, *Angewandte Chemie*, **29**(2), 138–175, 1990.
27. L. J. Hobson and W. J. Feast, Poly(amidoamine) hyperbranched systems: Synthesis, structure and characterization, *Polym. J*., **40**, 1279–1297, 1999.
28. Y. Zhao, X. Shuai, C. Chen, and F. Xi, Synthesis and characterization of star-shaped poly (L-lactide)s initiated with hydroxyl-terminated poly(amidoamine) (PAMAM-OH) dendrimers, *Chem. Mater*., **15**(14), 2836–2843, 2003.
29. R. Duncan, Dendrimers: Novel carriers for oral and parenteral drug delivery, *Polym. Mat. Sci. Eng*., **84**, 214, 2001.
30. P. Caliceti, S. Salmaso, A. Semerizato,T. Carofiglio, R. Fornasier, M. Fermeglia, M. Ferrone, and S. Prici, Synthesis and physicochemical characterization of folate-cyclodextrin bioconjugate for active drug delivery, *Bioconj. Chem*., **14**(5), 899–908, 2003.

31. C. M. Paleos, D. Tsiourvas, Z. Sideratou, and L. Tziveleka, Acid and salt-triggered multifunctional poly(propyleneimine) dendrimer as a prospective drug delivery system, *Biomacromolecules*, **5**, 524–529, 2004.
32. N. Malik, E. G. Evagorou, and R. Duncan, Dendrimer-platinate: A novel approach to cancer chemotherapy, *Anti-Cancer Drugs*, **10**(8), 767–776, 1999.
33. I. J. Majoros, B. Keszler, S. Woehler, T. Bull, and J. R. Baker, Acetylation of PAMAM dendrimer, *Macromolecules*, **36**, 5526, 2003.
34. R. Weissleder, Scaling down imaging: Molecular mapping of cancer in mice, *Nature Reviews*, *Cancer*, **2**, 1–8, 2002.
35. M. Brasuel, R. Kopelman, T. J. Miller, R. Tjalkens, and M. A. Philbert, Fluorescent nanosensors for intracellular chemical analysis: Decyl methacrylate iquid polymer matrix and ion-exchange-based potassium PEBBLE sensors with real-time application to viable rat C6 glioma cells, *Anal. Chem.*, **73**(10), 2221–2228, 2001.
36. C. Bremer, V. Ntziachristos, and R. Weissleder, Optical-based molecular imaging: Contrast agents and potential medical applications, *Eur. Radiol.*, **13**, 231–243, 2003.
37. B. Micheel, P. Jantscheff, V. Bottger, G. Scharte, G. Kaiser, P. Stolley, and L. Karawajew, The production and radioimmunoassay application of monoclonal antibodies to fluorescein isothiocyanate (FITC), *Journal of Immunological Methods*, **111**, 89–94, 1988.
38. S. Hong, P. R. Leroueil, I. J. Majoros, B. G. Orr, J. R. Baker, Jr., and M. M. Banaszak Holl, The binding avidity of a nano-particle-based

multivalent targeted drug delivery platform, *Chemistry and Biology*, **14**, 107–115, 2007

39. R. Shukla, T. P. Thomas, J. Peters, A. Kotlyar, A. Myc, and J. R. Baker Jr., Tumor angiogenic vasculature targeting with PAMAM dendrimer-RGD conjugates, *Chem. Comm.*, **46**, 5739–5741, 2005.
40. S. M. Moghimi, A. C. Hunter, and J. C. Murray, Long-circulating and target-specific nanoparticles: Theory to practice, *Pharm. Rev*., **53**, 283–318, 2001.
41. I. Brigger, C. Dubernet, and P. Couvreur, Nanoparticles in cancer therapy and diagnosis, *Adv. Drug Delivery Rev*., **54**, 631–651, 2002.
42. Y. Luo and G. D. Prestwich, Cancer-targeted polymeric drugs, *Curr. Cancer Drug Targets*, **2**, 209–226, 2002.
43. K. D. Jensen, A. Nori, M. Tijerina, P. Kopeckova, and J. Kopecek, Cytoplasmic delivery and nuclear targeting of synthetic macromolecules, *J. Controlled Release*, **87**, 89–105, 2003.
44. I. J. Majoros, T. P. Thomas, and J. R. Baker Jr., *Handbook of Theoretical and Computational Nanotechnology*; M. Rieth, W. Schommers, Eds.; Chapter 14: Molecular Engineering in Nanotechnology: Engineered Drug Delivery, **6**, 673–717, 2006.
45. D. Weitman, R. H. Lark, L. R. Coney, D. W. Fort, V. Frasca, V. R. Surawski, and B. A. Kamen, Distribution of the folate receptor GP38 in normal and malignant cell lines and tissues, *Cancer Res*., **52**, 3396–3401, 1992.
46. J. F. Ross, P. K. Chaudhauri, and M. Ratnam, Differential regulation of folate receptor isoforms in normal and malignant tissues *in vivo*

and in established cell lines. Physiologic and clinical implications, *Cancer*, **73**, 2432–2443, 1994.

47. G. Toffoli, Overexpression of folate binding protein in ovarian cancers, *Int. J. Cancer*, **74**, 193–198, 1997.
48. M. Wu, W. Gunning, and M. Ratnam, Expression of folate receptor type in relation to cell type, Malignancy, and differentiation in ovary, uterus, and cervix, *Cancer Epidemiol. Biomarkers Prev*., **8**, 775–782, 1999.
49. H. Wang, X. Zheng, F. G. Behm, and M. Ratnam, Differentiation-independent retinoid induction of folate receptor type beta, a potential tumor target in myeloid leukemia, *Blood*, **15**, 3529–3536, 2000.
50. Y. Lu and P. S. Low, Folate-mediated delivery of macromolecular anticancer therapeutic agents, *Adv. Drug Del. Rev*., **54**, 675–693, 2002.
51. C. P. Leamon, I. Pastan, and P. S. Low, Cytotoxicity of folate-Pseudomonas exotoxin conjugates toward tumor cells. Contribution of translocation domain. *J. Biol. Chem*., **268**, 24847–24854, 1993.
52. S. Li, H. M. Deshmukh, and L. Huang, Folate-mediated targeting of antisense oligodeoxynucleotides to ovarian cancer cells, *Pharm Res*., **15**, 1540–1545, 1998.
53. A. Bielinska, J. F. Kukowska-Latallo, J. Johnson, D. A. Tomalia, and J. R. Baker Jr., Regulation of *in vitro* gene expression using antisense oligonucleotides or antisense expression plasmids transfected using starburst PAMAM dendrimers, *Nucl. Acids Res*., **24**, 2176–2182, 1996.

54. J. F. Kukowska-Latallo, A. Bielinska, J. Johnson, R. Spindler, D. A. Tomalia, and J. R. Baker Jr., Efficient transfer of genetic material into mammalian cells using Starburst polyamidoamine dendrimers, *Proc. Natl. Acad. Sci*., **93**, 4897–4902, 1996.

55. R. J. Lee and P. S. Low, Delivery of liposomes into cultured KB cells via folate receptor-mediated endocytosis, *J. Biol. Chem*., **269**, 3198–3204, 1994.

56. R. J. Lee and P. S. Low, Folate-mediated tumor cell targeting of liposome-entrapped doxorubicin *in vitro*, *Biochim. Biophys. Acta*, **1233**, 134–144, 1995.

57. A. Gabizon, A. T. Horowitz, D. Goren, D. Tzemach, F. Mandelbaum-Shavit, M. M. Qazen, and S. Zalipsky, Targeting folate receptor with folate linked to extremities of poly(ethylene glycol)-grafted liposomes: *In vitro* studies, *Bioconj. Chem*., **10**, 289–298, 1999.

58. D. M. Kranz, T. A. Patrick, K. E. Brigle, M. J. Spinella, and E. J. Roy, Conjugates of folate and anti-T-cell-receptor antibodies specifically target folate- receptor-positive tumor cells for lysis, *Proc. Natl. Acad. Sci*., **92**, 9057–9061, 1995.

59. B. Stella, S. Arpicco, M. T. Peracchia, D. Desmaele, J. Hoebeke, M. Renoir, J. D'Angelo, L. Cattel, and P. Couvreur, Design of folic acid-conjugated nanoparticles for drug targeting, *J. Pharm. Sci*., **89**, 1452–1464, 2000.

60. Y. Ravindranath, Recent advances in pediatric acute lymphoblastic and myeloid leukemia, *Current Opinion in Oncology*, **15**(1), 23–35, 2003.

61. C. P. Leamon, M. A. Parker, I. R. Vlahov, L. C. Xu, J. A. Reddy, M. Vetzel, and N. Douglas, Synthesis and biological evaluation of EC20: A new folate-derived, (99m)Tc-based radiopharmaceutical, *Bioconj. Chem.*, **13**, 1200–1210, 2002.
62. S. D. Konda, S. Wang, M. Brechbiel, and E. C. Wiener, Biodistribution of a 153 Gd-folate dendrimer, generation = 4, in mice with folate-receptor positive and negative ovarian tumor xenografts, *Invest. Radiol.*, **37**, 199–204, 2002.
63. S. Mayor, K. G. Rothberg, and F. R. Maxfield, Sequestration of GPI-anchored proteins in caveolae triggered by cross-linking, *Science*, **264**, 1948–1951, 1994.
64. R. G. Anderson, B. A. Kamen, K. G. Rothberg, and S. W. Lacey, Potocytosis: Sequestration and transport of small molecules by caveolae, *Science*, **255**(5043), 410–411, 1992.
65. M. Wu, J. Fan, W. Gunning, and M. Ratnam, Clustering of GPI-anchored folate receptor independent of both cross-linking and association with caveolin, *J. Membr. Biol.*, **159**, 137–147, 1997.
66. C. P. Leamon, R. B. DePrince, and R. W. Hendren, Folate-mediated drug delivery: Effect of alternative conjugation chemistry, *J. Drug Target*, **7**, 157–169, 1999.
67. J. J. Turek, C. P. Leamon, and P. S. Low, Endocytosis of folate-protein conjugates: Ultrastructural localization in KB cells, *J. Cell Sci.*, **106**, 423–430, 1993.
68. J. T. Douglas, B. E. Rogers, M. E. Rosenfeld, S. I. Michael, M. Feng, and D. T. Curiel, Targeted gene delivery by tropism-modified adenoviral vectors, *Nat. Biotechnol.*, **14**, 1574–1578, 1996.

69. P. Ginobbi, T. A. Geiser, D. Ombres, and G. Citro, Folic acid-polylysine carrier improves efficacy of c-myc antisense oligodeoxynucleotides on human melanoma (M14) cells, *Anticancer Res*., **17**, 29–35, 1997.
70. J. Sudimack and R. J. Lee, Targeted drug delivery via the folate receptor, *Adv. Drug Delivery Rev*., **41**, 147–162, 2000.
71. D. Weitman, R. H. Lark, L. R. Coney, D. W. Fort, V. Frasca, V. R. Surawski, and B. A. Kamen, Distance of the folate receptor GP38 in normal and malignant cell lines and tissues, *Cancer Res*., **52**, 3396–3401, 1992.
72. F. Ross, P. K. Chaudhuri, and M. Ratnam, Differential regulation of folate receptor isoforms in normal and malignant tissues *in vivo* and in established cell lines. *Physiologic and Clinical Implications*, *Cancer*, **73**, 2432–2443, 1994.
73. X. Wang, G. Frederick, and M. Ratnam, Differentiation-independent retinoid induction of folate receptor type β, a potential tumor target in myeloid leukemia, *Blood*, **96**, 3529–3536, 2000.
74. C. T. Baillie, M. C. Winslet, and N. J. Bradley, Tumor vasculature — A potential therapeutic target, *Br. J. Cancer*, **72**, 257, 1995.
75. E. Ruoslahti, Specialization of tumour vasculature, *Nat. Rev. Cancer*, **2**, 83–90, 2002.
76. W. Arap, R. Pasqualini, and E. Ruoslahti, Cancer treatment by targeted drug delivery to tumor vasculature in a mouse model, *Science*, **279**, 377–380, 1998.
77. P. C. Brooks, R. A. F. Clark, and D. A. Cheresh, Requirement of vascular integrin alpha (V) beta (3) for angiogenesis, *Science*, **264**, 569–571, 1994.

78. O. Cleaver and D. A. Melton, Endothelial signaling during development, *Nat. Med*., **9**, 661–668, 2003.

79. R. Pasqualini, E. Koivunen, and E. Ruoslahti, Alpha v integrins as receptors for tumor targeting by circulating ligands, *Nat. Biotech*., **15**, 542–546,1997.

80. K. Kunath, T. Merdan, O. Hegener, H. Haberlein, and T. Kissel, Integrin targeting using RGD-PEI conjugates for *in vitro* gene transfer, *J. Gene. Med*., **5**, 588–599, 2003.

81. A. Mitra, J. Mulholland, A. Nan, E. McNeill, H. Ghandehari, and B. R. Line, Targeting tumor angiogenic vasculature using polymer-RGD conjugates, *J. Controlled Release*, **102**, 191, 2005.

82. X .Y. Chen, Y. Hou, M. Tohme, R. Park, V. Khankaldyyan, I. Gonzales- Gomez, J. R. Bading, W. E. Laug, and P. S. Conti, Pegylated Arg-Gly-Asp peptide: Cu-64 labeling and PET imaging of brain tumor alpha(v)beta(3)-integrin expression, *J. Nucl. Med*., **45**, 1776, 2004.

83. D. S. Salomon, R. Brandt, F. Ciardiello, and N. Normanno, Epidermal growth factor-related peptides and their receptors in human malignancies. *Critical Reviews in Oncology-Hematology*, **19**(3), 183–232, 1995.

84. R. Roskoski, Jr., The ErbB/HER receptor protein-tyrosine kinases and cancer, *Biochemical & Biophysical Research Communications*, **319**(1), 1–11, 2004.

85. J. R. Grandis, M. F. Melhem, W. E. Gooding, R. Day, V. A. Holst, M. M. Wagener, S. D. Drenning, and D. J. Tweardy, Levels of TGF-alpha and EGFR protein in head and neck squamous cell carcinoma

and patient survival, *Journal of the National Cancer Institute*, **90**(11), 824–832, 1998.

86. J. Mendelsohn and J. Baselga, Status of epidermal growth factor receptor antagonists in the biology and treatment of cancer, *Journal of Clinical Oncology*, **21**(14), 2787–2799, 2003.
87. C. H. Lee, E. C. Lee, S. T. Tsai, H. J. Kung, Y. C. Liu, and J. Hwang, An EGF-pseudomonas exotoxin A recombinant protein with a deletion in toxin binding domain specifically kills EGF receptor bearing cells, Protein Engineering, **16**(4), 433–440, 1993.
88. T. Suwa, M. Ueda, H. Jinno, S. Ozawa, Y. Kitagawa, N. Ando, and M. Kitajima, Epidermal growth factor receptor-dependent cytotoxic effect of anti-EGFR antibody-ribonuclease conjugate on human cancer cells, *Anticancer Research*, **19**(5B), 4161–4165, 1999.
89. S. V. Lutsenko, N. B. Feldman, G. V. Finakova, N. V. Gukasova, S. P. Petukhov, G. A. Posypanova, K. G. Skryabin, and S. E. Severin, Antitumor activity of alpha fetoprotein and epidermal growth factor conjugates *in vitro* and *in vivo*, *Tumour Biology*, **21**(6), 367–374, 2000.
90. M. Schmidt, E. Vakalopoulou, D. W. Schneider, and W. Wels, Construction and functional characterization of scFv(14E1)-ETA — a novel, highly potent antibody-toxin specific for the EGF receptor, *British Journal of Cancer*, **75**(11), 1575–1584, 1997.
91. P. Chen, M. Mrkobrada, K. A. Vallis, R. Cameron, J. Sandhu, A. Hendler, and R. M. Reilly, Comparative antiproliferative effects of (111)In-DTPA-hEGF, chemotherapeutic agents and gamma-radiation on EGFR-positive breast cancer cells, *Nuclear Medicine & Biology*, **29**(6), 693–699, 2002.

92. E. B. Kullberg, Q. Wei, J. Capala, V. Giusti, P. U. Malmstrom, and L. Gedda, EGF-receptor targeted liposomes with boronated acridine: Growth inhibition of cultured glioma cells after neutron irradiation, *International Journal of Radiation Biology*, **81**(8), 621–629, 2005.

93. W. Yang, R. F. Barth, D. M. Adams, M. J. Ciesielski, R. A. Fenstermaker, S. Shukla, W. Tjarks, and M. A. Caligiuri, Convection-enhanced delivery of boronated epidermal growth factor for molecular targeting of EGF receptor-positive gliomas, *Cancer Research*, **62**(22), 6552–6558, 2002.

94. J. Baselga, Why the epidermal growth factor receptor? The rationale for cancer therapy, *Oncologist*, **7**(4), 2–8, 2002.

95. C. S. Kang, Z. Y. Zhang, Z. F. Jia, G. X. Wang, M. Z. Qiu, H. X. Zhou, S. Z. Yu, J. Chang, H. Jiang, and P. Y. Pu, Suppression of EGFR expression by antisense or small interference RNA inhibits U251 glioma cell growth *in vitro* and *in vivo*, *Cancer Gene Therapy*, **13**(5), 530–538, 2006.

96. T. P. Thomas, R. Shukla, A. Kotlyar, B. Liang, Y. Ye, T. B. Norris, and J. R. Baker Jr., *In vitro* targeting of an epidermal growth factor-conjugated dendrimer nanoparticle, *Biomacromolecules*, 2007. Submitted.

97. J. P. Crowe, R. J. Patrick, L. A. Rybicki, P. F. Escobar, D. Weng, T. G. Budd, R. R. Tubbs, G. W. Procop, and D. G. Hicks, A data model to predict HER2 status in breast cancer based on the clinical and pathologic profiles of a large patient population at a single institution, *The Breast*, **15**, 728–735, 2006.

105. Y. Luo, M. R. Ziebell, and G. D. Prestwich, A hyaluronic acid-taxol antitumor bioconjugate targeted to cancer cells, *Biomacromolecules*, **1**(2), 208–218, 2000.

106. Z. Gao, A. N. Lukyanov, A. Singhal, and V. P. Torchilin, Diacyllipid-polymer micelles as nanocarriers for poorly soluble anticancer drugs, *Nano Lett.*, **2**(9), 979–982, 2002.

107. C. Liu, J. S. Strobl, S. Bane, J. K. Schilling, M. McCracken, S. K. Chatterjee, R. Rahim-Bata, and D. G. I. Kingston, Design, synthesis, and bioactivities of steroid-linked taxol analogues as potential targeted drugs for prostate and breast cancer, *J. Nat. Prod.*, **67**(2), 152–159, 2004.

108. Y. Hayashi, M. Skwarczynski, Y. Hamada, Y. Sohma, T. Kimura, and Y. Kiso, A novel approach of water-soluble paclitaxel prodrug with no auxiliary and no byproduct: Design and synthesis of isotaxel, *J. Med. Chem.*, **46**(18), 3782–3784, 2003.

109. I. J. Majoros, A. Myc, T. Thomas, C. B. Mehta, and J. R. Baker Jr., PAMAM dendrimer-based multifunctional conjugate for cancer therapy: Synthesis, characterization, and functionality, *Biomacromolecules*, **7**, 572–579, 2006.

110. Y. Luo and G. D. Prestwich, Synthesis and selective cytotoxicity of a hyaluronic acid-antitumor bioconjugate, *Bioconjugate Chem.*, **10**, 755–763, 1999.

111. H. Ogura, S. Nagai, and K. Takeda, A novel reagent (N-succinimidyl diphenyl phosphate) for synthesis of active ester and peptide, *Tetrahedron Lett.*, **21**, 1467–1468, 1980.

112. M. Islam, I. Majoros, and J. R. Baker Jr., HPLC analysis of PAMAM dendrim based multifunctional devices*, Journal of Chromatography. B.: Analytical Technologies in the Biomedical and Life Sciences*, **822**(1–2), 21–26, 2005.

113. I. J. Majoros, H. M. Chui, C. B. Mehta, S. R. Gopwani, and J. R. Baker Jr. UV properties of dendrimer based multifunctional devices, Unpublished data, 2007.

114. L. Mitnik, M. Novotny, and C. Felten, Recent advances in DNA sequencing by capillary and microdevice electrophoresis, *Electrophoresis*, **22**, 4104–4117, 2001.

115. J. S. Patrick and A. L. Lagu, Review applications of capillary electrophoresis to the analysis of biotechnology-derived therapeutic proteins, *Electrophoresis*, **22**, 4179–4196, 2001.

116. P. G. Righetti, Capillary electrophoretic analysis of proteins and peptides of biomedical and pharmacological interest, *Biopharm. Drug Dispos*., **22**, 337–351, 2001.

117. S. F. Y. Li, *Capillary Electrophoresis Theory & Practice*, Academic Press, San Diego, 1992.

118. X. Shi, I. J. Majoros, and J. R. Baker Jr., Capillary electrophoresis of poly(amidoamine) dendrimers: From simple derivatives to complex multifunctional medical nanodevices, *Mol. Pharm*., **2**(4), 278–294, 2005.

98. V. R. Fantin, M. J. Berardi, H. Babbe, M.V. Michelman, C. M. Manning, and P. Leder, A bifunctional targeted peptide that blocks HER-2 tyrosine kinase and disables mitochondrial function in HER-2-positive carcinoma cells, *Cancer Res*., **65**, 6891–6900, 2005.

99. H. Calvert, Folate status and the safety proile of antifolates, *Semin. Oncol*., **29**, 3–7, 2002.

100. I. D. Goldman and L. H. Matherly, The cellular pharmacology of methotrexate, *Pharmacol. Ther*., **28**, 77–102, 1985.

101. I. Majoros, T. Thomas, C. Mehta, and J. R. Baker Jr., PAMAM dendrimer-based multi-functional engineered nanodevice for cancer therapy, *Journal of Medicinal Chemistry*, **48**(19), 5892–5899, 2005.

102. S. Hong, A. U. Bielinska, A. Mecke, B. Keszler, J. L. Beals, X. Shi, L. Balogh, B. G. Orr, J. R. Baker Jr., and M. M. Banaszak Holl, Interaction of poly(amidoamine) dendrimers with supported lipid bilayers and cells: Hole formation and the relation to transport, *Bioconjugate Chem*., (Article), **15**(4), 774–782, 2004.

103. S. Hong, P. R. Leroueil, E. K. Janus, J. L. Peters, M.-M. Kober, M. T. Islam, B. G. Orr, J. R. Baker, Jr., and M. M. Banaszak Holl, Interaction of polycationic polymers with supported lipid bilayers and cells: Nanoscale hole formation and enhanced membrane permeability, *Bioconjugate Chem*., (Article), **17**(3), 728–734, 2006.

104. T.-H. Wang, H.-S. Wang, and Y.-K. Soong, Paclitaxel-induced cell death: Where the cell cycle and apoptosis come together, *Cancer*, **88**(11), 2619–2628, 2000.

This page intentionally left blank

Chapter 6

Biological Application of PAMAM Dendrimer Nanodevices *in vitro* and *in vivo*

Thommey P. Thomas & Jolanta F. Kukowska-Latallo

Outline

6.1 Introduction

Several conventional cancer chemotherapeutic protocols have been tested and used in the clinic over the past two decades, and the recent advancement in combination therapy using two or more drugs has significantly increased the survival rate of cancer patients. These drugs act through the interruption of cell proliferation via arresting cell division by inhibiting one of the biochemical pathways of cell division — for example, the inhibition of DNA replication or of the microtubule assembly that regulates cell division. The selectivity of conventional cancer therapeutic agents is based on the ability of a malignant cell to replicate faster than a normal cell. However, as all dividing cells will be destroyed by such treatments, a crucial factor that limits the success of such protocols has been drug toxicity. Any synergetic effects obtained due to combination therapy are also

normally accompanied by synergistic toxicity, leading to patient suffering. The cell toxicity is also accompanied in some cases with organ-specific toxicity, such as cardiotoxicity.

In addition to toxicity, there are other limitations in using chemotherapeutics. It may be difficult to maintain a small-molecule drug in the circulation system for sufficient time at an adequate concentration in order to catch all the tumor cells in the specific point of their cell cycle at which the drug interacts. Furthermore, although cancer cells initially respond to a chemotherapeutic agent, a relapse often occurs because the cells that survive the treatment become drug-resistant, further aggravating the cancer, owing to their lack of response to multiple drugs. Thus, the application of conventional chemotherapeutics as single agents or as combination therapy has always faced several setbacks not only because of their non-specific toxicity but also because of their poor solubility and long-term drug resistance.[1] In order to achieve an increased therapeutic index (cytotoxicity and killing of cancer cells versus normal cells), it is crucial that a more cancer cell-specific therapeutic approach is undertaken. This may be achieved by developing "targeted" drugs which would be preferentially taken up by the cancer cells, thus sparing normal cells.

Targeted therapy involves identifying biochemical molecules that are relatively more specifically expressed in the tumor cells and utilizing a mechanism similar to the "Trojan horse" to cause the death of the cells. There are two different major types of targeted therapeutic approaches. In the first approach, a molecule identified as being involved in the abnormal growth of the cancer cell is targeted using a drug that would block its deranged regulation. Examples of this type of targeted therapy is the application of

the antibody Herceptin®, which inhibits tumor growth through its binding onto the overexpressed HER2 receptor in certain breast tumors, and the usage of the small molecule Gleevec® in inhibiting the "c-abl" protein-mediated altered growth regulation in leukemia.[2]

In the second approach, a cell surface receptor overexpressed in the cancer cell that is qualitatively or quantitatively different from normal cells is identified and an apoptosis-inducing chemotherapeutic drug is delivered into the cell through this receptor, acting similarly to a guided missile, to disrupt the cell cycle and kill the cell. This is performed by using the receptor ligand directly linked to the drug or through a macromolecule carrier. In addition to the specificity achieved, targeted drug delivery overcomes the dilution effect of the drug in the body by effective homing of the drug into the tumor and maximizing the amount released into the cancer cell. Over the past decade several suitable drug conjugates using carriers such as liposomes, polymers, and dendrimers have been developed and studied.[3–6] A drug that is targeted through a cell surface receptor as well has other advantages — it uses different routes of endocytic pathways than the non-targeted free drug, which could lead to an increase in cellular retention and in the action of the drug and to a decrease in drug resistance.

The suitability of a macromolecular carrier for *in vivo* application is based on several properties: its ability to carry multiple targeting and drug molecules, its aqueous solubility, its uniformity, and its ability to pass through tissue barriers such as the vasculature and the interstitial fluid. In addition, the carrier-drug complex must bind and internalize into the cancer cell and release the drug into the appropriate cell compartment. It is

also important the carrier is non-toxic and non-immunogenic before and after biodegradation. Water-soluble macromolecular platforms as carriers of the drug also have the advantage of improved solubility and pharmacokinetics when compared to free drugs.[7]

Recent studies have shown that the water-soluble polymers termed "dendrimers" are one of the most suitable drug delivery platforms. This is because of properties such as their biocompatibility, dimension, and structural architecture, which mimic certain biomolecules such as the glycogen.[3,4,8,9] Dendrimers also fall under the category of "nanoparticles" because of their size — from 2.5 nm to 10 nm in diameter. Dendrimers can be synthesized as different "generations" in different molecular weights and sizes. For example, the poly(amidoamine) (PAMAM, Starburst™) dendrimer generations 3, 4, and 5 are about 3.6, 4.5, and 5.4 nm in diameter, and these resemble the sizes of the biological molecules insulin (3 nm), cytochrome C (4 nm), and hemoglobin (5 nm). Owing to their dimension and biocompatible architecture and properties (see below), the dendrimers can be termed "artificial" biomacromolecules.

During the past decade, various types of dendritic molecules have been tested as platforms for drug delivery, either as non-covalent "encapsulation complexes" or through the careful synthesis of covalent conjugates with multiple targeting and drug moieties. Several dendrimer platforms such as PAMAM, poly(propylene imine) (PPI), poly(aryl ether) branches, and those containing core molecules such as carbohydrate, calixarene have been described as possible drug delivery agents.[9–11] A variety of chemical linkages have been employed for the

conjugation of molecules onto the dendrimer, and core groups have been synthesized using different iterative synthetic strategies under controlled conditions. A selected synthetic strategy can direct the size, shape, and dimension of the dendrimers' interior molecular space.[3,12] A particular chemical method would also determine the number of surface functional groups by varying the core molecules and the nature of its branching points.

PAMAM dendrimers are the first dendrimer type to be synthesized, characterized, and tested in biological systems. The commercially available PAMAM ("Starburst") dendrimers are synthesized from an ethylene diamine (EDA) or NH_3 initiator core, with exhaustive Michael addition of methyl acrylate (MA) followed by condensation (amidation) reactions of the resulting ester with large excesses of EDA.[3,9,12–14] Each generation of growth doubles the number of termini and approximately doubles the molecular weight, with an increase of about 1 nm in diameter for each added generation. The detailed synthesis protocols, properties of different types of dendrimers, and characterization techniques have been described elsewhere in this book and in other recent reviews.[3,9,12,13,15] This chapter deals with the biological properties and the *in vivo* applicability of the PAMAM dendrimers as drug carriers. The goal of the research work conducted in our laboratory has been to investigate the usefulness of the PAMAM dendrimer as a platform for the specific cellular delivery of molecules such as a drug or an imaging agent into target cells, and our recent studies have unequivocally established the potential applicability of the PAMAM dendrimers as a molecular delivery platform.[15–19]

6.2 The Applicability of PAMAM Dendrimers as a Drug Targeting Platform

6.2.1 Methods for biological analysis of dendrimer conjugates

The specific targeting and tissue distribution of fluorescently tagged dendrimer conjugates are determined *in vitro* and *in vivo* by various fluorescence detection techniques such as flow cytometry, confocal microscopy and two-photon optical fiber fluorescence (TPOFF).[15,19,20] Flow cytometry allows quantification of the cellular binding of the conjugate, and confocal microscopy provides the cellular and sub-cellular localization. We have developed an optical fiber-based TPOFF technique to quantify tumor fluorescence that would not require the routine tissue processing needed for flow cytometry and confocal microscopy. In this method, an optical fiber is inserted into the tissue through a 30-gauge needle to quantify its fluorescence. Using this technique it is possible to measure the tumor fluorescence in live animals.[21] The details of the TPOFF analysis are given in a separate chapter. The extent of cytotoxicity induced by a dendrimer-drug conjugate is determined by XTT and clonogenic assays[19] and by monitoring apoptosis by other standard methods (described in a separate chapter).

6.2.2 Biological compatibility of PAMAM dendrimers

PAMAM dendrimers are largely non-immunogenic and their conjugation with certain molecules such as poly(ethylene glycol) (PEG) can make them devoid of any immunogenicity.[22] The surface charge, the dendrimer generation, and the route of administration ultimately determine the biological fate and compatibility of the PAMAM dendrimers.[23] Because the

mononuclear phagocyte system (MPS) present in the spleen, liver, lungs and bone marrow normally takes up hydrophobic particles larger than 100 nm in diameter, the hydrophilic PAMAM dendrimers (<10 nm) are excluded from the phagocytic pathway. PAMAM dendrimers which are not capped (surface amino groups neutralized by chemical reactions such as acetylation and hydroxylation) induce cytotoxicity in a concentration- and generation-dependent manner,[23–25] whereas capped (neutralized) dendrimers fail to show significant cytotoxicity.[15,16,19,24,26] The cytotoxicity of PAMAM dendrimers having free surface amino groups is thought to be due to its non-specific interaction with cellular membranes, which also leads to blood hemolytic activity *in vivo*.[23,27]

6.2.3 PAMAM-based drug conjugates as macromolecular targeting agent independent of enhanced permeability and retention

Because tumor vasculatures in general have the abnormal property of being leaky and able to permeate macromolecules (up to 400-nm pore size versus 2–6 nm in normal vasculature) through a process termed as "enhanced permeability and retention" (EPR), higher dendrimer generations may passively enter into the tumor tissue. Drug accumulation by the EPR effect is the due to the combined effects of tumor leakiness and poor lymphatic drainage from the tumor interstitial fluid. Smaller molecules which easily diffuse out of the tumor do not accumulate in the tumor by the EPR effect. Passive drug targeting via EPR has been attempted as a means for selective tumor uptake of drugs. However, EPR may be an

ineffective strategy because of the absence of the EPR effect in all areas of larger tumors and because of the inability of a carrier to non-specifically internalize into cells in these areas of the tumor passively following retention in the interstitial fluid. Therefore a targeted therapy that is not entirely dependent on EPR is required for the specific and effective targeting of a drug into the tumor.

The PAMAM dendrimers are suitable for specific drug targeting through mechanisms not dependent on an EPR effect. As described previously, PAMAM dendrimers are branched polymers with highly ordered spherical 3D structures. They possess positively charged amino groups on their periphery, which provide useful moieties for functional modification and they allow a variety of reactions to be performed under mild conditions. PAMAM dendrimer-conjugates with molecules such as folic acid, peptides, and antibodies have been synthesized, purified, characterized, and their biological properties reported in several recent studies.[18,28–31]

6.2.4 Applicability of PAMAM dendrimer as carrier through non-covalent interaction with molecules

A detailed description of PAMAM dendrimers as "nanocomposites" for carrying atoms or molecules into cells is in a separate chapter. In nanocomposites, the dendrimer-drug complex is generated through non-covalent interaction[9,32–34] through encapsulation and dispersal of small domains of the guest molecules within the dendrimer interior. Agents such as metal ions and drugs may be trapped inside the dendrimer through H-bonding,

ionic and van der Waals forces. The metal nanoparticles can be prepared by either *in situ* chemical reaction (for example, the reduction of metal ions to metal with zero valency) or by physical treatment (for example, irradiation). Preparation and *in vitro* applicability of gold-, silver- and drug-based nanoparticles have been described.[35–37] One undesirable biological property of the nanocomposites is that the entrapped molecules are released from the dendrimer in the presence of isotonic conditions despite their stability in water.[38] Thus, it is important to develop a covalent dendrimer-drug conjugate that is stable in the circulation but capable of releasing the drug or performing the function of the drug in cancer cells.

6.2.5 PAMAM dendrimer conjugates containing different functionalities for targeting, drug delivery and detection

Because of the presence of multiple free amino groups on the PAMAM, several functions such as a targeting molecule, a fluorescent detecting agent, an imaging agent, drugs, and an apoptosis-detecting agent can be covalently conjugated onto the dendrimer surface. The targeted drug delivery is based on the principle that if a receptor is specifically expressed or overexpressed on the surface of the cancer cell, the conjugate with the drug and a receptor ligand travels stably through the circulation and specifically binds, internalizes into the cell, and performs the action of the drug with or without releasing the free drug. The presence of additional functionalities such as a fluorescent sensing agent or an apoptosis-detecting agent along with the targeting molecule and the drug would enable simultaneous multifunctional analysis of the biological fate of the delivered drug.

6.2.6 *Targeting agents — small molecules (for example, FA and peptides) and biomacromolecules (for example, proteins and antibodies)*

The first step in creating a targeted drug delivery system is the identification of an appropriate cancer cell-specific cell surface receptor. These receptors may specifically bind a small molecule such as folic acid (FA), a protein, or an antibody. The most widely tested small molecule receptor is the FA receptor (FAR), which is known to be overexpressed in malignancies such as cancer of the ovary and breast.[39,40] There are three types of FAR — the α, β, and γ isoforms. The α and β isoforms are glycosylphosphatidylinositol (GPC)-anchored membrane proteins, and the γ isoform is a soluble protein. The α and β isoforms are membrane receptors identified respectively in epithelial and non-epithelial cells. The α isoform is overexpressed up to a hundred-fold in several human carcinomas, which provides optimal selectivity for targeting carcinomas using drug conjugates containing FA. FA binds to its receptor with high affinity (K_d = 0.1 to 1 nM) and is largely non-immunogenic.

Another advantage of FAR-targeting is that the expression of the FAR in transformed epithelial cells is higher on the basolateral surface ("blood side") of cancer cells in comparison to the predominant apical ("tissue side") expression in normal cells. Therefore, an intravenously administered dendrimer-FA conjugate will have additional cancer cell specificity of FA.[41] The small molecular size of FA allows easy tumor penetration and favorable pharmacokinetics. FA is easily available and is inexpensive, and the chemical conjugation of FA to a polymer such as a

dendrimer and the purification of the FA-conjugate complex are relatively simple. Because of these advantages, FA has been widely studied for the targeting of bioactive agents such as protein toxins, oligonucleotides, plasmids, liposome-entrapped drugs, radiopharmaceutical agents, and MRI agents.[3] Our *in vitro* as well as *in vivo* studies have shown that the FAR is a suitable target for dendrimer-based targeting (Figures 1 and 2).

Receptors of proteins and peptides have been tested as cancer-targeting cell surface molecules. Several receptors of growth factors such as EGFR, HER2 and FGF have been known to be overexpressed in certain tumor types. The natural protein ligands for the receptor or a ligand mimetic such as an antibody or a peptide (with <100 amino acids) can be used as the targeting molecule. Targeting using peptides or a peptide

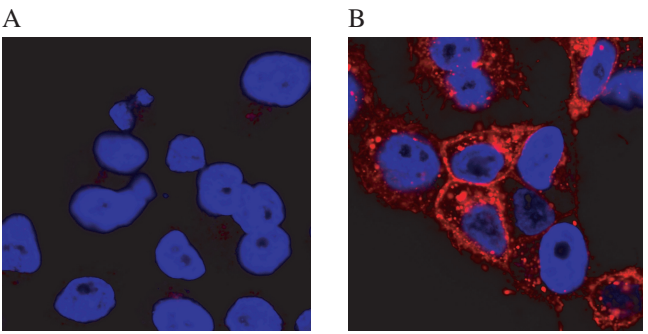

Figure 1: Confocal microscopy of KB cells treated with non-targeted (G5–6T, panel A) and targeted (G5–6T-FA, panel B) nanodevices. KB cells were incubated with 100 nM of the indicated dendrimers for 1 hour and confocal images were taken. (Reprinted with permission from T. P. Thomas, J. Y. Ye, C.-S. Yang, *et al*., "Tissue distribution and real-time fluroscence measurement of a tumor-targeted nanodevice by a two photon optical fiber fluroscence probe," in Nanobiophotonics and Biomedical Applications III, *Proceedings of the SPIE*, Vol. **6095**, 2006.)

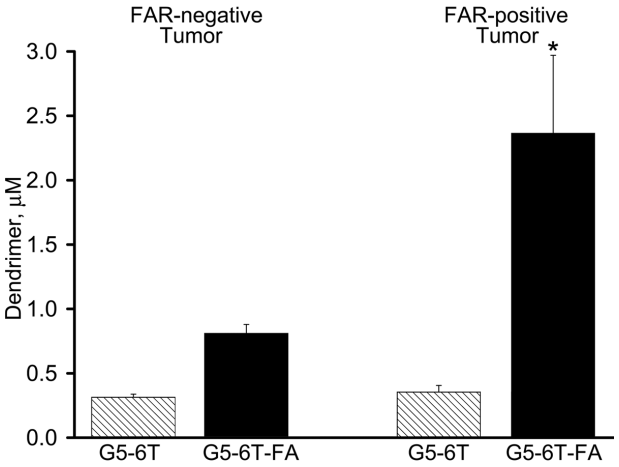

Figure 2: Tumor targeting of FA-conjugated dendrimer. KB (FAR-positive) and MCA207 (FAR-negative) cell tumors were developed in SCID mice. The mice were injected with 10 nmols of the dendrimers G5-6T or G5-6T-FA; after 15 hours, the tumor fluorescence was quantified by TPOFF. * $p = < 0.05$ vs. KB tumor injected with G5-6T and FAR-negative tumor injected with either G5-6T or G5-6T-FA. (Reprinted with permission from T. P. Thomas, M. T. Myaing, J. Y. Ye, *et al*., "Detection and analysis of tumor fluroscence using a two-photon optical fiber Probe," *Biophys. J*. **86**(6), 3959–3965, 2004.)

mimetic that would bind to an overexpressed growth factor receptor has several advantages over targeting using the intact protein ligands. The smaller size of the peptide would result in better pharmacokinetics and faster blood clearance than the parent protein. In addition, the conjugation chemistry with the peptides is easier and more stable in comparison to that using the intact protein.

Specific peptides that bind to a tumor cell can be determined by using random peptide phage libraries. In this procedure, random peptide

phage libraries are allowed to bind and internalize into the cell by the repeated cycling steps of cellular internalization, washing of surface bound phages, and amplification of the internalized phage in bacteria. The phage DNA purified from the final bacterial preparation is sequenced, and the corresponding peptide identified. Once a tumor-specific peptide has been identified, it must be determined whether the peptide is stable in the blood and whether or not it is readily hydrolyzed by peptidases. If the peptides are susceptible to plasma peptidases, the peptides have to be modified to inhibit the degradation by peptidases. Techniques such as peptide "end-capping", substitution of an L-amino acid with a D-amino acid, can be used to prevent hydrolysis by peptidases, provided these do not affect the binding of the peptide on the receptor. As the flexibility of the amino acids may be important for the binding of the peptide to the receptors, introduction of a spacer (such as an additional small peptide) between the active peptide and the polymer is important.

Peptides that bind to receptors such as integrins,[42] the human EGF receptor 2 (HER2),[43,44] and the leutenizing hormone-releasing hormone (LHRH)[45] have been tested. Our studies have shown that PAMAM conjugates of the $\alpha_v\beta_3$ integrin-binding cyclic peptide "RGD 4C" (Arg-Gly-Asp) bind and internalize into integrin-expressing cells *in vitro* (Figure 3).[30] As the integrin proteins are involved in the regulation of tumor neovascularization, the targeting of integrin would suppress tumor growth through nutrient and oxygen deprivation. One drawback of targeting the vascular cells is that, because the cancer cells are not directly targeted and killed, the effect on the cancer cells may be more cytostatic rather than cytotoxic.

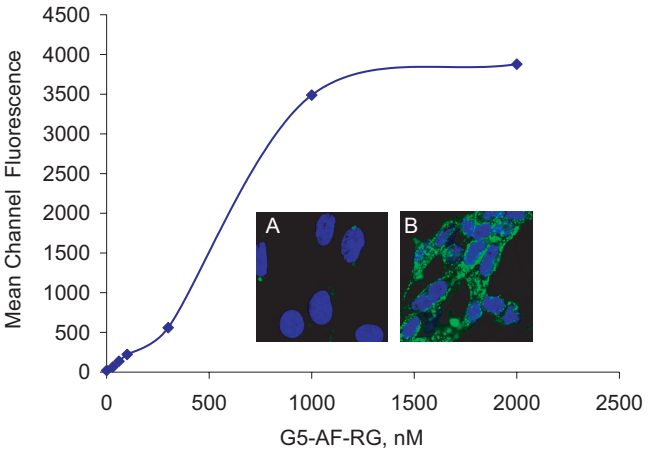

Figure 3: Binding and internalization of G5-AF-RGD (G5-AF-RG) on $\alpha_v\beta_3$ integrin-expressing HUVEC cells. Cells were incubated with different concentrations of the conjugate for 1 hour, and the fluorescence of the rinsed cells was taken in a flow cytometer. Inset: Confocal images of G5-AF-RGD-treated cells under similar conditions. Cells were cultured on coverslips and, after the treatment, fixed by paraformaldehyde and staining the nuclei with DAPI (blue stain). The results show the presence of the G5-AF-RGD (green stain) in the cytosolic compartment. Panels A and B show control and G5-AF-RGD-targeted cells, respectively. (*Chemical Communications*, **46**, 5739–5741, 2005.)

Antibodies which bind to cell surface antigens which are known to be overexpressed in tumor cells have been extensively studied as targeting agents.[46] We have tested several dendrimer-antibody conjugates *in vitro* and *in vivo*.[31,47,48] These antibodies include 60bca or J591 and Herceptin, which bind respectively to the antigen CD14, the prostate-specific membrane antigen (PSMA), and HER2. These conjugates target and internalize into the corresponding antigen-expressing cells *in vivo* (Figure 4). One disadvantage in using an intact antibody as the targeting molecule is the poor

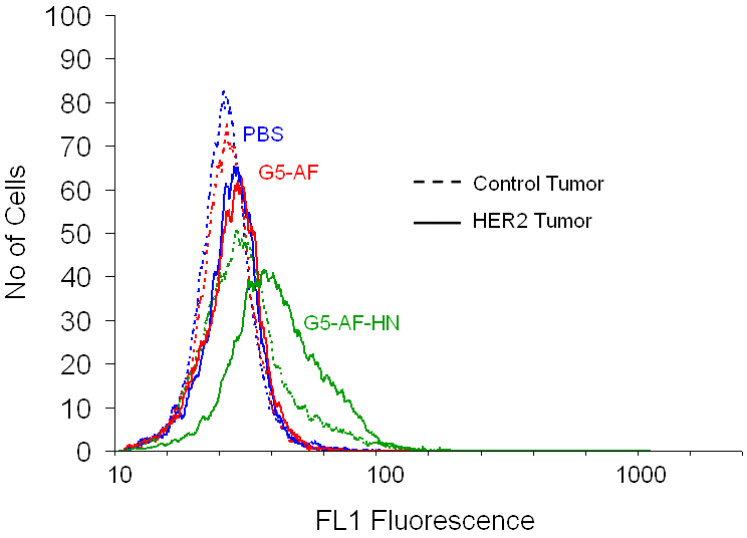

Figure 4: Binding of G5-Alexafluor (G5-AF) and G5-Alexafluor-Herceptin (G5-AF-HN) in Control- and HER2-expressing MCA 207 mice xenograft tumors *in vivo*. Tumors were developed in SCID mice by subcutaneous injection of the two cell lines, respectively on the left and right flank areas of the mice. When the tumors were about 0.7 cm in diameter, 2.4 nmols of the conjugates or its vehicle (PBS) were injected intravenously through the tail vein. The tumors were isolated after 15 hours, the cells were separated by collagenase digestion, and they were analyzed by flow cytometry. (Reprinted with permission from *Bioconjugate Chemistry* **17**(5), 1109–1115, 2006. Copyright (2006) American Chemical Society.)

targeting efficiency because of the very low tumor-to-blood ratio achieved. The Fc region is the primary recognition site for the immunogenecity of the antibody and for uptake into the liver, which lead to a host immune reaction and removal of the antibody conjugate in the liver.

The immunogenecity can be overcome by "humanizing" the antibody by recombining the immunogenic sites of the animal-derived antibody through genetic engineering technology. One alternative to using

an intact antibody is using antibody fragments such as the divalent $F(ab')_2$, the monovalent Fab, and the single chain Fv segment. These smaller-sized fragments, in addition to being smaller and providing better pharmacokinetics, will have reduced immunogenecity because of the removal of the Fc region. The association of the Fab fragment with carriers can further improve the biodistribution and tumor deposition of a Fab in comparison with an entire antibody molecule. Targeting of an albumin-Fab (trastuzumab derived) bifunctional molecule can be increased in comparison to the entire trastuzumab antibody (HERCEPTIN) in the mouse mammary tumor virus/HER2 allograft models *in vivo*.[49]

6.2.7 Chemotherapeutic drugs for inducing tumor cell apoptosis

Second to the selection of an appropriate targeting molecule, a chemotherapeutic drug that is suitable for inducing apoptosis of the targeted tumor cells has to be chosen. Although there are more than 100 FDA-approved cancer therapeutic drugs, only about 20 have been used for *in vivo* and clinical studies. Some of the commonly used chemo-therapeutic drugs include doxorubicin (intercalates into DNA and stops DNA replication), methotrexate (inhibits the enzyme dihydrofolate reductase and stops nucleotide and DNA synthesis), taxol (promotes microtubule assembly and causes cell cycle arrest), cisplatin, vincristine (inhibits microtubule assembly and causes cell cycle arrest), and 5-fluorouracil (inhibits thymidylate synthase). Any chemotherapeutic drug proven to be effective for anti-tumor therapy can be used for conjugation to the PAMAM dendrimer provided there are functional groups present on the drug for conjugation to the amine of the PAMAM dendrimer.[3]

Several dendrimer conjugates with drugs such as methotrexate 19 and taxo150 have been tested for conjugation with PAMAM dendrimer. PAMAM dendrimers with FA as the targeting molecule and methotrexate as the chemotherapeutic specifically target and kill FAR-expressing KB cells *in vitro* and *in vivo* (Figure 5).[15,16,19]

In vivo targeting of a nanoparticle conjugated drug improves the therapeutic response to anticancer MTX drug and allows the simultaneous monitoring of its uptake by tumors.[16] The conjugates are injected intravenously into immunodeficient mice bearing xenograft human KB tumors that overexpress the folic acid receptor. In contrast to non-targeted polymer, folate-conjugated nanoparticles concentrate in the tumor and liver tissue over four days after administration. The tumor tissue localization of

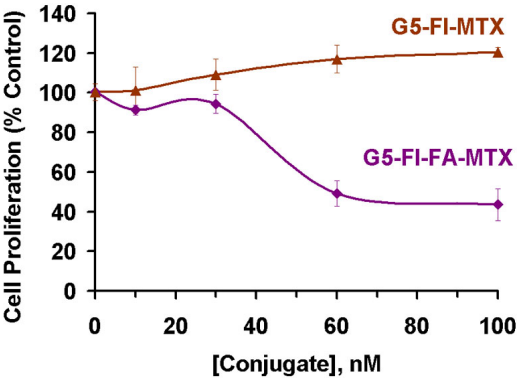

Figure 5: Comparison of cytotoxicity induced by G5-FI-MTX and G5-FI-FA-MTX. KB cells were exposed to different concentrations of the dendrimer conjugates shown for four days, and the XTT assay was performed. The data is plotted as percent growth of treated cells versus control cells incubated with the vehicle PBS.

the folate-targeted polymer can be attenuated by prior intravenous injection of free folic acid.

Confocal microscopy confirms the internalization of the drug conjugates into the tumor cells.[16] This is consistent with our *in vitro* binding and internalization studies of the multi-functional dendrimer conjugate.[19] Internalization coupled with a high cytosolic concentration of the drug provides the possibility of overcoming drug non-responsiveness due to the action of the membrane P-glycoprotein in resistant tumor cells.[51]

Significant improvements are achieved in the therapeutic index of a targeted polymer-drug conjugate over a free drug, and this could have occurred from both a decrease in the conjugate's toxicity and an increase in its effectiveness.[16] Prior studies from our group and others have shown that, when injected into the vascular system in mice, non-targeted PAMAM dendrimers distribute according to size with similar characteristics to proteins of the same molecular weight.[52] In addition, neutralization of the amine surface charge of the dendrimer is essential to preventing the toxicity and non-specific uptake of the drug conjugates.[15,53]

The anti-tumor activity of the targeting polymer therapeutic is equal, whether or not it carried FITC. This suggests that the four chemically distinct moieties on the conjugate — the folic acid, fluorescent dye, radiolabel, and methotrexate — function independently. Methotrexate conjugated to the dendrimer has significantly lower toxicity and a 10-fold higher efficacy compared with free MTX at an equal cumulative dose (Figure 6(a)). Higher doses of MTX on the conjugate compared with the free drug can be delivered due to the longer survival of mice receiving the therapeutic nanoparticle (Figure 6(b)).

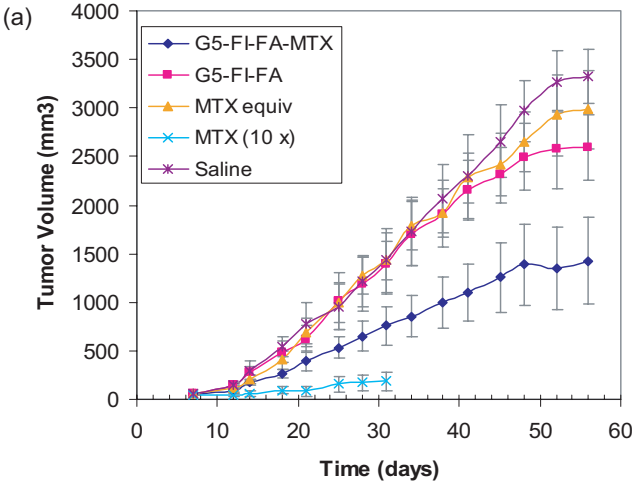

Figure 6(a): Tumor growth in SCID mice bearing KB xenografts during treatment with G5-FI-FA-MTX conjugate and free MTX. Tumor volume (mm^3) was calculated using the formula for a standard volume of an ellipsoid. The conjugate G5-FI-FA-MTX (blue) is effective in tumor growth delay. The dose of MTX (yellow) equivalent to the MTX dose of G5-FI-FA-MTX (blue) is equally ineffective as the saline (magenta) and the control G5-FI-FA conjugate (pink). A ten-times higher dose of free MTX inhibits tumor growth but affects about 30% of the mice's body weight and is lethal (LD 50) at 32 days. During 15 bi-weekly injections (56 days) of the experiment, the dose of free MTX equivalent to the MTX in the G5–FI-FA-MTX conjugate and all of the doses of the control treatments were not toxic. The values are the means ± SEM from five mice. (*Cancer Research*, **65**(12), 5317–5324, 2005.)

The biochemical events following the entry of the methotrexate conjugate into the targeted cell is not clearly understood. In the conjugate, the FA is linked through an amide linkage and the MTX through an ester linkage. The ester linkage was intended for allowing the release of the drug in the endosomes at acidic pH and through hydrolysis by the cellular

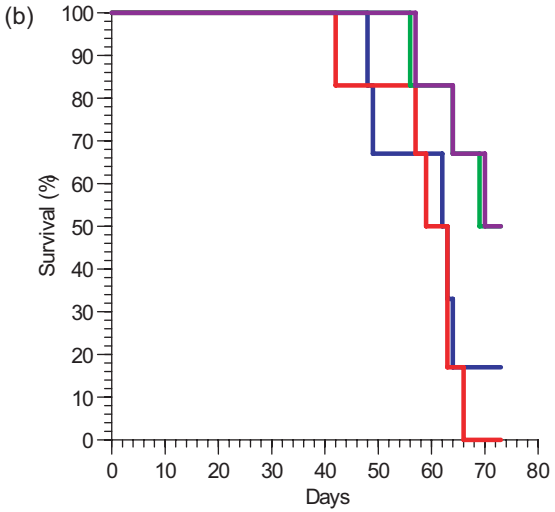

Figure 6(b): Representative survival rate of SCID mice bearing KB tumors. During 73 days of the trial, 50% of the mice receiving two different lots of G5–FA-MTX conjugates (green and purple) survived with significantly smaller tumors, compared with those treated with free methotrexate (red) and in the saline (blue) groups. (*Cancer Research*, **65**(12), 5317–5324, 2005).

esterases. Nevertheless, our studies *in vitro* using acidic conditions and in the presence of purified non-specific esterases have failed to show hydrolysis (unpublished observation). On the other hand, the conjugate inhibited purified DHFR with an IC_{50} similar to that of free methotrexate (Figure 7).

6.2.8 Dendrimer-based multifunctional nanoparticles for quantification of apoptosis

The mechanism through which a chemotherapeutic drug induces cell death is by a process called apoptosis or programmed cell death.[3,54] Real-time quantification of drug-induced apoptosis is important to following the

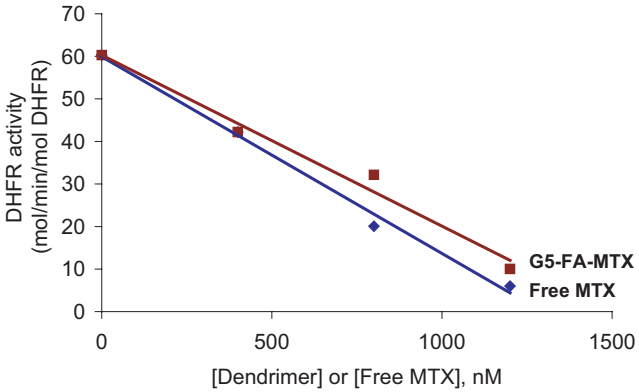

Figure 7: Inhibition of DHFR activity by free MTX and G5-FA-MTX. The reaction mixture contained 50 mM Tris HCl, pH 7.5, 150 mM KCl, 10 mM mercaptoethanol, 120 µM NADPH, 0.8 µM recombinant bacterial DHFR, 120 µM dihydrofolate, and different concentrations of free MTX or G5-FA-MTX in a total volume of 100 µl. The reaction was started by adding DHFR, and the absorbance at 340 nm was monitored for 4–5 minutes at room temperature in a Beckman spectrophotometer. The specific activity was calculated from the slope of the initial linear portion of the velocity curves.

physiological effectiveness of the drug. As the apoptotic process involves a cascade of biochemical changes, an intermediate biomolecule of the apoptosis pathway may be utilized to monitor fluorescence changes of a molecule delivered through the dendrimer. This may be done by the synthesis of fluorescence resonance energy transfer (FRET)-based dendrimer conjugates by conjugation of a donor-acceptor fluorophore to the dendrimer. For example, a donor and acceptor fluorophore can be coupled though the peptide "DEVD", a substrate of the apoptotic enzyme caspase-3, which will have a reduced fluorescence due to the FRET action between the dyes. The intracellular hydrolysis of this peptide will result in an

increase in fluorescence which can be quantified using appropriate techniques. A detailed description of the application of dendrimer-based conjugates in monitoring apoptosis is given in a separate chapter.

6.3 Dendrimer-Based Nanoparticles for Tumor MRI Imaging

The PAMAM dendrimer is a suitable platform for the conjugation and tumor targeting of magnetic resonance imaging (MRI) agents. A targeted contrast agent can be imaged using MRI non-invasively, and the method provides high temporal and spatial imaging resolution of up to 100 μm. Dendrimer-Gd complexes of different generations and sizes have been previously tested as MRI contrast agents. Amine-terminated PAMAM-Gd complexes with smaller size (<3 nm) are rapidly extravasated to diffuse throughout the body, whereas complexes between 3 nm and 6 nm are quickly excreted through the kidney. Dendrimers with sizes from 5 nm to 7 nm have a preference for extravasation into the tumor tissue, whereas those having a size between 7 nm and 12 nm are largely retained in the circulation.[28] Based on the observed differences in the body distribution of the conjugates, generations 5 and 6 of the PAMAM dendrimers appear to be ideal for tumor imaging/targeting, whereas sizes above 7 may be suitable for vascular imaging because of their retention in the vasculature.

6.4 Cluster Dendrimers Designed for Easy Conjugation of Multiple Functions

There are limitations for synthesizing different types of molecules onto the same dendrimer surface — such as decreased solubility, low yield, and steric

hindrance between molecules, etc. — due to the multiple synthetic and purification steps involved. We have attempted to overcome this problem by designing and synthesizing dendrimer clusters with each dendrimer molecule in the cluster carrying a specific function, such as being a targeting molecule or being an imaging agent.[55] This is done by linking two different dendrimer molecules carrying separate functions either covalently or through a DNA molecule. The advantage of such a cluster dendrimer is the easy combinatorial synthesis of a "custom" conjugate that would be specific for a patient's particular tumor type for imaging, specific targeting, and for the delivery of a drug that is effective for the tumor. Our *in vitro* studies show the applicability of a simple cluster dendrimer for tumor targeting, in which two dendrimer molecules with two different functions conjugated to complementary DNA molecules are allowed to anneal to form a cluster (Figure 8).

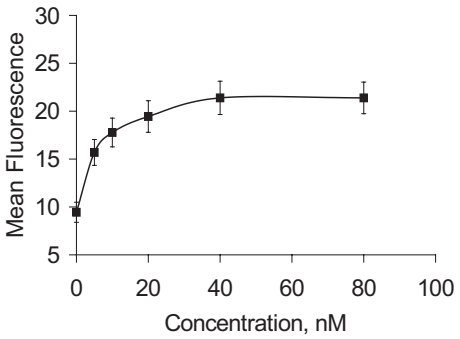

Figure 8: The concentration-dependent saturation binding of the DNA-linked cluster to KB cells overexpressing the folate receptor. FA- and FI-conjugated dendrimers were linked through DNA, purified, and the binding of the cluster to KB cells was determined in a flow cytometer following incubation for 1 hour at 37°C. (*Chemistry and Biology*, **12**, 35–43, 2005.)

6.5 Summary

PAMAM dendrimers are biocompatible nanosized macromolecules highly suitable for carrying and delivering molecules into tumor cells *in vitro* and *in vivo*. PAMAM dendrimers engineered to carry various functions on their surfaces may perform multiple biological tasks such as binding to a cancer cell, releasing a drug to induce apoptosis of the cancer cell and measuring the extent of cell death. Two or more dendrimer molecules can be designed by linking through DNA or other linkers for the relatively easier synthesis of a custom nanodevice. In addition to tumor targeting, the PAMAM-based targeting may be useful for the targeted delivery of other drugs for other diseases to minimize the toxicity of the free drug.

6.6 References

1. Y. Luo and G. D. Prestwich, Cancer-targeted polymeric drugs, *Current Cancer Drug Targets*, **2**(3), 209–226, 2002.
2. D. G. Savage and K. H. Antman, Imatinib mesylate — a new oral targeted therapy, [see comment], *New England Journal of Medicine*, **346**(9), 683–693, 2002.
3. I. J. Majoros, T. P. Thomas, and J. R. Baker Jr., Molecular engineering in nanotechnology: Engineered drug delivery. In, M. Rieth, W. Schommers, (Eds.), *Handbook of Theoretical and Computational Nanotechnology*, American Scientific Publishers, 2006.
4. R. Duncan and R. Duncan, The dawning era of polymer therapeutics, *Nature Reviews Drug Discovery*, **2**(5), 347–360, 2003.

5. L.Y. Qiu and Y. H. Bae, Polymer architecture and drug delivery, *Pharmaceutical Research*, **23**(1), 1–30, 2006.
6. M. J. Vicent and R. Duncan, Polymer conjugates: Nanosized medicines for treating cancer, *Trends in Biotechnology*, **24**(1), 39–47, 2006.
7. A. Nori and J. Kopecek, Intracellular targeting of polymer-bound drugs for cancer chemotherapy, *Advanced Drug Delivery Reviews*, **57**(4), 609–636, 2005.
8. A. K. Patri, I. J. Majoros, and J. R. Baker Jr., Dendritic polymer macro-molecular carriers for drug delivery, *Current Opinion in Chemical Biology*, **6**(4), 466–471, 2002.
9. S. Svenson and D. A. Tomalia, Dendrimers in biomedical applications-reflections on the field, *Advanced Drug Delivery Reviews*, **57**(15), 2106–2129, 2005.
10. H. F. Chow, T. K. Mong, M. F. Nongrum, and C. W. Wan , The synthesis and properties of novel functional dendritic molecules, *Tetrahedron*, **54**, 8534–8660, 1998.
11. M. Fischer and F. Vögtle, Dendrimers. From design to appplication — A progress report, *Angew. Chem. Int. Ed. Engl*., **38**, 884–905, 1999.
12. D. A. Tomalia and I. J. Majoros, Dendrimeric supramolecular and supramacro-molecular assemblies, In, A. Ciferri, Ed. *Supramolecular Polymers*, Marcel Dekker, NY, 359–435, 2002.
13. U. Boas and P. M. H. Heegaard, Dendrimers in drug research, *Chemical Society Reviews*, **33**(1), 43–63, 2004.
14. A. W. Bosman, H. M. Janssen, and E. W. Meijer, About dendrimers: Structure, physical properties, and applications, *Chem. Rev*., **99**, 1665–1668, 1999.

15. A. Quintana, E. Raczka, L. Piehler, I. Lee, A. Myc, I. Majoros, A. K. Patri, T. Thomas, J. Mule, and J. R. Baker Jr., Design and function of a dendrimer-based therapeutic nanodevice targeted to tumor cells through the folate receptor, *Pharmaceutical Research*, **19**(9), 1310–1316, 2002.

16. J. F. Kukowska-Latallo, K. A. Candido, Z. Cao, S. S. Nigavekar, I. J. Majoros, T. P. Thomas, L. P. Balogh, M. K. Khan, and J. R. Baker Jr., Nanoparticle targeting of anticancer drug improves therapeutic response in animal model of human epithelial cancer, *Cancer Research*, **65**(12), 5317–5324, 2005.

17. I. J. Majoros, B. Keszler, S. Woehler, T. Bull, and J. R. Baker Jr., Acetylation of poly(amidoamine) dendrimers, *Macromolecules*, **36**, 5526–5529, 2003.

18. I. J. Majoros, T. P. Thomas, C. B. Mehta, and J. R. Baker Jr., Poly(amidoamine) dendrimer-based multifunctional engineered nanodevice for cancer therapy, *Journal of Medicinal Chemistry*, **48**(19), 5892–5899, 2005.

19. T. P. Thomas, I. J. Majoros, A. Kotlyar, J. F. Kukowska-Latallo, A. Bielinska, A. Myc, and J. R. Baker Jr., Targeting and inhibition of cell growth by an engineered dendritic nanodevice, *Journal of Medicinal Chemistry*, **48**(11), 3729–3735, 2005.

20. T. P. Thomas, M. T. Myaing, J. Y. Ye, K. Candido, A. Kotlyar, J. Beals, P. Cao, B. Keszler, A. K. Patri, T. B. Norris, and J. R. Baker Jr., Detection and analysis of tumor fluorescence using a two-photon optical fiber probe, *Biophysical Journal*, **86**(6), 3959–3965, 2004.

21. T. P. Thomas, J. Y. Ye, C.-S. Yang, M. Myaing, I. J. Majoros, A. Kotlyar, Z. Cao, T. B. Norris, and J. R. Baker Jr., Tissue distribution and real-time fluorescence measurement of a tumor-targeted nanodevice by a two photon optical fiber fluorescence probe, *Proceedings of the SPIE*, 6095, 2006.
22. H. Kobayashi, S. Kawamoto, T. Saga, N. Sato, A. Hiraga, T. Ishimori, J. Konishi, K. Togashi, and M. W. Brechbiel, Positive effects of polyethylene glycol conjugation to generation-4 polyamidoamine dendrimers as macro-molecular MR contrast agents, *Magnetic Resonance in Medicine*, **46**(4), 781–788, 2001.
23. R. Duncan and L. Izzo, Dendrimer biocompatibility and toxicity, *Advanced Drug Delivery Reviews*, **57**(15), 2215–2237, 2005.
24. R. Jevprasesphant, J. Penny, R. Jalal, D. Attwood, N. B. McKeown, and A. D'Emanuele, The influence of surface modification on the cytotoxicity of PAMAM dendrimers, *International Journal of Pharmaceutics*, **252**(1–2), 263–266, 2003.
25. N. Malik, R. Wiwattanapatapee, R. Klopsch, K. Lorenz, H. Frey, J. W. Weener, E. W. Meijer, W. Paulus, and R. Duncan, Dendrimers: Relationship between structure and biocompatibility *in vitro*, and preliminary studies on the biodist-ribution of 125I-labelled polyamidoamine dendrimers *in vivo*, [erratum appears in *J. Control Release* 2000 Aug. 10, **68**(2), 299–302]. *Journal of Controlled Release*, **65**(1–2), 133–148, 2000.
26. S. Hong, A. U. Bielinska, A. Mecke, B. Keszler, J. L. Beals, X. Shi, L. Balogh, B. G. Orr, J. R. Baker Jr., and M. M. Banaszak Holl,

Interaction of poly(amido-amine) dendrimers with supported lipid bilayers and cells: Hole formation and the relation to transport, *Bioconjugate Chemistry*, **15**(4), 774–82, 2004.

27. J. C. Roberts, M. K. Bhalgat, R. T. Zera, J. C. Roberts, M. K. Bhalgat, and R. T. Zera, Preliminary biological evaluation of polyamidoamine (PAMAM) Starburst dendrimers, *Journal of Biomedical Materials Research*, **30**(1), 53–65, 1996.
28. H. Kobayashi and M. W. Brechbiel, Nano-sized MRI contrast agents with dendrimer cores, *Advanced Drug Delivery Reviews*, **57**(15), 2271–2286, 2005.
29. S. D. Konda, M. Aref, S. Wang, M. Brechbiel, and E. C. Wiener, Specific targeting of folate-dendrimer MRI contrast agents to the high affinity folate receptor expressed in ovarian tumor xenografts, *Magma*, **12**(2–3), 104–113, 2001.
30. R. Shukla, T. P. Thomas, J. Peters, A. Kotlyar, A. Myc, and J. R. Baker Jr., Tumor angiogenic vasculature targeting with PAMAM dendrimer-RGD conjugates, *Chem. Commun. (Camb.),* **46**, 5739–5741, 2005.
31. T. P. Thomas, A. K. Patri, A. Myc, M. T. Myaing, J. Yong Ye, T. B. Norris, and J. R. Baker Jr., *In vitro* targeting of synthesized antibody-conjugated dendrimer nanoparticles, *Biomacromolecules*, **5**(6), 2269– 2274, 2004.
32. L. Balogh and D. A. Tomalia, Poly (amidoamine) dendrimer-templated nanocomposites, 1: Synthesis of zerovalent copper nanoclusters, *J. Am. Chem. Soc*., **120**, 7355–7356, 1998.

33. N. Beck Tan, L. Balogh, and S. Trevino, Structure of metallo-organic nano-composites produced from dendrimer complexes, *Proceedings of ACS PMSE*, **77**, 120, 1997.
34. A. D'Emanuele and D. Attwood, Dendrimer-drug interactions, *Advanced Drug Delivery Reviews*, **57**(15), 2147–2162, 2005.
35. L. P. Balogh, D. R. Swanson, D. A. Tomalia, G. L. Hagnauer, and A. T. McManus, Dendrimer-silver complexes and nanocomposites as antimicrobial agents, *Nano Letters*, **1**, 18–21, 2001.
36. A. Bielinska, J. D. Eichman, I. Lee, J. R. Baker Jr., and L. P. Balogh, Imaging {Au0-PAMAM} gold-dendrimer nanocomposites in cell, *J. Nanoparticle Res*., **4**, 395–403, 2002.
37. N. Malik, E. G. Evagorou, R. Duncan, N. Malik, E. G. Evagorou, and R. Duncan, Dendrimer-platinate: A novel approach to cancer chemotherapy, *Anti-Cancer Drugs*, **10**(8), 767–776, 1999.
38. A. K. Patri, J. F. Kukowska-Latallo, and J. R. Baker Jr., Targeted drug delivery with dendrimers: Comparison of the release kinetics of covalently conjugated drug and non-covalent drug inclusion complex, *Advanced Drug Delivery Reviews*, **57**(15), 2203–2214, 2005.
39. A. R. Hilgenbrink and P. S. Low, Folate receptor-mediated drug targeting: From therapeutics to diagnostics, *Journal of Pharmaceutical Sciences*, **94**(10), 2135–2146, 2005.
40. N. Parker, M. J. Turk, E. Westrick, J. D. Lewis, P. S. Low, and C. P. Leamon, Folate receptor expression in carcinomas and normal tissues determined by a quantitative radioligand binding assay, *Analytical Biochemistry*, **338**(2), 284–293, 2005.

41. Y. Lu and P. S. Low, Folate-mediated delivery of macromolecular anticancer therapeutic agents, *Advanced Drug Delivery Reviews*, **54**(5), 675–693, 2002.

42. W. Arap, R. Pasqualini, and E. Ruoslahti, Cancer treatment by targeted drug delivery to tumor vasculature in a mouse model, [see comment], *Science*, **279**(5349), 377–380, 1998.

43. R. Murali, Q. Liu, X. Cheng, A. Berezov, M. Richter, K. Furuchi, M. I. Greene, and H. Zhang, Antibody like peptidomimetics as large scale immunodetection probes, *Cellular & Molecular Biology*, **49**(2), 209–216, 2003.

44. M. Shadidi and M. Sioud, Identification of novel carrier peptides for the specific delivery of therapeutics into cancer cells, *FASEB Journal*, **17**(2), 256–258, 2003.

45. S. S. Dharap, B. Qiu, G. C. Williams, P. Sinko, S. Stein, and T. Minko, Molecular targeting of drug delivery systems to ovarian cancer by BH3 and LHRH peptides, *Journal of Controlled Release*, **91**(1–2), 61–73, 2003.

46. D. Schrama, R. A. Reisfeld, and J. C. Becker, Antibody targeted drugs as cancer therapeutics, *Nature Reviews Drug Discovery*, **5**(2), 147–159, 2006.

47. A. K. Patri, A. Myc, J. Beals, T. P. Thomas, N. H. Bander, and J. R. Baker Jr., Synthesis and in vitro testing of J591 antibody-dendrimer conjugates for targeted prostate cancer therapy, *Bioconjugate Chemistry*, **15**(6), 1174–1181, 2004.

48. R. Shukla, T. P. Thomas, J. L. Peters, J. Kukowska-Latallo, A. K. Patri, A. Kotlyar, and J. R. Baker Jr., HER2 specific tumor targeting

with dendrimer conjugated anti-HER2 mAb, *Bioconjugate Chemistry*, **17**, 1109–1115, 2006.

49. M. S. Dennis, H. K. Jin, D. Dugger, R. H. Yang, L. McFarland, A. Ogasawara, S. Williams, M. J. Cole, S. Ross, and R. Schwall, Imaging tumors with an albumin-binding Fab, a novel tumor-targeting agent, *Cancer Research*, **67**(1), 254–261, 2007.
50. I. J. Majoros, A. Myc, T. Thomas, C. B. Mehta, and J. R. Baker Jr., PAMAM dendrimer-based multifunctional conjugate for cancer therapy: Synthesis, characterization, and functionality, *Biomacromolecules*, **7**(2), 572–579, 2006.
51. R. Krishna and L. D. Mayer, Multidrug resistance (MDR) in cancer. Mechanisms, reversal using modulators of MDR and the role of MDR modulators in influencing the pharmacokinetics of anticancer drugs, *Eur. J. Pharm. Sci*., **11**(4), 265–283, 2000.
52. J. C. Roberts, M. K. Bhalgat, and R. T. Zera, Preliminary biological evaluation of polyamidoamine (PAMAM) Starburst dendrimers, *J. Biomed. Mater. Res*., **30**(1), 53–65, 1996.
53. S. S. Nigavekar, L. Y. Sung, M. Llanes, A. El-Jawahri, T. S. Lawrence, C. W. Becker, L. Balogh, and M. K. Khan, 3H dendrimer nanoparticle organ/tumor distribution, *Pharm. Res*., **21**(3), 476–483, 2004.
54. D. R. Green and G. Kroemer, Pharmacological manipulation of cell death: Clinical applications in sight? *Journal of Clinical Investigation*, **115**(10), 2610–2617, 2005.

55. Y. Choi, T. Thomas, A. Kotlyar, M. T. Islam, and J. R. Baker Jr., Synthesis and functional evaluation of DNA-assembled polyamidoamine dendrimer clusters for cancer cell-specific targeting [see comment], *Chemistry & Biology*, **12**(1), 35–43, 2005.

This page intentionally left blank

Chapter 7

Dendrimer-based Targeted Apoptosis Sensors for Medical Application

Andrzej Myc, Chandan B. Mehta & István J. Majoros

Outline

7.1 Introduction

There are several criteria for proper selection of a targeted apoptosis sensors delivery system (ASDS). The targeting moiety of the system must target a specific receptor on the tumor. The ASDS must be soluble in aqueous body fluids and maintain its stability in blood before it arrives at the target. The ASDS must be able to penetrate through tissue barriers and should have the ability to migrate into the interstitial fluid to reach the cancer cells. Along with these characteristics, the ASDS must also be able to be endocytosed into the cancer cell and release the apoptosis sensors into the appropriate cell compartments to sense apoptosis. The exogenous

components of the system must also have the ability to be excreted from the body with or without undergoing biodegradation, and the monomer components of each macromolecule must be non-toxic so that, if the macromolecule undergoes biodegradation, the monomeric units will not cause toxicity to the system.

In recent years more and more techniques became available to measure the degree of apoptosis as a function of cell death. Apoptosis, often called "programmed cell death" (PCD), is a process in which a cell actively participates in its own destruction. PCD helps maintain tissue homeostasis, controls irregular cell growth, and regulates the immune system function.[1–5] Particular molecular, chemical, and morphological changes to a cell can trigger the apoptotic pathway. PCD leads to characteristic cell morphological changes such as cell fragmentation, chromatin condensation, membrane blebbing, and cytoplasmic shrinkage.[6] The central component of PCD is a cascade of proteolytic enzymes called caspases, a structurally related group of cysteine aspartate-specific proteases.[7] Caspase-3 is one of the most frequently activated cysteine proteases during the process of apoptosis. While apoptosis is possibly reversible if detected in its earliest stages, once caspase activity has begun (the final phases of apoptosis), the process becomes irreversible. Therefore, activation of the caspase family is one of the earliest markers of an apoptotic event. The function of caspase-3 includes protein degradation and DNA fragmentation. The high specificity of caspase-3 to cleave proteins containing a valine-aspartic acid sequence is of the utmost interest to our work.

In the treatment of cancer, tumor cells can respond to radio- or chemotherapy by undergoing apoptosis. For some tumors the degree of

apoptotic cell death has been shown to correlate with subsequent tumor growth delay and the rate of tumor cure.[8,9] The non-invasive detection of apoptosis is likely, therefore, to be a useful tool in the clinic, both for monitoring disease progression and for assessing the response to therapy.

The applicability of poly(amidoamine) (PAMAM) dendrimers as a platform for the targeted delivery of apoptosis sensors *in vitro* has been demonstrated.[10] The apoptosis sensors will help to monitor the responsiveness of cancer cells to the course of chemo- or radiotherapy and will facilitate the analysis and degree of apoptosis in targeted cells on a real-time basis. Below we show the synthesis, characterization, and *in vitro* targeting of an engineered PAMAM nanodevice in which folic acid (FA) is conjugated as the targeting molecule and either an $(Asp)_2$-R110 single dye sensor or a caspase-specific fluorescence resonance energy transfer (FRET)-based agent (PhiPhiLux™ G_1D_2) are used for detecting apoptosis. These conjugates specifically target FA-receptor (FAR)-positive cells.

Here we describe the synthesis and biological function of two kinds of targeted apoptosis sensors. One is the $(Asp)_2$-R110 single dye sensor and the other is a fluorescence resonance energy transfer (FRET)-based dye that becomes fluorescent in cells due to the actions of activated caspases.[11] Fluorescence resonance energy transfer (FRET) imaging agents, which contain two distinct dyes, are widely used to detect apoptosis. When these two conjugated dyes are cleaved by caspase-3, the fluorescent module is released and the amount of fluorescence can then be quantified by flow cytometry.[12,13]

7.2 Apoptosis as a Biological Event

Kerr *et al*. originally described two forms of cell death, necrosis and apoptosis, which may occur in the absence of pathological manifestations.[14] Apoptosis, or programmed cell death, is a normal physiologic process that occurs during embryonic development as well as in maintenance of tissue homeostasis. The overabundance or deficiency of apoptosis in cells can lead to recognizable disease. Many illnesses can be commonly associated with a defect in apoptosis, including cancer diseases. Cell growth becomes out of control and proliferation of these malignant cells continues, increasing the ratio of cancerous to healthy cells and eventually leading to death if left uncontrolled.[15] It must be emphasized that an enormous number of research articles have been made available over the past few years. Figure 1 below illustrates the huge increase in articles published in the past few years, which has left us with an enormous amount of research to sift through in order to present the clearest version of the course of apoptosis.

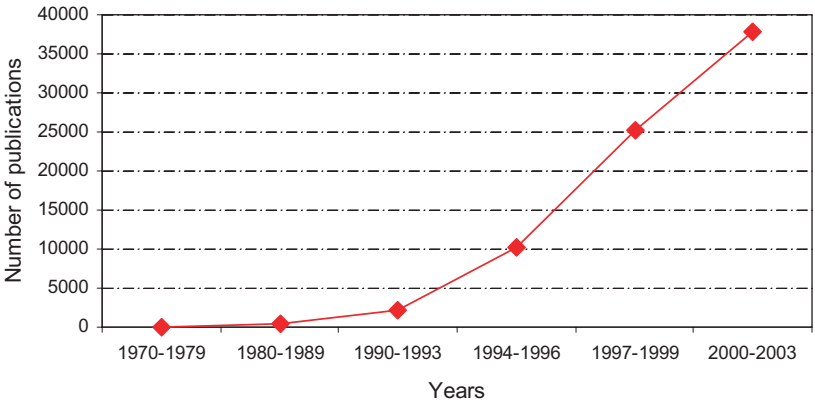

Figure 1: Chart of increase of journal articles published.

The term apoptosis, from the Greek word for "falling off" of leaves from a tree, is used to describe a process in which a cell actively participates in its own destructive processes. Certain morphological, biochemical and molecular changes characterize the apoptotic cascade. Events can be characterized to occur during the early, middle or late phases of the apoptotic process and are detected through the use of flow cytometry and fluorescence microscopy and through the newly developed atomic force microscopy (AFM). There are two pathways for induction of apoptosis via death signals, the mitochondria pathway and the death receptor pathway. Both pathways utilize caspases for the disassembly of cell structures, leading to cell death.

While the process of apoptosis is possibly reversible if detected in its earliest stages, once caspase activity has begun, the process becomes irreversible. Caspases, a structurally related group of cysteine aspartate-specific proteases, cleave peptide bonds following specific recognition sequences. They play a central role in activating apoptosis of vertebrate cells. Activation of the caspase family is one of the earliest markers of an apoptotic event. Early apoptotic events also consist of changes in the plasma membrane, including increased permeability, a loss of membrane symmetry, and construction of membrane-bound apoptotic bodies. Externalization of phosphatidyl serine from the inner to the outer plasma membrane leaflet also occurs (via caspase activation) and can be used as an indicator of the initialization of apoptosis.[16]

Additional events of apoptosis include the condensation of the cytoplasm and nucleus due to lysosomal rupture and cell shrinkage,

degradation of cellular proteins, membrane blebbing, condensation of nuclear chromatin, and inter-nucleosomal cleavage of DNA. In contrast to necrotic cell death, cell shrinkage is an elemental step in apoptosis for the instigation of death enzymes. Cells that have undergone shrinkage show an increased presence of caspase-3 like activity and have fragmented DNA.[16]

In the past few years, great emphasis has been placed on the mitochondria as important components to the apoptotic process. While there has been some uncertainty as to the order these events take place (caspase activation, then mitochondrial activity or, vice versa) or whether the mitochondria even play a vital role in the apoptotic process,[15] there are at least three general mechanisms occurring in the apoptotic cascade which involve cell mitochondria: (1) disruption of the electron transport chain, which means effectively, the loss of cell metabolism and ATP production; (2) the release of caspase activating proteins; and (3) alteration of the redox potential.[17]

The alteration of cell metabolism, largely due to a decrease in mitochondrial respiration, is a key step toward cell death.[18] Disruptions of the mitochondria begin with a decrease in membrane potential. Research by K. M. Heiskanen *et al*. supports that a decrease in membrane potential does not occur partially in all mitochondria within a cell, but occurs *fully* (full depolarization) within a finite proportion of mitochondria within a cell.[19] Opening of the mitochondrial permeability transition pore (PT pore) occurs as a result of this and allows for the passage of small molecules and ions, equilibrating the ion concentrations between the matrix and the inter-membrane space of the mitochondria. This equilibrium

causes destruction of the respiratory chain and rupturing of the mitochondrial outer membrane. Uncoupling of the respiratory chain leads to a decrease of ATP production in the mitochondria. The mitochondrial outer membrane ruptures due to the expansion of the matrix space inside the inner membrane (as a result of the equilibration of ion concentrations via the PT pore, the matrix experiences hyperosmolarity, causing it to swell). The folded cristae of the inner membrane allow for the inner membrane to have a much larger surface area than the outer membrane; therefore, the expansion of the inner membrane causes the outer membrane to rupture, leading to the release of cytochrome *c* and other caspase-activating proteins from the mitochondria into the cytosol.[17,19] The release of cytochrome *c* helps activate caspase-9, which cleaves procaspase-3 into its active form, caspase-3, which is largely responsible for the biochemical and morphological changes by which we so commonly characterize the apoptotic pathway. The final stage of apoptosis is characterized by the dying cells' fragmenting into "apoptotic bodies" which are rapidly eliminated by phagocytic cells without eliciting significant inflammatory damage to surrounding cells.

A variety of methods are used in order to detect whether or not apoptosis has occurred or is occurring within a cell. Double-dye fluorescence resonance energy transfer (FRET) detection as well as single-dye detection using rhodamine derivatives, Rhodamine 110, (which is used to detect caspase activity in cells), Rhodamine 123, and tetramethylrhodamine methyl ester (TMRM) and tetramethylrhodamine ethyl ester (TMRE) (which are used to measure membrane potential in mitochondria) are all commonly used as apoptosis detectors.

7.3 Apoptosis Detection Methods

Apoptosis detection methods are employed in order to determine if the apoptosis process has occurred or is in the process of occurring within cells. Apoptosis detection is most often performed using single- or double-dye detection methods. While there are a large variety of techniques in use, the following sections review the most commonly practiced. However, some methods are more valuable than others, as they are able to detect apoptosis *in vivo*. Most techniques nonetheless rely on *in situ* evaluation, as phagocytic tissues and cells quickly remove apoptotic cells left *in vivo*. Other detection methods require the cells to be fixed in order to detect the occurrence of apoptosis. Detection methods used to study apoptosis in fixed tissues are difficult to evaluate due to the structural complexity of cells and tissues; therefore, electron microscopy and two-photon microscopy are promising methods under investigation for further study of apoptosis in live tissues.[15]

Detectors are commonly made with one or two dyes, and by staining with these dyes or by coupling these dye reagents to a dendrimer or other delivery device, these dyes are delivered into the cell or attach to cell surfaces in order to determine whether apoptosis has occurred.

Detection methods can be categorized based on the phase of apoptosis they detect. Some techniques detect apoptotic activity based on membrane permeability and DNA fragmentation, while other methods detect activity based on chromatin condensation or caspase activity. Flow cytometry is widely used to quantify dye measurements as apoptotic, necrotic, and viable cells all exhibit different light scattering patterns. Most often,

apoptosis detection methods are used in combination with one another for better evaluation of the data. The majority of the methods of apoptosis detection are expensive as well as time-consuming and are subjected to a great deal of human error in handling and interpretation of test results; therefore, it is in an experimenter's best interest to fully utilize the methods available for proper evaluation of the data.[20] Table 1 lists apoptotic events, differentiated either by location in the cell or by type of event, that are detectable or made visible by imaging methods currently in use. These events are most commonly made detectable by surface staining dyes, flow cytometry, or by the other methods listed in italics. Research into imaging apoptosis is directed by the events below.

7.4 Single- and Double-Dye Apoptosis Sensors

Single-dye detection methods are often the less complex choice for apoptosis sensing. There are a wide variety of techniques in practice that utilize single dye detection. These include detection by coumarin-based dyes; rhodamine derivative dye; terminal deoxynucleotidyl transferase (TdT)-mediated end-labeling of DNA strand breaks; (TUNEL method); use of Annexin V for the detection of phosphatidyl serine on cell membranes and also in combination with propidium iodide (PI) for differentiation between apoptotic and necrotic cells; utilization of DNA-binding dyes such as the Hoechst dye and DAPI; use of green fluorescent protein (GFP) as a marker; and staining of cell surface and intracellular structures, which are measured quantitatively by flow cytometry.[21]

Detection of caspase-3 activity is often used to determine whether the apoptotic process is occurring. Coumarin-based fluorogenic substrates

Tab. 1. Detectable changes within a cell that denote the occurrence of an apoptotic event.

DNA Cleavage and Nuclear Events	*Biochemical Events*	*Mitochondrial Events*	*Changes in Surface Morphology and Composition*
Segmentation in chromatin, nuclei	Caspase activity, *FRET detection*, *Rhodamine derivatives,* various *fluorophores*	Permeability transition, detection by *vital dyes*	Time lapse characterization of surface morphology
Chromatin condensation	Detection of caspase cleavage products	Mitochondrial antigens	Phospholipid externalization, *Annexin V* binding
DNA cleavage *in situ* by *TUNEL method*, detection of DNA fragmentation, strand breaks	Transglutaminase activity	Cytochrome *c* release and alterations	Changes in membrane permeability, *DAPI, Hoechst*
Anti-single-stranded DNA antibody	PARP activity	Metabolic activity	
Hairpin Oligos to detected double-stranded breaks	Death antigens		

Note: Dyes and methods used for visualization of these events are italicized.

such as Ac-DEVD-AFC and Z-DEVD-AMC are often used to detect caspase-3 activity in cellular lysates; however, more effort has been placed on utilization of rhodamine-based derivatives for caspase-3 detection, as coumarin-based fluorogenic substrates have low extinction coefficients. It has been reported by Liu *et al*. that the $(Z\text{-DEVD})_2$-Rh 110 exhibits a much higher turnover rate than the coumarin-based Ac-DEVD-AFC substrate and is at least 10-fold times more sensitive than Z-DEVD-AMC under their assay conditions.[22] The products released from coumarin-based substrates also have short excitation and emission wavelengths, which limit assay sensitivity, and are cell impermeable; therefore, they only work with cellular extracts.[23]

Rhodamine derivatives including Rhodamine 110, Rhodamine 123, and others are often used to detect caspase activity as well as changes in mitochondrial membrane potential. There are many advantages to using rhodamine-based substrates over other dyes. They have longer excitation and emission wavelengths, which reduces interference from testing compounds; the uncleaved substrate does not fluoresce and therefore has a very low background signal, which makes it very clear as to whether apoptosis has occurred or not; and lastly, once cleaved, rhodamine has very strong fluorescent properties. Rhodamine and its derivatives are also cell-permeable, which allows for flow cytometry to measure the amount of fluorescence emitted and therefore to clearly verify the occurrence of the apoptotic process.[24]

While it is reportedly difficult to couple Rhodamine 110 to the tetrapeptide (a chain of four amino acids, D-E-V-D, which is cleaved by caspase-3 after the second D) in order to form the fluorogenic substrates,

sequential coupling of the amino acids to Rhodamine 110 has been the most suitable way of preparing the substrate.[22] Use of two DEVD blocking groups to prevent fluorescence of the substrate leads to the necessity of two hydrolysis reactions for cleavage of both the DEVD sites in $(Z\text{-DEVD})_2$-Rh 110. This limits the linear dynamic range of the substrate, and the creation of a Rhodamine 110-based substrate with only one hydrolysable amide group (one DEVD site) would allow for more efficiency in the use of the Rhodamine 110 derivative as a fluorogenic substrate.

A second method used for apoptosis detection is known as terminal deoxynucleotidyl transferase mediated digoxigenin nick end labeling, i.e., the "TUNEL" method. DNA fragmented by activated endonucleases into segments 180–200 bps in length are labeled by dUTP, which is later detected by light or fluorescence microscopy. This method is performed *in situ* for observation of apoptosis at the single cell level, where it is often difficult to distinguish between the occurrence of apoptosis or necrosis in a cell. While considered the standard for detection of DNA fragmentation, a hallmark of the apoptotic process, the TUNEL method often fails to distinguish between apoptosis and necrosis, as cells in late phases of necrosis undergo DNA damage, which would stain as a false positive for apoptosis. The TUNEL method detects all DNA damage and fragmentation, so artificial DNA breakage would be stained as well, also giving a false positive identification for apoptosis. Another drawback of this method is that it is unfeasible for use in live cells. Tissues must be frozen, then sectioned, mounted, and stained with the anti-digoxigenin antibody and conjugated with a fluorescent dye such as fluorescein.[25]

An early marker of the apoptotic process is indicated by the externalization of phosphatidyl serine from the inner to the outer plasma membrane leaflet. The Ca^{2+}-dependent protein Annexin V can be used to detect the presence of phosphatidyl serine on cell membranes. The externalization of phosphatidyl serine occurs via caspase activation; therefore, its presence, indicated by the binding of annexin V to the phosphatidyl serine, acts as a good marker of the initialization of apoptosis.[21] Due to the morphological differences that characterize apoptosis and necrosis, use of Annexin V in combination with use of propidium iodide (PI) staining makes it possible to differentiate between apoptotic and necrotic cells. As discussed previously, a fundamental difference between the two types of cell death is characterized by cell membrane permeability. Cells experiencing apoptotic cell death possess cell membranes that are impermeable until the final stages of the death process, while cells undergoing necrotic death possess membranes that are permeable. Due to the large molecular weight of PI and the impermeability of the membranes of cells undergoing apoptosis, cells that stain annexin V-positive and PI-negative are considered apoptotic, while cells that stain both annexin V- and PI-positive are labeled necrotic.[26] In the later stages of apoptosis, however, apoptotic cells may stain both annexin V- and PI-positive due to loss of membrane integrity, therefore making it difficult or near impossible to differentiate between apoptosis and necrosis during these stages.[27]

Another method of visualization can be achieved by the use of dyes that bind internally to DNA fragments. Use of the various Hoechst dyes (33342, 33258) is particularly prevalent. Hoechst 33342 is a fluorescent

dye that permanently stains DNA for visualization of chromatin condensation, changes in chromatin conformation, and nuclear fragmentation for qualitative determination of apoptosis. Hoechst 33342 is a simple method for detection of early and late events in the apoptotic process *in vivo*. It also has the ability to detect early changes in membrane permeability, as it can internally label DNA within apoptotic cells.[28] Other variations of Hoechst dyes work in similar ways.

Chromatin condensation and fragmentation and DEVD-like caspase activity can be analyzed by staining with DAPI and PhiPhiLux-G_1D_2, respectively. PhiPhiLux-G_1D_2 is a fluorogenic substrate that is cleaved in a DEVD-dependent manner to produce rhodamine molecules, which fluoresce red under a G2A filter, whereas DAPI stains apoptotic or viable nuclei blue under a DAPI filter.[29] PhiPhiLux, which is used to measure caspase activation via FACS, poorly penetrates the cell membrane and needs a longer incubation time.[23] It is not possible to measure apoptotic events shorter than the one-hour staining time necessary to produce visible results using this method.

Flow cytometry is used to quantify the amount of apoptosis occurring, based on the fact that light-scattering patterns of apoptotic cells are differentiated from light- scattering patterns of viable cells as well as from cells undergoing necrotic cell death. Apoptotic cells give lower forward and higher side scatter values than viable cells because of their smaller size and the differences in cytoplasm and nucleus consistency. Flow cytometry analysis is based on the detection of DNA fragmentation and loss and of morphological changes as well as changes in membrane permeability.[27] Various fluorogenic substrates as described previously can be used in

combination with this detection method in order to quantitatively determine if apoptosis is taking place.

Fluorescence resonance energy transfer (FRET) detection is used to examine structural and dynamic characteristics of biological molecules in aqueous solution.[30] Macromolecules that are to undergo examination are labeled with covalently linked donor and acceptor fluorophores. After a specific molecule has been chosen to undergo examination using FRET, the donor fluorophore of that molecule is excited by continuous laser illumination. The fluorophore donor transfers energy to the acceptor fluorophore, where it is re-emitted as fluorescence.

FRET detection measures non-covalent bonding events in biological and macromolecular systems. Due to the presence of caspase-3, which cleaves certain cellular substrates during apoptosis, and the effects of caspase-3 on fluorescence resonance energy transfer, FRET detection can be used to determine whether apoptosis has occurred. FRET detection can also be used to monitor the spontaneous folding and unfolding of molecules because of denaturing agents in the solution and to qualitatively map protein-protein interactions. There are two ways most generally used to measure the FRET effect with steady state microscopy. The first method of detection of the FRET effect measures the decrease of the donor fluorophore emission and the increase in the acceptor fluorophore emission in a two-dye system. The second method of detection of the FRET effect is called acceptor photobleaching. In this method, the donor is excited, the acceptor is photobleached, and the donor emission is measured before and after acceptor photobleaching.[31] However, this method cannot be used *in vivo*.

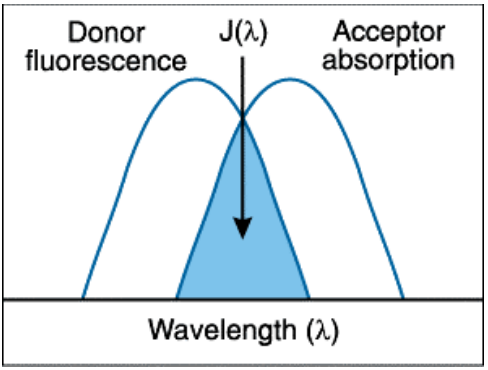

Figure 2: Image of overlapping acceptor/donor spectra. (J(λ) = spectral overlap integral of the absorption spectrum of the acceptor and fluorescence emission spectrum of the donor). The integral = $(\varepsilon_A(\lambda)_* F_D(\lambda)_* \lambda^4 d\lambda$, $[cm^3 M^{-1}]$ (ε_A = extinction coefficient of acceptor; F_D = fluorescence emission intensity of donor as a fraction of the total integrated intensity).

In order for the FRET effect to occur, it is necessary for the fluorescence emission band of the donor fluorophore molecule to overlap with the excitation band of the acceptor molecule within 20–80 Angstroms of the donor, as displayed in Figure 2.[32]

It is assumed that because of the peptide conformation in the aqueous solution, the donor and acceptor molecules are in close proximity to one another (10–100 Angstroms), which allows for the energy transference from the donor fluorophore to the acceptor fluorophore.

The transfer of energy due to the FRET effect can be detected by the reduction of fluorescence from the donor fluorophore and an increase in the intensity of the fluorescent emissions from the acceptor fluorophore. The temporal increase in fluorescent intensity by the acceptor is called "acceptor in-growth".[32] Donor fluorophore colors are restricted to blue

or cyan, which have limited fluorescent capabilities and also undergo auto fluorescence and are paired with green- or yellow- colored acceptor fluorophores.

As stated previously, the FRET effect is used to determine the conformation of biomolecules as well as to monitor biological processes such as apoptosis within a cell. FRET has great importance in the field of apoptosis detection and has been widely implemented in the study of programmed cell death. The detection of apoptosis in cells is again made possible by the activation of caspase-3. If the linker between the donor and acceptor fluorophores is synthesized to contain a cleavable substrate (containing the amino acid sequence D-E-V-D), then caspase-3, which actively cleaves cellular substrates possessing the sequence D-E-V-D, can be used to cleave the linker between the donor and acceptor fluorophores in the molecular probe.[33]

The presence of caspase-3, which is only active during apoptosis, is detected by the elimination of the FRET effect. This allows for the determination as to whether or not apoptosis is occurring.

Resulting cleavage of the peptide, by caspase-3, between valine and aspartic acid in the recognition sequence D-E-V-D results in the elimination of the FRET effect as the donor and acceptor fluorophores are no longer joined. Flow cytometry is used to quantify the amount of fluorescence present. By observing the intensity shift between the emissions of the donor and acceptor fluorophores, it is possible to determine the change in the FRET effect as a function of the cleavage of the linker by the enzyme caspase-3.[33] Figure 3 demonstrates an example of a peptide with a cleavable D-E-V-D site present. Cleavage of this

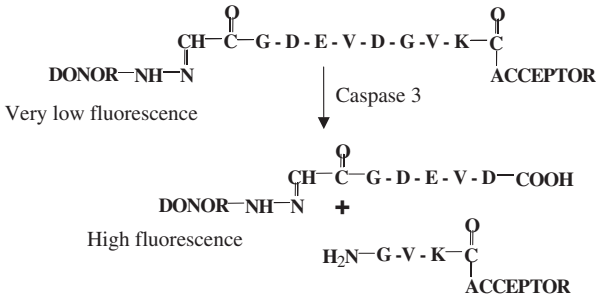

Figure 3: Peptide with cleavable valine-aspartic acid site.

site by caspase-3 results in a shift of low to high fluorescence of the donor.

There are, however, a few problems with the reliance on caspase-3 to cleave the D-E-V-D substrate within the linker between the donor and acceptor fluorophores. These problems lie within the fact that the linker might not be fully accessible for cleavage by the enzyme for various structural reasons, which would hinder the detection abilities of the FRET effect on apoptosis. The linker, for example, may be hindered from cleavage because of the orientation of the donor and acceptor fluorophores to one another and because of the distance between the two fluorophores.[33] This method, nonetheless, has shown to be able to detect apoptosis exceptionally well in living, intact cells.

7.5 Characterization of Folic Acid as a Targeting Component

The vitamin folic acid (FA) serves as a one-carbon source for synthesis of several intermediary metabolites, most importantly for the synthesis of nucleotides required for DNA synthesis and cell growth. The FA is taken

up into a cell either through a low-affinity reduced folate carrier (RFC) or through a high-affinity FA-receptor (FAR). The RFC is ubiquitously expressed in all cells and carries the naturally occurring reduced folates. FAR is expressed in low levels in normal cells and preferentially carries the oxidized FA into cells. Because of the high affinity and the cancer cell specificity, FA is the more suitable targeting agent when compared to the reduced folates. There are three types of FAR — the α, β, and γ isoforms. The α and β isoforms are glycosylphosphatidylinositol (GPC)-anchored membrane proteins, and the γ isoform is a soluble protein. The α and β isoforms are membrane receptors identified in epithelial and non-epithelial cells, respectively. The α isoform is over expressed in several human carcinomas, even up to a hundred-fold.[34–38] This provides striking selectivity for targeting carcinomas using drug conjugates containing FA.

In addition to the tumor specificity FAR-α in human carcinomas, there are other advantages for the selection of FA as a targeting agent. Expression of FAR in transformed epithelial cells is relatively enhanced on the basolateral surface ("blood side") of cancer cells, as compared to the predominant apical ("tissue side") expression in normal cells, which complements the cancer cell specificity of FA.[39] The small molecular size of FA allows easy tumor penetration and favorable pharmacokinetics. FA is easily available and is inexpensive, and the chemical conjugation of FA to a polymer such as a dendrimer and the purification of the FA-conjugate complex are relatively simple. FA binds to its receptor with high affinity (K_d = 0.1 to 1 nM) and is largely non-immunogenic. The tumor cell density of FA receptors tends to be elevated during tumor

progression, providing an increased therapeutic potential during later stages of the cancer. Because of these advantages, FA has been widely studied for the targeting of bioactive agents such as protein toxins, oligonucleotides, plasmids, liposome-entrapped drugs, radiopharmaceutical agents, and MRI agents.[36,40–48]

7.6 Characterization of Poly(amidoamine) Dendrimer as a Platform for Synthesis of Apoptosis Sensors

PAMAM dendrimers with well-defined and highly branched structures contain multiple surface primary amino groups ideal for conjugation of several molecules of FA and multiple other functions onto the surface amino groups of the dendrimer. FA-conjugated PAMAM dendrimers bind and internalize into FA receptor-expressing KB cells. Competition assay with free FA shows that the PAMAM dendrimer device (G5-Ac-FA) has a similar affinity for the folate receptor when compared to free FA. Therefore, the affinity of FA is not lost by conjugation with PAMAM dendrimer. The binding of the dendrimer device is relatively acid-resistant, compared to the binding of free FA. This is probably due to the increased avidity caused by multiple anchoring of the device to two or more adjacent receptor binding sites. Multivalent interactions of FA moieties have also been demonstrated in FA linked to PEGylated cyanoacrylate nanoparticles.[48] Multiple anchoring does not seem to influence internalization of the dendrimer, as confocal microscopic analysis indicated it has cytosolic and nuclear localization.[49]

The poly(amidoamine) dendrimer used in this synthesis is generation 5 (G5), well-characterized, uniform and mono dispersed.

Determination of the molecular weight and the number of primary amino groups is fundamental in designing reactions resulting in the synthesis of a precise conjugate structure. Potentiometric titration is initially performed to determine the average number of tertiary and primary amino groups. Although the theoretical numbers of primary and tertiary amino groups in the G5-PAMAM are 128 and 126 while the molecular weight is 28,826 g/mol,[50,51] the potentiometric analysis of different lots of dendrimers gives approximately 120 primary amines. Partial acetylation is used to neutralize a fraction of surface amino groups of the dendrimer device surface in order to prevent a charge-based non-specific interaction with a negatively charged cell membrane. The fraction of nonacetylated primary amines is used for the subsequent attachment of different kind of functional molecules. Figure 4 shows the GPC refractive index (RI)

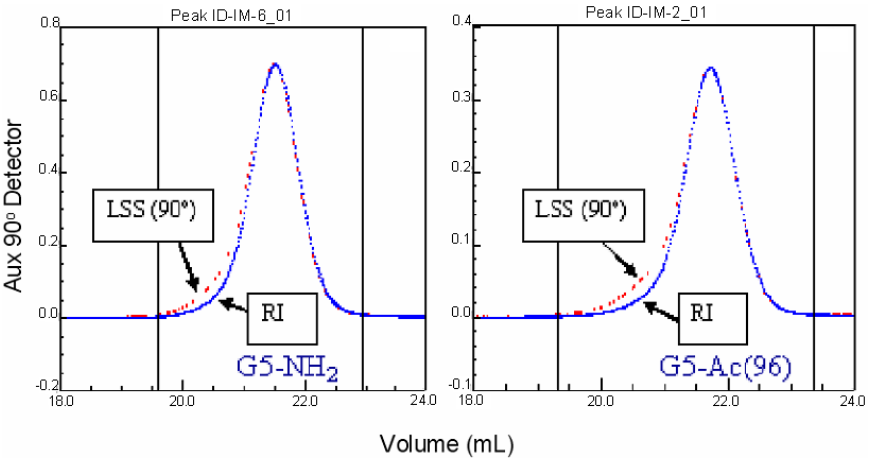

Figure 4: GPC RI and light scattering signal (90°) of the G5 dendrimer and G5-Ac(96) partially acetylated dendrimer. (Reprinted with permission from *Biomacromolecules* **8**, 13–18, 2007 Copyright (2007) American Chemical Society.)

as a concentration detector and light scattering signal (90°) of the G5 dendrimer (M_n = 26,530 g/mol) and G5-Ac(96) (M_n = 29,970 g/mol) partially acetylated dendrimer. As shown the RI signal and laser light-scattering signal, LSS overlaps at 90° indicating that there is very low level of defect in the analyzed structure.

7.7 Synthesis and Biological Activity of a Dendrimer-Based Single Dye Sensor Detect Apoptosis in Targeted Cells

In this section we demonstrate how to synthesize a sensing agent based on the dye rhodamine 110 and how to conjugate this substrate to the functionalized G5 dendrimer designed specifically to detect apoptosis. In contrast to the FRET-based detectors, this device contains only one dye. The single dye apoptosis sensor (SDAS) as attached to the dendritic nanodevice is not fluorescent. It becomes fluorescent upon enzymatic cleavage by caspase-3, which is only active in apoptotic cells.

7.7.1 The synthesis of N-pentafluorobenzoyl-rhodamine 110

Pentafluorobenzoyl chloride is added dropwise to a solution of rhodamine 110 and *N*,*N*-diisopropylethylamine in dimethylformamide at –42°C. The solution is stirred for 10 minutes at –42°C; then it is warmed to room temperature and stirred at room temperature for two hours. It is diluted with ice water and extracted with ethyl acetate. The extracts are washed with brine, dried over Na_2SO_4, and concentrated to give the crude product, which is purified by column chromatography (hexane:EtOAc 1:1). The result is that *N*-pentafluorobenzoylrhodamine 110 is obtained.

7.7.2 The synthesis of N-[Ac-Asp(OBu-t)-Glu(OBu-t)-Val-Asp(OBu-t)]-N′-pentafluorobenzoyl-rhodamine 110

To a solution of Ac-Asp(OBu-*t*)-Glu(OBu-*t*)-Val-Asp(OBu-*t*)-CO_2H in an anhydrous 1:1 mixture of dimethylformamide and pyridine at 0°C is added 1-[3-(dimethylamino)-propyl]-3-ethylcarbodiimide hydrochloride (EDC). The solution is stirred for 20 minutes, and then *N*-pentafluorobenzoylrhodamine 110 is added. It is stirred at room temperature for five days, then diluted with water and extracted with ethyl acetate. The extracts are washed with 1 N HCl and water, dried over Na_2SO_4, and concentrated to give the crude product, which is purified by column chromatography (EtOAc:CH_2Cl_2 2:3). As a result the *N*-[Ac-Asp(OBu-*t*)-Glu(OBu-*t*)-Val-Asp(OBu-*t*)]-*N′*-pentafluorobenzoylrhodamine 110 is obtained.

7.7.3 The synthesis of N-*(Ac-Asp-Glu-Val-Asp)-N′-pentafluorobenzoyl-rhodamine 110*

To a solution of *N*-[Ac-Asp(OBu-*t*)-Glu(OBu-*t*)-Val-Asp(OBu-*t*)]-*N′*-pentafluorobenzoylrhodamine 110 in methylene chloride cooled to 0°C is added 50% trifluoroacetic acid in methylene chloride. The solution is stirred at room temperature for 4 hours. The solvent is removed, and the residue is redissolved in a solvent mixture of EtOAc:MeOH (1:1). The solution is added dropwise into hexane to obtain precipitate, which is filtered and dried. The resulting material is *N*-(Ac-Asp-Glu-Val-Asp)-*N′*-pentafluorobenzoylrhodamine 110. The sequence of reactions for the in-house designed and synthesized *N*-(Ac-Asp-Glu-Val-Asp)-*N′*-pentafluorobenzoylrhodamine 110 is depicted in Figure 5.

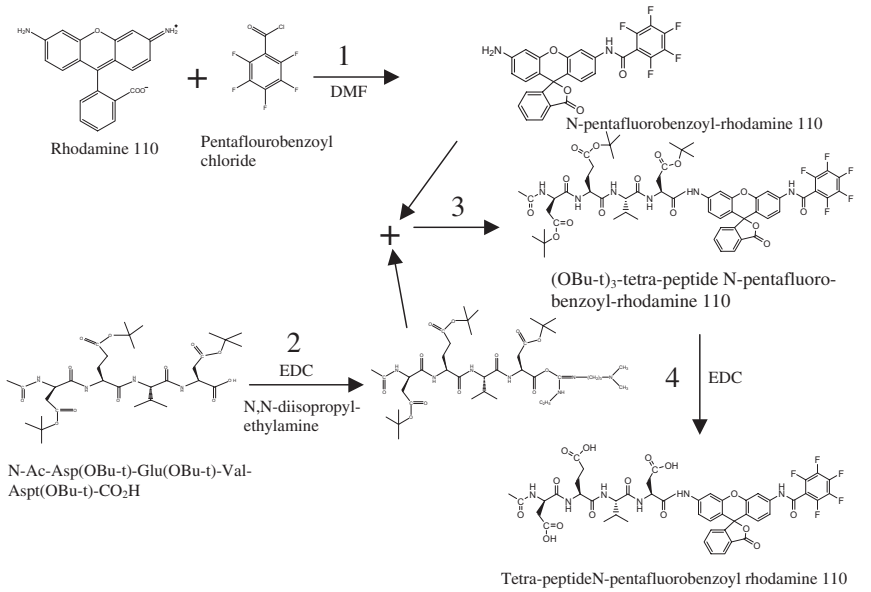

Figure 5: The reaction sequence for designed and synthesized apoptosis detector.

*7.7.4 The synthesis of G5-Ac-FA-(*N*-(Ac-Asp-Glu-Val-Asp)-N′-pentafluorobenzoyl-rhodamine 110)*

A solution of *N*-(Ac-Asp-Glu-Val-Asp)-*N′*-pentafluorobenzoylrhodamine 110 and EDC in DMF and DMSO (3:1) is stirred for one hour at room temperature. This is added to a solution of G5-Ac-FA in DI water and stirred for three days at room temperature under N_2 in dark. The reaction mixture is dialyzed in DI water for two days and then lyophilized. The conjugation of *N*-(Ac-Asp-Glu-Val-Asp)-*N′*-pentafluorobenzoylrhodamine 110 to the G5-Ac-FA is schematically shown in Figure 6.

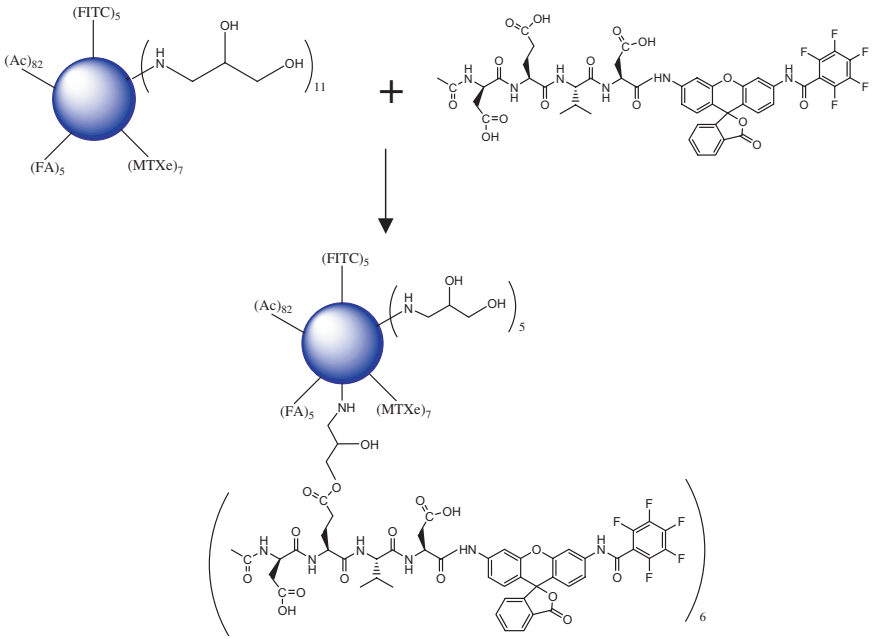

Figure 6: Conjugation of tetra-peptide-N-pentafluorobenzoyl-rhodamine 110 to the tri-functional nanodevice completes the synthesis of the four-functional nanodevice.

*7.7.5 Biological function of G5-Ac-FA-(*N*-(Ac-Asp-Glu-Val-Asp)-N′-pentafluorobenzoyl-rhodamine 110*

The G5-Ac-FA-*N*-(Ac-Asp-Glu-Val-Asp)-*N′*-pentafluorobenzoylrhodamine 110 was tested for its activity to detect apoptosis. In order to examine the biological activity the synthesized nanodevice was incubated with cell lysates obtained from control and apoptotic KB cells. The nanodevice incubated with the apoptotic cell lysate showed an increase in fluorescence when compared to incubation with the control cell lysate (Figure 7). Furthermore, the nanodevice detected apoptosis in KB folate

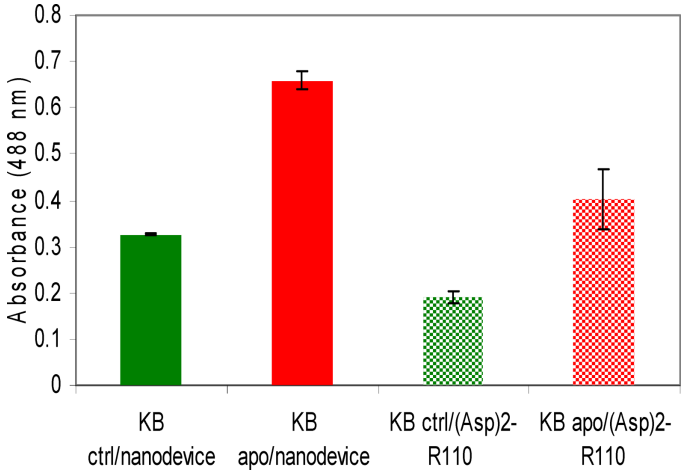

Figure 7: KB cells were untreated or treated with 2 μM staurosporine for 11 hours. Then the cells were harvested, washed, pelleted and frozen. Before the assay, cells were lysed with lysis buffer (10 mM HEPES, 2 mM EDTA, 0.1% CHAPS, pH 7.3) and protein content was measured (KB ctrl – 34.8 mg/ml; KB apo – 18.8 mg/ml). Aliquots of cell lysates were mixed with 10 mM of apoptosis detectors and incubated at 37°C for 12 hours. After incubation fluorescence was measured at 488 nm using an ELISA reader.

receptor-upregulated cells as shown in Figure 8. By attaching anti-cancer drugs like methotrexate, one may synthesize a tetra-functional dendrimer — G5-**FA**(targeting moiety)-**AlexaFluor 660**(reporting moiety)-**Rh110**(apoptosis sensor)-**MTX**(anti-cancer drug).

7.8 Synthesis and *in vitro* Function of Dendrimer-Based FRET Apoptosis Sensor to Target Cancer Cells

Figure 9 below demonstrates the synthetic steps necessary to produce a nanodevice for apoptosis detection. Evaluation of the FRET effect necessitates

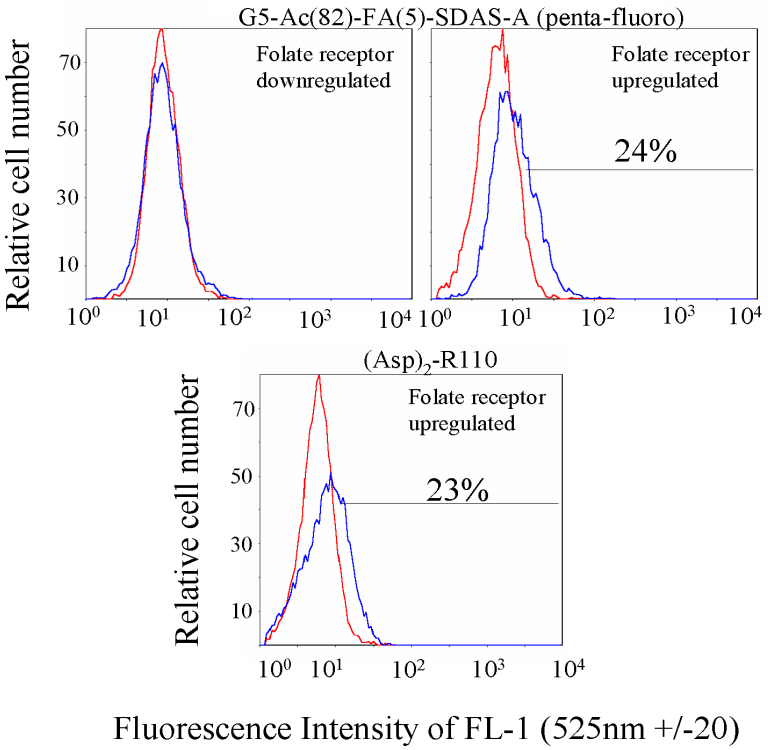

Figure 8: KB cells with upregulated and downregulated folate receptor were treated with either DMSO control cells (red histograms) or staurosporine (blue histograms) for six hours. The apoptosis sensor nanodevice detected the apoptosis (approximately 24%) only in KB cells with upregulated folate receptor and treated with staurosporine. The control apoptosis detector $(Asp)_2$-Rh110 (the fluorochrome used in synthesis of the apoptosis sensor nanodevice) stained apoptotic cells to an extent similar to the nanodevice.

the calculation of the transfer efficiency of the photons between the donor and the acceptor. The number of photons emitted from the donor and the acceptor are counted within a certain timeframe, and the ratio of these numbers is called the energy-transfer efficiency.

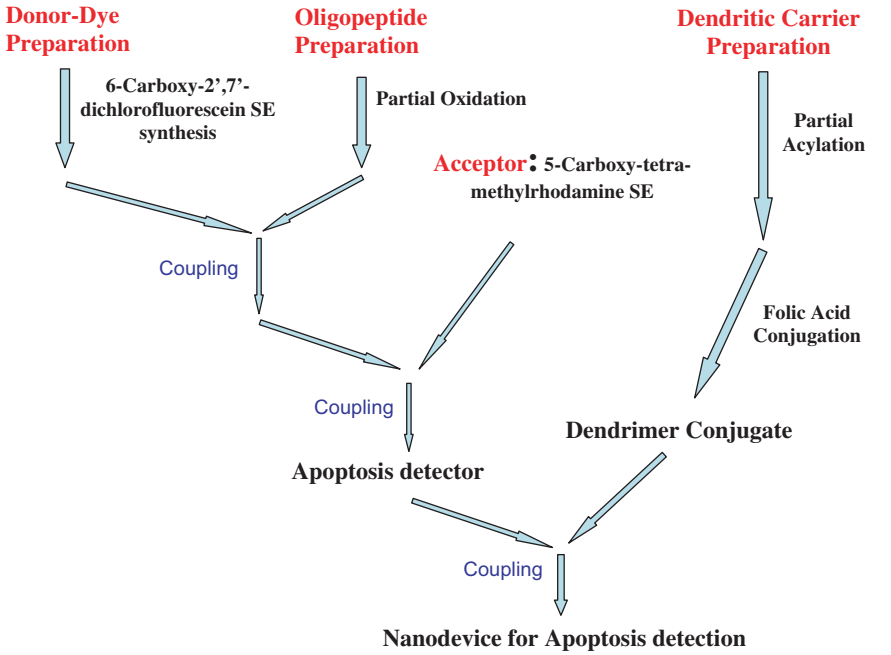

Figure 9: Strategy for FRET reagent and dendritic device synthesis.

This ratio is dependent on the distance between the donor and acceptor fluorophores. The distance between the two fluorophores must be calculated in order to determine the dynamic and conformational changes of the macromolecule under consideration.[52] The efficiency of the energy transfer can be calculated using the following formula:

$$E(r) = (1 + (r / R_0)^6)^{-1}$$

where $E(r)$ — the efficiency of the Förster energy transfer between the fluorophore donor and acceptor,

r — the distance between the donor and acceptor fluorophores, and

R_0 — Förster radius, (i.e., the distance at which the efficiency is ½).

The larger the efficiency *E(r)* of the energy transfer, the shorter the distance (*r),* between the fluorophores. This formula is valid due to the angular averaging of the dipole-dipole interaction, which occurs because of the fast movement of the fluorophores. It must be noted, however, that the value *r* fluctuates as a result of the dynamics of the macromolecule to which it is attached, as the molecule under observation will change shape and undergo folding and unfolding of its structure and other various conformational changes.[52] If the time window of observation is such that enough photons have been emitted for calculation and the distance between the donor and acceptor fluorophores does not change, then the efficiency can be turned into a useful calculation of distance *r*.

It must also be noted that at a constant concentration of free and associated FRET pairs, the emission of the FRET donor is inversely proportional to the mole fraction of associated molecules.[32]

While double-dye (fluorophore) FRET detection is the most commonly used FRET detection technique, use of triple- and possible quadruple-dye detection has also been under study.[30] Research by Liu and Lu has shown that it is possible to label biomolecules that possess many arms with three or even four dyes for maximal detection of conformational changes as a result of fluorescent resonance energy transfer. The labeling of the radiating arms of dendrimers independently of one another using fluorophores of different colors allows for determination of temporal and spatial locations of each pair of arms as well as for the assessment of overall changes in structural dynamics. One problem encountered, however, with using four dyes for detection is the possible non-overlaps of the spectra between the donor and acceptor fluorophores, a prerequisite for the

FRET effect, thus preventing energy transfer between that particular pair of fluorophores.[30] This, however, (although a small inefficiency) does not eliminate the capabilities that using four dyes can have, as the detection capabilities with this number of dyes can have a great positive influence on determining the structural changes within a biomolecule.

Below we show the synthesis, characterization and *in vitro* targeting of an engineered PAMAM nanodevice in which folic acid (FA) is conjugated as the targeting molecule and a caspase-specific FRET-based agent (PhiPhiLux™ G_1D_2) as the apoptotic detecting agent. Fluorescence resonance energy transfer (FRET) is the transfer of photon energy from an excited fluorophore (the donor) to another fluorophore (the acceptor) when both are located within close proximity (1–10 nm). An excited fluorophore (the donor) transfers its excited state energy to a light-absorbing molecule (the acceptor). This transfer of energy is non-radiative, due primarily to a dipole-dipole interaction between the donor and acceptor, and leads to a reduction in the donor's fluorescence intensity and a decreased lifetime in the excited state. If the acceptor molecule is no longer present, the donor increases fluorescence intensity.[53]

7.8.1 Synthesis of G5-Ac-FA-PhiPhiLux™ G_1D_2

The synthetic scheme for production of dendritic devices is given in Figure 10. The G5 PAMAM dendrimer was synthesized and characterized at the Michigan Nanotechnology Institute for Medicine and Biological Sciences (MNIMBS), University of Michigan.

The synthesized dendrimer was analyzed by using NMR, HPLC, GPC and potentiometric titration.[51] The molecular weight was found to be

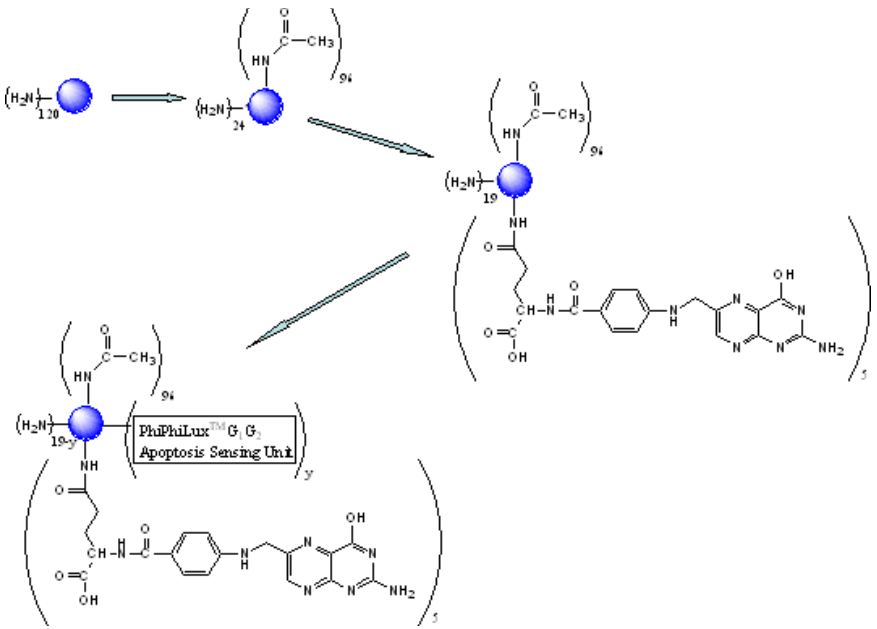

Figure 10: Synthetic scheme for bi-functional PAMAM dendritic devices. Order of syntheses: (1) G5 carrier, (2) G5-Ac(96), (3) G5-Ac(96)-FA, (4) G5-Ac(96)-FA-PhiPhiLux™ G_1D_2. (Reprinted with permission from *Biomacromolecules* **8**, 13–18, 2007 Copyright (2007) American Chemical Society.)

27,500 g/mol by GPC and the average number of primary amino groups was determined by potentiometric titration to be 120. Following, there is a step-by-step description of G5-Ac-FA-PhiPhiLux™ G_1D_2 synthesis.

7.8.1.1 Acetylation of G5 PAMAM

Partial acetylation is needed to neutralize a fraction of the surface amino groups of the dendrimer device surface and thereby prevent a charge-based non-specific interaction with a negatively charged cell membrane. The fraction of nonacetylated primary amines is used for the subsequent

attachment of different kinds of functional molecules. G5 PAMAM dendrimer in absolute methanol (MeOH) is allowed to react with acetic anhydride in the presence of triethylamine for 14 hours. After intensive dialysis in DI water and lyophilization, the resulting product is G5-Ac(96). The average number of acetyl groups (96) is determined based on ^{1}H NMR calibration.[54]

7.8.1.2 Synthesis of G5-Ac(96)-FA

FA is attached to the G5-Ac(96) carrier primarily through the γ-carboxylic group of FA because of its higher reactivity during carbodiimide-mediated coupling to the primary amino groups as compared to the α-carboxyl group.[55] The affinity of FA for binding to FAR is not affected when linked through the γ-carboxylic group. NMR was also used to confirm the number of FA molecules attached to the dendrimer (Figure 11). In the case that free FA is present in the sample; sharp peaks would appear in the spectrum (at the broad aromatic peaks). The broadening of the aromatic proton peaks in the G5-Ac(96)-FA spectrum indicates the presence of a covalent bond between the FA and the dendrimer. Based on the integration values of the methyl protons in the acetamide groups (1.84 ppm) and the aromatic protons in the FA (6.64, 7.55 and 8.52 ppm), the number of attached FA molecules was calculated to be 4.9. In a separate study using UV spectroscopy and using a concentration calibration curve of free FA, the number of FA molecules was estimated to be 5.3 (data not shown).

Analytical HPLC showed that the G5-Ac(96)-FA(5) conjugate clearly indicates the removal of free FA before (1) and after (2) membrane filtration purification (Figure 12). Briefly, the FA is allowed to react with

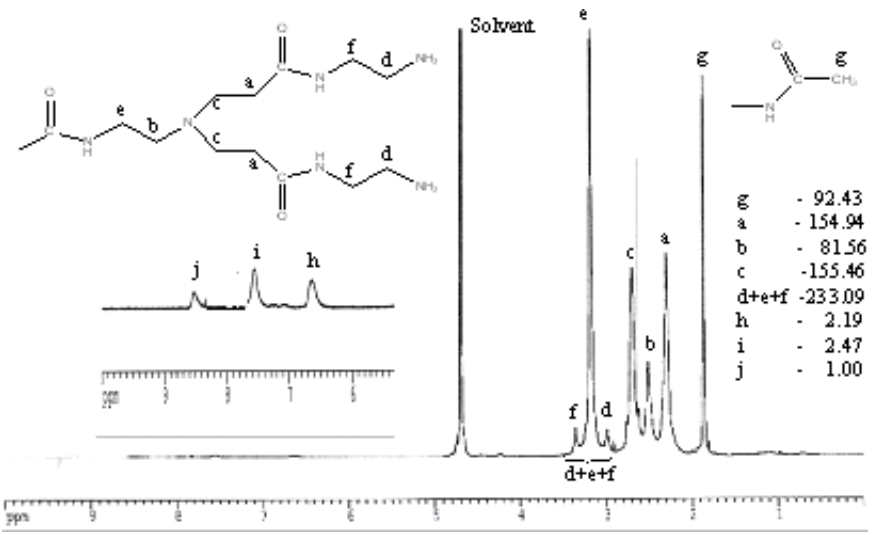

Figure 11: ^{1}H NMR of the G5-Ac(96)-FA(5) conjugate. The inserts depict aromatic peaks which belong to the conjugated FA and integral values of the individual peaks of the dendrimer protons. (Reprinted with permission from *Biomacromolecules* **8**, 13–18, 2007 Copyright (2007) American Chemical Society.)

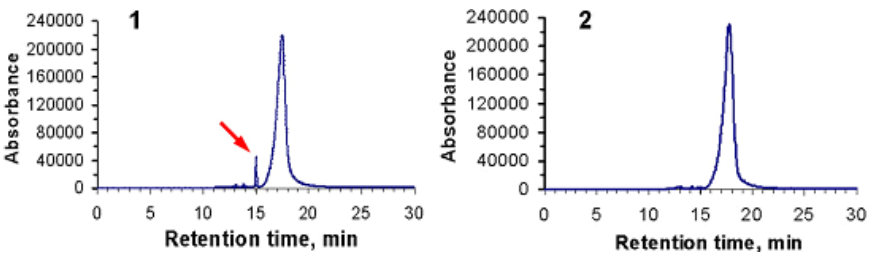

Figure 12: HPLC eluogram of the G5-Ac(96)-FA(5) conjugate (1) before and after (2) membrane filtration purification. (Reprinted with permission from *Biomacromolecules* **8**, 13–18, 2007 Copyright (2007) American Chemical Society.)

a 14-fold excess of EDC in a solvent mixture of DMF and DMSO at room temperature for 1 hour, and the FA-active ester formed is added dropwise to an aqueous solution of the partially acetylated product G5-Ac(96) in

water, and the reaction time is three days at room temperature. After dialysis in DI water, repeated membrane filtration, and lyophilization, the resulting product is G5-Ac(96)-FA as shown in Figures 10 and 11.

7.8.1.3 Synthesis of G5-Ac(96)-FA-PhiPhiLux™ G_1D_2

PhiPhiLux™ G_1D_2 was attached to the G5-Ac(96)-FA mono-functional dendrimer conjugate in two successive reactions. PhiPhiLux™ G_1D_2 is allowed to react with a 14-fold excess of EDC in a solvent mixture of DMF and DMSO at room temperature for one hour. This PhiPhiLux™ G_1D_2-active ester solution was added dropwise to an aqueous solution of the partially acetylated mono-functional dendrimer conjugate G5-Ac(96)-FA in water, and the reaction time is two days. After repeated membrane filtration (using PBS and DI water) and lyophilization, the final product G5-Ac(96)-FA-PhiPhiLux™ G_1D_2 is obtained.

7.8.2 In vitro function of G5-Ac-FA-PhiPhiLux™ G_1D_2

The purified G5-Ac(96)-FA-PhiPhiLux™ G_1D_2 nanodevice was examined for its functionality in the FAR-positive KB cells and the FAR-negative UMSCC-38 cells.[10] As shown in Figure 13, the control KB cells showed some non-specific increase in fluorescence intensity when compared to the control unstained cells. However, the apoptotic KB cells increased the fluorescence intensity to a much greater degree and were easily distinguished from the nonspecifically stained control cells (Figure 13(a)). In contrast, the apoptotic UMSCC-38 cells did not show any increase in fluorescence intensity over the background fluorescence of the stained control cells (Figure 13(b)), suggesting the nanodevice was not internalized.

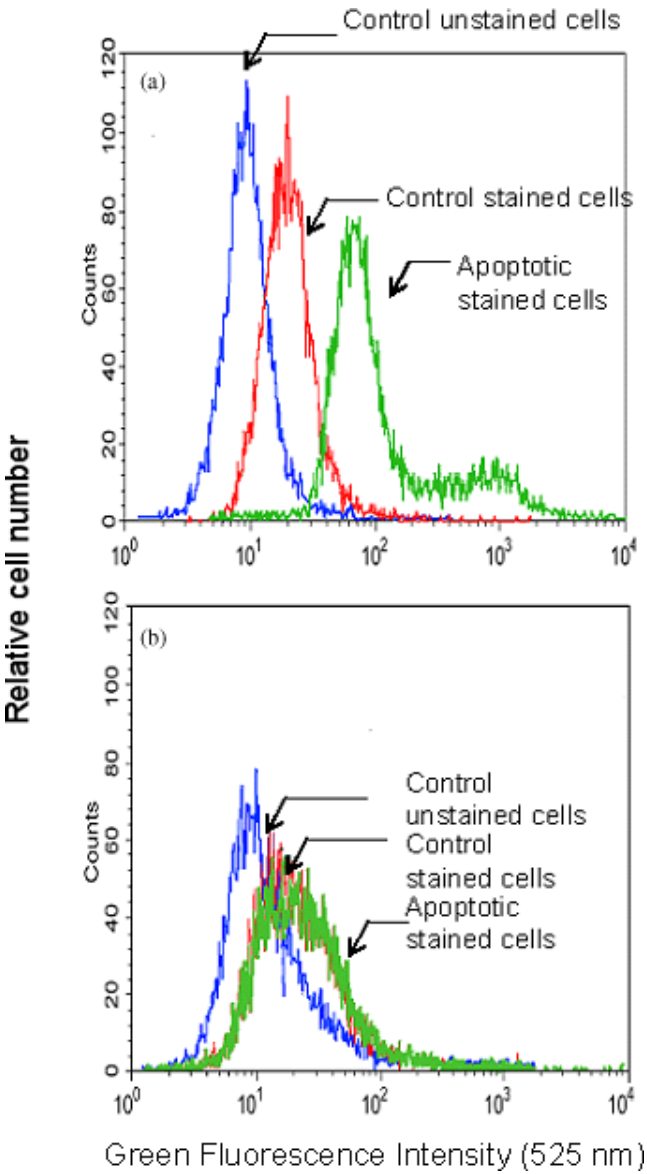

Figure 13: Fluorescence intensity of KB (a) and UMSCC-38 (b) cells treated and untreated with Staurosporine and stained with the G5-Ac(96)-FA-PhiPhiLux™ G_1D_2 nanodevice. (Reprinted with permission from *Biomacromolecules* **8**, 13–18, 2007 Copyright (2007) American Chemical Society.)

These results suggest that KB cells actively internalized the nanodevice through folate receptors during the first 30 minutes of incubation, and, after induction of apoptosis, the active caspase-3 cleaved the bond between donor and acceptor on PhiPhiLux™ G_1D_2 conjugated to the dendrimer, thereby increasing the fluorescence intensity in the apoptotic KB cells. Importantly, the nanodevice is not internalized by cells lacking the folate receptor, indicating the specificity of the nanodevice.

7.9 Summary and Future Directions

In view of the limitations of the techniques currently available to detect apoptosis *in vivo*, we set out to develop novel nanostructures containing a targeting agent and an apoptosis detection agent. They detect the activity of caspase-3. Caspase-3 is one of the cysteine proteases most frequently activated during the process of apoptosis (programmed cell death). In response to a pro-apoptotic stimulus, the 32 kDa pro-caspase-3 is processed to an active enzyme essential for the progression of apoptosis, resulting in the degradation of cellular proteins. Activated caspase-3 cleaves proteins, which contain the sequence valine-aspartic acid, with a high specificity. Based on this principle, several fluorogenic peptide substrates have been developed to detect active caspase-3 in cells. In the absence of active caspase-3, these substrates do not fluoresce due to fluorescence resonance energy transfer between dyes at each end of the substrate peptide. In apoptotic cells, active caspase-3 cleaves the oligopeptide between a valine-aspartic acid pair, destroying the fluorescence resonance energy transfer. The resulting fluorescence can be quantified by flow cytometry or confocal microscopy.

The functional studies clearly show the feasibility of targeting cancer cells with apoptosis sensors. Since we have demonstrated that similar molecules can deliver cancer drugs *in vivo,* this allows the potential for specifically targeting apoptosis detectors to tumors to monitor their response to therapy. However, the fluorescence measurement using conventional techniques such as flow cytometry or confocal microscopy is not applicable for *in vivo* fluorescence quantification. We have recently made advances in overcoming this problem using a two-photon optical fiber device.[56] In this method an optical fiber is inserted through 27-gauge needle to quantify the fluorescence of a targeted nanodevice in live mouse tumors. We believe systems such as this can be further developed to quantify the changes in FRET-based tissue fluorescence targeted through a carrier such as the dendrimer.

We conclude that noninvasive *in vivo* detection and imaging of organs and tissues undergoing apoptosis is possible. The ability to image apoptosis *in vivo* may lead to more expeditious and precise assessment of therapeutic interventions. It would be especially useful for diagnostic imaging of cancer patients who are starting a new treatment modality after a previous therapy has failed. Serial treatment failures with the affiliated waste of money and time, and the side effects endured through these highly toxic treatments could thus be avoided.

7.10 References

1. M. J. Arends, A. H. Wyllie, M. J. Arends, and A. H. Wyllie, Apoptosis: Mechanisms and roles in pathology, *International Review of Experimental Pathology,* **32**, 223–254, 1991.

2. H. Okada, T. W. Mak, H. Okada, and T. W. Mak, Pathways of apoptotic and non-apoptotic death in tumour cells, *Nature Reviews Cancer,* **4**, 592–603, 2004.
3. C. M. Rudin, C. B. Thompson, C. M. Rudin, and C. B. Thompson, Apoptosis and disease: Regulation and clinical relevance of programmed cell death, *Annual Review of Medicine,* **48**, 267–281, 1997.
4. C. B. Thompson and C. B. Thompson, Apoptosis in the pathogenesis and treatment of disease, *Science,* **267**, 1456–1462, 1995.
5. C. P. Zou, E. M. Youssef, C. C. Zou, T. E. Carey, R. Lotan, C. P. Zou, E. M. Youssef, C. C. Zou, T. E. Carey, and R. Lotan, Differential effects of chromosome 3p deletion on the expression of the putative tumor suppressor RAR beta and on retinoid resistance in human squamous carcinoma cells, *Oncogene*, **20**, 6820–6827, 2001.
6. A. H. Wyllie, J. F. Kerr, A. R. Currie, A. H. Wyllie, J. F. Kerr, and A. R. Currie, Cell death: The significance of apoptosis. *International Review of Cytology,* **68,** 251–306, 1980.
7. E. A. Slee, C. Adrain, S. J. Martin, E. A. Slee, C. Adrain, and S. J. Martin, Serial killers: Ordering caspase activation events in apoptosis, *Cell Death & Differentiation,* **6**, 1067–1074, 1999.
8. R. E. Meyn, L. C. Stephens, K. K. Ang, N. R. Hunter, W. A. Brock, L. Milas, and L. J. Peters, Heterogeneity in the development of apoptosis in irradiated murine tumours of different histologies, *International Journal of Radiation Biology,* **64**, 583–591, 1993.
9. R. E. Meyn, L. C. Stephens, N. R. Hunter, and L. Milas, Apoptosis in murine tumors treated with chemotherapy agents, *Anti-Cancer Drugs,* **6**, 443–450, 1995.

10. A. Myc, I. J. Majoros, T. P. Thomas, and J. R. Baker Jr., Dendrimer-based targeted delivery of an apoptotic sensor in cancer cells, *Biomacromolecules,* **8**, 13–18, 2007.
11. Z. Darzynkiewicz, X. Huang, M. Okafuji, and M. A. King, Cytometric methods to detect apoptosis, *Methods in Cell Biology,* **75**, 307–341, 2004.
12. P. Pozarowski, X. Huang, D. H. Halicka, B. Lee, G. Johnson, and Z. Darzynkiewicz, Interactions of fluorochrome-labeled caspase inhibitors with apoptotic cells: A caution in data interpretation, *Cytometry Part A, The Journal of the International Society for Analytical Cytology,* **55**, 50–60, 2003.
13. F. Belloc, M. A. Belaud-Rotureau, V. Lavignolle, E. Bascans, E. Braz-Pereira, F. Durrieu, and F. Lacombe, Flow cytometry detection of caspase 3 activation in preapoptotic leukemic cells, *Cytometry,* **40**, 151–160, 2000.
14. J. F. Kerr, A. H. Wyllie, and A.R. Currie, Apoptosis: A basic biological phenomenon with wide-ranging implications in tissue kinetics, *British Journal of Cancer,* **26**, 239–257, 1972.
15. E. Finkel and E. Finkel, The mitochondrion: Is it central to apoptosis? [comment], *Science,* **292**, 624–626, 2001.
16. N. Zurgil, Y. Shafran, D. Fixler, and M. Deutsch, Analysis of early apoptotic events in individual cells by fluorescence intensity and polarization measurements, *Biochemical & Biophysical Research Communications,* **290**, 1573–1582, 2002.
17. D. R. Green and J. C. Reed, Mitochondria and apoptosis. *Science,* **281**, 1309–1312, 1998.

18. M. Demoy, T. Minko, P. Kopeckova, and J. Kopecek, Time- and concentration-dependent apoptosis and necrosis induced by free and HPMA copolymer-bound doxorubicin in human ovarian carcinoma cells, *Journal of Controlled Release,* **69**, 185–196, 2000.
19. K. M. Heiskanen, M. B. Bhat, H. W. Wang, J. Ma, and A. L. Nieminen, Mitochondrial depolarization accompanies cytochrome c release during apoptosis in PC6 cells, *Journal of Biological Chemistry,* **274**, 5654–5658, 1999.
20. H. Kobayashi, S. Kawamoto, S. K. Jo, N. Sato, T. Saga, A. Hiraga, J. Konishi, S. Hu, K. Togashi, M. W. Brechbiel, and R. A. Star, Renal tubular damage detected by dynamic micro-MRI with a dendrimer-based magnetic resonance contrast agent, *Kidney International,* **61**, 1980–1985, 2002.
21. A. Strebel, T. Harr, F. Bachmann, M. Wernli, and P. Erb, Green fluorescent protein as a novel tool to measure apoptosis and necrosis, *Cytometry,* **43**, 126–133, 2001.
22. J. Liu, M. Bhalgat, C. Zhang, Z. Diwu, B. Hoyland, and D. H. Klaubert, Fluorescent molecular probes V: A sensitive caspase-3 substrate for fluorometric assays, *Bioorganic & Medicinal Chemistry Letters,* **9**, 3231–3236, 1999.
23. H. Hug, M. Los, W. Hirt, and K. M. Debatin, Rhodamine 110-linked amino acids and peptides as substrates to measure caspase activity upon apoptosis induction in intact cells, *Biochemistry,* **38**, 13906–13911, 1999.
24. H. Z. Zhang, S. Kasibhatla, J. Guastella, B. Tseng, J. Drewe, and S. X. Cai, N-Ac-DEVD-N′-(Polyfluorobenzoyl)-R110: novel

cell-permeable fluorogenic caspase substrates for the detection of caspase activity and apoptosis, *Bioconjugate Chemistry,* **14**, 458–463, 2003.

25. S. Yasuhara, Y. Zhu, T. Matsui, N. Tipirneni, Y. Yasuhara, M. Kaneki, A. Rosenzweig, and J. A. J. Martyn, Comparison of comet assay, electron microscopy, and flow cytometry for detection of apoptosis, *Journal of Histochemistry & Cytochemistry,* **51**, 873–885, 2003.
26. R. Sgonc, and J. Gruber, Apoptosis detection: An overview, *Experimental Gerontology,* **33**, 525–533, 1998.
27. L. F. R. Span, A. H. M. Pennings, G. Vierwinden, J. B. M. Boezeman, R. A. P. Raymakers, and T. de Witte, The dynamic process of apoptosis analyzed by flow cytometry using Annexin-V/propidium iodide and a modified *in situ* end labeling technique, *Cytometry,* **47**, 24–31, 2002.
28. A. M. Steff, M. Fortin, C. Arguin, and P. Hugo, Detection of a decrease in green fluorescent protein fluorescence for the monitoring of cell death: An assay amenable to high-throughput screening technologies, *Cytometry,* **45**, 237–243, 2001.
29. D. M. Finucane, E. Bossy-Wetzel, N. J. Waterhouse, T. G. Cotter, and D. R. Green, Bax-induced caspase activation and apoptosis via cytochrome c release from mitochondria is inhibitable by Bcl-xL, *Journal of Biological Chemistry,* **274**, 2225–2233, 1999.
30. J. Liu and Y. Lu, FRET study of a trifluorophore-labeled DNAzyme, *Journal of the American Chemical Society,* **124**, 15208–15216, 2002.

31. C. Berney and G. Danuser, FRET or no FRET: A quantitative comparison, *Biophysical Journal,* **84**, 3992–4010, 2003.

32. S. R. Stauffer and J. F. Hartwig, Fluorescence resonance energy transfer (FRET) as a high-throughput assay for coupling reactions. Arylation of amines as a case study, *Journal of the American Chemical Society,* **125**, 6977–6985, 2003.

33. K. Q. Luo, V. C. Yu, Y. Pu, and D. C. Chang, Application of the fluorescence resonance energy transfer method for studying the dynamics of caspase-3 activation during UV-induced apoptosis in living HeLa cells, *Biochemical & Biophysical Research Communications,* **283**, 1054–1060, 2001.

34. J. F. Ross, P. K. Chaudhuri, and M. Ratnam, Differential regulation of folate receptor isoforms in normal and malignant tissues *in vivo* and in established cell lines, physiologic and clinical implications, *Cancer,* **73**, 2432–2443, 1994.

35. G. Toffoli, C. Cernigoi, A. Russo, A. Gallo, M. Bagnoli, and M. Boiocchi, Overexpression of folate binding protein in ovarian cancers, *International Journal of Cancer,* **74**, 193–198, 1997.

36. H. Wang, X. Zheng, F. G. Behm, and M. Ratnam, Differentiation-independent retinoid induction of folate receptor type beta, a potential tumor target in myeloid leukemia, *Blood,* **96**, 3529–3536, 2000.

37. S. D. Weitman, R. H. Lark, L. R. Coney, D. W. Fort, V. Frasca, V. R. Zurawski, Jr., and B. A. Kamen, Distribution of the folate receptor GP38 in normal and malignant cell lines and tissues, *Cancer Research,* **52**, 3396–3401, 1992.

38. M. Wu, W. Gunning, and M. Ratnam, Expression of folate receptor type alpha in relation to cell type, malignancy, and differentiation in ovary, uterus, and cervix, *Cancer Epidemiology*, *Biomarkers & Prevention,* **8**, 775–782, 1999.

39. Y. Lu and P. S. Low, Folate-mediated delivery of macromolecular anticancer therapeutic agents, *Advanced Drug Delivery Reviews,* **54**, 675–693, 2002.

40. A. Bielinska, J. F. Kukowska-Latallo, J. Johnson, D. A. Tomalia, and J. R. Baker, Jr., Regulation of *in vitro* gene expression using antisense oligonucleotides or antisense expression plasmids transfected using starburst PAMAM dendrimers, *Nucleic Acids Research,* **24**, 2176–2182, 1996.

41. A. Gabizon, A. T. Horowitz, D. Goren, D. Tzemach, F. Mandelbaum-Shavit, M. M. Qazen, and S. Zalipsky, Targeting folate receptor with folate linked to extremities of poly(ethylene glycol)-grafted liposomes: *In vitro* studies, *Bioconjugate Chemistry,* **10**, 289–298, 1999.

42. D. M. Kranz, T. A. Patrick, K. E. Brigle, M. J. Spinella, and E. J. Roy, Conjugates of folate and anti-T-cell-receptor antibodies specifically target folate-receptor-positive tumor cells for lysis, *Proceedings of the National Academy of Sciences of the United States of America,* **92**, 9057–9061, 1995.

43. J. F. Kukowska-Latallo, A. U. Bielinska, J. Johnson, R. Spindler, D. A. Tomalia, and J. R. Baker Jr., Efficient transfer of genetic material into mammalian cells using Starburst polyamidoamine dendrimers,

Proceedings of the National Academy of Sciences of the United States of America, **93**, 4897–4902, 1996.

44. C. P. Leamon, I. Pastan, and P. S. Low, Cytotoxicity of folate-pseudomonas exotoxin conjugates toward tumor cells. Contribution of translocation domain, *Journal of Biological Chemistry,* **268**, 24847–24854, 1993.
45. R. J. Lee and P. S. Low, Delivery of liposomes into cultured KB cells via folate receptor-mediated endocytosis, *Journal of Biological Chemistry,* **269**, 198–204, 1994.
46. R. J. Lee and P. S. Low, Folate-mediated tumor cell targeting of liposome-entrapped doxorubicin in vitro, *Biochimica et Biophysica Acta,* **1233**, 134–144, 1995.
47. S. Li, H. M. Deshmukh, and L. Huang, Folate-mediated targeting of antisense oligodeoxynucleotides to ovarian cancer cells, *Pharmaceutical Research,* **15**, 1540–1545, 1998.
48. B. Stella, S. Arpicco, M. T. Peracchia, D. Desmaele, J. Hoebeke, M. Renoir, J. D'Angelo, L. Cattel, and P. Couvreur, Design of folic acid-conjugated nanoparticles for drug targeting, *Journal of Pharmaceutical Sciences,* **89**, 1452–1464, 2000.
49. Y. Ravindranath and Y. Ravindranath, Recent advances in pediatric acute lymphoblastic and myeloid leukemia, *Current Opinion in Oncology,* **15**, 23–35, 2003.
50. R. Esfandand and D. A. Tomalia, Poly(amidoamine) (PAMAM) dendrimers: From biomimicry to drug delivery and biomedical applications, *Drug Discovery Today,* **6**, 427–436, 2001.

51. I. J. Majoros, C. B. Mehta, and J. R. Baker Jr., Mathematical description of dendrimer structure, *Journal of Computational and Theoretical Nanoscience,* **1**, 193–198, 2004.

52. I. V. Gopichand and A. Szabo, Single-macromolecule fluorescence resonance energy transfer and free-energy profiles, Vol. **107**, 5058–5063, 2003.

53. E. A. Jares-Erijman and T. M. Jovin, FRET imaging, *Nature Biotechnology,* 21, 1387–1395, 2003.

54. I. J. Majoros, T. P. Thomas, C. B. Mehta, and J. R. Baker Jr., Poly(amidoamine) dendrimer-based multifunctional engineered nanodevice for cancer therapy, *Journal of Medicinal Chemistry,* **48**, 5892–5899, 2005.

55. A. Quintana, E. Raczka, L. Piehler, I. Lee, A. Myc, I. Majoros, A. K. Patri, T. Thomas, J. Mule, and J. R. Baker Jr., Design and function of a dendrimer-based therapeutic nanodevice targeted to tumor cells through the folate receptor, *Pharmaceutical Research,* **19**, 1310–1316, 2002.

56. T. P. Thomas, M. T. Myaing, J. Y. Ye, K. Candido, A. Kotlyar, J. Beals, P. Cao, B. Keszler, A. K. Patri, T. B. Norris, and J. R. Baker Jr., Detection and analysis of tumor fluorescence using a two-photon optical fiber probe, *Biophysical Journal,* **86**, 3959–3965, 2004.

Chapter 8

MRI Using Targeted Dendrimer Contrast Agents

Scott D. Swanson & Christopher R. Williams

Outline

8.1 Introduction

Advances in medical imaging have revolutionized diagnosis of disease in the last 30 years. One of the most important contributions to imaging

was the discovery in 1972 by Paul Lauterbur that it would be possible to create a map of the spatial distribution of nuclear spins by using nuclear magnetic resonance (NMR).[1] From this discovery, the field of magnetic resonance imaging (MRI) was born. Of all of the advances in medicine in the last 30 years, MRI and x-ray CT imaging have made the most important contribution to health care.[2] This point was emphasized by awarding the 2003 Nobel Prize in Medicine or Physiology to Paul Lauterbur and Sir Peter Mansfield for their work in MRI.[3–7]

MRI has created a new diagnostic landscape for the physician. High-resolution, three-dimensional images of soft tissue in the brain, abdomen, and knee joints are routinely obtained. One often hears of an athlete requiring an MRI to rule out sports injuries such as tears of the anterior cruciate ligament (ACL).[8] The popular press contains numerous stories about "brain scans" that show the inner workings of our thought processes.[9] The National Cancer Institute has recently issued recommendations that women at high risk for breast cancer obtain an MRI to look for cancer lesions.[10,11] These examples demonstrate how MRI has come to change the way we diagnose disease and understand how the human body works.

To aid in visualization of cancer and other diseases in the body, MRI procedures often use contrast agents to increase the signal difference between the lesion and background tissue. Contrast agents currently approved for clinical studies are either chelated gadolinium ions or iron oxide nanoparticles.[12,13] The current generation of clinical contrast agents has no specific molecular targeting. It is widely thought that the next

generation of MRI will consist of both targeted contrast agents that bind to specific receptor sites on cells in diseases such as cancer or will be so-called "smart" imaging agents that become active only upon enzymatic activation.[14]

Dendrimer macromolecules are well suited to become a platform for both targeting molecules and contrast agents. The branches of PAMAM dendrimer macromolecules provide numerous possibilities for attaching molecular ligands with specific functions.[15] For targeted contrast agents, a subset of the dendrimer branches can be used to attach the targeting agent, and the remaining branches can be used to attach the contrast enhancing molecule. This chapter provides a review of the general properties of T_1 (the spin lattice relaxation time) contrast agents and outlines the contributions that dendrimer macromolecules have made — and have the possibility to make — in the field of targeted contrast agents.

8.2 Principles of MRI

Understanding contrast and contrast agents in MRI requires a basic knowledge of how NMR and MRI work. NMR was discovered independently in 1946 by Edward Purcell[16] and Felix Bloch[17] and is used extensively in physics, chemistry, and biological chemistry for identification in the study of the structure and dynamics of molecules. Magnetic resonance imaging uses the physical principles of NMR to create a map or image of the concentration and magnetic properties of nuclear spins. A complete description of NMR and MRI are beyond the scope of this chapter and can be found in many excellent books.[18–20]

The following is a sketch of how MRI works:

- Nuclei with magnetic moments (e.g., ^{1}H, ^{13}C, ^{23}Na) are NMR active. Water is the most common molecule *in vivo* (about 70% by weight of soft tissue) and water protons (spin I = 1/2) create the largest MRI signal.
- The protons of hydrogen in water molecules, when placed in a strong magnetic field, align either with or against the magnetic field. The net difference between this spin up and spin down is small — about 1 in 100,000 — and determines the signal strength in MRI.
- The patient is placed in a strong magnetic field, typically 1.5 Tesla. By comparison, earth's magnetic field is about 50 micro Tesla.
- A combination of radio frequency (RF) pulses and magnetic field gradients records a map of the water proton magnetization in an inverse spatial coordinate system called k-space with units of cm^{-1}.
- The data are processed with a multi-dimensional Fourier Transform and a map of the water proton magnetization is constructed.

Other Information:

- RF pulsing destroys the nuclear magnetization each time it is measured.
- Magnetization is restored by a process called T_1 or spin-lattice relaxation.
- The T_1 of various tissues can be different.

- A primary goal of targeted contrast agent development is to selectively create a short T_1 so that the nuclear magnetization is restored more quickly in regions where the targeted contrast agent binds than it is in regions where it does not bind.

To understand dendrimer contrast agents, we first need a basic understanding of NMR, relaxation mechanisms in NMR, and how NMR can lead to imaging of water.

8.2.1 Basics of NMR

The signal in NMR is generated by inducing transitions between energy levels of nuclear spins in a large magnetic field. Spin, like mass and charge, is a fundamental property of matter.[18] When a collection of nuclear spins is placed in a magnetic field, the individual nuclear spins will each be quantized into one of the $2I + 1$ energy levels, where I is the spin angular momentum quantum number. Protons, with spin, $I = 1/2$ have two energy levels given by $-\frac{1}{2}\gamma\hbar B_0$ and $+\frac{1}{2}\gamma\hbar B_0$, where γ is the proton gyromagnetic ration, $\hbar$ is Plank's constant divided by 2π, and B_0 is the static magnetic field strength. The two spin states are typically referred to as spin up, $|+1/2\rangle$, and spin down, $|-1/2\rangle$. The difference in energy levels is given by $\Delta E = \gamma\hbar B_0$ and determines the frequency required to cause transitions from one level to another level, $\nu = \Delta E/h$ (the Larmor frequency). For common magnetic field strengths, the frequency is in the radio frequency range of the electromagnetic spectrum, resulting in two important advantages for medical imaging. First, radio frequencies (63 MHz at 1.5 Tesla) easily penetrate the body and allow uniform signal transmission

and reception in the body. Second, the low-energy RF radiation is not ionizing and, other than RF heating, has no known adverse bioeffects on tissue.

Though beneficial for imaging, the small energy level separation is not without cost. The signal intensity in NMR or MRI is proportional to the difference between the energy level number of the spins in the $|+1/2\rangle$, state and the number of spins in the $|-1/2\rangle$, state. Because the nuclear spin energy level spacing is very small relative to thermal energy levels, the population difference between the spin up and spin down levels is very small.

The ratio of the population is given by the Boltzmann relationship as,[18]

$$\frac{N^{+1/2}}{N^{-1/2}} = e^{E/kT}, \tag{1}$$

where $N^{+1/2}$ and $N^{-1/2}$ are the number of spins in the $|+1/2\rangle$ and $|-1/2\rangle$ spin states, E is the energy difference between the two levels, and T is the temperature in Kelvin.

In a sample with one million water molecules, NMR sees only about 10 molecules. The reason that MRI can be successfully performed is due to the large concentration of water molecules in the body. Pure water has a concentration of 55 M, and the hydrogen atom concentration is 110 M. Water concentration *in vivo* is approximately 70 w/w%; therefore, the hydrogen atom concentration is about 80 M.

8.2.2 Diamagnetic relaxation of water

Initially, the nuclear spin magnetization is quantized along the axis of the main magnetic field, B_0. To detect the nuclear magnetization, the

spin-lattice or longitudinal magnetization must be converted into transverse magnetization. This is typically done with a RF pulse.[19] The RF pulse tips the magnetization from the *z* axis into the transverse, or *xy* plane; once in the transverse plane, the nuclear spin magnetization can be detected by the coil or probe tuned to the Larmor frequency of the spins.

Following excitation with a tip angle 90° pulse, the longitudinal magnetization is destroyed. If there were no mechanism to restore the Boltzmann spin polarization, NMR and MRI would not be useful. The process of restoring nuclear magnetization to the Boltzmann levels is called spin-lattice relaxation. Detailed explanation of relaxation requires an understanding of quantum mechanics and is outside the scope of this chapter but can be found elsewhere.[18,19] However, to understand dendrimer contrast agents, a working knowledge of basic relaxation theory is needed and presented here.

Relaxation in NMR consists of two physical components; an energy interaction and a molecular motion that provides a time-dependent modulation of the energy interaction. This can be written as,

$$\frac{1}{T_1} = R_1 = (Interaction) \times (Modulation), \tag{2}$$

where T_1 is the spin lattice relaxation time and R_1 is the rate constant for relaxation.

In one of the most important manuscripts in the field of magnetic resonance, Bloembergen, Purcell and Pound[21] developed general relaxation theory and outlined how magnetic interactions between neighboring

spins cause magnetization to return to the Boltzmann levels. This is now referred to as the BPP theory of relaxation. The dominant process for T_1 relaxation for water protons is modulation of the magnetic dipole-dipole interaction. Two processes contribute: intra-molecular and inter-molecular. The intra-molecular interaction is the dipole-dipole coupling between the two protons shown in Figure 1, and the inter-molecular interaction is the dipolar coupling present between other water molecules. We consider only the intra-molecular relaxation mechanism given by

$$\frac{1}{T_1} = \frac{1}{10}\frac{\gamma^4 h^2}{r_{IS}^6}\left\{\frac{\tau_R}{1+\omega_H^2\tau_R^2} + \frac{2\tau_R}{1+4\omega_H^2\tau_R^2}\right\}, \tag{3}$$

where r_{IS} is the distance between the two water protons and τ_R is the rotational correlation time of water. The first set of terms in this equation correspond to the magnitude of the proton-proton dipole-dipole interaction, the interaction part of Eq. (2), and the terms within the brackets correspond

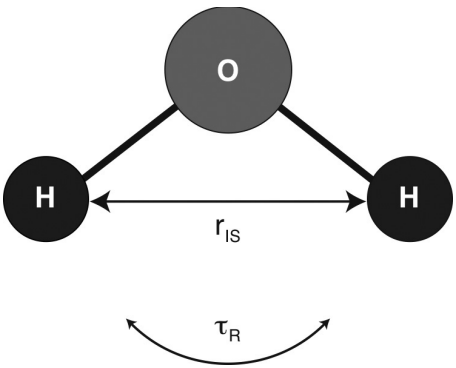

Figure 1: Structure of water. The inter proton distance r_{IS} = 1.6 Å and the rotational correlation time determine the relaxation rate of pure water.

to the modulation of the dipole-dipole interaction created by the Brownian motion of the spins. In pure water, the rotational correlation time is very short, about 4 picoseconds (ps). The rotational correlation time of water can be increased by changing the viscosity of the water, either by changing the temperature or by adding an additional solute such as glycerin.

Figure 2 shows the proton relaxation rate as a function of the Larmor frequency for three different rotational correlation times. This type of graph, called a nuclear magnetic relaxation dispersion (NMRD) plot,[22] is reflective of the spectral density of motions occurring in the spin system. Figure 2 shows that the relaxation rate is constant for a given correlation

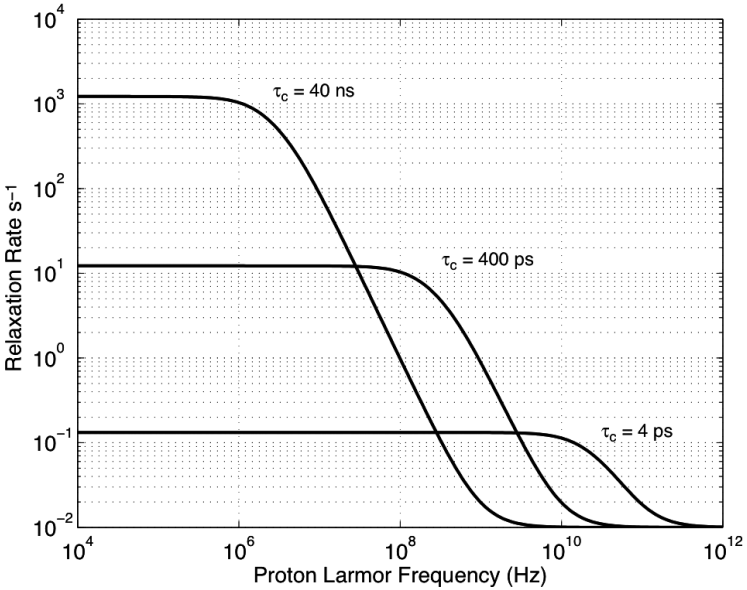

Figure 2: Proton relaxation rate as a function of proton Larmor frequency for three different correlation times.

time until $\omega_0 > \tau_c^{-1}$. At that point the relaxation rate decreases or disperses with increasing magnetic field strength. When the correlation time is short, the intensity of the spectral density at any given Larmor frequency is low and the dispersion occurs at a very high magnetic field. At longer correlation times, e.g., 40 ns, random motions of water molecules are confined to these slower motions, but the spectral density of each of the slower motions is larger and, therefore, the relaxation rate is higher. The total spectral density of motions, the integrated area under each of the three curves, is the same for each of the three correlation times shown. For short correlation times, the spectral densities are spread out over a large range. For long correlation times, the spectral densities are concentrated in the low frequency region. Understanding these important physical concepts provides deeper understanding into the design and performance of MRI contrast agents.

Spin-lattice relaxation is driven by random fluctuation of the dipole-dipole interaction. This process causes transitions from spin up to spin down and vice versa. Figure 3 shows that the relaxation rate for a given Larmor frequency is at a maximum when the correlation time is on the order of the inverse of the Larmor frequency. Under these conditions, the correlation time of the spins is effectively tuned to the Larmor frequency. This makes physical sense. Random fluctuations of the dipole-dipole Hamiltonian act as a molecular RF generation system. Just as the RF coil must be tuned to the spins to efficiently excite and detect them, so too must the correlation time be tuned to create the most efficient relaxation. Unlike an RF coil, which has a very narrow spectral profile, the random Brownian motion of the spins

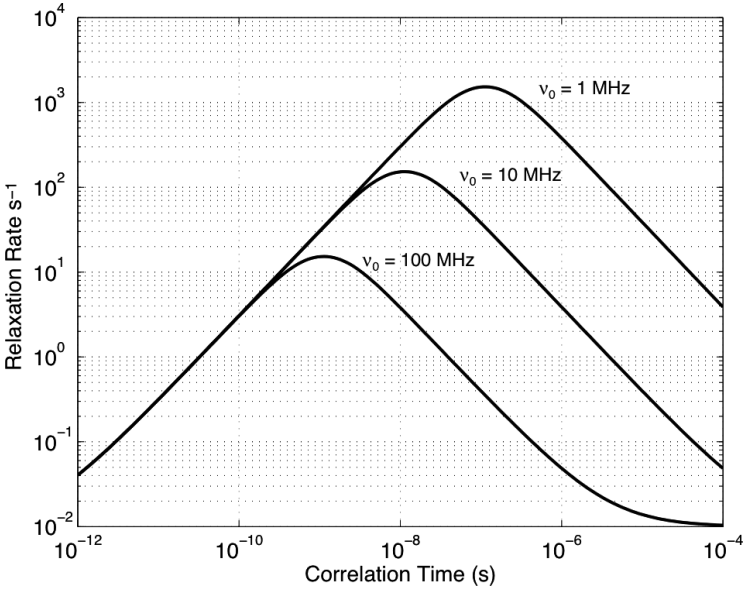

Figure 3: Proton relaxation rate as a function of correlation time for three different magnetic field strengths. The relaxation rate is at a maximum when $\tau_c \approx \omega_0^{-1}$.

creates a broad spectrum of frequencies or spectral densities, as seen in Figure 3.

Another way of saying this is that when the spins are moving at approximately the Larmor frequency, they generate random transitions that tend to restore the populations of the energy levels to the Boltzmann equilibrium values. Random Brownian motions of nearby magnetic moments of either nuclear or electron spins cause transitions between the two spin states. Relaxation is most efficient when the correlation time of the dipole-dipole interaction τ_c, is the same value as the inverse of the Larmor frequency of the spin, $\tau_c \cong 1/\omega_0$. Under these conditions the tumbling rate of the molecules is tuned to the spin precession rate and relaxation is efficient.

8.2.3 Paramagnetic Relaxation Enhancement (PRE) of water

For diamagnetic water relaxation, the only correlation time involved in the intramolecular dipole-dipole interaction is the rotational correlation time of the water molecule, $\tau_c = \tau_R$. For relaxation of water protons by paramagnetic contrast agents, the situation is more complicated but the basic principle still holds; to achieve maximum relaxation efficiency it is beneficial to tune the modulation of the dipole-dipole interaction to the inverse of the Larmor frequency.

The electron magnetic moment is 658 times greater than the proton magnetic moment.[18] A Gadolinium ion (Gd^{3+}) is a lanthanide rare earth metal ion with seven unpaired electrons (with spin S = 7/2). In an aqueous solution, the large electron magnetic moment of Gd^{3+} creates a strong electron-nuclear dipole-dipole interaction and a very efficient pathway for water proton relaxation. The increase in the water proton relaxation rate by addition of a paramagnetic species is called the proton relaxation enhancement (PRE)[23–25] and is the physical basis for most contrast agents in MRI. Gadolinium itself is toxic and must be chelated to be a viable contrast agent.[26] Currently, chelates of Gd(III) are the most widely used contrast agents in MRI.[12]

Figure 4 shows a schematic diagram of the interaction of water with chelated Gd^{3+}. Four different time constants are seen. (1) The rotational correlation time, τ_R, of the Gd complex; (2) the time constant for exchange of the Gd bound water with bulk water τ_M, and (3 and 4) the electron T_1 and T_2.

BPP theory, described earlier, was expanded by Solomon[27] and Bloembergen and Morgan[28] to include relaxation of water protons by

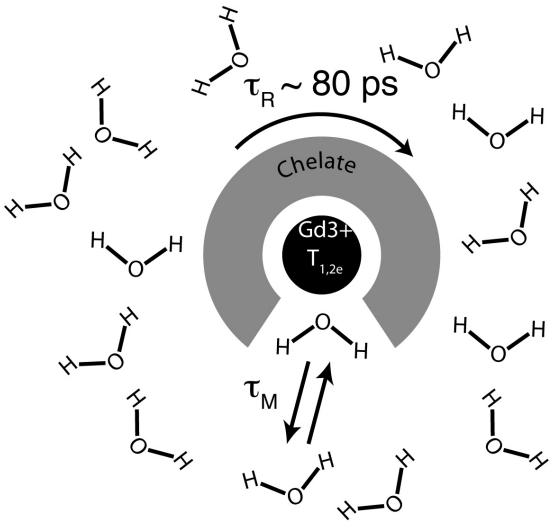

Figure 4: Schematic of the mechanism of a conventional contrast agent. The Gd^{3+} ions, with seven unpaired electrons, create a relaxation sink for water proton magnetization through the electron-nuclear dipole-dipole interaction. Chelating groups, such as DOTA or DTPA, shield the toxic Gd ion from the body. One water exchange site remains available for close water-Gd contact.

paramagnetic ions. Now called Solomon, Bloembergen, Morgan (SBM) theory, it has become the standard model to understand PRE. (See Lauffer[29] for a more detailed review.)

We start by considering the water proton relaxation rate,

$$R_{1p} = \frac{P_M}{\tau_M + T_{1M}}, \tag{4}$$

where R_{1p} is the bulk water proton relaxation rate, P_M is the mole fraction of waters in the first coordination sphere, τ_M is the time constant for

exchange of water between innersphere and bulk water, and T_{1M} is the T_1 of water protons in the inner-sphere. Equation 4 describes how the magnetization of the water bound to the Gd complex is transferred to bulk water in the sample.

The electron-nuclear dipole-dipole contribution to T_{1M} is given by

$$\frac{1}{T_{1M}} = \frac{2}{15} S(S+1) C_{dd}^2 \left\{ \frac{3\tau_{C1}}{1+\omega_H^2 \tau_{C1}^2} + \frac{7\tau_{C2}}{1+\omega_S^2 \tau_{C2}^2} \right\}, \tag{5}$$

where S is the electron spin (= 7/2 for Gd), C_{dd} is the proton-electron dipole-dipole interaction, ω_H is the proton Larmor frequency, and ω_S is the electron Larmor frequency. Equation 5 looks remarkably similar to Eq. (3). Indeed, it has the same structure of an interaction (here the electron-nuclear dipole-dipole interaction) modulated by a spectral density function. In Eq. (3), the correlation time was simply the rotational correlation time of water. For PRE, there are two correlation times, τ_{C1} and, τ_{C2} given by

$$\frac{1}{\tau_{C1}} = \frac{1}{\tau_R} + \frac{1}{\tau_M} + \frac{1}{T_{1e}} \text{ and} \tag{6}$$

$$\frac{1}{\tau_{C2}} = \frac{1}{\tau_R} + \frac{1}{\tau_M} + \frac{1}{T_{2e}}, \tag{7}$$

where τ_R is the rotational correlation time, τ_M is the time constant for exchange, and $T_{1,2e}$ are the electron T_1 and T_2. The electron T_1 is the spin-lattice relaxation time constant for recovery of the electron magnetization. The electron T_2 is the time constant for the decay of electron magnetization

in the transverse plane. The relaxation time constants for the unpaired Gd electrons are a function of magnetic field strength and are given by

$$\frac{1}{T_{1e}} = \frac{1}{5}\tau_{S0}^{-1}\left\{\frac{1}{1+\omega_H^2\tau_v^2} + \frac{4}{1+4\omega_S^2\tau_v^2}\right\} \text{ and} \tag{8}$$

$$\frac{1}{T_{2e}} = \frac{1}{10}\tau_{S0}^{-1}\left\{3 + \frac{5}{1+\omega_H^2\tau_v^2} + \frac{2}{1+4\omega_S^2\tau_v^2}\right\}, \tag{9}$$

where τ_{S0} is the electron T_1 at zero field and τ_v is the correlation time for the modulation of the Gd electronic orbitals by molecular collisions with water.

What do all these equations mean and why are they important for dendrimer-based contrast agents? The crux of the problem lies in the value of the correlation time of the electron-nuclear dipole-dipole interaction. In small molecules, like Gd(DOTA), the rotational correlation time of the Gd complex is short (in the picosecond range). In that case τ_R^{-1} is large and will dominate the other terms in Eqs. (6) and (7) and determine the value of the electron-nuclear dipole-dipole correlation time. It turns out that under these conditions, the correlation time of the electron-proton dipole-dipole interaction is not tuned to the water proton Larmor frequency, and the relaxation enhancement, though useful for medical imaging, is relatively weak. The relaxivity or relaxation rate of water protons per millimole of Gd for Gd(DOTA) is approximately 3.9 $s^{-1}mM^{-1}$ at clinical field strengths (1.5 T). The lower plot in Figure 6 shows the relaxivity of a Gd complex with a rotational correlation time of 100 ps — similar to the 80 ps rotational correlation time of Gd(DOTA) — as a function of proton Larmor frequency.

Increasing the rotational correlation time decreases the value of τ_R^{-1} in Equations 6 and 7 and allows the other time constants to come into play. In addition, the electron T_1 and T_2, which are a function of magnetic field strength as seen in Equations 8 and 9, create a condition perfect for efficient relaxation. That is, the correlation time of the electron-nuclear dipole-dipole interaction becomes tuned to the proton Larmor precession time.

Examination of Figure 6 shows that the relaxivity for a Gd complex with a 5 ns-rotational correlation time is enhanced over only a limited range of proton Larmor frequencies. Fortunately, at 1.5 T — the field strength of most clinical MRI systems — the relaxivity is dramatically greater for Gd on dendrimers than for conventional MRI contrast agents.

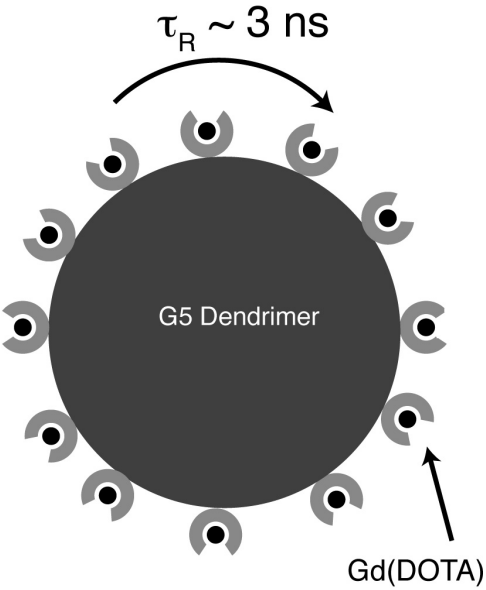

Figure 5: G5-Gd increases the number of Gd(DOTA) per molecule and the rotational correlation time.

At either higher or lower field strengths, the resonance condition between the correlation time and the precession time is broken and relaxivity decreases.

Equations (5)–(9) contain several assumptions adopted to reduce complexity. The primary assumption is that Gd(DOTA) or Gd(DTPA) when bonded to the dendrimer behaves as a rigid particle with no dynamic flexibility. This assumption is not valid as has been recently shown.[30,31] The effect of dendrimer internal motion is to smooth out and decrease the peak in relaxivity seen between 10 and 100 MHz in Figure 6. Nonetheless, the main features remain.

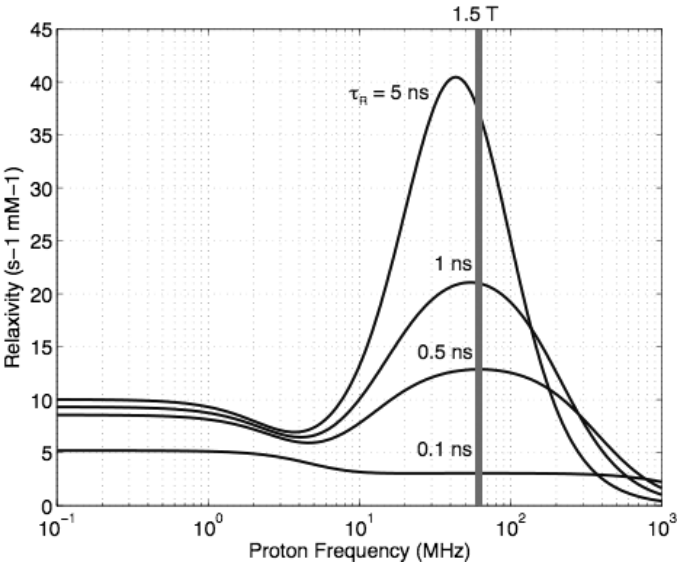

Figure 6: Water proton relaxivity as a function of proton Larmor frequency for $\tau_R = 0.1$, 0.5, 1.0, and 5.0 ns. At longer rotational correlation times, relaxation efficiency is dramatically increased between 10 and 100 MHz. A line is drawn for 1.5 T, the most common field strength for clinical imaging.

In summary, short electron T_1 (relative to proton T_1), large electron magnetic dipole moment, dipole-dipole interactions between the proton and electron, and exchange of water in the first coordination sphere create an efficient pathway for water proton spin-lattice relaxation. Figure 5 shows that the dendrimer nanoparticle has many Gd(DOTA) residues. The size of the dendrimer and attached Gd(DOTA) residues results in an increase of the rotational correlation time, τ_R from about 80 ps to about 3 ns. This increase in τ_R has profound changes in the relaxivity of the dendrimer-Gd complex. Most of the changes in relaxivity created by the increased rotational constant occur in the inner-sphere, dipole-dipole contribution to the spin lattice relaxation.

In addition to the increase in relaxivity created by the long rotational correlation time, numerous Gd(DOTA) residues can be added to single G5 dendrimer, further enhancing the sensitivity of each dendrimer macromolecule. This is especially important for targeted contrast agents since there may be a limited number of targeting sites.

8.2.4 Image acquisition and contrast in MRI

Recording the NMR signal in the presence of a magnetic field gradient allows collection of a one-dimensional image or profile of the sample. This concept is very straightforward. The magnetic field gradient adds an additional element to the NMR equation. Because the frequency of the spins is proportional to the magnetic field strength, the magnetic field gradient causes spins in different locations to resonate at different frequencies. A magnetic field gradient along the *x* direction Gx creates a linear ramp of the strength of the magnetic field as a function of the *x*. Because the

frequency of the spins is now a function of the distance, recording the NMR signal as a function of time creates a superposition of all of the signals. The NMR signal is said to be "frequency encoded". Fourier transform of this signal yields a one-dimensional image of the sample.

Rather than viewing the signal as being acquired as a function of time, it is possible to rearrange the variables in the time-evolution of the signal and create a new parameter, *k*. The *k* has dimensions of inverse space (cm^{-1}, for instance). Therefore, Fourier transformation of the signal creates a graph of signal intensity as a function of distance, a projection image.

The second (or third) dimension of an image is more difficult to acquire and more difficult to understand. These additional dimensions are said to be "phase encoded" because the phase of the spins is incremented over a series of acquisitions. One is effectively stepping through *k*-space in the second or third dimension. For a detailed account of phase-encoding, *k*-space, and MRI in general, see Haacke.[20]

There are two time constants in magnetic resonance that are called T_1 and T_2. T_1 is the time that it takes to restore the spin-lattice magnetization to the equilibrium level, and T_2 is the time constant for the decay of transverse or detected magnetization. T_1 ranges from about 2 s for fluid-like materials such as CSF to about 100 ms for unsaturated hydrocarbon chains in fat deposits.

A primary reason that MRI is useful for medical imaging is that different water molecules have different relaxation properties, depending on the surrounding tissue. An important and striking example of this is found in the brain, where T_1 and T_2 of white matter and gray matter differ. At 1.5 T,

white matter T_1 is approximately 750 ms and gray matter T_1 is about 1.0 s, whereas white matter T_2 is 75 ms and gray matter T_2 is 90 ms.[32]

Spins relax differently because they are in a different molecular environment and are exposed to different interactions. MRI pulse sequences require numerous RF pulses and signal acquisitions in order to obtain an appropriate sample of *k*-space.[20] If the repetition time (TR) is less than 5 times T_1, the longitudinal magnetization will not return to equilibrium but will achieve a steady state value. This value is easily calculated and can be shown to be $M_x(s.s.) = M_0(1 - e^{-TR/T1})$ when the flip angle is 90°.

Figure 7 shows that by pulsing at a repetition TR of approximately 500 ms, the signal difference between spins with a T_1 = 300 ms and T_1 = 600 ms is maximized. This is the typical operating mode for a T_1

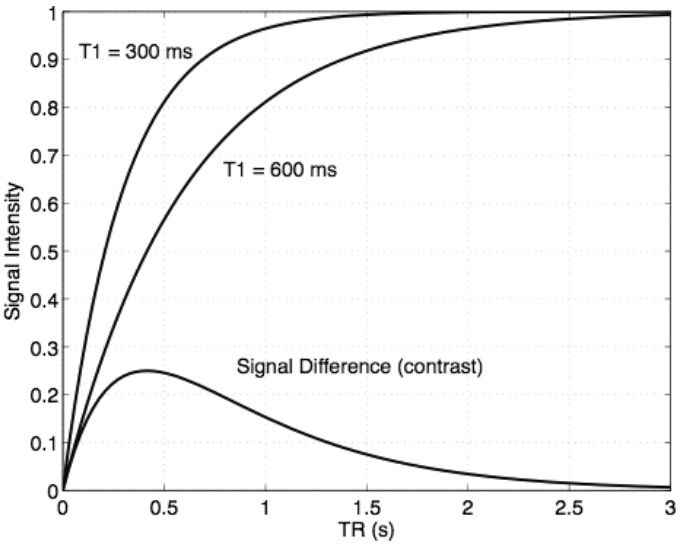

Figure 7: Signal intensity as a function of repetition time, TR, for T_1 = 300 and 600 ms, and the difference between the two signals. The signal intensity is the steady-state magnetization.

weighted pulse sequence. T_1 contrast agents are effective because they create regions with more efficient water proton spin lattice relaxation and therefore shorter T_1 times. The shorter T_1 times then create increased signal intensities on T_1-weighted images. T_1 contrast agents are said to be "positive" contrast agents because they increase the SNR where present.

8.3 Dendrimer Contrast Agents

8.3.1 Targeted dendrimers

A primary reason that dendrimers are attractive candidates for MRI contrast agents is the ability to attach different ligands to different branches or limbs of the dendrimers. The multiple arms allow attachment of different functional groups for targeting specific binding sites and molecules with Gd(III) for increased T_1 relaxation. Dendrimer contrast agents currently in published research have incorporated either Folic Acid[33] or Avidin[34] as a targeting agent. Other targeting agents that have been conjugated to dendrimer nanodevices include Herceptin, epidermal growth factor (EGF), and Arg–Gly–Asp (RGD). Targeting strategies are described more in depth in Chapter 5, Section 4 of this book.

8.3.2 Dendrimer contrast agents: Practice

The idea of using dendrimer-based MRI contrast agents was first put into practice by Erik Wiener *et al*.[35] in the early 1990s. They created two functional contrast agents by chelating both G2 and G6 PAMAM dendrimers with the metal chelate 2-(4-isothiocyanatobenzyl)-6-methyldiethylenetriaminepentaacetic acid to create PAMAM-TU-DTPA.

The PAMAM-TU-DTPA would then be complexed with Gd^{3+} to form functional contrast agents. NMR spectroscopy and/or gel electrophoresis showed that the G2 and G6 contrast agents held, on average, 11 and 170 surface chelates, respectively. Saturation of the G2 and G6 chelate PAMAM-TU-DTPA with Gd^{3+} displayed enhanced relaxivities equivalent to 43 and 1074 molecules of Gd^{3+}-DTPA (Magnevist), respectively.[35] Perhaps an equally important advantage exhibited from dendrimer contrast agents over Gd^{3+}-DTPA is the increase in blood pool retention time. Some of the more complex MRI procedures, such as three-dimensional MRI, can be very time consuming and should not be rushed. Keeping a substantial concentration of contrast agent in the blood for a longer period of time can lend toward maximizing the quality of the MRI. The G6 poly-chelate exhibited a prolonged half-life eight times that of Gd^{3+}-DTPA.[35] These optimistic results were just the first of many indicating the applicability of dendrimer-based contrast agents.

Most published research since this initial study has been aimed at producing contrast agents for specific purposes. The broad versatility of the dendrimer allows scientists to customize these nanodevices to the highest degree. While the basic concept of a chelated dendrimer remains the same, variations in size, structure, and composition can be altered to improve imaging of certain tissues or organs. Non-targeted PAMAM dendrimers, especially those of higher generations, tend to remain in the bloodstream for longer periods of time when injected intravenously.[36] By attaching targeting agents to dendrimers, as described previously in this book, contrast agents will accumulate in a specific tissue or organ of interest.[34,37]

Improving methods for cancer diagnosis is one particular area of interest in which dendrimer contrast agents have been implemented. Many types of cancer over-express folic acid receptors to supply the increased demand for folic acid. During mitosis, folic acid is required for DNA synthesis.[38] This knowledge has been exploited by several groups to create targeted nanodevices to deliver chemotherapy drugs specifically to those types of cancer cells. Utilization of folic acid for targeting has also been established as a successful method for improving contrast agent specificity.[33] The accumulation of Gd^{3+} in tumors causes them to be highlighted in respect to surrounding tissue. Improved tumor contrast on an MR image eases visual detection and thereby bestows greater confidence of an accurate diagnosis.

Several other papers have described specific purposes to which PAMAM dendrimers may benefit. One study has shown that employing PAMAM-based contrast agents improves the clarity of intratumoral angiography.[39] Intratumoral vasculature is often described as being "leaky" because of the observed increase in perfusion, when compared to normal vasculature. High-molecular-weight dendrimer contrast agents exhibit reduced excretion, which leads to higher intra- to extra-vasculature contrast.[39] The same concept applies to MR lymphangiography in mice models.[40] Again, high molecular weight contrast agents provide for better contrast of small vessels within the deep lymphatic system.[40] Figure 8 illustrates the detail that a 3D MRI image can display when used with dendrimer-based contrast agents.[41]

Often finding the best dendrimer construct for a specific application involves considering factors that have little to do with MRI technology

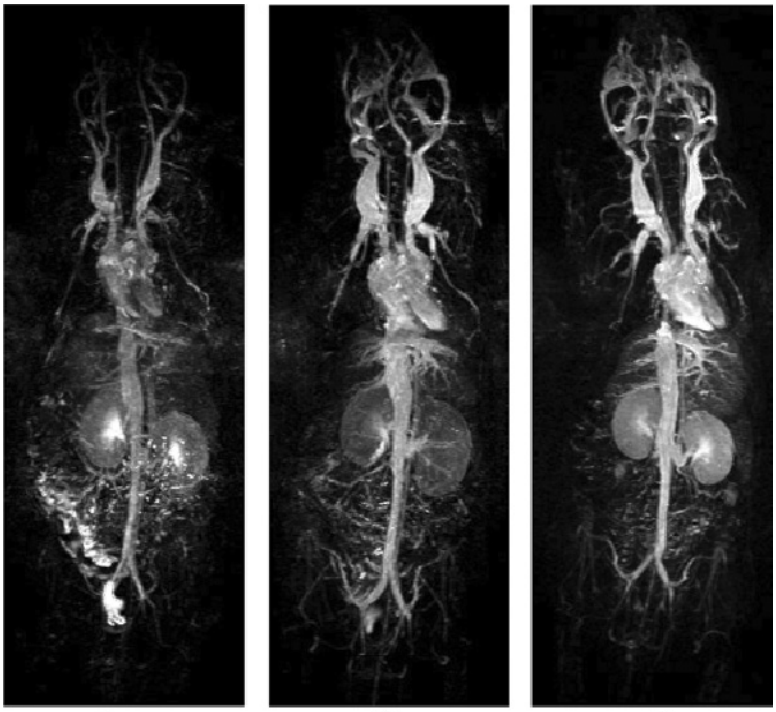

Figure 8: This T_1-weighted 3D image obtained from MRI illustrates the detail which can be observed using dendrimer-based contrast agents. The difference between pictures (a), (b), and (c) is the linker between the G4 PAMAM dendrimer and the Gd(III) chelate.[41] (Reprinted with permission from the *Journal of Medicinal Chemistry* **50**(13), 3185–3193, 2007 Copyright (2007) American Chemical Society.)

itself. A study aimed at imaging acute renal failure found that, while both polypropylenimine diaminobutyl (DAB) dendrimer and PAMAM dendrimer-based contrast agents provided similar functional images, the DAB dendrimer exhibited favorable excretion and pharmacokinetics.[42] The increase in blood pool retention of PAMAM-DTPA conjugates

consequently decreases the hepatic uptake of the contrast agent, thereby again making DAB dendrimer contrast agents more favorable for some liver imaging applications.[36] The relaxivity of a G2 polypropyleneimine (PPI) dendrimer contrast agent was found to be comparable to that of higher generation PAMAM dendrimers while being only a fraction of the size.[43] This finding advocates an alternative contrast agent for use when PAMAM dendrimers are not well suited for a specific application. These are just a few of the published examples that illustrate the diversity of dendrimer functionality.

Recent work in our laboratory has explored the use of targeted dendrimer contrast agents to selectively image tumors in immune-suppressed mice with KB human epithelial cancer cells expressing folate receptor (FAR). Both targeted and non-targeted dendrimer macromolecules were studied.[44] We find that the targeted dendrimer complex shows a statistically significant enhancement of the tumor when compared to the non-targeted dendrimer (Figure 9).

8.4 Conclusion and Future Directions

Dendrimer macromolecules possess many favorable properties for use as MRI contrast agents. First, the large number of dendrimer arms allows attachment of different ligands for different functional needs. This property has been exploited by attaching folic acid to serve as a targeting agent and Gd(DOTA) to serve as a contrast agent. Second, since each dendrimer contains many Gd(DOTA) residues, the relaxation efficiency per targeted site is greatly enhanced. And third, the high molecular weight of the

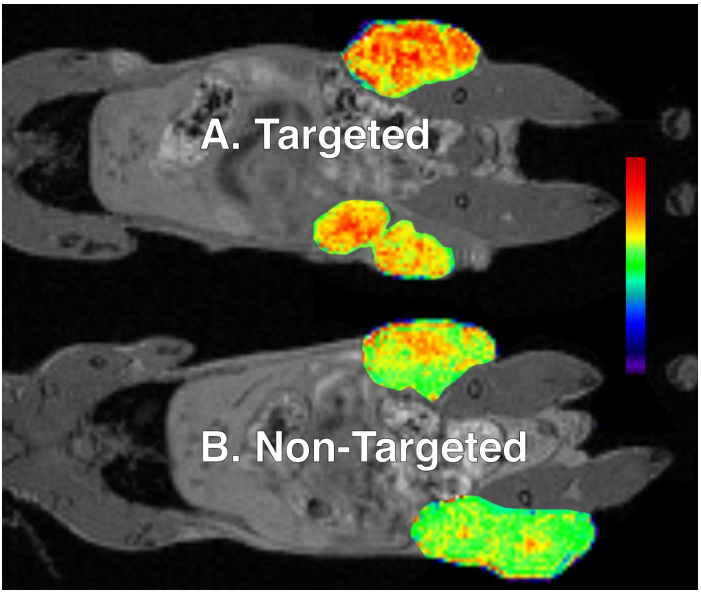

Figure 9: Images of SCID mice acquired with a T_1 weighted, 3D gradient-echo MRI pulse sequence. These images were acquired four hours after injection of either the targeted (A) or the non-targeted (B) contrast agent. The areas with tumors are colorized (the color lookup table is shown on the right of the figure). Red and yellow indicate high signal intensity on the T_1-weighted images and green indicates lower signal intensity. The tumors of the mice injected with a targeted contrast agent show significant enhancement when compared to the tumor of mice injected with non-targeted contrast agent.

dendrimer creates a significant increase in the relaxivity (relaxation rate per millimole of Gd) relative to conventional Gd contrast agents at the magnetic field strengths of clinical magnets.

This chapter has outlined the physical reasons that dendrimer macromolecules are ideal candidates for future applications of molecular imaging. The flexibility of dendrimer architecture allows many different

permutations of targeting, contrast enhancement, and therapy. Other recent reviews outline additional configurations and applications.[45–49] At the cutting edge of NMR research, dendrimers have been used to carry hyperpolized xenon for use as a biosensor.[50] The future of dendrimers in NMR and MRI is limited only by our imagination.

8.5 References

1. P. C. Lauterbur, Image formation by induced local interactions — examples employing nuclear magnetic-resonance, *Nature*, **242**, 190–191, 1973.
2. V. R. Fuchs and H. C. Sox, Jr., Physicians views of the relative importance of thirty medical innovations, *Health Aff (Millwood)*, **20**, 30–42, 2001.
3. F. W. Wehrli, On the 2003 Nobel Prize in medicine or physiology awarded to Paul C. Lauterbur and Sir Peter Mansfield, *Magn. Reson. Med.*, **51**, 1–3, 2004.
4. G. Vogel, 2003 Nobel Prize. Physicists honored for their medical insights. *Science*, **302**, 382–383, 2003.
5. J. Gore, Out of the shadows — MRI and the Nobel Prize, *N. Engl. J. Med.*, **349**, 2290–2292, 2003.
6. P. Mansfield and A. A. Maudsley, Medical imaging by NMR, *Br. J. Radiol.*, **50**, 188–194, 1977.
7. P. Mansfield, Snapshot magnetic resonance imaging (Nobel lecture), *Angew. Chem. Int. Ed. Engl.*, **43**, 5456–5464, 2004.
8. N. E. Rose and S. M. Gold, A comparison of accuracy between clinical examination and magnetic resonance imaging in the diagnosis of

meniscal and anterior cruciate ligament tears, *Arthroscopy*, **12**, 398–405, 1996.

9. F. Di Salle, E. Formisano, D. E. Linden, R. Goebel, S. Bonavita, A. Pepino, F. Smaltino, and G. Tedeschi, Exploring brain function with magnetic resonance imaging, *Eur. J. Radiol*., **30**, 84–94, 1999.
10. M. Kriege, C. T. Brekelmans, C. Boetes, P. E. Besnard, H. M. Zonderland, I. M. Obdeijn, R. A. Manoliu, T. Kok, H. Peterse, M. M. Tilanus-Linthorst, S. H. Muller, S. Meijer, J. C. Oosterwijk, L. V. Beex, R. A. Tollenaar, H. J. de Koning, E. J. Rutgers, and J. G. Klijn, Efficacy of MRI and mammography for breast-cancer screening in women with a familial or genetic predisposition, *N. Engl. J. Med*., **351**, 427–437, 2004.
11. S. K. Plevritis, A. W. Kurian, B. M. Sigal, B. L. Daniel, D. M. Ikeda, F. E. Stockdale, and A. M. Garber, Cost-effectiveness of screening BRCA1/2 mutation carriers with breast magnetic resonance imaging, *Journal of the American Medical Association*, **295**, 2374–2384, 2006.
12. P. Caravan, J. J. Ellison, T. J. McMurry, and R. B. Lauffer, Gadolinium (III) Chelates as MRI contrast agents: Structure, dynamics, and applications, *Chem. Rev*., **99**, 2293–2352, 1999.
13. C. W. Jung and P. Jacobs, Physical and chemical properties of superparamagnetic iron oxide MR contrast agents: Ferumoxides, ferumoxtran, ferumoxsil, *Magn. Reson. Imaging*., **13**, 661–674, 1995.
14. G. J. Strijkers, W. J. Mulder, G. A. van Tilborg, and K. Nicolay, MRI contrast agents: Current status and future perspectives, *Anticancer Agents Med. Chem*., **7**, 291–305, 2007.

15. A. K. Patri, J. F. Kukowska-Latallo, and J. R. Baker, Jr., Targeted drug delivery with dendrimers: Comparison of the release kinetics of covalently conjugated drug and non-covalent drug inclusion complex, *Advanced Drug Delivery Reviews*, **57**, 2203–2214, 2005.
16. E. M. Purcell, H. C. Torrey, and R. V. Pound, Resonance absorption by nuclear magnetic moments in a solid, *Physical Review*, **69**, 37–38, 1946.
17. F. Bloch, W. W. Hansen, M. Packard, Nuclear induction, *Physical Review*, **69**, 127–127, 1946.
18. A. Abragam, *The Principles of Nuclear Magnetism*, Oxford, Clarendon Press, 1961.
19. R. R. Ernst, G. Bodenhausen, and A. Wokaun, *Principles of Nuclear Magnetic Resonance in One and Two Dimensions*, Oxford, New York, Clarendon Press, Oxford University Press, 1988.
20. E. M. Haacke, *Magnetic Resonance Imaging: Physical Principles and Sequence Design*, New York, Wiley-Liss, 1999.
21. N. Bloembergen, E. M. Purcell, and R. V. Pound, Relaxation effects in nuclear magnetic resonance absorption, *Physical Review*, **73**, 679–712, 1948.
22. S. H. Koenig, R. G. Bryant, K. Hallenga, and G. S. Jacob, Magnetic cross-relaxation among protons in protein solutions, *Biochemistry*, **17**, 4348–4358, 1978.
23. R. A. Dwek, R. E. Richards, K. G. Morallee, E. Nieboer, R. J. Williams, and A. V. Xavier, The lanthanide cations as probes in biological systems. Proton relaxation enhancement studies for model systems and lysozyme, *Eur. J. Biochem*., **21**, 204–209, 1971.

24. C. F. Geraldes, A. D. Sherry, R. D. Brown, 3rd, and S. H. Koenig, Magnetic field dependence of solvent proton relaxation rates induced by Gd^{3+} and Mn^{2+} complexes of various polyaza macrocyclic ligands: implications for NMR imaging, *Magn. Reson. Med.*, **3**, 242–250, 1986.

25. S. H. Koenig, C. Baglin, R. D. Brown, 3rd, and C. F. Brewer, Magnetic field dependence of solvent proton relaxation induced by Gd^{3+} and Mn^{2+} complexes, *Magn. Reson. Med.*, **1**, 496–501, 1984.

26. W. P. Cacheris, S. C. Quay, and S. M. Rocklage, The relationship between thermodynamics and the toxicity of gadolinium complexes, *Magn. Reson. Imaging*, **8**, 467–481, 1990.

27. I. Solomon, Relaxation processes in a system of 2 spins, *Physical Review*, **99**, 559–565, 1955.

28. N. Bloembergen and L. O. Morgan, Proton relaxation times in paramagnetic solutions effects of electron spin relaxation, *Journal of Chemical Physics*, **34**, 842–850, 1961.

29. R. B. Lauffer, Paramagnetic metal-complexes as water proton relaxation agents for Nmr imaging — Theory and design, *Chemical Reviews*, **87**, 901–927, 1987.

30. S. Laus, A. Sour, R. Ruloff, E. Toth, and A. E. Merbach, Rotational dynamics account for pH-dependent relaxivities of PAMAM dendrimeric, Gd-based potential MRI contrast agents, *Chemistry-a European Journal*, **11**, 3064–3076, 2005.

31. G. M. Nicolle, E. Toth, H. Schmitt-Willich, B. Raduchel, and A. E. Merbach, The impact of rigidity and water exchange on the relaxivity

of a dendritic MRI contrast agent, *Chemistry-a European Journal*, **8**, 1040–1048, 2002.

32. P. A. Bottomley, T. H. Foster, R. E. Argersinger, and L. M. Pfeifer, A review of normal tissue hydrogen NMR relaxation times and relaxation mechanisms from 1–100 MHz: Dependence on tissue type, NMR frequency, temperature, species, excision, and age, *Med. Phys*., **11**, 425–448, 1984.
33. S. D. Konda, M. Aref, M. Brechbiel, and E. C. Wiener, Development of a tumor-targeting MR contrast agent using the high-affinity folate receptor: Work in progress, *Invest. Radiol*., **35**, 50–57, 2000.
34. H. Kobayashi, S. Kawamoto, T. Saga, N. Sato, T. Ishimori, J. Konishi, K. Ono, K. Togashi, and M. W. Brechbiel, Avidin-dendrimer-(1B4M-Gd)(254): A tumor-targeting therapeutic agent for gadolinium neutron capture therapy of intraperitoneal disseminated tumor which can be monitored by MRI, *Bioconjugate Chemistry*, **12**, 587–593, 2001.
35. E. C. Wiener, M. W. Brechbiel, H. Brothers, R. L. Magin, O. A. Gansow, D. A. Tomalia, and P. C. Lauterbur, Dendrimer-based metal chelates: A new class of magnetic resonance imaging contrast agents, *Magn. Reson. Med*., **31**, 1–8, 1994.
36. H. Kobayashi, T. Saga, S. Kawamoto, N. Sato, A. Hiraga, T. Ishimori, J. Konishi, K. Togashi, and M. W. Brechbiel, Dynamic micromagnetic resonance imaging of liver micrometastasis in mice with a novel liver macromolecular magnetic resonance contrast agent DAB-Am64-(1B4M-Gd)(64), *Cancer Research*, **61**, 4966–4970, 2001.
37. S. D. Konda, M. Aref, M. Brechbiel, and E. C. Wiener, Development of a tumor-targeting MR contrast agent using the high-affinity folate

receptor — Work in progress, *Investigative Radiology*, **35**, 50–57, 2000.

38. S. W. Choi and J. B. Mason, Folate and carcinogenesis: An integrated scheme, *J. Nutr.*, **130**, 129–132, 2000.
39. H. Kobayashi, N. Sato, S. Kawamoto, T. Saga, A. Hiraga, T. Ishimori, J. Konishi, K. Togashi, and M. W. Brechbiel, 3D MR angiography of intratumoral vasculature using a novel macromolecular MR contrast agent, *Magnetic Resonance in Medicine*, **46**, 579–585, 2001.
40. H. Kobayashi, S. Kawamoto, R. A. Star, T. A. Waldmann, Y. Tagaya, and M. W. Brechbiel, Micro-magnetic resonance lymphangiography in mice using a novel dendrimer-based magnetic resonance imaging contrast agent, *Cancer Res.*, **63**, 271–276, 2003.
41. H. Xu, C. A. Regino, M. Bernardo, Y. Koyama, H. Kobayashi, P. L. Choyke, and M. W. Brechbiel, Toward improved syntheses of dendrimer-based magnetic resonance imaging contrast agents: New bifunctional diethylenetriamine-pentaacetic acid ligands and non-aqueous conjugation chemistry, *J. Med. Chem.*, **50**, 3185–3193, 2007.
42. J. W. Dear, H. Kobayashi, M. W. Brechbiel, and R. A. Star, Imaging acute renal failure with polyamine dendrimer-based MRI contrast agents, *Nephron. Clin. Pract.*, **103**, c45–49, 2006.
43. S. J. Wang, M. Brechbiel, and E. C. Wiener, Characteristics of a new MRI contrast agent prepared from polypropyleneimine dendrimers, generation 2, *Investigative Radiology*, **38**, 662–668, 2003.
44. S. D. Swanson, A. K. Patri, J. F. Kukowska-Latilla, and J. R. Baker Jr., Targeted contrast using gadolinium labeled G5 dendrimers. In,

ISMRM, Fourteenth Scientific Meeting and Exhibition, Seattle, WA, 2006.

45. S. H. Bai, C. Thomas, A. Rawat, and F. Ahsan Recent progress in dendrimer-based nanocarriers, *Critical Reviews in Therapeutic Drug Carrier Systems*, **23**, 437–495, 2006.
46. V. Gajbhiye, P. V. Kumar, R. K. Tekade, and N. K. Jain, Pharmaceutical and biomedical potential of PEGylated dendrimers, *Current Pharmaceutical Design*, **13**, 415–429, 2007.
47. S. D. Caruthers, S. A. Wickline, and G. M. Lanza, Nanotechnological applications in medicine, *Current Opinion in Biotechnology*, **18**, 26–30, 2007.
48. D. A. Tomalia, L. A. Reyna, and S. Svenson, Dendrimers as multi-purpose nanodevices for oncology drug delivery and diagnostic imaging, *Biochemical Society Transactions*, **35**, 61–67, 2007.
49. S. Svenson and D. A. Tomalia, Commentary — Dendrimers in biomedical applications — reflections on the field, *Advanced Drug Delivery Reviews*, **57**, 2106–2129, 2005.
50. J. L. Mynar, T. J. Lowery, D. E. Wemmer, A. Pines, and J. M. J. Frechet, Xenon biosensor amplification via dendrimer-cage supramolecular constructs, *Journal of the American Chemical Society*, **128**, 6334–6335, 2006.

This page intentionally left blank

Chapter 9

Nanoparticle — Membrane Interactions: Mechanism for Enhanced Permeability

Seungpyo Hong, Almut Mecke, Pascale Leroueil, Mark M. Banaszak Holl & Bradford G. Orr

---

Outline

9.1 Introduction

The use of nanoparticles holds tremendous promise in a number of applications. The economic impact of these products is predicted to grow exponentially and reach $1 trillion by 2015.[1] This enormous enthusiasm, in both the research and business communities, stems from the emerging and merging capabilities of a number of scientific disciplines including: material science, chemistry, medicine, physics, and scientific computation. The central tenant is that we will soon have the ability to design and synthesize nanometer structures that are able to perform tasks that were previously only found in science fiction. Examples include advanced medicines that target disease and reduce deleterious side effects, materials that repair themselves when broken and molecular computer components that vastly reduce size and power requirement from today's devices. This truly appears to be the dawn of a new age of "Better Things for Better Living … Through Chemistry."[2]

However, as with any new technology, care must be exercised in first determining possible unintended consequences. History (such as with DDT pesticide, asbestos and formaldehyde insulations) has taught us to be careful before introducing new manmade compounds and materials into the environment until extensive studies have been performed to understand their effects. With regard to nanoparticles these types of environmental and toxicological studies are still in their infancy. However, several reports

already point to the need to take care in understanding the possible effects of these particles.[3–6]

To study this question we have examined the interaction of a particular type of nanoparticle, a dendritic polymer called a dendrimer, with biological material (for a review of dendrimers see ref. 7). Dendrimers have been called "artificial proteins" due to their similarity in size and constituent components to naturally occurring proteins. The nanoparticle can be formed via a layer-by-layer synthesis starting from a core molecule. Dendrimers are a very useful model system because their size and end group chemistry can be precisely controlled and the synthesized particles are quite homogeneous. Specifically, the particles that have been used in these studies have an ethylene diamine core with three to seven branching layers surrounding it, see Figure 1. Such nanoparticles are named generation *N* poly(amidoamine) dendrimers and abbreviated as G*N* PAMAM dendrimers. Additionally, the functional end-groups can be synthesized with various termini so as to vary their charge when the particle is in aqueous physiological conditions. At pH 7, amine terminated dendrimers protonate and have a positive charge, carboxyl end-groups become negatively charged and acetyl termini remain neutral. The final important characteristic of these nanoparticles is the high degree of homogeneity. Polydispersity index values near 1.0 allow confidence that as particle properties are systematically varied the behavior is due to the bulk of the particles and not outliers in the distribution.

There is, of course, nothing new about the introduction of foreign nanoparticles into living systems. Evolution has equipped plants and animals with a number of mechanisms for dealing with foreign proteins, viruses etc. What is relatively new and unusual is our ability to create

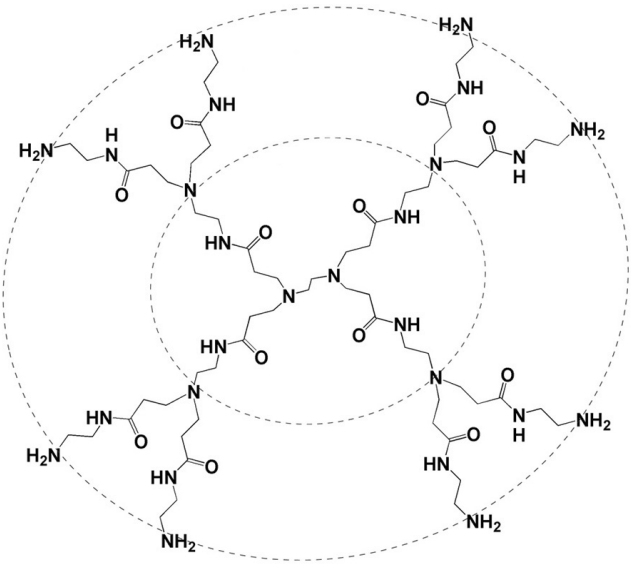

Figure 1: Structure of amine terminated poly(amidoamine) (PAMAM) dendrimer generation 1. (Reprinted with permission from A. Mecke *et al*., "Lipid bilayer disruption by polycationic polymers: The roles of size and chemical functional group," *Langmuir*, **21**(23), 10348–10354, 2005. Copyright (2005) American Chemical Society.)

nanostructures having specific functional properties. The possible introduction of foreign particles of this same scale into biological systems begs the question "How will living systems deal with these particles that are the same size as the fundamental engines of life?"

9.2 Cellular Membrane Disruption Upon Exposure to Dendrimers

There is considerable data pointing to the ability of dendrimers to disrupt cell membranes.[8,9] These particles have been used for over a decade as

transfection agents enhancing transport across cell membranes.[10,11] Dendrimers are not the only artificial polymer to act in this manner; however, in this chapter we will concentrate on dendrimers, as a model, and later mention findings that appear to be generally applicable to other polycationic polymers. Several groups have examined the interaction of PAMAM dendrimers with phosphatidylethanolamine-containing vesicles as a first step towards examining the interaction with cells.[9] In summary, efficient cross-membrane transport and membrane disruption were observed. The efficacy was strongly dependent on the size of the dendrimer (generation), chemical structure and composition of the vesicle membrane. These results demonstrate strong interactions between dendrimers and simple lipid bilayers. However cellular membranes are much more complex with the inclusion of cholesterol, sugars and proteins. Would the same internalization be observed for dendrimers and biological cells?

To determine this we have performed a series of experiments exposing several lines of cells to dendrimers having different sizes and end-group functionalizations.[12]

The experiments consisted of examining the transport of fluorescently labeled dendrimers across cell membranes and the diffusion of dyes into and out of cells exposed to dendrimers, Figure 2. Specifically we investigated the interaction of G7-NH_2, G5-NH_2, and G5-Ac PAMAM dendrimers with KB and Rat2 cell membranes. NH_2 and Ac denote amine and acetamide groups as end groups, respectively. We have evaluated the release of two cytosolic enzymes, lactate dehydrogenase (LDH) and luciferase (Luc), from the cells upon exposure to dendrimers in terms of generation and

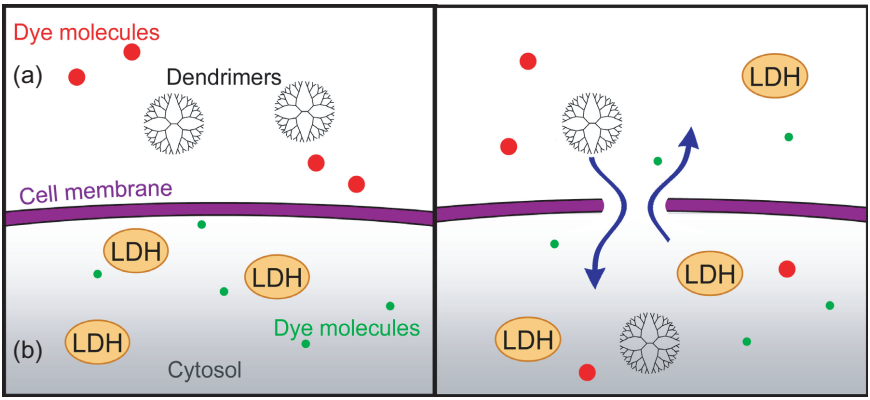

Figure 2: Schematic view of how dendrimers might increase the transport of small molecules across the cell membrane.

the identity of surface functional group (amine or acetamide). The temperature dependence of the binding and internalization has also been studied.

It was found that G7-NH_2 and G5-NH_2 PAMAM dendrimers induce significant leakage of LDH and Luc whereas G5-Ac does not. Similarly, the presence of G5-NH_2 was shown to make the cell membrane permeable to the small molecules such as propidium iodide (PI indicating diffusion into cells) and fluorescein (indicating diffusion out of cells) even though the cells were still viable.

9.3 Dendrimer-Induced Enzyme Leakage from Cells

The effects of G7-NH_2, G5-NH_2, and G5-Ac dendrimers on the membrane permeability of KB and Rat2 cells were investigated using LDH and Luc assays. Concentration dependent dendrimer-induced LDH release at 37 and 6°C is shown in Figure 3.

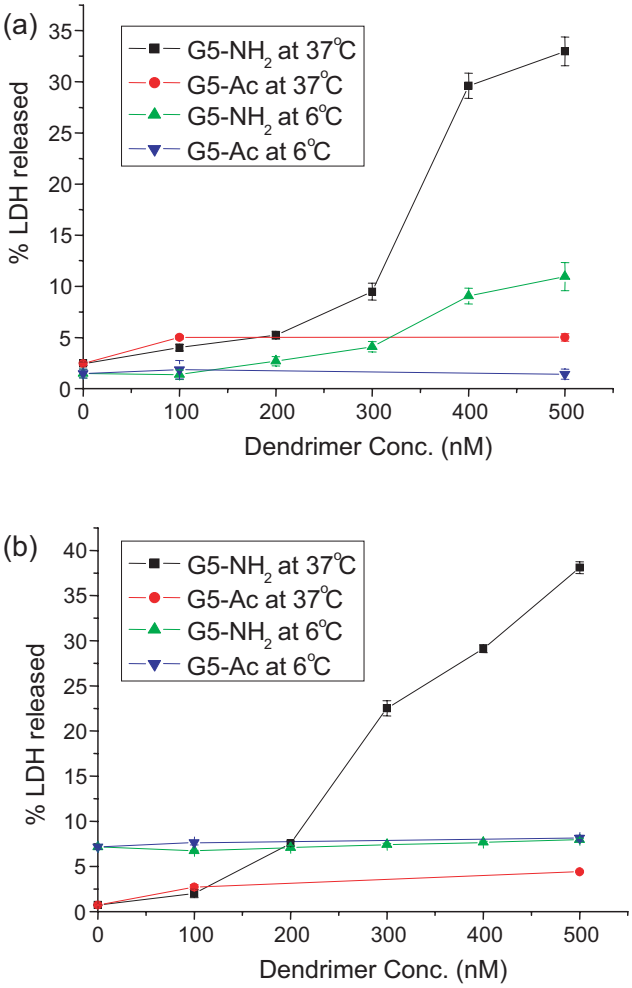

Figure 3: Dose-dependent LDH release from (a) KBpLuc and (b) Rat2pLuc cell lines at 37°C and 6°C by G5-NH_2 and G5-Ac-PAMAM dendrimers. (Reprinted with permission from S. Hong *et al.*, "Interaction of poly(amidoamine) dendrimers with supported lipid bilayers and cells: Hole formation and the relation to transport, *Bioconjugate Chem.*, **15**(4), 774–782, 2004. Copyright (2004) American Chemical Society.)

As the concentration of G5-NH_2 increases, the LDH release from both KBpLuc and Rat2pLuc increases. In contrast, neither cell line releases a significant amount of LDH as a result of exposure to G5-Ac. KBpLuc and Rat2pLuc cells incubated with both G5-NH_2 and G5-Ac at 6°C exhibited no LDH release. Luc release followed the same general trend observed for LDH release (Figure 4). For the Luc release tests, both cell lines were transfected using dendrimers to induce expression of the Luc gene as described elsewhere.[10]

To further investigate the binding and internalization of dendrimers, fluorescence images of Rat2 cells were taken after incubation with dendrimer-FITC conjugates at different temperatures, Figure 5. Rat2, a fibroblast cell line, was chosen in this experiment due to its stable surface adherence. DNA in the cell nucleus was stained by DAPI. The stained nuclei can be seen as blue spots in the images while dendrimer-FITC conjugates emit green fluorescence (Figure 5(b)) shows a fluorescence image of Rat2 cells incubated with 200 nM of G5-NH_2–FITC at 37°C for 1 hr. Dendrimers are apparent both inside the cells as well as associated with the membrane. This indicates that the G5-NH_2–FITC dendrimers interact with the cell membrane and enter the cell at physiological temperature (37°C). At 6°C, however, although the dendrimers associate with the cell membrane, no significant internalization was observed (Figure 5(c)). Identical experiments employing G5-Ac-FITC at 200 nM concentration indicate no association with the cell membrane or internalization into the cell (Figure 5(d)).

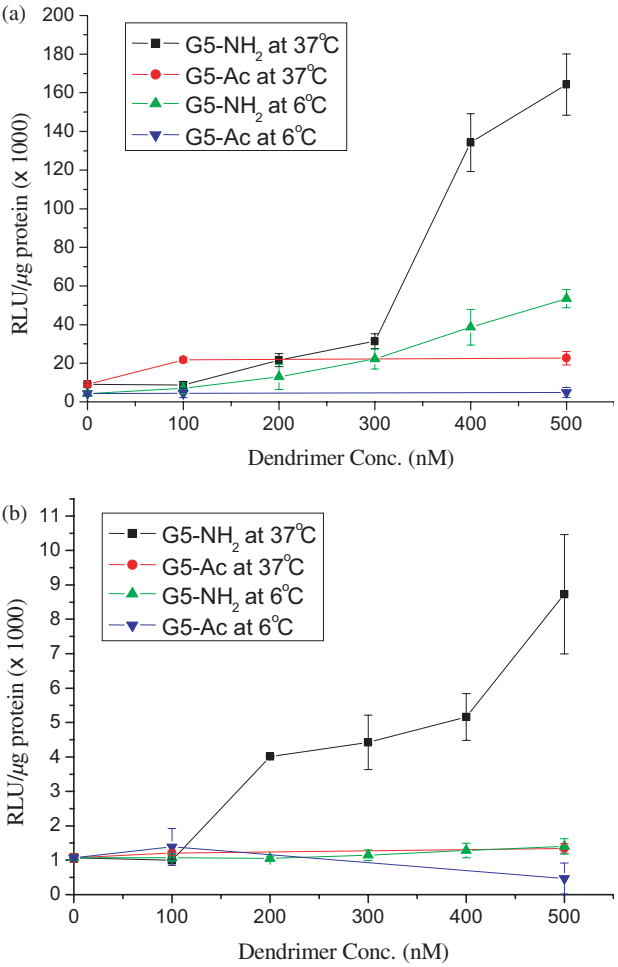

Figure 4: Dose-dependent Luc release from (a) KBpLuc and (b) Rat2pLuc cell Lines at 37°C and 6°C by G5-NH_2 and G5-Ac-PAMAM dendrimers. (Reprinted with permission from S. Hong *et al.*, "Interaction of poly(amidoamine) dendrimers with supported lipid bilayers and cells: Hole formation and the relation to transport, *Bioconjugate Chem.*, **15**(4), 774–782, 2004. Copyright (2004) American Chemical Society.)

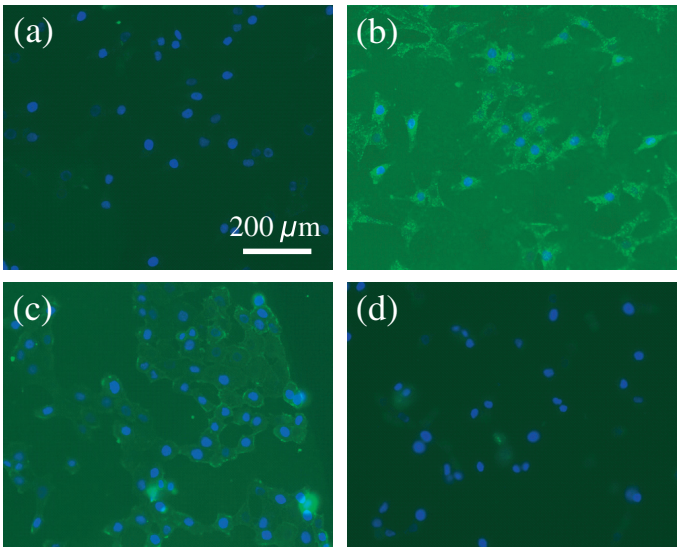

Figure 5: Fluorescence microscopy of (a) untreated Rat2 cells (control), (b) Rat2 cells incubated with 200 nM G5-NH2–FITC at 37°C for 1 hr, (c) Rat2 cells incubated with 200 nM G5-NH2–FITC at 6°C for 1 hr, and (d) Rat2 cells incubated with 200 nM G5-Ac-FITC at 37°C for 1 hr. Blue spots represent the cell nucleus stained by DAPI and green spots are dendrimer-FITC conjugates. (Reprinted with permission from S. Hong *et al.*, "Interaction of poly(amidoamine) dendrimers with supported lipid bilayers and cells: Hole formation and the relation to transport, *Bioconjugate Chem.*, **15**(4), 774–782, 2004. Copyright (2004) American Chemical Society.)

9.4 Reversibility of Dendrimer-Induced Membrane Permeability

The reversibility of the dendrimer-induced membrane permeability was tested by replacing a solution of G5-NH_2 dendrimer with dendrimer-free PBS and monitoring the LDH release. The dendrimer-induced membrane

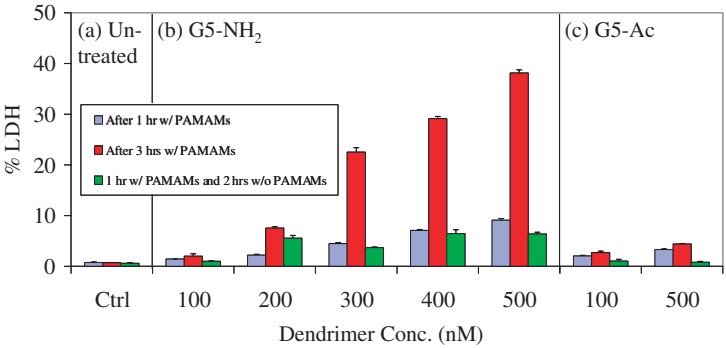

Figure 6: AFM height images of DMPC bilayer (a) before, and (b–f) 7–32 minutes after adding G5-acetamide. Gray scale height 0–20 nm. (Reprinted with permission from S. Hong *et al.*, "Interaction of poly(amidoamine) dendrimers with supported lipid bilayers and cells: Hole formation and the relation to transport, *Bioconjugate Chem.*, **15**(4), 774–782, 2004. Copyright (2004) American Chemical Society.)

permeability of cell lines in the presence of G5-NH_2 was not permanent and cells recovered their membrane integrity upon removal of dendrimer/PBS solutions (Figure 6), as indicated by LDH release. This "re-sealing" behavior is consistent with the observation that G5-NH_2 dendrimers are not cytotoxic up to 500 nM, as after removal of the dendrimer solution the cell can return the membrane permeability back to the normal level.

9.5 The Role of Dendrimer Surface Functionalization: Amine vs. Acetamide

To test possible mechanisms of internalization and their implications for cytosolic enzyme release (Figure 7), comparisons between G5-NH_2,

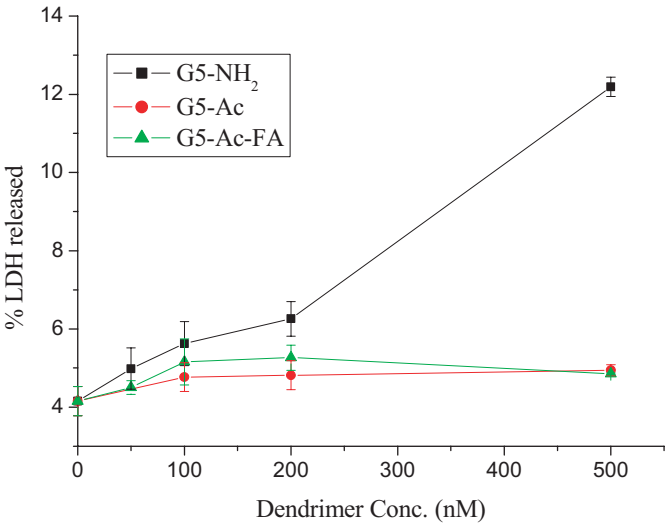

Figure 7: Comparison of interaction of G5-NH_2, G5-Ac, and G5-Ac-FA with FAR-KB cell line. Note that G5-Ac-FA is internalized by receptor mediated endocytosis. (Reprinted with permission from S. Hong *et al.*, "Interaction of poly(amidoamine) dendrimers with supported lipid bilayers and cells: Hole formation and the relation to transport, *Bioconjugate Chem.*, **15**(4), 774–782, 2004. Copyright (2004) American Chemical Society.)

G5-Ac, and G5-Ac-FA were carried out using the LDH assay. It has been demonstrated that internalization of G5-Ac-FA occurs through receptor-mediated endocytosis, initiated by binding of folic acid (FA) to folic acid receptors (FAR) on KB cells.[13] Under the same conditions, no uptake of G5-Ac is observed. The LDH assay results show no significant LDH release from KB cells following a three-hour incubation with G5-Ac-FA or G5-Ac. However, incubation with G5-NH_2 induced significant LDH release, consistent with previous experiments.

9.6 Effect of Dendrimer Generation on Cell Membrane Permeability

It is well known that high generation PAMAM dendrimers are unusually effective at disrupting cell membranes.[9,14] In order to test this effect upon LDH release, G5-NH_2 and G7-NH_2 dendrimers were analyzed at 37 and 6°C. The results of an LDH assay comparing enzymatic leakage for both KB and Rat2 cell lines after exposure to varying concentration of G5-NH_2 and G7-NH_2 are shown in Figure 8. At 37°C, G7-NH_2 causes a greater release of LDH than G5-NH_2 at all concentrations. In addition, whereas LDH release was not observed for G5-NH_2 at 6°C, the G7-NH_2 was still capable of causing LDH release (Figure 8(b)).

9.7 Tests for Diffusion of Dyes

To study passive diffusion in and out of the cell, small molecular probes (PI and FDA) were used according to a modification of a previous literature method.[15] PI is readily internalized into cells with disrupted membranes, but is excluded from cells with intact membranes. On the other hand, fluorescein diacetate (FDA), a non-fluorescent compound, readily enters intact cells and then undergoes hydrolysis by endogenous esterase, resulting in release of fluorescein into the cytosol. The cytosolic fluorescein is not able to transverse a normal cell membrane without holes. Thus, the FDA is used as a marker for diffusion-out. Consequently, it is presumed that fluorescence intensity of PI should be increased and that of fluorescein should be decreased if the presence of G5-NH_2 makes the membrane permeable to these dyes.

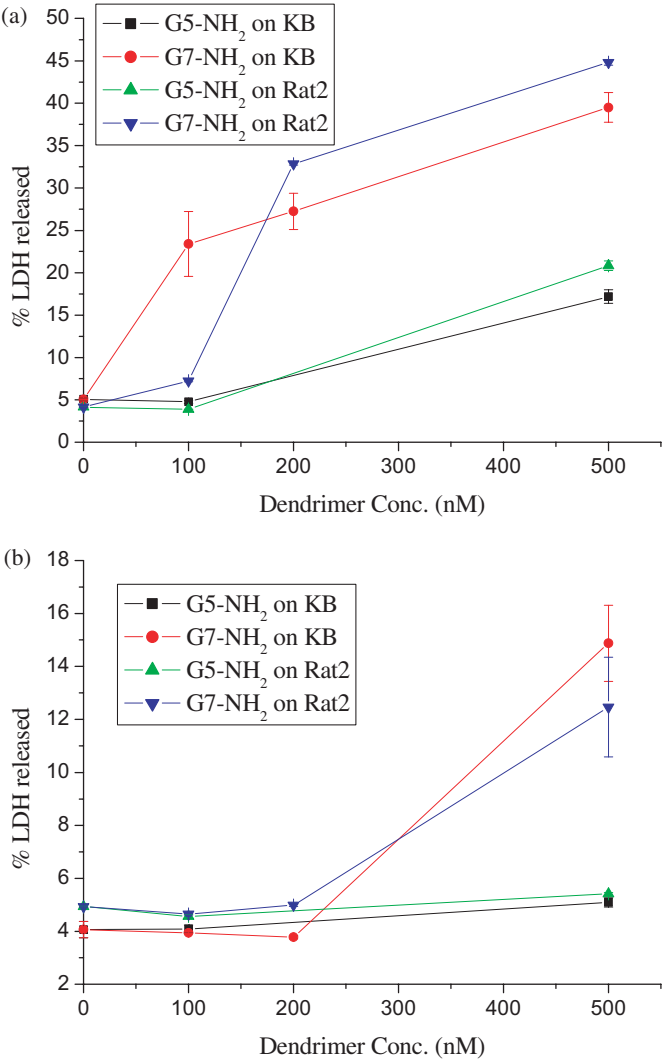

Figure 8: Comparison of different dendrimer generations. Enzyme release from KB and Rat2 cells after incubation with G5-NH_2 and G7-NH_2 (a) 37°C and (b) 6°C. (Reprinted with permission from S. Hong *et al.*, "Interaction of poly(amidoamine) dendrimers with supported lipid bilayers and cells: Hole formation and the relation to transport, *Bioconjugate Chem.*, **15**(4), 774–782, 2004. Copyright (2004) American Chemical Society.)

Figure 9 shows flow cytometer data of Rat2 cells incubated with G5 PAMAM dendrimers and then stained with PI. As illustrated in Figures 9(a)–(c) and 9(e), PI is internalized into the cells in a G5-NH_2 concentration dependent manner. In the case of G5-Ac, however, no significant difference in PI incorporation was observed as compared to the control cells. (Figure 9(d)).

Fluorescence intensity of fluorescein in cells as a function of G5-NH_2 dendrimer concentration is illustrated in Figure 10. Consistent with previous results,[15] FDA was internalized through intact cell membranes, resulting in a substantial signal for free fluorescein in Rat2 cells. As the G5-NH_2 concentration increased, however, the signal intensity of the fluorescein significantly decreased, indicating that the membrane had become permeable (Figure 10(e)). Rat2 cells incubated with G5-Ac did not show any noticeable difference from the control experiment (Figure 10(d)).

The release of cytosolic enzymes, LDH and Luc, demonstrates an increase in membrane permeability (Figures 3 and 4). The larger enzyme of the two, LDH, is a 135–140 kDa complex protein with a hydrodynamic radius of ~4.3 nm.[16] The smaller 62 kDa enzyme, Luc composed of α- and β-subunits, should be able to diffuse through a similar sized hole. The overall dimensions of this heterodimer are reported as 7.5 nm × 4.5 nm × 4.0 nm (~2.7 nm in radius).[17] Membrane permeability returns to normal following removal of the dendrimer-containing solution. Presumably, the cell has additional lipid available and can regenerate its membrane within two hours (as assayed by permeability in Figure 6).

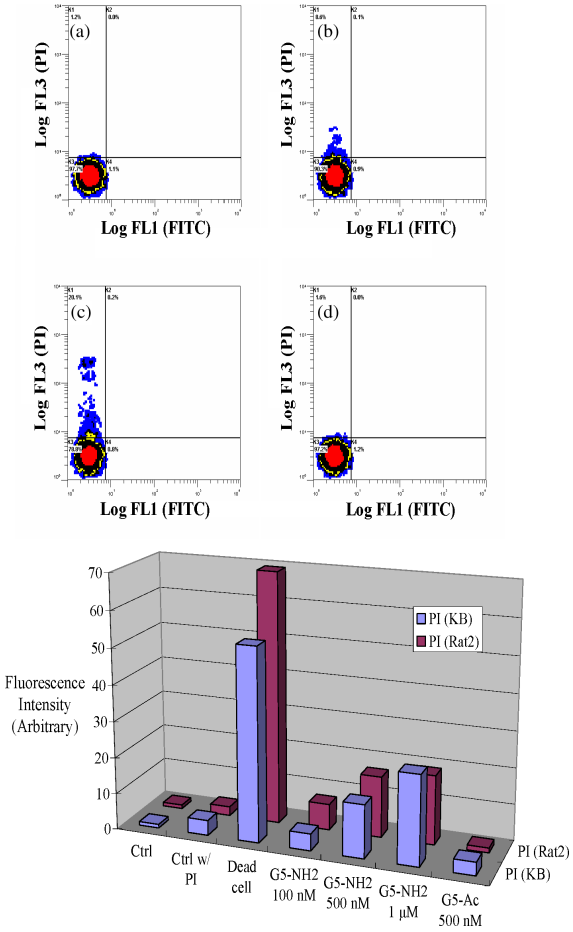

Figure 9: Flow cytometer diagrams of Rat2 cells at several representative conditions. (a) Untreated, (b) incubated with PI, (c) incubated with 500 nM G5-NH_2 and PI, and (d) incubated with 500 nM G5-Ac and PI at 37°C for 1 hr. (e) Signal intensity of PI fluorescence for KB and Rat2 cells after incubation with dendrimers. Controls (first three columns): cells in pure PBS buffer, cells in the buffer with PI, and dead cells incubated with 30% ethanol solution for 30 min. (Reprinted with permission from S. Hong *et al.*, "Interaction of poly(amidoamine) dendrimers with supported lipid bilayers and cells: Hole formation and the relation to transport, *Bioconjugate Chem.*, **15**(4), 774–782, 2004. Copyright (2004) American Chemical Society.)

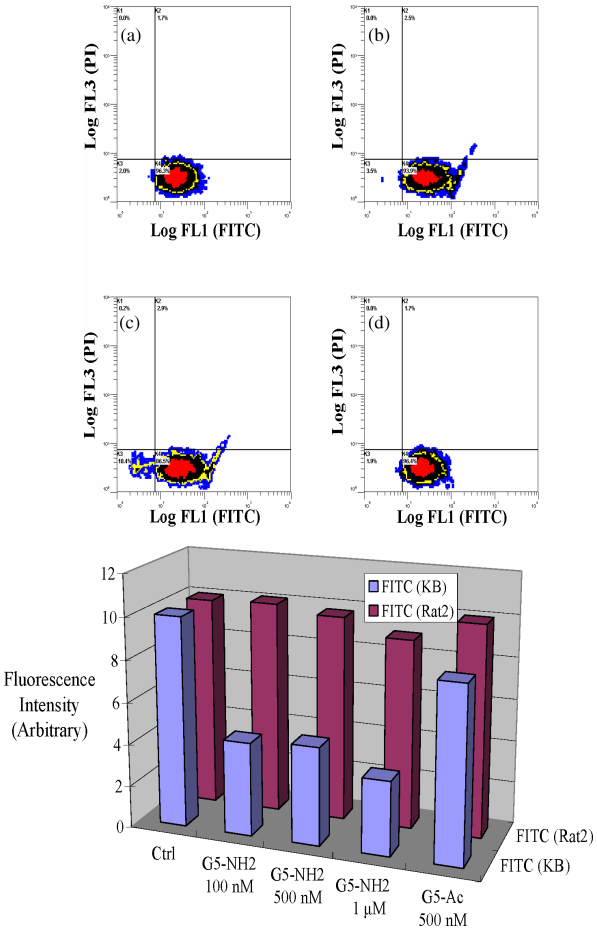

Figure 10: Flow cytometer diagrams of Rat2 cells at several representative conditions. (a) Untreated, (b) incubated with FDA and 500 nM G5-NH_2, (c) incubated with FDA and 1 μM G5-NH_2, and (d) incubated with FDA and 500 nM G5-Ac at 37°C for 1 hr. (e) Signal intensity of fluorescein fluorescence for KB and Rat2 cells after incubation with dendrimers. Control (first column): cells in pure PBS buffer. (Reprinted with permission from S. Hong *et al*., "Interaction of poly(amidoamine) dendrimers with supported lipid bilayers and cells: Hole formation and the relation to transport, *Bioconjugate Chem.*, **15**(4), 774–782, 2004. Copyright (2004) American Chemical Society.)

9.8 Mechanism of Nanopartical Penetration of Membranes

A generally accepted method of charged nanoparticle transmembrane transport is polycation-mediated endocytosis.[18,19] This process has three steps: binding with the phospholipids and/or glycolipids in the membrane, internalization into cells, and exit from the endosome. However, dendrimer-membrane interactions are present even in the absence of the cellular machinery needed for endocytosis. What is the mechanism for dendrimer internalization in cells? Is it possible that these nanoparticles interact with the membrane directly and enhance transport via a physical process rather than a biological one? In this section we will present atomic force microscopy studies that examine the interaction of dendrimers with lipid bilayers. The studies focus on the following dendrimer properties: size, chemical functionality, and charge and examine the role they play in the disruption of a model membrane system, a supported lipid bilayer. The goal of these experiments is the development of a general model that can explain the effects of these three properties that of polymers on membrane disruption.

Early atomic force microscopy (AFM) studies revealed that G7 PAMAMs have the ability to create damage in lipid bilayers and that this effect can be influenced by a change in macromolecular architecture.[20] In search of an underlying mechanism for this behavior, further AFM experiments of dendrimers interacting with supported lipid bilayers were performed. The size, chemical functionality, and charge of the dendrimer were varied to examine the effect upon defect formation. From this data a model that explicitly includes the interaction between dendrimer and lipid

was used to estimate the stability and expected size of the resulting dendrimer/lipid assemblies.[21]

These studies investigated PAMAM dendrimers with amine-terminated (R-NH_2, generations 3, 5, and 7) and acetamide-terminated[22] (R-NHC(O)CH_3, generations 5 and 7) branches, respectively. The preparation of supported lipid bilayers as well as the AFM imaging procedures are described in detail in the literature.[20] Briefly, supported DMPC bilayers were formed by vesicle fusion on freshly cleaved mica. All images were taken in tapping mode with a liquid cell and standard silicon nitride cantilever (spring constant 0.32 N/m, length 100 μm). The temperature inside the liquid cell during imaging was determined to be ~28°C and therefore above the gel-transition temperature of supported DMPC bilayers.[20,23] As initially formed, bilayers frequently contained defects resulting from incomplete vesicle fusion (see Figures 11(a), 13(a), 14(a), 15(a)). The presence of these defects is quite useful for verifying bilayer formation and thickness (~5 nm for DMPC[13]). Once it was confirmed that a bilayer had formed, 20–30 μl of a dilute dendrimer solution was injected into the sample volume of approximately 100 μl for a final concentration in the range of 1.4–42 nM polymer at pH 6. The corresponding total number of *functional end-groups* (i.e. amine or acetamide, respectively) in the sample volume ranged from 0.5–5 μM. Note that the concentration of lower generation dendrimers was increased to reach at least the same molar concentration of functional groups as for the case of high generation dendrimers. Imaging continued for up to two hours after injection in order to observe the interaction of the dendrimers with the bilayer. The

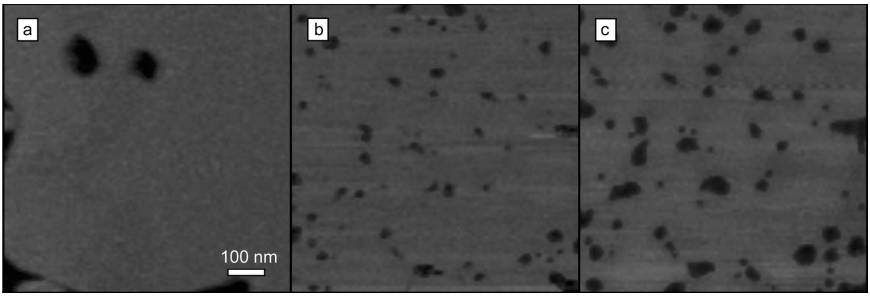

Figure 11: AFM height images of DMPC bilayer (a) before adding dendrimers, (b) 20 min after exposure to G7-amine, and (c) 60 min after exposure to G7-amine. Grey areas: top surface of lipid bilayer. Black areas: substrate supporting the lipid bilayer. The corresponding step height between substrate and top of bilayer is about 5 nm. Color height scale: 0–20 nm. (Reprinted with permission from A. Mecke *et al*., "Lipid bilayer disruption by polycationic polymers: The roles of size and chemical functional group," *Langmuir*, **21**(23), 10348–10354, 2005. Copyright (2005) American Chemical Society.)

effect of decreasing dendrimer generation on the ability to form defects in lipid bilayers is illustrated in Figures 11–13.

Adding G7-NH_2 PAMAMs to the lipid bilayer caused the formation of small, isolated holes (typical diameters range from 15–40 nm) in previously intact parts of the bilayer. This hole formation occurred within two minutes, i.e. faster than the time between two consecutive AFM scans.[20] Figure 11 shows AFM images of a DMPC lipid bilayer at three different time points, before and after the exposure to G7-NH_2. Once the holes had formed, their position and size changed very little for time periods of up to one hour (Figures 11(b) and (c)). Some erosion of the bilayer was observed at the edges of existing bilayer defects.

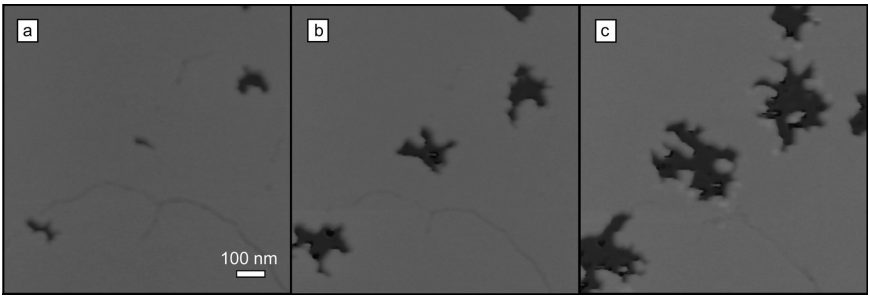

Figure 12: AFM height images of the same area of DMPC bilayer (a) 12 min — (c) 19 min after exposure to G5-amine. Color height scale 0–20 nm. (Reprinted with permission from A. Mecke *et al*., "Lipid bilayer disruption by polycationic polymers: The roles of size and chemical functional group," *Langmuir*, **21**(23), 10348–10354, 2005. Copyright (2005) American Chemical Society.)

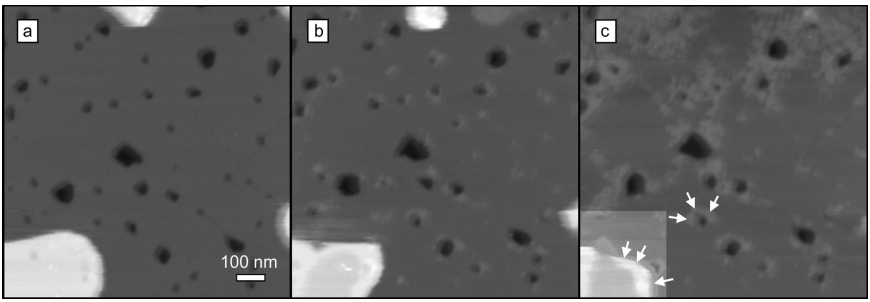

Figure 13: AFM height images of DMPC bilayer (a) before adding dendrimers as well as (b) 3 min and (c) 5 min after adding G3-amine. In these images the lipid molecules form two bilayers (seen in grey and white) each with a thickness of about 5 nm. Note that dendrimer adsorption occurs at lipid boundaries of both layers (see arrows in panel c). The color contrast in the lower left corner of panel (c) has been adjusted to better show dendrimers adsorbed to the bilayer edge. (Reprinted with permission from A. Mecke *et al*., "Lipid bilayer disruption by polycationic polymers: The roles of size and chemical functional group," *Langmuir*, **21**(23), 10348–10354, 2005. Copyright (2005) American Chemical Society.)

The smaller G5–NH_2 dendrimers had a greatly reduced ability to remove lipid molecules from the surface (Figure 12), even when the concentration of charged end-groups was increased five times as compared to the case of G7. Although G5-NH_2 dendrimers removed lipids, they did so more slowly and mostly from the edges of existing bilayer defects, as can be seen in Figures 12(a) (12 minutes after adding dendrimers) — 12(c) (19 minutes after adding dendrimers). This resulted primarily in the growth of existing defects rather than the formation of isolated small holes as in the case of G7.

When the size of the dendrimers was reduced still further, they were no longer able to remove lipids from the surface, see Figure 13. G3-NH_2 PAMAMs adsorbed preferentially to bilayer edges forming a layer approximately 1.5 nm in height along the boundary of the lipid bilayer as indicated by arrows in panel 13(c).

These first three experiments all involved dendrimers carrying a positive charge since their surface primary amines were determined to be protonated at pH < at least 11.[15,24] The next two figures show the effect of PAMAMs with acetamide-terminated — i.e. charge neutral — branches on a lipid bilayer. The molar concentration of end-groups in the following experiments with G7-acetamide and G5-acetamide was the same as in the case of G7-NH_2.

As can be seen in Figure 14, G7-acetamide PAMAM dendrimers behaved similarly to G7-NH_2 PAMAMs. Hole formation also occurred very quickly, although resulting in a lower density of holes than for G7-NH_2. For lower generation acetamide dendrimers the interaction with

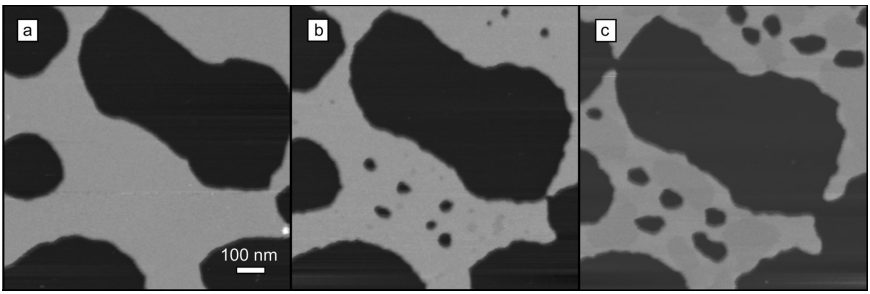

Figure 14: AFM height images of DMPC bilayer (a) before adding dendrimers, (b) 3 min after exposure to G7-acetamide, and (c) 17 min after exposure to G7-acetamide. Color height scale 0–20 nm. (Reprinted with permission from A. Mecke *et al*., "Lipid bilayer disruption by polycationic polymers: The roles of size and chemical functional group," *Langmuir*, **21**(23), 10348–10354, 2005. Copyright (2005) American Chemical Society.)

the lipid bilayer changed dramatically as compared to the amine case (Figure 15).

G5-acetamide PAMAMs no longer caused the formation or expansion of defects in the lipid bilayer. As in the previous examples, the dendrimers were attracted to the edges of existing bilayer defects. However, the acetamide dendrimers did not adsorb to the top of the bilayer substrate, as in the case of G3-NH_2 shown in Figure 13, but instead they caused the formation of ledges surrounding the bilayer defects. The height of these ledges, measured from the top of the bilayer, was between 3 and 3.5 nm, i.e. less than the thickness of a DMPC bilayer. The leading edge of the ledges moved inward into the bilayer over time as indicated in Figure 15(c). Due to the different

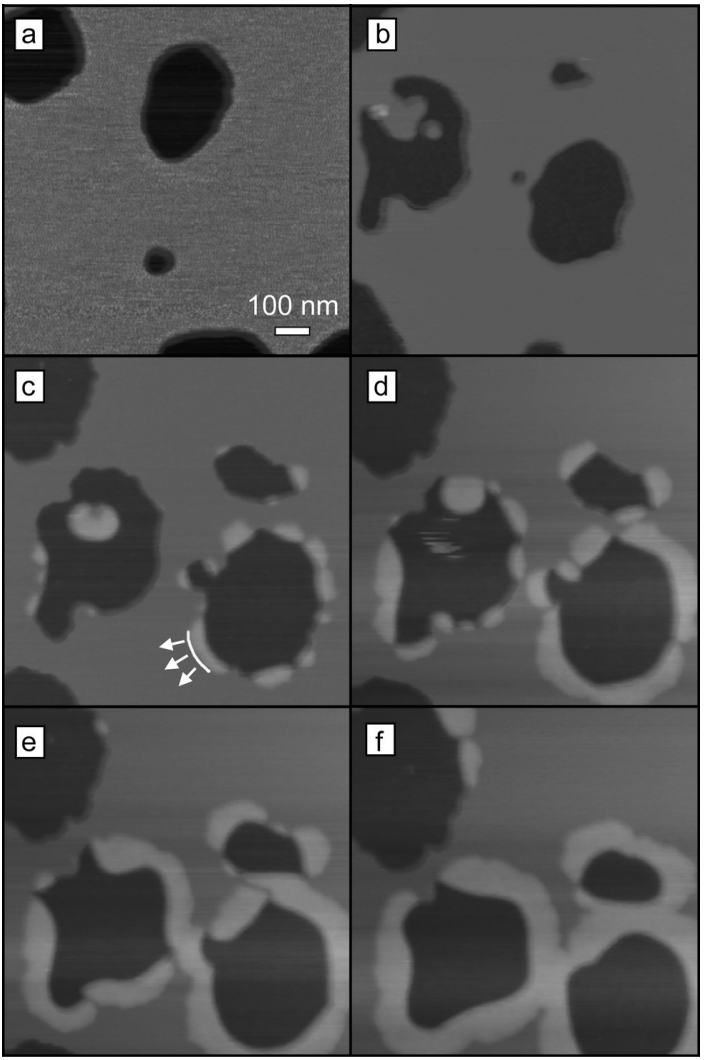

Figure 15: AFM height images of DMPC bilayer (a) before, and (b–f) 7–32 minutes after adding G5-acetamide. Color height scale is 0–20 nm. (Reprinted with permission from A. Mecke *et al*., "Lipid bilayer disruption by polycationic polymers: The roles of size and chemical functional group," *Langmuir*, **21**(23), 10348–10354, 2005. Copyright (2005) American Chemical Society.)

appearance, height of the ledge, and surface chemistry of the acetamide dendrimers, we speculate that they intercalate into the middle of the lipid bilayer.

Having now examined both the *in vitro* data indicating enhanced cellular leakage and enzyme permeability, as well as the AFM experiments on supported lipid bilayers, the question is can a mechanism be postulated that explains the totality of the experimental data? The AFM data clearly indicates that defects, holes, are being formed in the lipid layers. The size of the holes is sufficient to allow rapid diffusion of the enzymes through the membrane. The role of the surface functionality observed in the cell studies — i.e., positively charged dendrimers more effectively cause membrane penetration — was similarly observed in the AFM studies. The trend with dendrimer generation is the same in both sets of experiments; larger dendrimers caused more leakage in cells and more disruption in supported lipid layers. In all aspects the AFM experiments agree very well with those presented above for the *in vitro* cell data. The following section introduces a general mechanism explaining the experimental results.

9.9 Model for the Self-Assembly of Dendrimer-Filled Lipid Vesicles

The experimental data shows that dendrimers are able to remove lipid molecules from a membrane leaving behind defects. The data further shows that the ability of the dendrimer to form the defects is sensitive to both size and charge. This leads to the proposal that dendrimers can remove lipid molecules off the substrate and form a dendrimer-filled

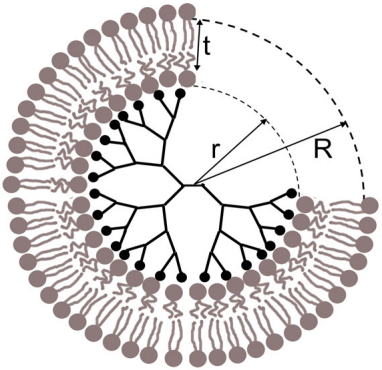

Figure 16: Schematic cross section of proposed dendrimer-lipid vesicle. Number of dendrimer end-groups (black circles) = *M*. Number of lipid head groups in contact with dendrimer surface (inner ring of grey circles) = *m*. (Reprinted with permission from A. Mecke *et al*., "Lipid bilayer disruption by polycationic polymers: The roles of size and chemical functional group," *Langmuir*, **21**(23), 10348–10354, 2005. Copyright (2005) American Chemical Society.)

vesicle (Figure 16). Since these particles are no longer attached to the substrate they cannot be imaged by the AFM tip. Dynamic light scattering measurements as well as ^{31}P NMR data support this hypothesis.[14] In what follows, a model is presented that analyzes the stability of dendrimer-lipid vesicles. The model is then applied to explain the influence of dendrimer generation — i.e. size — on the ability to remove lipids from lipid bilayers as demonstrated in AFM experiments and cell culture.

Considering a G7 PAMAM, the experimentally determined dendrimer diameter is about 8 nm.[25,26] Computer simulations have shown that PAMAM dendrimers with fully extended branches (due to strong repulsive end-group interactions) can reach somewhat larger sizes.[23,27]

Extrapolating from those results, the expected total diameter of a dendrimer-lipid vesicle with a bilayer thickness of 4.5 nm[28] is expected to lie between 17 and 22 nm — depending on whether one assumes a more compact or fully extended branching structure for the dendrimer. This is below the diameter of small unilamellar vesicles (SUV's), in the range of 25–30 nm, that can be obtained by ultrasonication of aqueous phospholipid suspensions.[29] Therefore, the proposed dendrimer-filled vesicles will only be able to self-assemble if a lipid double layer can form stabilizing bonds to the dendrimer functional groups inside of the vesicle.

The geometry of lipid assemblies such as bilayers, micelles and vesicles can be successfully predicted by considering the free energy associated with molecular interaction coupled with geometric constraints imparted by the choice of lipid. Although entropy favors structures with small aggregation numbers, packing constraints of the double-chained DMPC lipids energetically resist the formation of arbitrarily small structures below a critical radius R_C.[30,31] Israelachvili *et al*. combined thermodynamic and geometric principles to derive physical properties of self-assembled lipid vesicles such as their size distribution. They used the "opposing forces" model to describe the interaction between the lipid molecules, each occupying a surface area a at the hydrocarbon water interface of a lipid layer. In this approach the free energy μ_N per molecule in a vesicle of aggregation number N is expressed as the sum of an attractive and a repulsive contribution

$$\mu_N = \gamma a + C / a. \tag{1}$$

Here $\gamma = 5 \cdot 10^{-25}$ kJ/Å^2 is the interfacial free energy per unit area that seeks to decrease the molecular area a. The strength determined by the constant C, which represents interactions between the lipid head groups of the repulsive contributions in the free energy μ_N reaches its minimum when the area per lipid molecule is equal to the optimum surface area $a_0 = \sqrt{C/\gamma}$.

Below the critical radius R_C, where the surface area a_0 can no longer be maintained due to lipid chain crowding, the free energy per molecule can be written as a function $\mu_N(R)$ of the vesicle radius R. In order to describe bilayer vesicles enclosing a dendrimer (as depicted in Figure 16), this model has been modified to allow for different surface free energies, γ_1 and γ_2, for the inside and outside monolayer that can be adjusted to account for the change in interfacial free energy due to the interaction with the dendrimer.

Following the notation of Israelachvili *et al.*,[31] the mol fraction concentration X_N of lipids incorporated into vesicles of aggregation number N is

$$X_N = N\left(\frac{X_{ref}}{N_{ref}}\right)^{N/N_{ref}} \cdot e^{\frac{N}{kT}(\mu_{ref}-\mu_N(R))} \quad \text{for } R < R_C. \tag{2}$$

The subscript "*ref*" denotes the quantities of the chosen reference state, a vesicle of radius R_C. The result for the modified free energy per lipid in the dendrimer-lipid vesicle is

$$\mu_N = 2a_1\gamma_1 + \frac{n\gamma_2}{Na}(a-a_2)^2 + 2\frac{n}{N}(a_2\gamma_2 - a_1\gamma_1). \tag{3}$$

Here $a_1 = \sqrt{C/\gamma_1}$ and $a_2 = \sqrt{C/\gamma_2}$ are the optimum surface areas for lipids respectively in the inside and outside monolayers, total number of lipids $N \approx 4\pi (R - t)^2/a_1 + 4\pi R^2/a_2$, t is the thickness of the hydrocarbon layer, and $n \approx 4\pi R^2/a_2$ is the number of lipids in the outer monolayer. The effective surface free energy per unit area for molecules in the inner monolayer is written as $\gamma_1 = \gamma_2 + \Delta\gamma$. Since $\Delta\gamma$ is assumed to be the result of the interaction between dendrimer branch ends with the inside of the vesicle it is of the form.

$$\Delta\gamma = \frac{M\varepsilon}{4\pi r^2} \tag{4}$$

with M = number of dendrimer end-groups, ε = energy per bond (expected to lie in the range of 12–30 kJ/mol for typical hydrogen bonds), r = dendrimer radius.

For empty vesicles $\gamma_1 = \gamma_2$ which corresponds to the previously studied case.[31]

The vesicle size distributions X_N both *with* and *without* the contribution $\Delta\gamma$ is shown in Figure 8. These curves were obtained using the values appropriate for G7 PAMAMs and DMPC lipids: M = 512, r = 45 Å, = 45 Å^2, t = 29 Å, length of carbon chains = 16.7 Å, volume of lipid tails = 667 Å^3, as well as ε = 24 kJ/(mol·N_{Avogadro}), T = 298 K (see also Refs. 28 and 32). Considering the generic nature of the chosen model for the lipid-lipid and lipid-dendrimer interactions, the results are in excellent agreement with predictions. While the empty lipid vesicles are expected to have a diameter of 28 nm (dashed line in Figure 17), the dendrimer-filled

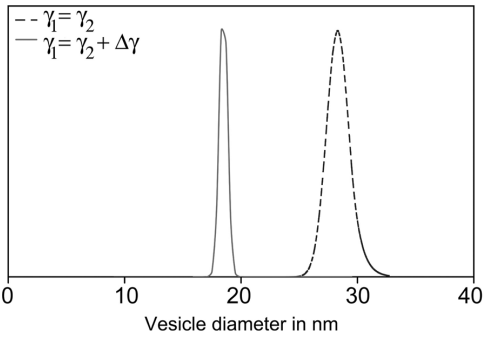

Figure 17: Probability distribution of unilamellar vesicle sizes according to Eq. (2) without dendrimer (using $g_1 = g_2 = 5 \cdot 10^{-25}$ kJ/Å^2, dashed line) and with enclosed dendrimer (using parameter $g_1 = g_2 + Dg = 7 \cdot 10^{-25}$ kJ/Å^2, solid line). (Reprinted with permission from A. Mecke *et al*., "Lipid bilayer disruption by polycationic polymers: The roles of size and chemical functional group," *Langmuir*, **21**(23), 10348–10354, 2005. Copyright (2005) American Chemical Society.)

vesicles have a diameter of 18 nm (solid line in Figure 17). This is in the range of 17–22 nm for the expected diameter of a dendrimer-filled vesicle as described in Figure 16.

A G5 dendrimer, on the other hand, only has $M = 128$ end-groups. Therefore $\Delta\gamma$ will be smaller than for a G7 dendrimer, see Eq. (4). This in turn implies that the interaction between a single G5 PAMAM and the lipid bilayer would not be strong enough to create a hole in the bilayer by forming a dendrimer-filled vesicle. It is however possible that multiple dendrimers combined are still able to remove lipids by forming larger aggregates. The experimental data suggests that, in particular, edges of bilayer defects are more vulnerable to dendrimer disruption, probably due to a different packing structure at the rims, see Figures 13–15.

A second argument for the stability of dendrimer-lipid vesicles can be made by calculating the ratio *m/M* of lipid head groups in the inside monolayer to the number of dendrimer branch ends, see Figures 16 and 17. In order to arrive at a uniform increase in surface tension across the inside lipid layer (as proposed in Eq. (4) this ratio should be small.

For a G7 PAMAM the number *m* is between 500 and 1400 for diameters ranging from 8–13 nm[25–27,33,34] and the packing density of lipids used above. Since a G7 PAMAM has 512 end-groups the ratio *m/M* of lipid head groups per dendrimer end-group is between 1 and 3. For the example discussed in Figure 17, the ratio is 2:1. Figure 18 illustrates how two factors — dendrimer size and end-group density — contribute to dendrimer-vesicle stability. It shows *m/M* as a function of dendrimer generation. Although the maximum possible diameter for a G5-filled vesicle is about 19 nm, the number *m/M* reaches 6 in this case. This implies that the G5 dendrimer cannot easily form enough stabilizing bonds between its functional groups and the lipid molecules. This analysis also explains the observation that G3 PAMAMs did not remove lipids from a bilayer (Figure 14). They are much smaller, disk-like rather than spherical molecules with only 32 end-groups.[33,35]

In addition to the number *M*, the parameter γ which depends on dendrimer end-group polarity plays an important role for vesicle formation. As pointed out earlier, it is well-known that charge-neutral dendrimers do not have as strong an effect on membrane integrity as charged ones. This is consistent with the calculation presented above as well as with the AFM experiments on lipid bilayers, i.e. while positively charged G5-NH_2 PAMAMs were able to remove lipids from the bilayer

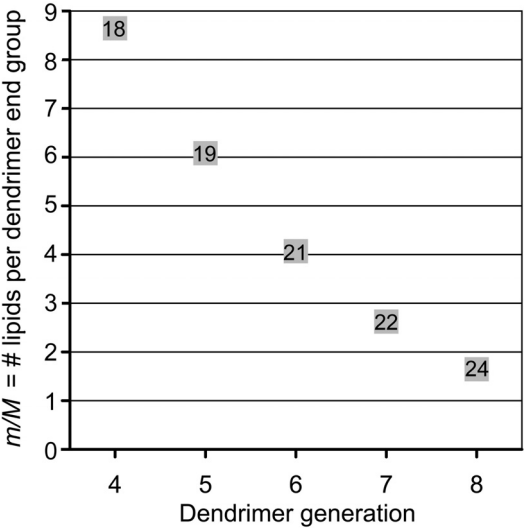

Figure 18. Measure for the stability of dendrimer-lipid vesicles (see Figure 7): *m/M* = Average number of lipid head groups per dendrimer end-group given as function of generation. The numbers inside the squares are the corresponding maximum diameter of the dendrimer-lipid vesicle given in nm. (Reprinted with permission from A. Mecke *et al*., "Lipid bilayer disruption by polycationic polymers: The roles of size and chemical functional group," *Langmuir*, **21**(23), 10348–10354, 2005. Copyright (2005) American Chemical Society.)

(Figure 13), neutral G5-acetamide PAMAMs were not able to remove lipids (Figure 15).

Although the energetics discussed above point to the possibility of vesicle formation the reaction pathway and the barriers to formations are unknown. A study has been performed to examine the energies of deformation for dendrimers. The major question poised was, is there sufficient binding energy in the dendrimer-surface interaction to cause the dendrimer

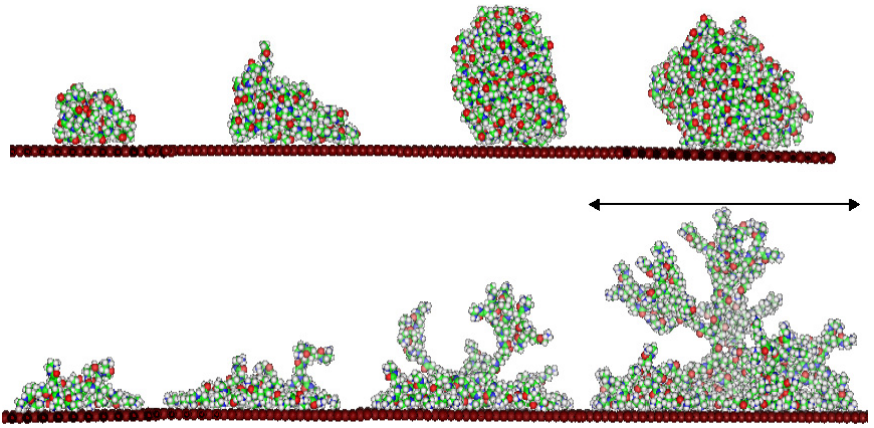

Figure 19: Simulation images of acetamide (a) and amine (b) PAMAMs after interacting with surface. Shown are generations 2–5, q = – 0.05.

to flatten into a "pancake" shape thereby allowing the majority of charged end groups to come in contact with the membrane. Figure 19 shows the conformation of dendrimers of varying generation when attracted to a sheet of positive charge. It is clear that the particles with the charged end groups (amine dendrimers) bring many more of the branch termini in contact with the surface than does the neutral acetimide dendrimer.

In this section we have focused on the analysis of a monodisperse dendrimer-lipid complex in order to facilitate an analytical solution. Although these simple pictures and conclusions allow forming a reasonable hypothesis, we caution that more complex mixtures of dendrimers and lipids could also follow the same general energetics outlined here (for example aggregates of dendrimers nucleating a lipid vesicle). However, our experimental data to date is most consistent with the monodendrimer core model.

9.10 Summary and Remarks on the Relevance of PAMAM Dendrimer Nanoparticles to the Expected Behavior of Other Nanoparticles

Amine-terminated PAMAM dendrimers, a monodisperse class of polycationic polymers, have been shown to create holes in supported DMPC lipid bilayers. The experimental data revealed that the ability to generate holes depends upon both the size and the charge of the dendrimer. Similar size and charge densities are common for many classes of nanoparticles. Given the generality of the model that is able to explain the observations, one might expect that these results are indicative of a common trend for the behavior of nanoparticles with supported lipid bilayers and by extension, with cell membranes. The mechanistic model suggests a general ability of nanoparticles to disrupt cell membranes, particularly if the nanoparticle is similar in scale to the intrinsic small unilamellar vesicle size.

PAMAM dendrimers were employed for these studies because they can be made with excellent control of size and surface modification. How relevant is this work to other kinds of nanoparticles? The PAMAM dendrimers fit into a large class of polycationic organic polymers including poly-(L-lysine) (PLL), polyethyleneimine (PEI), and (diethylaminoethyl)-Dextran (DEAE-Dextran). All of these materials form nanoscale particles, are known to be efficient methods for inducing permeability in cell membranes, and are effective methods of transfecting cells via DNA translocation across the cell membrane.[36,37] Recall also that gold particles with polycationic surfaces behave similarly.[38,39] The similarities in practical applications and in detailed behavior at the cellular level

suggest additional experimentation is called for to determine if the formation of nanoscale holes is also an important mechanistic step for these materials.

The observations made for the dendrimer,[12,20] gold,[38,39] and carbon[40] nanoparticle systems all indicate that control of surface chemistry is key to obtaining the desired degree of interaction with biological membranes. The results from the dendrimer experiments also indicate that the interactions can be altered by nanoparticle size. Given the wide range of nanoparticle sizes and surface modifications, and the wide variety of relevant environmental conditions, it is clear that additional research is needed to understand and explore the ability of nanoparticles to induce membrane permeability. The relationship of these parameters to nanoscale hole formation and other permeation mechanisms, and the relevance of all of these parameters to nanoparticle uptake and biodistribution needs to be determined. Finally, detailed toxicology studies are required to see if the supported lipid bilayer models and the *in vitro* cell models are useful predictors for the toxic effects of nanoparticles in the environment.

In summary, the interaction of DMPC supported lipid bilayers has been investigated by AFM and a novel physical mechanism for the observed formation of holes in the bilayer has been proposed. High generation dendrimers (G7) caused the formation and growth of holes in model membranes whereas the ability to remove lipids from bilayers was reduced for G5 and completely lost for G3. Hole formation by G5 PAMAMs could be avoided by replacing their amine end-groups with acetamide groups.

A mechanism was developed to account for the effect of size and surface chemistry on the propensity for hole formation. It is proposed that small bilayer patches can wrap around the dendrimers forming dendrimer-filled vesicles. Those assemblies are expected to be most stable for large dendrimers with a high number of polar functional groups such as G7-NH_2 PAMAMs. The results help elucidate the importance of size and charge for understanding and controlling the toxicity of polymers and nanoparticles used in biological applications.

9.11 References

1. P. J. Bond, Undersecretary of Commerce for Technology US Department of Commerce. Technology Administration Nanotechnology: Economic Opportunities, Societal & Ethical Challenges (Keynote Address), in NanoCommerce, 2003.
2. DuPont advertising slogan, 1939.
3. G. Oberdörster, Z. Sharp, V. Atudorei, A. Elder, R. Gelein, W. Kreyling, and C. Cox, Translocation of inhaled ultrafine particles to the brain*, Inhalation Toxicology*, **16**(6–7), 437–445, 2004.
4. C. M. Sayes, R. Wahi, P. A. Kurian, Y. Liu, J. L.West, K. D. Ausman, D. B. Warheit, and V. L. Colvin, Correlating nanoscale titania structure with toxicity: A cytotoxicity and inflammatory response study with human dermal fibroblasts and human lung epithelial cells, *Toxicological Sciences*, **92**(1), 174–185, 2006.
5. J. P. Ryman-Rasmussen, J. E. Riviere, and N. A. Monteiro-Riviere, Penetration of intact skin by quantum dots with diverse physicochemical properties, *Toxicological Sciences*, **91**(1), 159–165, 2006.

6. S. Hong, J. A. Hessler, M. M. B. Holl, P. Leroueil, A. Mecke, and B. G. Orr, Physical interactions of nanoparticles with biological membranes: The observation of nanoscale hole formation, *Chemical Health and Safety*, **13**, 16–20, 2006.
7. A. W. Bosman, H. M. Janssen, and E. W. Meijer, About dendrimers: Structure, physical properties, and applications, *Chem. Rev*., **99**, 1665–1688, 1999.
8. Z-Y. Zhang and B. D. Smith, High-generation polycationic dendrimers are unusually effective at disrupting anionic vesicles: Membrane bending model, *Bioconjugate Chemistry*, **11**(6), 805–814, 2000.
9. N. Karoonuthaisiri, K. Titiyevskiy, and J. L. Thomas, Destabilization of fatty acid-containing liposomes by polyamidoamine dendrimers, colloids and surfaces B-biointerfaces, **27**(4), 365–375, 2003.
10. A. Bielinska, J. F. Kukowska-Latallo, J. Johnson, D. A. Tomalia, and J. R. Baker, Jr., Regulation of *in vitro* gene expression using antisense oligonucleotides or antisense expression plasmids transfected using starburst PAMAM dendrimers, *Nucleic Acids Research*, **24**(11), 2176–2182, 1996.
11. J. F. Kukowska-Latallo, E. Raczka, A. Quintana, C. Chen, M. Rymaszewski, and J. R. Baker Jr., Intravascular and endobronchial DNA delivery to murine lung tissue using a novel, nonviral vector, *Human Gene Therapy*, **11**(10), 1385–1395, 2000.
12. S. Hong, A. U. Bielinska, A. Mecke, B. Keszler, J. L. Beals, X. Shi, L. Balogh, B. G. Orr, J. R. Baker Jr., and M. M. Banaszak Holl, The interaction of polyamidoamine (PAMAM) dendrimers with supported

lipid bilayers and cells: Hole formation and the relation to transport, *Bioconjugate Chemistry*, **15**, 774–782, 2004.

13. A. Quintana, E. Raczka, L. Piehler, I. Lee, A. Myc, I. Majoros, A. K. Patri, T. Thomas, J. Mule, and J. R. Baker Jr., Design and function of a dendrimer-based therapeutic nanodevice targeted to tumor cells through the folate receptor, *Pharmaceutical Research*, **19**(9), 1310–1316, 2002.
14. R. Jevprasesphant, J. Penny, R. Jalal, D. Attwood, N. B. McKeown, and A. D'Emanuele, The influence of surface modification on the cytotoxicity of PAMAM dendrimers, *International Journal of Pharmaceutics*, **252**(1–2), 263–266, 2003.
15. M. F. Ottaviani, F. Montalti, M. Romanelli, N. J. Turro, and D. A. Tomalia, Characterization of starburst dendrimers by EPR. 4. Mn(II) as a probe of interphase properties, *J. Phys. Chem.*, **100**, 11033–11042, 1996.
16. M. M. Andersson, R. Hatti-Kaul, and W. Brown, Dynamic and static light scattering and fluorescence studies of the interactions between lactate dehydrogenase and poly(ethyleneimine), *Journal of Physical Chemistry B*, **104**(15), 3660–3667, 2000.
17. T. O. Baldwin, J. A. Christopher, F. M. Raushel, J. F. Sinclair, M. M. Ziegler, A. J. Fisher, and I. Rayment, Structure of bacterial luciferase, *Curr. Opin. Struct. Biol.*, **5**, 798–809, 1995.
18. J. Rejman, V. Oberle, I. S. Zuhorn, and D. Hoekstra, Size-dependent internalization of particles via the pathways of clathrin- and caveolae-mediated endocytosis. *Biochemical Journal*, **377**, 159–169, 2004.

19. I. Kopatz, J. S. Remy, and J. P. Behr, A model for non-viral gene delivery: Through syndecan adhesion molecules and powered by actin. *Journal of Gene Medicine*, **6**(7), 769–776, 2004.
20. A. Mecke, S. Uppuluri, T. J. Sassanella, B. G. Orr, M. M. Banaszak Holl, and J. R. Baker, Direct observation of lipid bilayer disruption by poly(amidoamine) dendrimers. *Chemistry and Physics of Lipids*, **132**, 3–14, 2004.
21. A. Mecke, I. J. Majoros, A. K. Patri, J. R. Baker Jr., M. M. Banaszak Holl, and B. G. Orr, Lipid bilayer disruption by polycationic polymers: The roles of size and chemical functional group, *Langmuir*, **21**, 10348–10354, 2005.
22. I. J. Majoros, B. Keszler, S. Woehler, T. Bull, and J. R. Baker, Jr., Acetylation of poly(amidoamine) dendrimers, *Macromolecules*, **36**(15), 5526–5529, 2003.
23. F. Tokumasu, A. J. Jin, and J. A. Dvorak, Lipid membrane phase behaviour elucidated in real time by controlled environment atomic force microscopy, *J. Electron. Microsc*., **51**(1), 1–9, 2002.
24. R. C. van Duijvenbode, M. Borkovec, and G. J. M. Koper, Acid-base properties of poly(propylene imine) dendrimers, *Polymer*, **39**, 2657–2664, 1998.
25. C. L. Jackson, H. D. Chanzy, F. P. Booy, B. J. Drake, D. A. Tomalia, B. J. Bauer, and E. J. Amis, Visualization of dendrimer molecules by transmission electron microscopy (TEM): Staining methods and Cryo-TEM of vitrified solutions, *Macromolecules*, **31**(18), 6259–6265, 1998.
26. T. J. Prosa, B. J. Bauer, E. J. Amis, D. A. Tomalia, and R. Scherrenberg., A SAXS study of the internal structure of dendritic

polymer systems, *Journal of Polymer Science Part B-Polymer Physics*, **35**(17), 2913–2924, 1997.

27. I. Lee, B. D. Athey, A. W. Wetzel, W. Melxner, and J. R. Baker Jr., Structural molecular dynamics studies on polyamidoamine dendrimers for a therapeutic application: Effects of pH and generation, *Macromolecules*, **35**, 4510–4520, 2002.
28. S. J. Johnson, T. M. Bayerl, D. C. McDermott, G. W. Adams, A. R. Rennie, R. K. Thomas, and E. Sackmann, Structure of an adsorbed dimyristolyphosphatidyl-choline bilayer measured with specular reflection of neutrons, *Biophys. J.*, **59**, 289–294, 1991.
29. C. Hauang, Studies on phosphatidylcholine vesicles, *Biochemistry*, **8**, 344–351, 1969.
30. J. N. Israelachvili, D. J. Mitchell, and B. W. Ninham, Theory of self-assembly of hydrocarbon amphiphiles into micelles and bilayers, *Journal of the Chemical Society-Faraday Transactions Ii*, **72**, 1525–1568, 1976.
31. J. N. Israelachvili, D. J. Mitchell, and B. W. Ninham, Theory of self-assembly of lipid bilayers and vesicles, *Biochimica Et Biophysica Acta*, **470**(2), 185–201, 1977.
32. R. R. C. New, *Liposomes*. Oxford University Press, UK, 1990.
33. S. Uppuluri, S. E. Keinath, D. A. Tomalia, and P. R. Dvornic, Rheology of dendrimers. I. Newtonian flow behavior of medium and highly concentrated solutions of polyamidoamine (PAMAM) dendrimers in ethylenediamine (EDA) solvent, *Macromolecules*, **31**(14), 4498–4510, 1998.

34. A. Mecke, I. Lee, J .R. Baker Jr., M. M. Banaszak Holl, and B. G. Orr, Deformability of poly(amidoamine) dendrimers, *Eur. Phys. J. E-Soft Matter*, **14**, 7–16, 2004.

35. A. M. Naylor, W. A. Goddard III, G. E. Kiefer, and D. A. Tomalia, Starburst dendrimers: 5. Molecular shape control, *Am. Chem. Soc*., **111**, 2339–2341, 1989.

36. S. Hong, P. R. Leroueil, E. K. Janus, J. L. Peters, M.-M. Kober, M. T. Islam, B. G. Orr, J. R. Baker, Jr., and Mark M. Banaszak Holl, Interaction of polycationic polymers with supported lipid bilayers and cells: Nanoscale hole formation and enhanced membrane permeability, *Bioconjugate Chemistry*, **17**(3), 728–734, 2006.

37. D. Fischer, Y. Li, B. Ahlemeyer, J. Krieglstein, and T. Kissel, *In vitro* cytotoxicity testing of polycations: Influence of polymer structure on cell viability and hemolysis, *Biomaterials*, **24**(7), 1121–1131, 2003.

38. C. M. Goodman, C. D. McCusker, T. Yilmaz, and V. M. Rotello, Toxicity of gold nanoparticles functionalized with cationic and anionic side chains, *Bioconjugate Chemistry*, **15**(4), 897–900, 2004.

39. K. K. Sandhu, C. M. McIntosh, J. M. Simard, S. W. Smith, and V. M. Rotello, Gold nanoparticle-mediated transfection of mammalian cells, *Bioconjugate Chemistry*, **13**(1), 3–6, 2002.

40. C. M. Sayes, J. D. Fortner, W. Guo, D. Lyon, A. M. Boyd, K. D. Ausman, Y. J. Tao, B. Sitharaman, L. J. Wilson, J. B. Hughes, J. L. West, and V. L. Colvin., The differential cytotoxicity of water-soluble fullerenes, *Nano Letters*, **4**(10), 1881–1887, 2004.

This page intentionally left blank

Chapter 10

Computer Simulations of Dendrimers

Senthil K. Kandasamy, Hwankyu Lee &
Ronald G. Larson

Outline

10.1 Introduction

The flexible and symmetric architecture of dendrimers makes them suitable for many biological applications. Their structure, typically drawn (unrealistically) as concentric layers, one for each generation, suggests that the mass density ought to be low in the core and increase towards the periphery. The presumed "hollow" interior led to an interesting speculation that dendrimers might be used to house small molecules in their cores and transport them into

cells and, for this reason, dendrimers have been actively considered for drug transport in the past decade or so. To design dendrimers that provide optimal functionality, one needs to understand their structure and dynamics. Although experimental techniques such as small-angle neutron scattering can provide structure factors, which can be used to calculate the radius of gyration, the detailed three-dimensional architecture of the dendrimer is not obtained from such methods. Hence, several theoretical and computational studies have been undertaken to investigate the dendrimer structure. For an excellent review article of these studies, please refer to Ballauff and Likos.[1] Since the dendrimers are hyper-branched polymers, the earliest theoretical attempts to characterize dendrimers used simple theories similar to those applied to linear polymers. Later, more refined coarse-grained and all-atom molecular simulations were employed. In this chapter, we will briefly review the theoretical and simulation studies that have been carried out to elucidate the structure and dynamics of dendrimers. First (Section 10.2), we will describe theoretical and coarse-grained studies in which the monomer units are treated in a continuum fashion or as simplified, coarse-grained beads. Next (Section 10.3), we will review studies in which the dendrimers are treated in an all-atom manner. In Section 10.4, we will briefly review simulations of the interaction of dendrimers with biologically relevant molecules such as lipids and DNA.

10.2 Theoretical and Coarse Grained Models of Dendrimer

10.2.1 Neutral dendrimers

The earliest theoretical study of dendrimers by de Gennes and Hervet,[5] using a modified form of the self-consistent field model, showed that the

density profile for the monomer units of the dendrimer had a minimum at the core and increased monotonically outward toward the edges. This is consistent with the conventional "hollow core and dense shell" picture of dendrimers. However, Lescanec and Muthukumar[11] used a simple lattice model to show that, in contrast to the findings of de Gennes and Hervet,[5] the monomer density had a maximum at the core and decreased monotonically toward the edges. This is known as the "dense core" model. Several subsequent theoretical simulation studies[2,31,33] have lent support to the dense core model. Currently, it is well accepted that dendrimers, at least the uncharged ones, indeed have a dense core and a hollow shell. The simple physical argument behind this[2] is that the dendrimer configuration is decided by the interplay between entropic and energetic contributions from its monomers, and it turns out that the monomers at the periphery can easily access the interior regions of the dendrimer, leading to significant back-folding and a dense core. It should be pointed out that these results, achieved by simple theoretical models, do not take into account the specific chemical structure of the monomers. Thus the exact density profile will depend on the specific chemical structure, the nature of the solvent, the ionization state of the monomers, etc. However, the general conclusion that neutral dendrimers possess a dense core is still largely valid.

Several coarse-grained simulations have been performed in order to understand the dendrimer architecture. These simulations can be further categorized as molecular dynamics, Brownian dynamics, or Monte Carlo. A list of coarse-grained simulations has been summarized in Table 1, adapted from the review article by Ballauff and Likos.[1]

Tab. 1. Coarse-grained simulations of the structure of dendrimers.

Authors	*Year*	*Method*	*Comments*
Lescanec and Muthukumar[11]	1990	Monte Carlo	Neutral dendrimer; dense core
Mansfield and Klushin[21]	1993	Monte Carlo	Neutral dendrimer; dense core
Murat and Grest[26]	1996	Molecular Dynamics	Neutral dendrimer; dense core
Chen and Cui[4]	1996	Monte Carlo	Neutral dendrimer; dense core
Lue and Prausnitz[16]	1997	Monte Carlo	Neutral dendrimer; dense core
Welch and Muthukumar[32]	1998	Monte Carlo	Charged dendrimer; transition from dense core to hollow core as a function of salt concentration.
Lyulin *et al.*[18]	2000	Brownian Dynamics	Neutral dendrimer; dense core
Karatasos *et al.*[10]	2001	Molecular Dynamics	Neutral dendrimer; dense core
Sheng *et al.*[30]	2002	Monte Carlo	Neutral dendrimer; dense core
Timoshenko *et al.*[31]	2002	Monte Carlo	Neutral dendrimer; dense core
Gotze and Likos[7]	2003	Monte Carlo	Neutral dendrimer; dense core

While minor discrepancies were observed among the different studies, the overwhelming conclusion was that neutral dendrimers have a dense core, validating the pioneering study by Lescanec and Muthukumar.[11] Dendrimers were found to be highly flexible, with a significant amount of back-folding. The other important conclusion from

most of these studies is that the radius of gyration scales is $R_g \sim N^{1/3}$, where N is the number of monomers in the dendrimer. This scaling behavior was valid for a large range of N values, with slight deviations at extremely small and extremely large values of N. The radius of gyration was also found to be dependent on the quality of the solvent.

10.2.2 Charged dendrimers

While neutral dendrimers were shown to have a dense core, in charged dendrimers, charge-charge repulsions are likely to force the monomers apart. This may lead to a hollow core architecture with potential for applications as a delivery vehicle. Welch and Muthukumar,[32] using coarse-grained model Monte Carlo simulations, hypothesized that the structure of the dendrimers will depend not only on their charges but also on the pH of the surrounding environment. They used a simple bead-spring model, with the springs described by a FENE potential, the bead-bead interactions described by a Morse potential, and the repulsive coulomb interactions by a Debye-Hückel potential. By varying the inverse Debye screening length, they were able to change the effective added salt concentration. The potential falls off rapidly at high salt concentrations and is long-ranged at low salt concentrations.

The most important conclusion from the study of Welch and Muthukumar is that charged dendrimers exhibit "smart" behavior, in which the structure of the dendrimer changes from a hollow core to a dense core on addition of salt. This behavior is reversible, which they observed by cycling the Debye screening length from a low to a high value. The results are shown in Figure 1. At low electrostatic screening (low salt), the termini

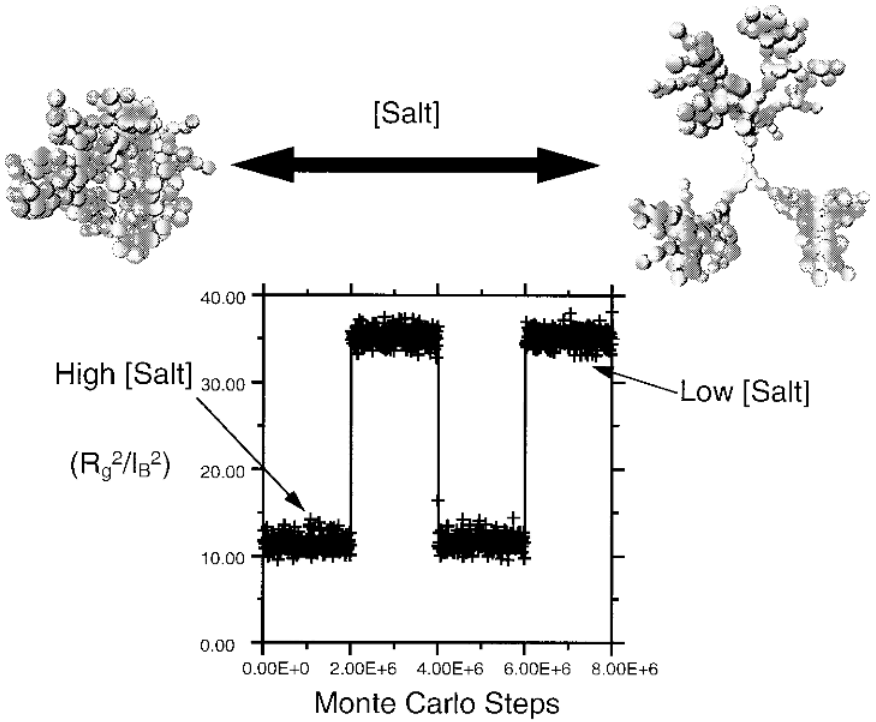

Figure 1: "Smart" behavior of dendrimers. Figure reproduced from Welch and Muthukumar.[32] (Reprinted with permission from "Tuning the density profile of dendritic polyelectrolytes," *Macromolecules*, **31**(17), 5892–5897, 1998. Copyright (1998) American Chemical Society.)

of the dendrimer are at the periphery (hollow core), while at high salt concentrations, the termini sample all regions of the dendrimer. This observation has important implications for the application of dendrimers as drug delivery vehicles. As stated by Welch and Muthukumar,[32] "one might imagine trapping a small molecule inside a polyelectrolyte dendrimer at low salt concentration or low pH. Then, the small molecule, a drug for example, may be delivered by placing the guest-host complex in a high salt or

neutral pH medium to affect a rearrangement of the density profile. This rearrangement may be expected to eject the guest from its dendritic cage."

This result was the first simulation study to convincingly show the possibility of using dendrimers as vehicles to deliver cargo into cells.

Following up this pioneering work, Gurtovenko *et al.*[8] recently performed a coarse-grained MD simulation of charged dendrimers, with explicit counter ions added to the system. They found that including explicit counter ions can have a dramatic effect on the structure and dynamics of charged dendrimers, and, under certain conditions, they cannot be treated implicitly. Thus, implicit approaches, such as using the Debye-Hückel approximation used by Welch and Muthukumar,[32] have to be used with caution. Nevertheless, coarse-grained simulations of charged dendrimers have been able to predict qualitatively and correctly the dense-core to hollow-core transition.

10.3 All-Atom Simulations of Dendrimers

Coarse-grained simulations (CG model) have been able to predict the size, shape and density profile of dendrimers of different generations remarkably well, considering that the monomers are typically represented by just one or two beads. There are several reasons for using coarse-grained models rather than the more accurate atomistic models. The most important reasons are lower computational costs and the fact that the underlying physics is universal and should not depend on the specific chemical architecture of the dendrimer. While CG models may be sufficient for studying the overall shape and size of the dendrimers, atomistic models are required in order to capture the more subtle interactions, such as those between the

dendrimer and (1) an encapsulated drug or small molecule, (2) lipid molecules, (3) DNA molecules, and others.

The first all-atom simulation of dendrimers was performed by Naylor *et al*.,[27] in 1989. They simulated the first seven generations of the poly(amidoamine) (PAMAM) dendrimer in vacuum using the AMBER force field. They found that generations 1–3 were highly asymmetric, while generations 5–7 were nearly spherical. Large voids were found in the interior of the dendrimer, suggesting that these structures are capable of encapsulating small molecules. However, it is not clear from their work whether the structures were well equilibrated or not, and no estimates of the size were made. Another all-atom study was performed by Cavallo and Fraternali[3] on a poly(propylene-imine) dendrimer, in vacuum. This work showed that the dendrimers had a dense core, as predicted by the earlier coarse-grained and theoretical models. They also showed that the dendrimers had significant back-folding, and the radius of gyration roughly followed the 1/3rd scaling law. Around the same time, Peerlings and Meijer[28] and Miklis *et al*.[25] performed simulations of a small molecule, "Bengal rose," encapsulated in dendrimers and including explicit solvent. These studies demonstrated that atomic and theoretical models can be used to design and test dendrimer encapsulation systems in advance of experiments.

Several subsequent simulation studies considered more accurate dendrimer models, using explicit solvents, and for longer timescales, so that true equilibration was achieved, enabling direct comparison of the simulation results with experimentally obtained structural values. A list of several of the all-atom simulations, in both implicit and explicit solvent, is shown in Table 2.

Tab. 2. Atomistic simulations of the structure of dendrimers.

Authors	*Year*	*Solvent*	*Dendrimer Generations*	*Comments*
Naylor *et al.*[27]	1989	Vacuum	G1-G7	First atomistic simulations of dendrimers
Cavallo and Fraternali[3]	1998	Vacuum	G1-G5	Dense core predicted
Lee *et al.*[12]	2002	Implicit Explicit	G2-G6 G2	Neutral and charged dendrimers
Maiti *et al.*[19]	2004	Vacuum	G1-G11	Dense core; limiting generation explored
Han *et al.*[9]	2005	Explicit	G1-G7	Dense core; ~15 ns simulations
Maiti *et al.*[20]	2005	Explicit	G4-G6	Neutral and charged; dense core
Lin *et al.*[15]	2005	Explicit	G5	Dynamics of water explored
Lee *et al.*[13]	2006	Explicit	G5	Effect of solvent studied

Lee *et al.*[12] performed extensive simulations of G2 PAMAM dendrimers in explicit water at different pH values. The dendrimers were fully charged (terminal and interior amine groups charged), partially charged (only terminal amine groups charged), or uncharged, corresponding to low, neutral, or high pH, respectively. Simulations were performed for up to 2 ns. The final configurations from these simulations are shown in Figure 2. These simulations were compared to a series of G2 simulations in implicit solvent to obtain an optimal set of parameters for implicit solvation. These

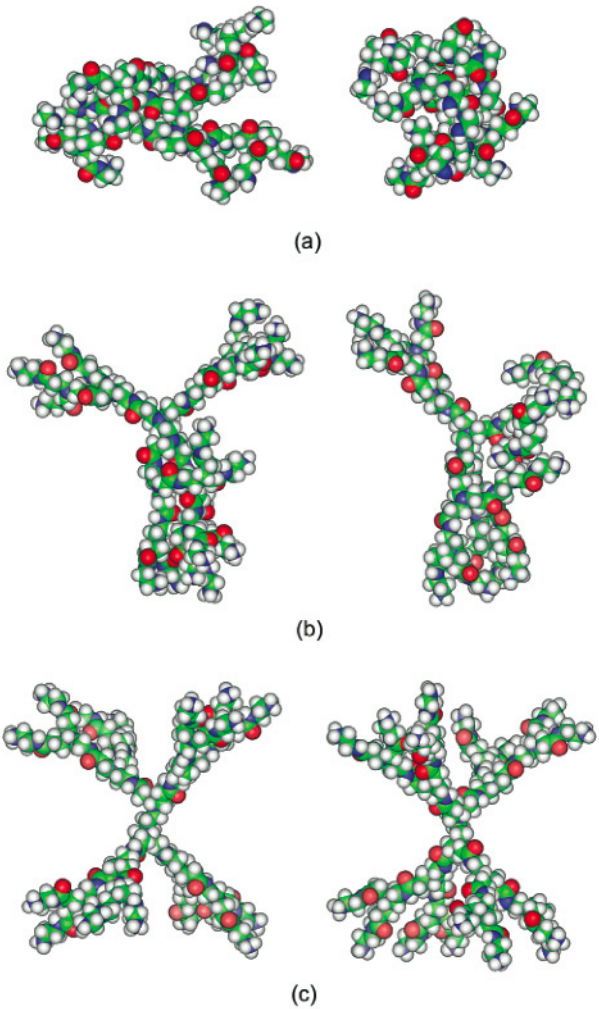

Figure 2: Structure of G-2 PAMAM dendrimers at (a) high, (b) neutral, and (c) low pH. Snapshots at the end of two independent simulations are shown in each case. The figure is reproduced from Lee *et al.*[12] (Reprinted with permission from "Structural molecular dynamics studies on polyamidoamine dendrimers for a therapeutic application: Effects of pH and generation," *Macromolecules*, **35**(11), 4510–4520, 2002. Copyright (2002) American Chemical Society.)

parameters were then used to simulate larger dendrimers (G3–G6) in implicit solvent. These simulations showed that at low pH (<4) the core is hollow, while at neutral pH significant back-folding occurs. The simulations also showed that a significant change in volume occurred between the neutral and low pH regimes for generations 5 and larger, leading to the possibility of cargo encapsulation in these dendrimers. This also explains the experimentally observed improved levels of gene expression for generations G5 and larger when dendrimers are used as a gene-delivery vehicle.

Maiti *et al.*[19] simulated the first 11 generations of the PAMAM dendrimer in vacuum to understand the structure, size, and back-folding characteristics and to determine the number of generations to which a dendrimer can grow before steric effects prohibit further growth, which is the "limiting generation" issue first raised by de Gennes.[5] Computational costs prohibited them from performing these simulations in explicit solvent. Due to steric hindrances, the construction of dendrimers of larger generations is a major challenge. Maiti *et al.*[19] used a continuous configurational Boltzman biased (CCBB) Monte Carlo method to generate the dendrimer conformations. Since this was supposed to be a gas [vacuum] phase simulation; all the termini were neutral. Once their initial configurations were generated, the dendrimers were simulated for up to 200 ps, and the radii of gyration for several generations were found to match the experimental results, within the experimental error. They also calculated other properties such as asphericity, terminal group distribution, and monomer density, and their results largely matched those from earlier theoretical, CG, and experimental results. They also observed large cavities in the interior of the dendrimer, into which, presumably, small molecules can partition. Using an

expression derived by de Gennes (1983) for PAMAM dendrimers, they determined that the limiting generation is ~10.2. Maiti *et al*.[19] calculated the strain energy for all generations and found that it increased dramatically for generations 10 and 11, providing an indirect confirmation of de Gennes' prediction. However, the structures of the larger dendrimers in this study are not very reliable due to the absence of solvent. Nevertheless, their study provided good insights into various structural aspects of dendrimers.

In subsequent work, Maiti *et al.*[20] performed all-atom simulations of G4 to G6 dendrimers in explicit solvent. This more accurate treatment enabled them to study the effect of pH (degree of ionization) on the dendrimer structure and dynamics. For each generation, they studied the effect of low, neutral, and high pH. Simulations were performed for 200 ps each, which seemed sufficient to equilibrate properties such as the radius of gyration. They found that the size of the dendrimer was highly dependent on the pH, and the calculated radii of gyration matched the experimentally measured values accurately. In a following study,[15] the same group of researchers investigated in detail the structure of water inside and around the dendrimers, which is important to understanding the binding of dendrimers to small molecules, DNA, and proteins. Two distinct relaxation behaviors were observed for water, one at the surface of the dendrimer and the other inside the dendrimer. They also found that the protonation of the amines increased the relaxation time scales of water in the interior of the amines, suggesting that the binding of cargo molecules into the dendrimer interior at low pH might be much slower than at high pH.

More recent all-atom simulations of the PAMAM dendrimers by Han *et al*.[9] include generations 1 through 7. They performed explicit

Tab. 3. Radius of gyration (R_g) of dendrimers. These values are compared with experiments and other simulations.

	Radius of Gyration (nm)					
	Experiment		*Simulation*			
	Prosa et al.[29]	*Choi et al.*[6]	*Lee et al.*[13]	*Maiti et al.*[19]	*Lee et al.*[12*]	*Maiti et al.*[20*]
Un-acetylated G5 in water	—	2.50	2.51 ± 0.01	2.22 ± 0.01	3.28	1.83
Un-acetylated G5 in methanol	2.41	—	2.57 ± 0.01	—	—	—
90%-acetylated G5 in water	—	2.35	2.11 ± 0.01	—	—	—
90%-acetylated G5 in methanol	—	—	2.33 ± 0.01	—	—	—

* These simulations were performed without explicit water.

solvent simulations of unprotonated dendrimers of different generations (1 to 7) for up to 15 ns. They also observed that Rg scales with the power ~1/3 as a function of the number of monomers. Significant back-folding of the outer generations was also observed. In another study by Lee *et al*.,[13] simulations were performed on uncharged and 10% charged dendrimers in explicit water and methanol. Simulations were performed for ~5 ns, and the results showed that the radii of gyration matched experimentally observed values. Table 3 summarizes the values of the radii of gyration from several all-atom MD simulations.

It is thus clear that all-atom simulations are able to predict accurately the size, shape, and conformation of dendrimers of several

generations, validating a large body of earlier work performed using theoretical and coarse-grained simulation methods. Although different all-atom force fields were used, the various simulations have yielded similar quantitative results, indicating the inherent robustness of using all-atom simulations. However, to date, not many studies have been performed on the interactions of dendrimers with other biologically relevant molecules such as drugs, protein, DNA and lipids. All atom-simulations are ideally suited — and perhaps necessary — for such studies where the specific interactions cannot be captured by coarse-grained models. We will briefly discuss such simulations in the following sections.

10.4 Interactions of Dendrimers with Other Molecules

The desired use of dendrimers as vehicles to carry cargo into cells involves the interaction of the dendrimers with several biological moieties.

1) With the cargo: Typically a drug or a small molecule is partitioned into the dendrimer core.
2) With lipid bilayers: Dendrimers need to interact with and penetrate the exterior lipid bilayer membrane of the cell to facilitate cargo delivery.
3) With proteins: Once inside the cells, the dendrimers are likely to interact with specific protein targets.
4) With DNA: For gene therapy, DNA might itself be a cargo; the positively charged dendrimers are also likely to interact with the negatively charged DNA molecules inside the cell.

It is important to study all of the above-mentioned interactions to get a clearer picture of the mechanism of dendrimer-based cargo delivery. While we have discussed the various CG and all-atom studies that have been carried out to study the structure and dynamics of dendrimers in solution, very few studies have looked at the interactions of dendrimers with other moieties.

However, Mecke *et al*.[23] studied the interactions of PAMAM dendrimers with an atomically flat mica substrate. Like membranes, mica possesses a negative surface charge. While comparatively simpler than a realistic biological membrane, mica is nevertheless a useful model that is easier to study by experimental scanning probe techniques than are biological membranes. Their experimental work and molecular dynamics simulations showed that the dendrimers in solution tended to flatten from their oblate shape on contact with mica. Both charged and uncharged dendrimers exhibited this behavior. Figure 3 shows the flattened dendrimer profile on a mica substrate.

A more recent study by Lee and Larson[14] used a coarse-grained dendrimer model to investigate dendrimer-lipid interactions. AFM

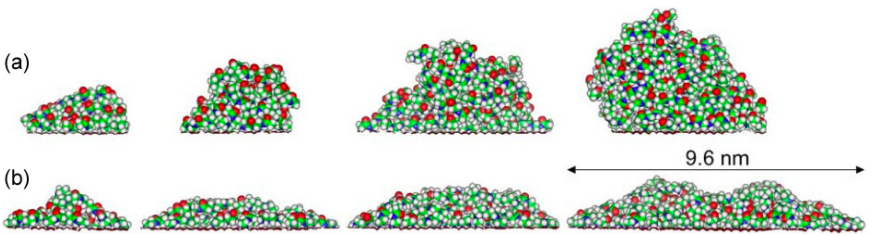

Figure 3: Images of flattened PAMAM dendrimers (G2 to G5) on a mica substrate. (a) Partially charged. (b) Fully charged. Image reproduced from Mecke *et al*.[23]

experiments had shown that unacetylated (charged) G7 PAMAM dendrimers form large holes in dimyristoyl-phosphatidyl-choline (DMPC) bilayers, while G5 dendrimers are capable of expanding smaller holes.[23] The CG simulations by Lee *et al.*[14] used a simplified coarse-grained model developed for lipid bilayers by Marrink *et al.*[22] In this model, roughly four heavy (non-hydrogen) atoms are lumped into one CG bead, and the PAMAM dendrimer can essentially be approximated by four different types of beads. After coarse-graining, a G5 dendrimer has 506 CG beads, which is approximately half an order of magnitude smaller than the corresponding all-atom system. Lee *et al.*[14] systematically studied the interactions of the CG dendrimer with CG lipid bilayers by varying the surface charge density of the dendrimer from uncharged to 50% charged to 100% charged (mimicking different pH values) and by varying the dendrimer size (G3 and G5). The simulations were begun by placing the equilibrated dendrimers close to the bilayer surface and were run for up to 500 ns. These simulations showed that acetylated (uncharged) G3 and G5 dendrimers were not inserted into the bilayer. The unacetylated (100% charged) and partially acetylated (50% charged) G5 dendrimers fully inserted into the bilayer. Snapshots from one of the simulations are shown in Figure 4. The results from the simulations agree qualitatively with experimental results and this is the only simulation study to date to offer insights into the bilayer-penetrating mechanism of dendrimers.

DNA-dendrimer interactions have also been studied using simplified Brownian dynamics simulations[18] of cationic dendrimers interacting with oppositely charged linear polymers representing the DNA. The results show that most of the linear chain monomers are present close to

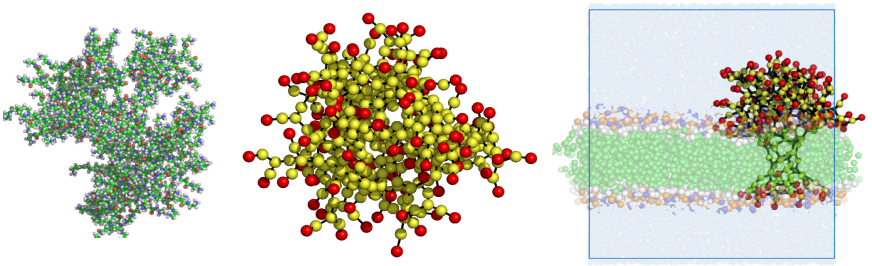

Figure 4: All-atom (left) and coarse-grained (center) representations of G5 dendrimers. Right: Interaction of a coarse-grained G5 dendrimer with a DMPC bilayer, leading to pore formation.

the dendrimer terminal groups. At linear chain lengths longer than necessary for charge neutralization with the dendrimer, strong adsorption between the dendrimer and linear polymers was observed. This adsorption, in turn, has a strong effect on the chain radius of gyration and radial distribution of the dendrimer. These simulations provide qualitative insights into DNA-dendrimer interactions, relevant for gene therapy and other applications.

10.5 Conclusions and Future Outlook

Theories and simulations have shown definitively that for uncharged dendrimers,

1) The monomer density is highest in the core (dense-core).
2) The dendrimers are extremely flexible, with a large degree of back-folding of the outer generations
3) The radius of gyration scales as ~$N^{1/3}$, where N is the number of monomers.

The simulations also show that charged dendrimers undergo a structural transition when moved from low pH to a high pH solution. Simple coarse-grained simulations have been sufficient in predicting most of the structural properties of dendrimers in solution rather accurately, showing that the underlying physics is universal and does not depend on the specific chemical structure of the monomer unit. However, there are some issues that have not yet been conclusively demonstrated through simulations. The issue of a "limiting-generation," raised originally by de Gennes and beyond which the dendrimers cannot be grown, is still unresolved.

While coarse-grained modeling has helped to explain the physics of dendrimers in solution, such modeling is not detailed enough to capture the specific interactions of dendrimers with biological moieties such as lipids, proteins and DNA. While CG models have indeed attempted to capture some of these interactions, the results are at best qualitative. This leads to the inference that appropriately parameterized all-atom simulations are indeed necessary to study the interactions of dendrimers with biological molecules. The primary argument against all-atom simulations is the prohibitive cost. However, over the past decade or so, as faster computers have become available, all-atom molecular dynamics simulations of dendrimers have become more common. Starting with the early simulations of small (G1 to G5) dendrimers in vacuum or in implicit solvent, the most recent simulations have been able to access tens of nanoseconds in explicit solvent for dendrimers as large as the biologically relevant G7 dendrimers. Over this time scale, most of the structural properties of dendrimers in

solution are fully equilibrated. However, the next major challenge is to be able to simulate the interaction of dendrimers with lipids, DNA, and other materials using reasonably long time scales so that the desired property of interest is well equilibrated.

The recent coarse-grained simulations of Lee and Larson[14] on the interactions of G5 dendrimers with DMPC lipid bilayers matched experiments qualitatively. Their simulation system consisted of 512 CG lipids, ~20,000 CG water beads and a single G5 dendrimer. The simulations were performed for 500 ns to observe pore formation. To perform the same simulation using an all-atom approach would require a system with ~100,000 atoms. Presumably, the same physical phenomenon of pore formation could be simulated using the all-atom model over similar time scales (hundreds of nanoseconds) and using accurate electrostatic calculations such as the particle mesh Ewald (PME) method. While the CG simulation can be performed in a matter of weeks on a single computational node, all-atom simulation would require several (tens of) nodes and months of computation. While this is still computationally expensive, with ever-increasing computer speeds, all-atom simulations of such systems will become rather routine within a few years. Thus, we can foresee all-atom simulations of higher generation dendrimers interacting with lipids, DNA, proteins and drug molecules and providing useful insights into the medicinally relevant molecular aspects that cannot be observed experimentally. Finally, all-atom simulations can guide the design and engineering of newer classes of dendrimers, which can be manipulated to achieve variable shapes and sizes while being optimized for biological functionality.

10.6 References

1. M. Ballauff and C. N. Likos, Dendrimers in solution: Insight from theory and simulation, *Angewandte Chemie — International Edition*, **43**(23), 2998–3020, 2004.
2. D. Boris and M. Rubinstein, A self-consistent mean field model of a starburst dendrimer: Dense core vs. dense shell, *Macromolecules*, **29**(22), 7251–7260, 1996.
3. L. Cavallo and F. Fraternali, A molecular dynamics study of the first five generations of poly(propylene imine) dendrimers modified with N-tBoc-L-phenylalanine, *Chemistry — A European Journal*, **4**(5), 927–934, 1998.
4. Z. Y. Chen and S. M. Cui, Monte Carlo simulations of star-burst dendrimers, *Macromolecules*, **29**(24), 7943–7952, 1996.
5. P. G. de Gennes and H. Hervet, Statistics of "starburst" polymers, *J. Phys. Lett,* **44**, L351–L360, 1983.
6. Y. S. Choi, A. Mecke, B. G. Orr, M. M. B. Holl, and J. R. Baker Jr., DNA-directed synthesis of generation 7 and 5 PAMAM dendrimer nanoclusters, *Nano Letters,* **4**(3), 391–397, 2004.
7. I. O. Gotze and C. N. Likos, Conformations of flexible dendrimers: A simulation study, *Macromolecules*, **36**(21), 8189–8197, 2003.
8. A. A. Gurtovenko, S. V. Lyulin, M. Karttunen, and I. Vattulainen, Molecular dynamics study of charged dendrimers in salt-free solution: Effect of counterions, *Journal of Chemical Physics*, **124**(9), Art. No. 094904, 2006.

9. M. Han, P. Q. Chen, and X. Z. Yang, Molecular dynamics simulation of PAMAM dendrimer in aqueous solution, *Polymer*, **46**(10), 3481–3488, 2005.
10. K. Karatasos, D. B. Adolf, and G. R. Davies, Statics and dynamics of model dendrimers as studied by molecular dynamics simulations, *Journal of Chemical Physics*, **115**(11), 5310–5318, 2001.
11. R. L. Lescanec and M. Muthukumar, Configurational characteristics and scaling behavior of starburst molecules — A computational study, *Macromolecules*, **23**(8), 2280–2288, 1990.
12. I. Lee, B. D. Athey, W. A. Wetzel, W. Meixner, and J. R. Baker Jr., Structural molecular dynamics studies on polyamidoamine dendrimers for a therapeutic application: Effects of pH and generation, *Macromolecules*, **35**(11), 4510–4520, 2002.
13. H. Lee, J. R. Baker Jr., and R. G. Larson, Molecular dynamics studies of the size, shape, and internal structure of 0% and 90% acetylated fifth-generation poly(amidoamine) dendrimers in water and methanol, *Journal of Physical Chemistry B*, **110**(9), 4014–4019, 2006.
14. H. Lee, R. G. Larson, Molecular dynamics simulation of PAMAM dendrimer-induced pore formation in DPPC bilayers with coarse-grained model, *Journal of Physical Chemistry B*, **110**(37), 18204–18211, 2006.
15. S. T. Lin, P. K. Maiti, and W. A. Goddard, Dynamics and thermodynamics of water in PAMAM dendrimers at subnanosecond time scales, *Journal of Physical Chemistry B*, **109**(18), 8663–8672, 2005.

16. L. Lue and J. M. Prausnitz, Structure and thermodynamics of homogeneous-dendritic-polymer solutions: Computer simulation, integral-equation, and lattice-cluster theory, *Macromolecules*, **30**(21), 6650–6657, 1997.
17. A. V. Lyulin, G. R. Davies, and D. B. Adolf, Location of terminal groups of dendrimers: Brownian dynamics simulation, *Macromolecules*, **33**(18), 6899–6900, 2000.
18. S. V. Lyulin, A. A. Darinskii, and A. V. Lyulin, Computer simulation of complexes of dendrimers with linear polyelectrolytes, *Macromolecules*, **38**(9), 3990–3998, 2005.
19. P. K. Maiti, T. Cagin, G. F. Wang, and W. A. Goddard, Structure of PAMAM dendrimers: Generations 1 through 11, *Macromolecules*, **37**(16), 6236–6254, 2004.
20. P. K. Maiti, T. Cagin, S. T. Lin, and W. A. Goddard, Effect of solvent and pH on the structure of PAMAM dendrimers, *Macromolecules*, **38**(3), 979–991, 2005.
21. M. L. Mansfield and L. I. Klushin, Monte Carlo studies of dendrimer, *Macromolecules*, **26**(16), 4262–4268, 1993.
22. S. J. Marrink, A. H. de Vries, and A. E. Mark, Coarse grained model for semiquantitative lipid simulations, *Journal of Physical Chemistry B*, **108**(27), 750–760, 2004.
23. A. Mecke, S. Uppuluri, T. M. Sassanella, D. K. Lee, A. Ramamoorthy, J. R. Baker Jr., B. G. Orr, and M. M. B. Holl, Direct observation of lipid bilayer disruption by poly(amidoamine) dendrimers, *Chemistry and Physics of Lipids*, **132**(1), 3–14, 2004.

24. A. Mecke, I. Lee, J. R. Baker Jr., M. M. B. Holl, and B. G. Orr, Deformability of poly(amidoamine) dendrimers, *European Physical Journal E*, **14**(1), 7–16, 2004.

25. P. Miklis, T. Cagin, and W. A. Goddard, Dynamics of Bengal Rose encapsulated in the Meijer dendrimer box, *Journal of the American Chemical Society*, **119**(32), 7458–7462, 1997.

26. M. Murat and G. S. Grest, Molecular dynamics study of dendrimer molecules in solvents of varying quality, *Macromolecules*, **29**(4), 1278–1285, 1996.

27. A. M. Naylor, W. A. Goddard, G. E. Kieffer, and D. A. Tomalia, Starburst dendrimers. 5. Molecular shape control, *Journal of the American Chemical Society*, **111**(6), 2339–2341, 1989.

28. H. W. I. Peerlings and E. W. Meijer, Chirality in dendritic architectures, *Chemistry — A European Journal*, **3**(10), 1563–1570, 1997.

29. T. J. Prosa, B. J. Bauer , E. J. Amis, D. A. Tomalia, R. Scherrenberg, A SAXS study of the internal structure of dendritic polymer systems, *Journal of Polymer Science Part B — Polymer Physics*, **35**(17), 2913–2924, 1997.

30. Y. J. Sheng, S. Y. Jiang, and H. K. Tsao, Radial size of a starburst dendrimer in solvents of varying quality, *Macromolecules*, **35**(21), 7865–7868, 2002.

31. E. G. Timoshenko, Y. A. Kuznetsov, and R. Connolly, Conformations of dendrimers in dilute solution, *Journal of Chemical Physics,* **117**(19), 9050–9062, 2002.

32. P. Welch and M. Muthukumar, Tuning the density profile of dendritic polyelectrolytes, *Macromolecules*, **31**(17), 5892–5897, 1998.

33. T. C. Zook and G. T. Pickett, Hollow-core dendrimers revisited, *Physical Review Letters*, **90**(1), Art. No. 015502, 2003.

Chapter 11

Dendrimer-Entrapped and Dendrimer-Stabilized Metal Nanoparticles for Biomedical Applications

Xiangyang Shi & Su He Wang

Outline

11.1 Introduction

In recent years, dendrimer-entrapped and dendrimer-stabilized metal nanoparticles (NPs) have received immense scientific and technological interest because of their promising applications in a broad range of fields, such as catalysis, optics, electronics, and biomedical applications. Dendrimers are a class of highly branched, monodispersed, synthetic macromolecules with well-defined composition and structure,[1–4] which makes them ideal templates or stabilizers for the synthesis and modification of various metal, and

semiconductor NPs. Dendrimer-entrapped NPs (DENPs) are formed using dendrimers as templates, where each metal or other inorganic NP is entrapped within each dendrimer molecule, while dendrimer-stabilized NPs (DSNPs) are formed using dendrimers as stabilizers, where each metal or other inorganic NP is surrounded or protected by multiple dendrimer molecules on its surface. Detailed synthesis, characterization, and applications of DENPs and DSNPs in catalysis, optics, or other applications not related to biomedical sciences can be found in several reviews.[5–9] The unique properties of dendrimers as well as their excellent biocompatibility and non-immunogenicity lead to the synthesis of various metal dendrimer composite NPs for a range of biomedical applications. The major advantage of using dendrimers to synthesize NPs is their tunable surface chemistry, providing many opportunities for the functionalization of NP surfaces. This chapter provides a glimpse of various metal DENPs and DSNPs and how these nanocomposite materials have been designed and used in biomedical applications.

11.2 Dendrimer-Entrapped Nanoparticles (DENPs)

DENPs are often formed using fast reduction (e.g., sodium borohydride reduction) and nucleation chemistry. The formed DENPs are usually smaller than 5 nm. The formation of DENPs consists of two steps. In the first step, metal ions are preorganized by the dendrimer host through ligand/metal-ion interactions, salt formation, acid-base and donor-acceptor interactions, covalent bond formation, steric confinement, various types of weaker forces (van der Waals, hydrogen bonding, etc.), and combinations thereof.[5] Meanwhile, due to many possible overlapping equilibrium processes (involving several different geometries), the binding of metal ions within dendrimer host

usually appears as a non-stoichiometric process. The preorganization results in dendrimer-metal complexes, which are in dynamic equilibrium with the template and metal ions. The dynamic equilibrium permits equal distribution of the metal ions between all the equivalent ligands in the dendrimer molecules and diffusion provides a homogenous distribution of metal ions among the dendrimer template. In the second step, a reduction of preorganized metal ions results in the formation of DENPs. A scheme for the synthesis of Au DENPs[10–12] (Scheme 1) gives an example how the two steps lead to the formation of metal DENPs. A wide range of metal ions including Cu^{2+}, Au^{3+}, Ag^{+}, Pd^{2+}, Pt^{2+}, Ni^{2+}, Ru^{3+} can be preorganized with PAMAM dendrimer hosts to form metal DENPs.[5] Dendrimer-entrapped semiconductor quantum dots, such as CdS, can also be prepared by reacting Cd (II)/dendrimer complexes with sulfide (II) ions.[13,14]

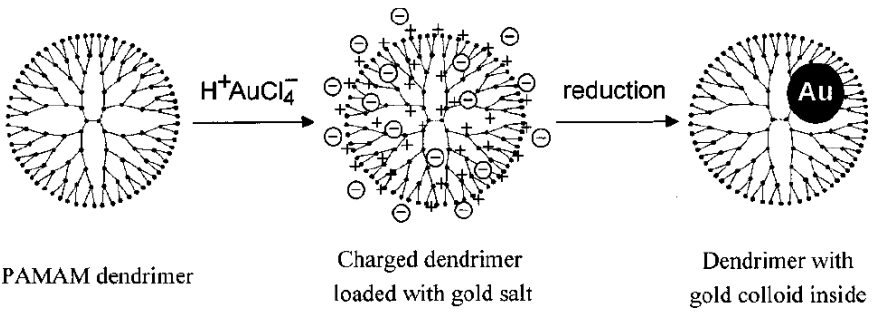

Scheme 1: Dendrimer nanotemplating in aqueous solution. In a first step, the dendrimer is loaded with a precursor salt ($H^{+}AuCl_4^{-}$), resulting in a charged dendrimer with the precursor as counterions. In a second step, the chemical reduction is performed which yields a colloid inside the dendrimer. (Reprinted with permission from [Grohn, *et al*. *Macromolecules*, **33**, 6042–6050]. Copyright (2000) American Chemical Society.)

Compared with regular/classic composite materials, DENPs possess nanometer-sized inorganic domains and organic host, which make them display unique physical and chemical properties that are characteristic of both the nanosized host and the nanodispersed guest. A range of physical properties come from the nanodispersed inorganic domains, instead of PAMAM dendrimer alone, which affords DENPs with many unique applications in a wide range of areas, including catalysis, optics, environmental, sensing, etc. While many unique properties and applications of DENPs are derived from the nanodispersed inorganic domain, dendrimer in itself is also indispensable in the stabilization of the inorganic domains. In DENPs, most of the interaction between guest atoms and their microenvironment (metal-metal and metal-solvent interactions) are substituted with the metal-dendrimer and dendrimer-solvent interactions, which makes the DENP solutions stable for a relatively long time in appropriate solvent systems.

For biological applications, the surface of DENPs has to be modified in order to avoid toxicity and non-specific membrane binding. In literature, the absence of biological applications of DENP systems is largely due to the technical difficulties with DENP toxicity and surface manipulation. Gold NPs have recently received immense scientific and technological interest because of their extensive applications in biology, catalysis, and nanotechnology.[15,16] Although functionalized dendrimers have been used to prepare dendrimer-entrapped gold or other noble metal NPs with different functionalities,[17,18] in most circumstances dendrimer-entrapped gold NPs (Au DENPs) are prepared using amine-terminated PAMAM dendrimers. This is due to the commercial availability of this material, but this yields particles with high cytotoxicity and non-specific membrane binding

due to the amine surface on the dendrimers, limiting the biological application of these particles. Preparation of non-toxic, biocompatible {$(Au^0)_n$-PAMAM} DENPs is of great importance for applications in various biological systems.

It is well documented that decreasing the surface charge of amine-terminated PAMAM dendrimers toward neutral reduces their toxicity.[19,20] We have developed a new, facile approach to surface modification of Au DENPs by replacing the terminal amine groups of the dendrimers after the entrapment of Au NPs.[21] Au DENPs formed using ethylenediamine core amine-terminated generation 5 PAMAM dendrimers (G5.NH_2) as templates were reacted with acetic anhydride or glycidol molecules to form acetamide or hydroxyl-functionalized Au DENPs (see Scheme 2). The formed Au DENPs after surface functionalization are stable, water-soluble, and display similar sizes, size distributions, and optical properties as the original DENPs, however the surface charge changes and the biocompatibility is significantly improved. Using this approach, one can directly tailor the surface functionalities of preformed Au DENPs.

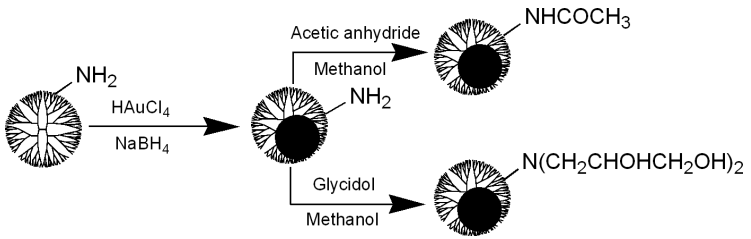

Scheme 2: Reactions to modifying Au DENPs prepared using amine-terminated G5.NH_2 dendrimers as templates. (*Soft Matter,* 2007, **3**, 71–74 — Reproduced by permission of The Royal Society of Chemistry.)

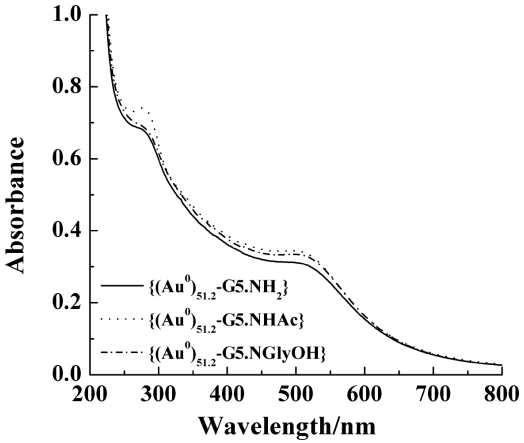

Figure 1: UV-Vis spectra of the synthesized and modified Au DENPs. (*Soft Matter,* 2007, **3**, 71–74 — Reproduced by permission of The Royal Society of Chemistry.)

The optical properties of the modified Au DENPs were investigated using UV-Vis spectrometry. $\{(Au^0)_{51.2}$–G5.$NH_2\}$, $\{(Au^0)_{51.2}$–G5.NHAc}, and $\{(Au^0)_{51.2}$–G5.NGlyOH} DENPs (Figure 1) exhibit a similar absorption behavior, with surface plasmon bands around 510 nm, indicating their similar size and size distribution. The corresponding surface modified dendrimers in the absence of the Au NPs do not show any absorption features at wavelengths above 250 nm. The Au DENPs are soluble and stable in water, and no aggregates formed for at least 10 months after synthetic modifications with either acetic anhydride or glycidol molecules.

The morphology and size distribution of the synthesized Au DENPs were characterized by transmission electron microscopy (TEM) imaging (Figure 2). All Au DENPs regardless of modification are relatively monodispersed and small, with sizes ranging from 2.0 ± 0.4 to 2.4 ± 0.5 nm. The size range of the Au DENPs is consistent with their UV-Vis

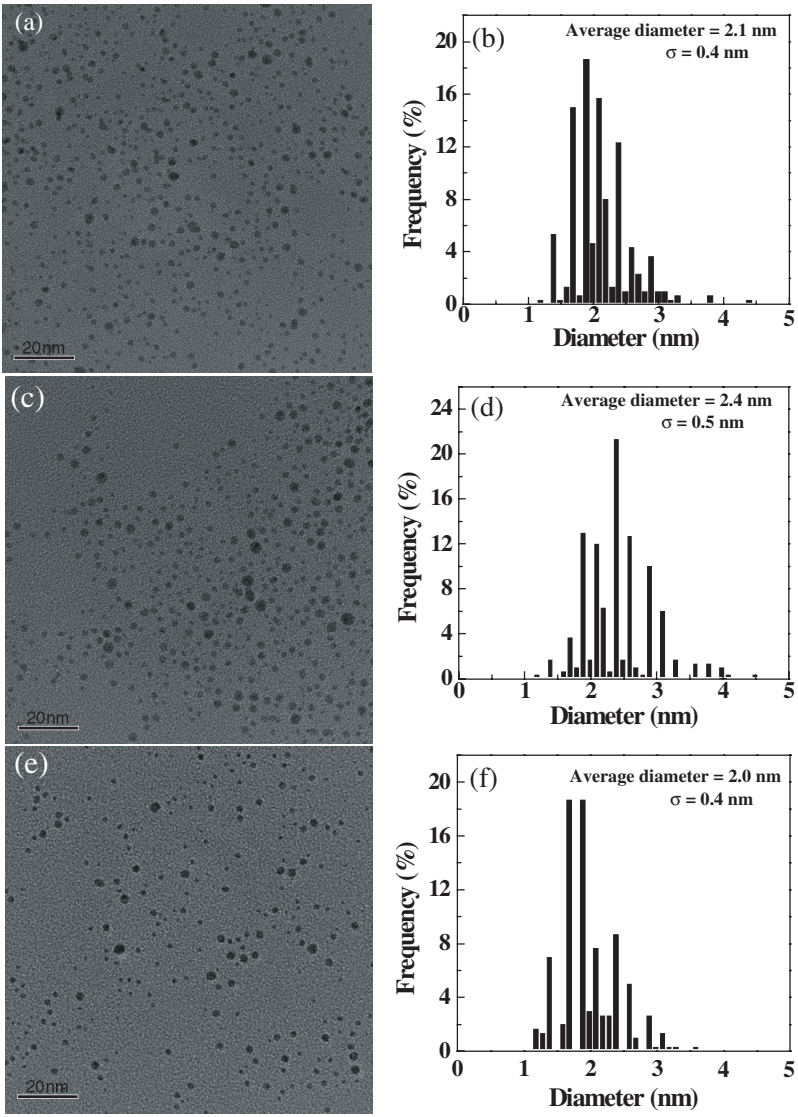

Figure 2: TEM micrographs of the $\{(Au^0)_{51.2}$–G5.$NH_2\}$ (a), $\{(Au^0)_{51.2}$–G5.NHAc} (c), $\{(Au^0)_{51.2}$–G5.NGlyOH} (e) DENPs; (b), (d) and (f) are size distribution histograms of the $\{(Au^0)_{51.2}$–G5.$NH_2\}$, $\{(Au^0)_{51.2}$–G5.NHAc}, and $\{(Au^0)_{51.2}$–G5.NGlyOH} DENPs, respectively. (*Soft Matter,* 2007, **3**, 71–74 — Reproduced by permission of The Royal Society of Chemistry.)

absorption characteristics (Figure 1) exhibiting a surface plasmon band around 510 nm.[22,23] High-resolution TEM images show that all Au DENPs are crystalline, as lattices of Au crystals are clearly observed. The crystalline nature of the Au DENPs was also confirmed using selected area electron diffraction (SAED). The (111), (200), (220) and (311) rings in the SAED patterns indicate the face-centered-cubic (*fcc*) crystal structures. Energy dispersive spectroscopy (EDS) of each of the Au DENP samples indicates the existence of Au elements.

Although the optical properties and sizes of all Au DENPs are very similar, their surface charges change. Zeta potential measurements show marked changes in the surface potentials of Au DENPs, with $\{(Au^0)_{51.2}$–G5.$NH_2\}$ at + 36.86 mV, $\{(Au^0)_{51.2}$–G5.NGlyOH} at + 23.47 mV, and $\{(Au^0)_{51.2}$–G5.NHAc} at + 4.27 mV. The zeta potential changes reflect the successful surface modification of $\{(Au^0)_{51.2}$–G5.$NH_2\}$ DENPs, suggesting that the surface potentials of Au DENPs can be manipulated through conventional organic reactions with the dendrimers.

Further PAGE analyses of the synthesized and modified Au DENPs and the corresponding dendrimer derivatives (Figure 3) show that Au DENPs exhibit migration patterns similar to those of the corresponding dendrimer derivatives. $\{(Au^0)_{51.2}$–G5.NGlyOH} migrates faster than G5.NGlyOH dendrimer, which is due to the less complete hydroxylation reaction with dendrimers in the presence of Au NPs. This is consistent with our NMR results.

The cytotoxicity of the synthesized Au DENPs was evaluated by an MTT (3-(4,5-dimethylthiazol-2-yl)-2,5-diphenyltetrazolium bromide) assay of KB cells (a human epithelial carcinoma cell line) (Figure 4).

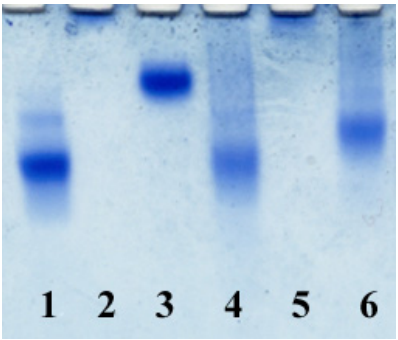

Figure 3: PAGE electropherograms of Au DENPs and the corresponding dendrimers. Lane 1: G5.NH_2; Lane 2: G5.NHAc; Lane 3: G5.NGlyOH; Lane 4: {$(Au^0)_{51.2}$–G5.NH_2}; Lane 5: {$(Au^0)_{51.2}$–G5.NHAc}; Lane 6: {$(Au^0)_{51.2}$–G5.NGlyOH}. (*Soft Matter,* 2007, **3**, 71–74 — Reproduced by permission of The Royal Society of Chemistry.)

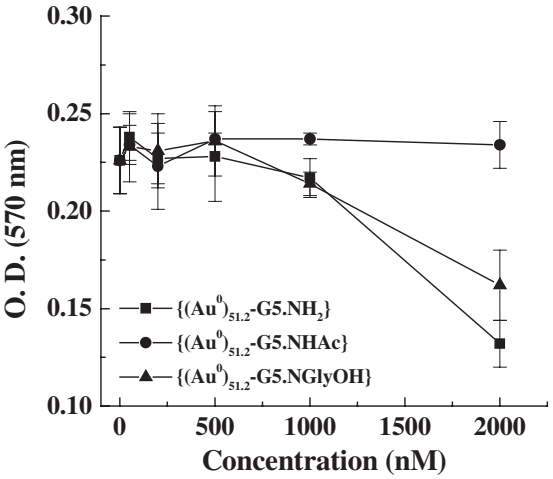

Figure 4: An MTT assay of KB cell viability after treatment with {$(Au^0)_{51.2}$–G5.NH_2}, {$(Au^0)_{51.2}$–G5.NHAc}, and {$(Au^0)_{51.2}$–G5.NGlyOH} DENPs for 24 hours. The data are expressed as mean ± S. D. (*Soft Matter,* 2007, **3**, 71–74 — Reproduced by permission of The Royal Society of Chemistry.)

Results show that all Au DENPs are non-toxic below the concentration of 1.0 μM. Above 1.0 μM, the cytotoxicity of Au DENPs follows the order of $\{(Au^0)_{51.2}$–G5.$NH_2\}$ > $\{(Au^0)_{51.2}$–G5.NGlyOH} > $\{(Au^0)_{51.2}$–G5.NHAc}, which was related to the degree of cationic surface charge. Acetylation of $\{(Au^0)_{51.2}$–G5.$NH_2\}$ DENPs neutralizes the surface charges of Au NPs, as confirmed by PAGE and zeta-potential measurements, making them highly compatible with biological systems. In contrast to the acetylation reaction, much less complete hydroxylation of $\{(Au^0)_{51.2}$–G5.$NH_2\}$ DENPs (as compared with hydroxylation of G5.NH_2 dendrimers) cannot effectively neutralize their positive charges; therefore, the formed $\{(Au^0)_{51.2}$–G5.NGlyOH} DENPs still display some cytotoxicity at high concentrations. It implies that post-synthetic modification of Au DENPs is a straightforward approach to designing non-toxic Au NPs for biological applications. It is interesting to note that we also attempted to synthesize non-toxic Au NPs using preformed G5.NHAc and G5.NGlyOH dendrimers as templates under similar conditions. In both cases, black precipitates were formed. It seems that the complexation of $AuCl_4^-$ ions with either the acetamide or glycidol hydroxyl-terminated G5 dendrimer is much weaker than that with amine-terminated G5 dendrimers, significantly decreasing the stability of the Au NPs. The approach used for functionalization of Au NPs may be applied to a range of different dendrimer-templated metal NPs and different organic syntheses and opens a new avenue to tailoring the particle surface functionality for various applications.

In the area of targeted cancer imaging and therapeutics, one great challenge is that the used NPs lack specific binding with cancerous cells. The ability to chemically functionalize preformed Au DENPs without

significantly changing their sizes and size distributions led us to develop these Au DENPs as a multifunctional platform for cancer cell targeting, imaging, and treatment as we have done with dendrimers.[20,24] The Au DENP-based nanoplatform should be able to be localized in targeted cells and tissues due to the high electron density contrast of the Au NPs. It is also possible that multifunctional Au DENPs can be used for targeted hyperthermia treatment of cancers through inductive heating of cells that have internalized these particles.

We demonstrate that dendrimer-entrapped gold nanoparticles (Au DENPs) can be covalently linked with targeting ligands and imaging molecules for cancer cell targeting and imaging.[25] Au DENPs linked with defined numbers of folic acid (FA) and fluorescein isothiocyanate (FI) molecules are water-soluble, stable, and biocompatible. We show that the FA- and FI-modified Au DENPs can specifically bind to KB cells that overexpress high affinity folate receptors and be internalized predominantly into lysosomes of target cells within 2 h. These findings document a facile approach to use Au DENPs as a platform for the targeting and imaging of cancer cells.

Au DENPs were prepared using G5.NH_2 dendrimers as templates according to previously described procedures.[11,12,26] The formed Au DENPs are relatively monodispersed with a mean diameter of 2.1 nm.[21] The approach to functionalize the Au DENPs with defined numbers of targeting molecules (e.g., FA) and dyes (e.g., FI) (Scheme 3) are slightly modified from the methods been used to functionalize dendrimers (without entrapped metal nanoparticles) for targeting and imaging of cancer cells.[19,20,27] One of the key steps in the preparation of FA- and FI-modified

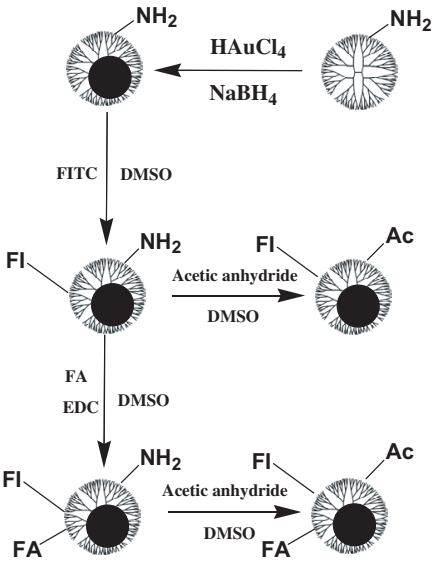

Scheme 3: Schematic representation of the reactions involved in modifying Au DENPs for cancer cell targeting and imaging. (Reprinted with permission from Wiley-VCH GmbH & Co KG, *Small*, 2007, **3**, 1245–1252.)

Au DENPs is to keep the surface charges on the particles neutral in order to avoid toxicity and non-specific binding. This can be accomplished by a final acetylation step to convert the remaining amine groups of G5.NH_2 dendrimers to acetamides (Scheme 3). Zeta potential measurements show that after the final acetylation step, the surface potentials of the formed $\{(Au^0)_{51.2}$–G5-FI_5-Ac$\}$ (ξ = −1.11 mV) and $\{(Au^0)_{51.2}$–G5-FI_5-FA_5-Ac$\}$ (ξ = −2.30 mV) DENPs (Ac denotes acetyl) are close to neutral, indicating the success of the acetylation reaction. The slight negative charges of both DENPs may be derived from the deprotonated carboxyl groups in both FI and FA moieties being conjugated. The numbers of FI and FA moieties conjugated onto each Au DENP can be estimated by comparing the

differences between the integration values of ^{1}H NMR signals associated with dendrimers and the FI and FA moieties, as we did for dendrimer (without entrapped Au nanoparticles) conjugation.[20,27] The average numbers of FI and FA moieties conjugated onto each Au DENP were estimated to be 4.0 and 4.5, respectively.

A dynamic simulated image of Au DENP with Au NP size of 3 nm is shown in Figure 5(a). It appears that the Au NP is not necessarily situated at the center of the G5 dendrimer interior. In this case, the conjugated FI molecules display certain molecular space that would not allow the complete quenching of the fluorescence in the presence of metal Au. This is very important for Au DENPs to be used for confocal microscopic imaging purposes. A dynamic simulated image of Au DENP with FI and FA modified on the surface, followed by acetylation is shown in Figure 5(b).

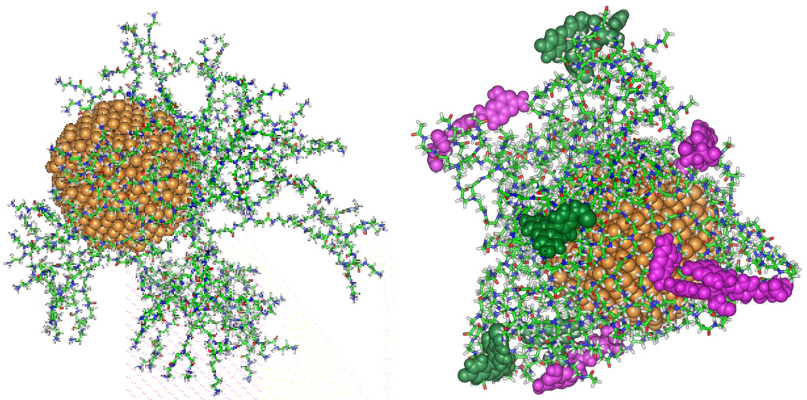

(a) (b)

Figure 5: (a) A configuration of Au (diameter = 3 nm) NP entrapped in an amine-terminated, fully protonated G5 dendrimer. (b) A configuration of Au (diameter = 3 nm) DENP with surface FI and FA moieties, followed by acetylation. This is about 50 psec simulation image (simulated by Inhan Lee).

This reflects that from both theoretical model and simulation and experimental data, it is possible to modify the Au DENP platform for cancer cell targeting and imaging.

TEM images show that the sizes of $\{(Au^0)_{51.2}$–G5-FI_5-Ac$\}$ and $\{(Au^0)_{51.2}$–G5-FI_5-FA_5-Ac$\}$ DENPs are 3.4 ± 0.6, and 3.2 ± 0.7 nm (Figures 6(a)–(d)), respectively. The somewhat larger size compared with the pristine $\{(Au^0)_{51.2}$–G5.$NH_2\}$ DENPs (2.1 nm) may be due to multiple surface modifications, which facilitate Ostwald ripening of the Au DENPs. UV-vis spectrometry (Figure 6(e)) verified the conjugation of FI and FA moieties onto Au DENPs. The $\{(Au^0)_{51.2}$–G5-FI_5-FA_5-Ac$\}$ DENPs show characteristic absorption peaks at both 500 nm and 280 nm for respective FI and FA moieties, while only the characteristic absorption peak at 500 nm related to FI moiety is observed with $\{(Au^0)_{51.2}$–G5-FI_5-Ac$\}$ DENPs. In addition, a band representing an overlap of the surface plasmon resonance of Au DENPs (510 nm) with the absorption of FI moiety is also observed. The functionalized Au DENPs are stable, and no precipitation of the solution appeared even after periods of storage as long as nine months. An MTT assay of KB cells shows that the functionalized Au DENPs are not cytotoxic even at a concentration up to 2000 nM (Figure 6(f)), implying that the final acetylation step creates biocompatible nanoparticles.

FA has been extensively investigated for targeting various cancer cells, including ovary, kidney, uterus, testis, brain, colon, lung, and myelocytic blood that overexpress FA receptors (FAR).[28–31] The high-affinity FAR for FA (K_d = 0.1–1 nM) affords specific binding and internalization of FA-modified nanoparticles to cancer cells in the presence of normal cells through receptor-mediated endocytosis. KB cells were selected for the

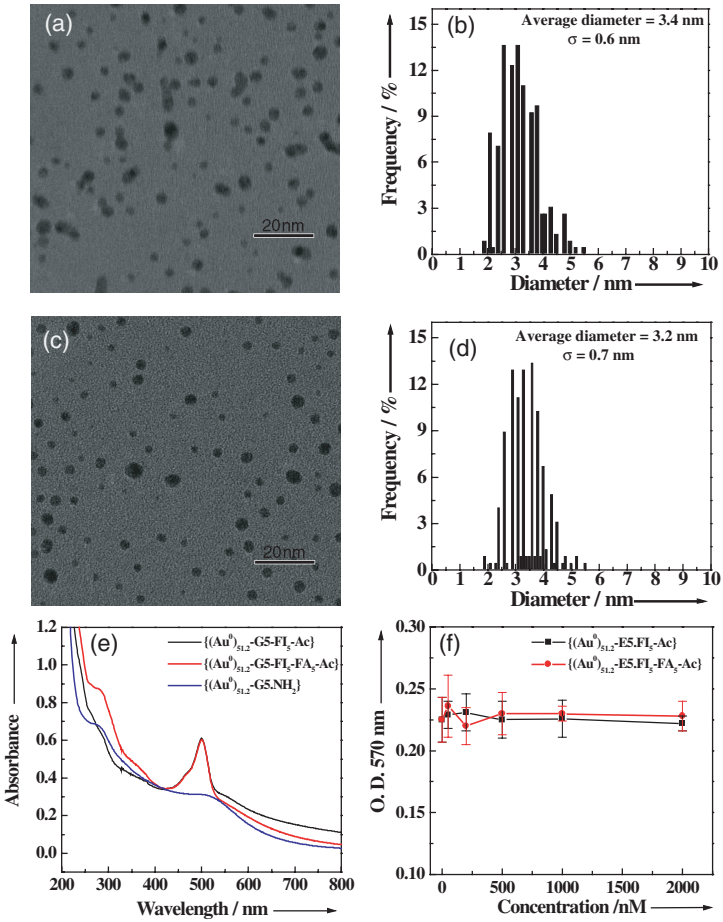

Figure 6: Characterization and toxicity test of functionalized Au DENPs. (a) and (c) TEM images of the functionalized $\{(Au^0)_{51.2}$–G5-FI_5-Ac$\}$ and $\{(Au^0)_{51.2}$–G5-FI_5-FA_5-Ac$\}$ DENPs, respectively. (b) and (d) The size distribution histograms of $\{(Au^0)_{51.2}$–G5-FI_5-Ac$\}$ and $\{(Au^0)_{51.2}$–G5-FI_5-FA_5-Ac$\}$ DENPs, respectively. (e) UV-vis spectra of the starting $\{(Au^0)_{51.2}$–G5.$NH_2\}$ and functionalized $\{(Au^0)_{51.2}$–G5-FI_5-Ac$\}$ and $\{(Au^0)_{51.2}$–G5-FI_5-FA_5-Ac$\}$ DENPs. (f) An MTT assay of KB cell viability after treatment with $\{(Au^0)_{51.2}$–G5-FI_5-Ac$\}$ and $\{(Au^0)_{51.2}$–G5-FI_5-FA_5-Ac$\}$ DENPs for 24 h. The data are expressed as mean ± S. D. (Reprinted with permission from Wiley-VCH GmbH & Co KG, *Small*, 2007, **3**, 1245–1252.)

specific binding with functionalized Au DENPs. KB cells with both high- and low-levels of FAR were respectively incubated with {$(Au^0)_{51.2}$–G5-FI_5-FA_5-Ac} and {$(Au^0)_{51.2}$–G5-FI_5-Ac} DENPs for 1 h. Figures 7(a)–(d) shows the flow cytometric analyses of KB cells that express both high- and low-level FAR after exposure to functionalized Au DENPs (25 nM) for 1 h. It is clear that the treatment of KB cells expressing high-level FAR with {$(Au^0)_{51.2}$–G5-FI_5-FA_5-Ac} DENPs results in a significant increase in the fluorescence signal within the cells. In contrast, the same KB cells treated with {$(Au^0)_{51.2}$–G5-FI_5-Ac} DENPs without FA display a similar fluorescence signal to cells treated with PBS buffer (Figure 7(a)), suggesting no binding of the {$(Au^0)_{51.2}$–G5-FI_5-Ac} DENPs. KB cells with low-level FAR treated with either {$(Au^0)_{51.2}$–G5-FI_5-FA_5-Ac} or {$(Au^0)_{51.2}$–G5-FI_5-Ac} DENPs show a similar fluorescence intensity to the PBS control (Figure 7(b)). These results indicate that the specificity of {$(Au^0)_{51.2}$–G5-FI_5-FA_5-Ac} DENPs binding to KB cells is restricted to cells containing high levels of FAR. The cellular uptake of the FA-functionalized Au DENPs shows a dose-dependent fashion, with saturation and 50% binding occurring at approximately 50 nM and 18 nM, respectively (Figure 7(c)), which is comparable with the binding capacity of FA-modified G5 dendrimers.[24] For KB cells with low-level FAR, neither {$(Au^0)_{51.2}$–G5-FI_5-FA_5-Ac} nor {$(Au^0)_{51.2}$–G5-FI_5-Ac} DENPs shows any significant binding, even at a concentration up to 300 nM (Figure 7(d)).

The conjugation of FI moiety onto Au DENPs also affords confocal microscopic imaging of the intracellular uptake. Figures 7(e), 7(f), and 7(g) show that only KB cells with high-level FAR treated with FA-modified {$(Au^0)_{51.2}$–G5-FI_5-FA_5-Ac} DENPs display fluorescence signals,

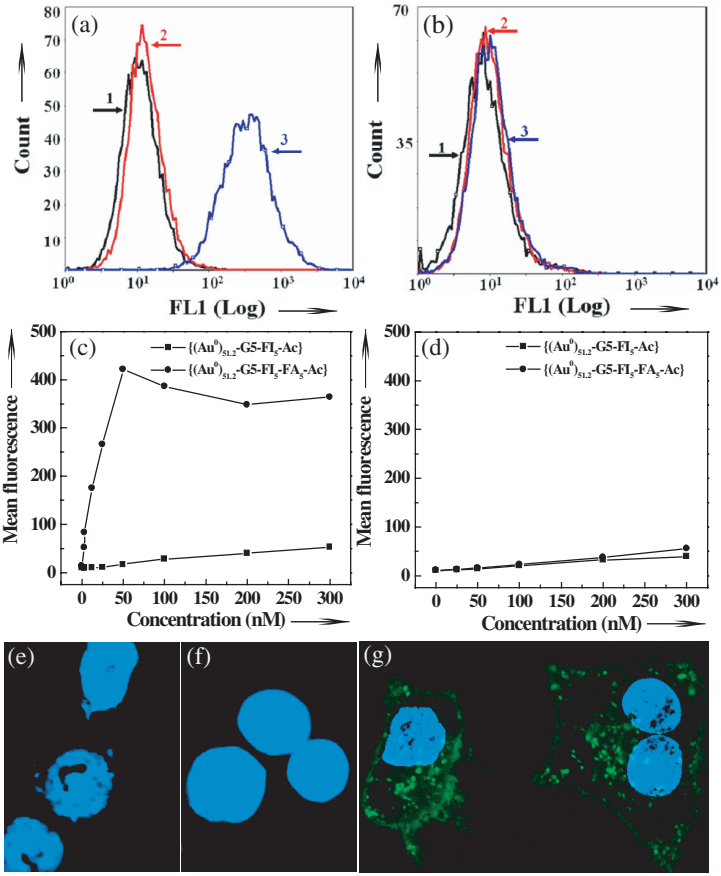

Figure 7: Flow cytometric and confocal microscopic studies of the binding of functionalized Au DENPs with KB cells. (a) and (b), Binding of $\{(Au^0)_{51.2}$–G5-FI_5-Ac$\}$ and $\{(Au^0)_{51.2}$–G5-FI_5-FA_5-Ac$\}$ DENPs (25 nM) with KB cells with high- and low-levels of FAR, respectively. 1. PBS control; 2. $\{(Au^0)_{51.2}$–G5-FI_5-Ac$\}$; 3. $\{(Au^0)_{51.2}$–G5-FI_5-FA_5-Ac$\}$. (c) and (d), Dose-dependent binding of $\{(Au^0)_{51.2}$–G5-FI_5-Ac$\}$ and $\{(Au^0)_{51.2}$–G5-FI_5-FA_5-Ac$\}$ DENPs with KB cells expressing high- and low-levels of FAR, respectively. (e–g) Confocal microscopic images of KB cells with high-level FAR treated with PBS buffer (e), $\{(Au^0)_{51.2}$–G5-FI_5-Ac$\}$ (25 nM) (f), and $\{(Au^0)_{51.2}$–G5-FI_5-FA_5-Ac$\}$ (25 nM) (g) DENPs for 2 h, respectively. (Reprinted with permission from Wiley-VCH GmbH & Co KG, *Small*, 2007, **3**, 1245–1252.)

which is associated with the specific internalization of $\{(Au^0)_{51.2}$–G5-FI_5-FA_5-Ac$\}$ DENPs into the cytoplasm of the cells (Figure 7(g)). In contrast, the same KB cells treated with $\{(Au^0)_{51.2}$–G5-FI_5-Ac$\}$ DENPs without FA modification do not show any fluorescence signals (Figure 7(f)), which is the same case as with KB cells treated with PBS buffer (Figure 7(e)). This result suggests that the binding and intracellular uptake do not occur in the cells treated with non-FA modified Au DENPs.

One major advantage of using functionalized Au DENPs to image cancers is its ability to differentiate cancer cells from surrounding cells or tissues by using contrast agents with high electron density. Dendrimers without entrapped metal nanoparticles cannot achieve this goal.[20,24] By using the TEM imaging technique, we can clarify the distribution of functionalized Au DENPs in different compartments inside targeted cells. This also aids in understanding the mechanism for targeted drug delivery and therapeutics, using dendrimer-based nanodevices. Upon 2 h incubation of functionalized Au DENPs, the FA-modified $\{(Au^0)_{51.2}$–G5-FI_5-FA_5-Ac$\}$ DENPs were predominantly located in the lysosomes of KB cells with high-level FAR expression (Figures 8(a) and (b)). We also observed that a small portion of $\{(Au^0)_{51.2}$–G5-FI_5-FA_5-Ac$\}$ DENPs situated in vacuoles and the nucleus. However, we did not see any uptake of the $\{(Au^0)_{51.2}$–G5-FI_5-Ac$\}$ DENPs without FA modification in the lysosomes of the same KB cells (Figure 8(c)). A very small quantity of $\{(Au^0)_{51.2}$–G5-FI_5-Ac$\}$ DENPs were observed in the vacuoles of some cells, and this was undetectable using confocal microscopy. This uptake is believed to be associated with diffusion-driven non-specific binding since control cells not exposed to Au DENPs show no internalized metal nanoparticles. The TEM studies

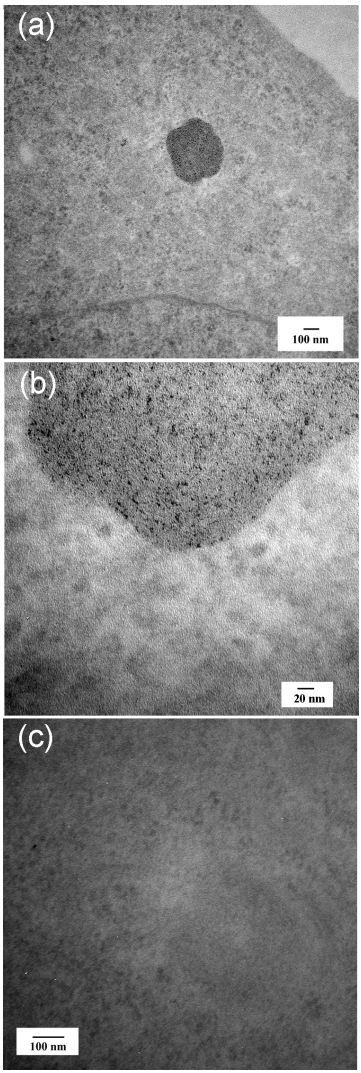

Figure 8: TEM images of cellular uptake of Au DENPs. (a–c), TEM images of KB cells with high-level FAR treated with $\{(Au^0)_{51.2}$–G5-FI_5-FA_5-Ac$\}$ (a and b) and $\{(Au^0)_{51.2}$–G5-FI_5-Ac$\}$ DENPs (c) for 2 h, respectively. (b) A magnified area of the lysosome of the same cell shown in (a). The concentration for both Au DENPs is maintained at 50 nM. (Reprinted with permission from Wiley-VCH GMbH & Co KG, *Small*, 2007, **3**, 1245–1252.)

highlighted the high specificity of FA-modified Au DENPs for targeting KB cells with high-level FAR expression, and corroborate the confocal imaging data.

This approach to functionalizing Au DENPs can be applied to various other biological ligands (e.g., sugars, peptides, proteins, and antibodies) for targeting and imaging various biological systems. It is anticipated that drug molecules can be conjugated onto Au DENPs, thereby providing an approach for imaging and targeted treatment to various forms of cancers.

11.3 Dendrimer-Stabilized Nanoparticles (DSNPs)

DSNPs are referred to a nanostructure, where one metal or other inorganic NP is surrounded with multiple dendrimer molecules. Metal DSNPs are usually formed under mild reduction conditions to assist slow nucleation of the particles. The formation of DSNPs also depends on the structure of dendrimers used. In some cases, if low generation dendrimers (G1–G3) are used as templates, even fast reduction and nucleation can still afford the formation of DSNPs (instead of DENPs) because the limited terminal amines and open structures cannot entrap metal NPs inside the dendrimers. Besides the metal DSNPs, other inorganic metal sulfide DSNPs can also be formed using dendrimers as stabilizers.[32–35]

Several groups pioneered the research on dendrimer stabilized metal NPs as well as specifically on Au DSNPs.[36–38] The preparation of dendrimer-stabilized Au NPs (Au DSNPs) usually involves complexation of gold salts (e.g. $HAuCl_4$) with PAMAM dendrimers, followed by physical or chemical reduction.[7,8,37] It is well established that the size of the

Au DSNPs is mainly dependent on the molar ratio between dendrimers and Au atoms.[7] The mechanistic studies show that dendrimer terminal amines are extremely effective in the stabilization of Au NPs.[11,38] Although there are a number of reports showing that DSNPs can be formed by simple thermo treatment,[39,40] UV-irradiation,[36,41] or laser ablation[42] of the dendrimer-metal complexes, a majority of the work related to the synthesis of DSNPs were performed by chemical reduction.

In our previous work,[43] we utilize amine-terminated PAMAM dendrimers of generation 2 through 6 as stabilizer to synthesize Au DSNPs by hydrazine reduction chemistry. For all Au-DSNPs, the molar ratio between dendrimer terminal amines (DTA) and Au atoms are kept consistent at 1:0.4. Figure 9(a) shows the UV-Vis spectra of Au DSNPs prepared using G2.NH_2 through G6.NH_2. The plasmon peak at around 525 nm, which is

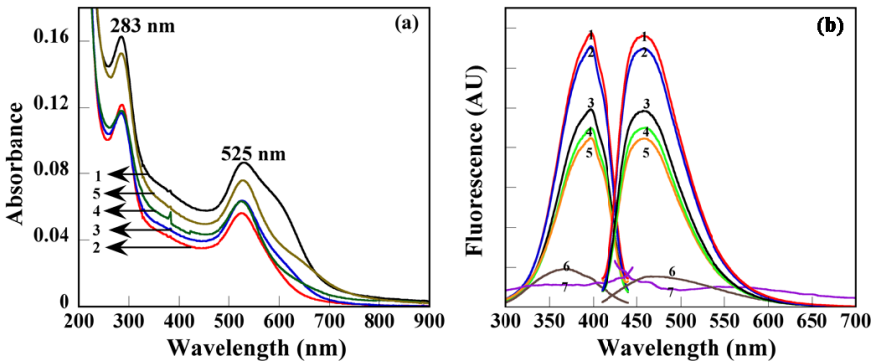

Figure 9: UV-Vis (a) and fluorescence (b) spectra of Au DSNPs. Curves 1, 2, 3, 4, and 5 correspond to {$(Au^0)_6$–G2.NH_2}, {$(Au^0)_{12}$–G3.NH_2}, {$(Au^0)_{24}$–G4.NH_2}, {$(Au^0)_{57}$–G5.NH_2}, and {$(Au^0)_{98}$–G6.NH_2}, respectively. In (b), 6 and 7 indicate gold colloids with diameter of 5 and 100 nm, respectively. (Reprinted with permission from *Nanotechnology*, 2006, **17**, 1072–1078, IOP Publishing Limited.)

attributed to collective oscillation of free electrons in gold NPs,[23] is clearly observed for all samples. The gradual increase of absorption below 400 nm for all samples is due to the interband transition of gold. The absorbance peak at 283 nm for all Au DSNPs is assigned to certain carbonyl compounds formed presumably by oxidation of the dendrimers.[36] The same UV-Vis spectrometric features related to Au DSNPs were also observed by other groups.[36,37] Figure 9(b) shows the fluorescence spectra of Au DSNPs and commercial Au colloid particles (5 nm and 100 nm). All Au DSNPs were found to be fluorescent and display strong blue photoluminescence. The maximum excitation and emission wavelengths were around 397 nm and 458 nm, respectively, in agreement with the literature data.[44] In contrast, commercial gold colloids (5 nm and 100 nm) that are prepared using citric acid reduction and protection approach do not exhibit fluorescence emission, suggesting that the dendrimer stabilizers contribute to the fluorescence properties of the formed Au DSNPs. A recent report from Imae's group shows that both PAMAM and polypropyleneimine (PPI) dendrimers exhibit strong intrinsic fluorescence emission at certain concentration ranges.[45] They proposed that the backbone of dendrimers plays a key role in forming the fluorescence center. The fluorescent properties of the formed Au DSNPs make them potentially useful as fluorescent markers for cell labeling and biological sensing studies.

The size distribution and morphology of the synthesized Au DSNPs were studied by TEM. Figure 10 shows TEM images of Au DSNPs prepared using PAMAM dendrimers of different generations. The sizes of the formed Au DSNPs are 15.4 ± 5.8 nm, 12.0 ± 2.8 nm, 9.1 ± 3.2 nm, 8.6 ± 2.8 nm, and 7.1 ± 1.9 nm for $\{(Au^0)_6$–G2.$NH_2\}$, $\{(Au^0)_{12}$–G3.$NH_2\}$,

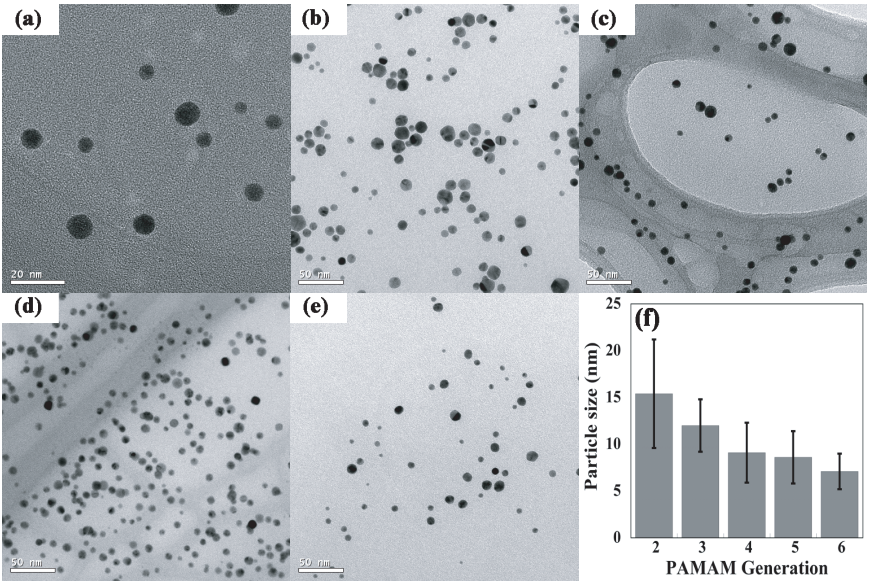

Figure 10: Large scale TEM images of (a) $\{(Au^0)_6$–G2.$NH_2\}$; (b) $\{(Au^0)_{12}$–G3.$NH_2\}$; (c) $\{(Au^0)_{24}$–G4.$NH_2\}$; (d) $\{(Au^0)_{57}$–G5.$NH_2\}$; and (e) $\{(Au^0)_{98}$–G6.$NH_2\}$. The plot of their sizes as a function of the number of dendrimer generations is shown in (f). (Reprinted with permission from *Nanotechnology*, 2006, **17**, 1072–1078, IOP Publishing Limited.)

$\{(Au^0)_{24}$–G4.$NH_2\}$, $\{(Au^0)_{57}$–G5.$NH_2\}$, and $\{(Au^0)_{98}$–G6.$NH_2\}$, respectively. It is clear that all the Au DSNPs are relatively monodispersed except $\{(Au^0)_6$–G2.$NH_2\}$. $\{(Au^0)_6$–G2.$NH_2\}$ displays larger size and higher polydispersity, which is attributed to limited number of amines of G2.NH_2 dendrimer to stabilize Au NPs. This result is in good agreement with the reported data.[46] The size of the Au DSNPs decreases with the increase of the number of dendrimer generations (Figure 10(f)), suggesting the different nucleation and growth mechanisms for gold nanocrystals in the presence of PAMAM dendrimers. At basic pH conditions (pH ≈ 10.4 when

dendrimers are dissolved in water), $AuCl_4^-$ anions bind preferably to the protonated amines of PAMAM dendrimers through electrostatic interaction. Larger generation PAMAM dendrimers have denser structures that would significantly limit the nucleation, movement, and growth of gold nanocrystals. In contrast, smaller generation PAMAMs have relatively open structures, which hinder the growth of gold nanocrystals less significantly than larger generation PAMAMs. It is interesting to note that the synthesized Au DSNPs in this work are significantly larger than Au DENPs reported in the literature.[10–12,21,46] The reduction potential of NH_2-NH_2 (–0.09 V) used in this work is significantly smaller than $NaBH_4$ (–0.481 V) which was used by other groups.[47,48] Therefore, the slower reaction rate favors the formation of larger Au DSNPs, accordingly the formed Au DSNPs are covered with a monolayer of dendrimer molecules. Compared with Au DENPs synthesized using $NaBH_4$ reduction chemistry, the size dispersity of Au DSNPs is rather large, mainly due to the fact that slow nucleation process of NPs occurs because of slow reduction reaction. However, the size dispersity of Au DSNPs synthesized using hydrazine reduction chemistry is comparable with those synthesized under UV or laser radiation.[36,42] All the synthesized Au DSNPs are highly polycrystalline as shown by both the high- resolution TEM images and SAED patterns (Figure 11).[43] These larger Au nanoparticles will be very useful in cellular labeling and imaging studies.

Zeta potential measurements confirmed that all the synthesized Au DSNPs are positively charged with zeta potentials ranging from 26.42 to 41.11 mV. This further indicates that after the formation of the hybrid nanostructures the terminal amines of dendrimers are still available to be

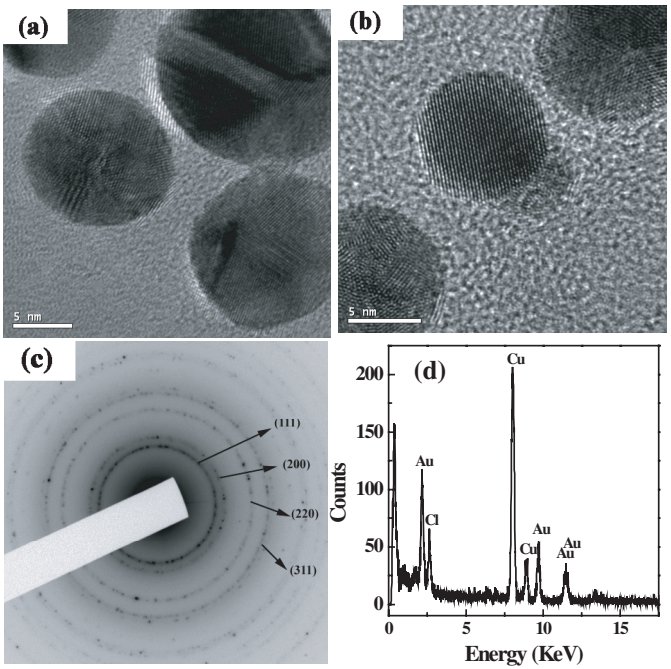

Figure 11: High-resolution TEM images of $\{(Au^0)_{12}$–G3.$NH_2\}$ (a) and $\{(Au^0)_{57}$–G5.$NH_2\}$ (b) DSNPs, a typical SAED pattern of $\{(Au^0)_{98}$–G6.$NH_2\}$ DSNPs (c) and an EDS spectrum of $\{(Au^0)_{24}$–G4.$NH_2\}$ DSNPs (d). (Reprinted with permission from *Nanotechnology*, 2006, **17**, 1072–1078, IOP Publishing Limited.)

protonated. The surface charge polarity of Au DSNPs is similar to the protonated corresponding dendrimers, which was further confirmed by polyacrylamide gel electrophoresis (PAGE) measurements (Figure 12).[43] Shown in Figure 12 is the PAGE electropherograms of both Au DSNPs and the corresponding dendrimer stabilizers. The Au DSNPs display very similar migration patterns as those of their respective dendrimer stabilizers. In some cases, the difference is that the Au DSNPs exhibit somewhat lower electrophoretic mobility than their corresponding dendrimer stabilizers

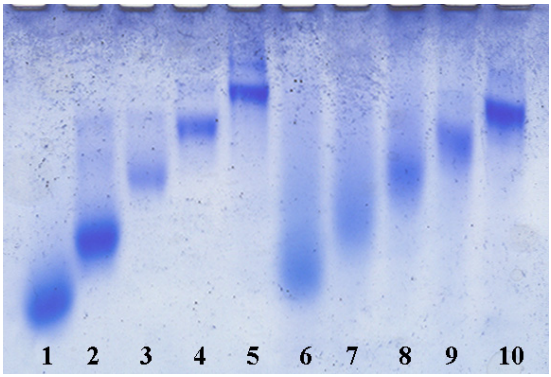

Figure 12: PAGE electropherograms of Au DSNPs and their corresponding dendrimer stabilizers. Lane 1: G2.NH_2; Lane 2: G3.NH_2; Lane 3: G4.NH_2; Lane 4: G5.NH_2; Lane 5: G6.NH_2; Lane 6: {$(Au^0)_6$–G2.NH_2}; Lane 7: {$(Au^0)_{12}$–G3.NH_2}; Lane 8: {$(Au^0)_{24}$–G4.NH_2}; Lane 9: {$(Au^0)_{57}$–G5.NH_2}; and Lane 10: {$(Au^0)_{98}$–G6.NH_2}. (Reprinted with permission from *Nanotechnology*, 2006, **17**, 1072–1078, IOP Publishing Limited.)

due to their lower charge/mass ratios after "loading" with Au nanocrystals. PAGE measurements verified the existence of dendrimers for each Au DSNPs, because the comassie-stained bands of Au DSNPs are exclusively related to stained dendrimers. In contrast, commercial negatively citric acid-protected Au NPs migrate reversely to upside of the gel (toward cathode) during electrophoresis under the reverse polarity. The PAGE results also indicate that the formed Au DSNPs are highly stable and both Au nanocrystals and dendrimers do not separate from each other during the electrophoresis at pH 8.3.

The biological application of metal DSNPs is inherently related to the properties of metal NPs. For example, Ag DSNPs have been found to display antimicrobial activity without the loss of solubility and activity,

even in the presence of sulfate or chloride ions.[49] Radioactive Au^{198} NPs can be used to detect the organ/tissue biodistribution of the NPs.[50] In most cases, metal DSNPs have been widely used as biomarkers for cellular imaging because of the high electron density contrast as compared with cellular or tissue structures.

In a previous work, Bielinska *et al*. utilized positively charged Au DSNPs as DNA carriers to transfect gene with similar efficiency to the corresponding dendrimers in the absence of Au NPs.[51] It appears that in this gene transfection process, large pDNA-PAMAM clusters form (containing many DNA molecules and many dendrimers), which then undergo endocytosis after surface binding (Figure 13). Another example was the case of

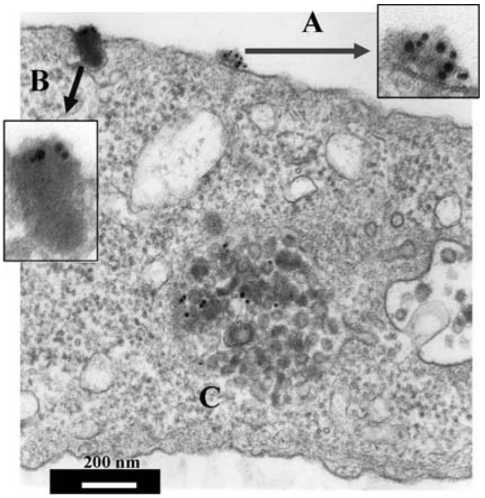

Figure 13: Visualization of gene transfection with plasmid DNAgold/ PAMAM nanocomposite complex aggregates. (A) Cell surface attachment, (B) complex aggregate just undergoing endocytosis, (C) complexes localized in lysozome. (Reprinted with permission from Springer, *Journal of Nanoparticle Research*, 2002, **4**, 395–403.)

lipid bilayers, where the positively charged Au DSNPs easily penetrated into the polar zone of the bilayer structure thereby rendering them visible by TEM. The use of Au DSNPs makes the gene tranfection process visible through TEM imaging, which is impossible for the use of dendrimers in the absence of metal NPs. The diffusion of various metal DSNPs is controlled rather by the surrounding dendrimers than by the stabilized metal NPs. Therefore, by varying the charge and lipophilicity of the dendrimers, the metal particle can be internalized and interact with various biologic entities.

In another recent study, we have shown that Ag DSNPs synthesized using amino-, hydroxyl-, and carboxyl-terminated ethylenediamine core generation 5 poly(amidoamine) dendrimers (G5.NH_2, G5.NGlyOH, and G5.NSAH) as stabilizers are biocompatible, fluorescent and can be used as cell labeling markers.[41] The Ag DSNPs were synthesized by UV irradiation of Ag (I)-dendrimer complexes and are water-soluble and stable. The fluorescent properties of Ag DSNPs are from the dendrimer templates, which has been demonstrated by our groups and others.[43,45,52] The {$(Ag^0)_{25}$–PAMAM_G5.NH_2}, {$(Ag^0)_{25}$–PAMAM_G5.NGlyOH}, and {$(Ag^0)_{25}$–PAMAM_G5.NSAH} DSNPs are fluorescent in the wavelength range of 400–500 nm. The fluorescence properties of Ag DSNPs allow us to image the intracellular uptake of Ag DSNPs using confocal microscopy. Figure 14 displays representative TEM images collected for NIH3T3 (A and B) and U937 (C and D) cell lines incubated with {$(Ag^0)_{25}$–G5.NH_2} DSNPs. After 1 h incubation at 37°C, Ag DSNPs were observed in the form of randomly dispersed single particles or agglomerates on the surface of cellular

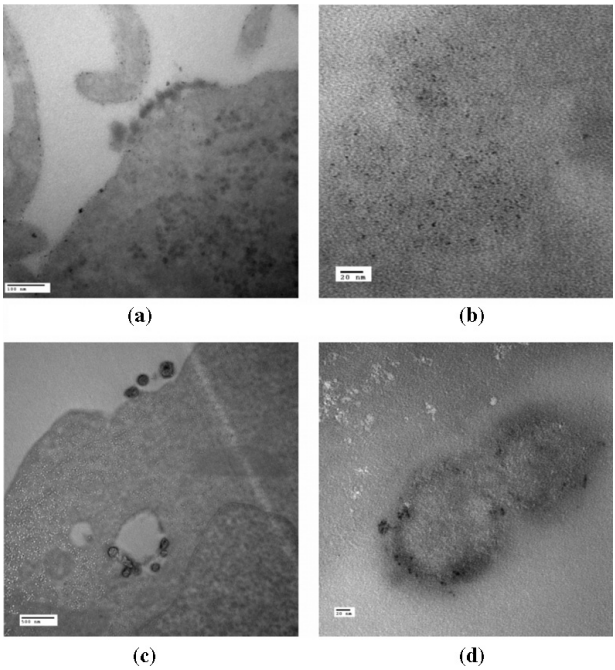

Figure 14: Representative TEM images of NIH3T3 and U937 cell lines incubated with $\{(Ag^0)_{25}$–G5.$NH_2\}$ nanoparticles for 1 h at 37°C and at 500 nM DSNP concentration. (a and b) NIH3T3 cell showing DSNPs located on the surface of the cell and randomly dispersed single particles in the cytoplasm, respectively; (c and d) U937 cell viewing the agglomerates of DSNPs located on the surface of the cell and trapped in the phagocytic or endocytic vesicles. (Reprinted with permission from *Nano Lett.*, **5**(11), 2123–2130. Copyright (2005) American Chemical Society.)

membranes, in the cytoplasm, or trapped by the phagocytic or endocytic vesicles. It seems that internalization of the polycationic $\{(Ag^0)_{25}$–G5.$NH_2\}$ DSNPs may occur through two distinct mechanisms: both phagocytosis and diffusion via cell walls may take place. Similar results were obtained for the polyanionic $\{(Ag^0)_{25}$–PAMAM_G5.NSAH}

DSNPs, whereas cellular uptake of $\{(Ag^0)_{25}$–G5.NGlyOH$\}$ with charge close to neutral was low.

The cellular uptake and potential application of $\{(Ag^0)_{25}$–G5.$NH_2\}$, $\{(Ag^0)_{25}$–G5.NGlyOH$\}$, and $\{(Ag^0)_{25}$–G5.NSAH$\}$ DSNPs as cell labels was further studied by confocal microscopy. Rat2 cells incubated with $\{(Ag^0)_{25}$–G5.$NH_2\}$ DSNPs exhibited a measurable increase of intracellular fluorescence proving that (a) the fluorescence is not quenched and (b) the nanoparticles were internalized within the cells and visibly located in the cytoplasm. There are also small areas exhibiting relatively strong fluorescence; we speculate that these areas might correspond to the nanocomposite aggregates trapped in the endocytic or phagocytic vesicles, as seen in TEM images. Similar results were obtained for the negatively charged $\{(Ag^0)_{25}$–G5.NSAH$\}$ DSNPs, whereas incubation of Rat2 cells with $\{(Ag^0)_{25}$–G5.NGlyOH$\}$ DSNPs with charge close to neutral did not result in elevated intracellular fluorescence. Overall, the results indicate that the toxicity and uptake of investigated silver DSNPs correlate with the surface charge of nanoparticles and testing of different cells indicates that the presented behavior of silver DSNPs is not limited to specific cell lines.

11.4 Concluding Remarks and Outlooks

This review has described the synthesis, characterization, and biomedical applications of metal DENPs and DSNPs. The unique aspects of dendrimer structure (the chemistry of the terminal groups, the generation-dependent size, the 3-dimensional structure, and the interior coordination chemistry) afford immense interest in the preparation of these nanostructured materials. Metal DENPs and DSNPs prepared using dendrimers as

templates and stabilizers offers a wide range of opportunities for biomedical applications because of the functionalizable nature of the dendrimer materials and the controlled size, dimension, and crystalline structures of the metal NPs. The synthesized metal DENPs and DSNPs will find a wide range of biomedical applications, including imaging, sensing, and treatment of various biological systems.

Many efforts have been devoted to surface modification of metal DENPs and DSNPs for biological applications. Since the discovery of metal dendrimer nanocomposite in 1998, the fabrication and biomedical applications of these NPs still remains an open area and great challenges. For example, metal DSNPs currently used in biological systems lack specificity to particular biological systems, which is largely due to the technical difficulty in modifying them with specific biological moieties. TEM imaging of *in vivo* tumor models is expected to be very difficult because of the 3-dimensional heterogeneity of tumor structures. Hyperthermia treatment of cancer using the current metal DENPs or DSNPs will be limited to skin tumors because the laser wavelength used for hyperthermia is short (e.g., 510–530 nm for Au DENPs and Au DSNPs in order to match their surface plasmon resonance absorption). Developing Au DENP or DSNP-based Au nanoshell structure will be necessary to overcome the disadvantage, in the latter case, the Au nanoshell structure displays surface plasmon resonance absorption at near infrared (NIR) wavelength range (700–1100 nm), which allows the used laser at this range of wavelength to penetrate tissues and bloods for deep tumor therapy. All these challenges will drive the effective collaboration of scientists working in chemistry, materials, engineering, and biomedical

fields to develop effective dendrimer-related nanostructures for various biological applications.

11.5 References

1. D. A. Tomalia, H. Baker, J. R. Dewald, M. Hall, G. Kallos, S. Martin, J. Roeck, J. Ryder, and P. Smith, A new class of polymers: Starburst®-Dendritic Macromolecules, *Polymer J.,* **17**, 117, 1985.
2. D. A. Tomalia, H. Baker, J. R. Dewald, M. Hall, G. Kallos, S. Martin, J. Roeck, J. Ryder, and P. Smith, Dendritic macromolecules: Synthesis of starburst dendrimers, *Macromolecules,* **19**, 2466–2468, 1986.
3. D. A. Tomalia, A. M. Naylor, and W. A. Goddard III., Starburst dendrimers: Control of size, shape, surface chemistry, topology and flexibility in the conversion of atoms to macroscopic materials, *Angew. Chem. Int. Ed. Engl.,* **29**, 138, 1990.
4. D. A. Tomalia and J. M. J. Frechet, *Dendrimers and Other Dendritic Polymers*, John Wiley & Sons Ltd., New York, 2001.
5. R. M. Crooks, M. Zhao, L. Sun, V. Chechik, and L. K. Yeung, Dendrimer-encapsulated metal nanoparticles: Synthesis, characterization, and applications to catalysis, *Accounts Chem. Res.,* **34**, 181–190, 2001.
6. R. W. J. Scott, O. M. Wilson, and R. M. Crooks, Synthesis, characterization, and applications of dendrimer-encapsulated nanoparticles, *J. Phys. Chem., B* **109**, 692–704, 2005.
7. K. Esumi, Dendrimers for nanoparticle synthesis and dispersion stabilization, *Top. Curr. Chem.,* **227**, 31–52, 2003.

8. K. Esumi, Dendrimer-metal nanocomposites, *Encyclopedia of Nanoscience and Nanotechnology,* **2**, 317–326, 2004.
9. T. Goodson III., O. Varnavski, and Y. Wang, Optical properties and applications of dendrimer-metal nanocomposites, *International Reviews in Physical Chemistry,* **23**, 109–150, 2004.
10. F. Grohn, B. J. Bauer, Y. A. Akpalu, C. L. Jackson, and E. J. Amis, Dendrimer templates for the formation of gold nanoclusters, *Macromolecules,* **33**, 6042–6050, 2000.
11. A. Manna, T. Imae, K. Aoi, M. Okada, and T. Yogo, Synthesis of dendrimer-passivated noble metal nanoparticles in a polar medium: Comparison of size between silver and gold particles, *Chem. Mater.,* **13**, 1674–1681, 2001.
12. Y.-G. Kim, S.-K. Oh, and R. M. Crooks, Preparation and characterization of 1–2 nm dendrimer-encapsulated gold nanoparticles having very narrow size distributions, *Chem. Mater.,* **16**, 167–172, 2004.
13. B. I. Lemon and R. M. Crooks, Preparation and characterization of dendrimer-encapsulated CdS semiconductor quantum dots, *J. Am. Chem. Soc.,* **122**, 12886–12887, 2000.
14. X. C. Wu, A. M. Bittner, and K. Kern, Synthesis, photoluminescence, and adsorption of CdS/dendrimer nanocomposites, *J. Phys. Chem. B*., **109**, 230–239, 2005.
15. N. L. Rosi and C. A. Mirkin, Nanostructures in biodiagnostics, *Chem. Rev.,* **105**, 1547–1562, 2005.
16. M.-C. Daniel and D. Astruc, Gold nanoparticles: Assembly, supramolecular chemistry, quantum-size-related properties, and

applications toward biology, catalysis, and nanotechnology, *Chem. Rev.,* **104**, 293–346, 2004.

17. S.-K. Oh, Y.-G. Kim, H. Ye, and R. M. Crooks, Synthesis, characterization, and surface immobilization of metal nanoparticles encapsulated within bifunctionalized dendrimers, *Langmuir,* **19**, 10420–10425, 2003.
18. M. R. Knecht, J. C. Garcia-Martinez, and R. M. Crooks, Hydrophobic dendrimers as templates for Au nanoparticles, *Langmuir,* **21**, 11981–11986, 2005.
19. A. Quintana, E. Raczka, L. Piehler, I. Lee, A. Myc, I. Majoros, A. K. Patri, T. Thomas, J. Mule, and J. R. Baker Jr., Design and function of a dendrimer-based therapeutic nanodevice targeted to tumor cells through the folate receptor, *Pharm. Res.,* **19**, 1310–1316, 2002.
20. J. F. Kukowska-Latallo, K. A. Candido, Z. Cao, S. S. Nigavekar, I. J. Majoros, T. P. Thomas, L. P. Balogh, M. K. Khan, and J. R. Baker Jr., Nanoparticle targeting of anticancer drug improves therapeutic response in animal model of human epithelial cancer, *Cancer Res.,* **65**, 5317–5324, 2005.
21. X. Shi, S. Wang, H. Sun, and J. R. Baker Jr., Improved biocompatibility of surface functionalized dendrimer-entrapped gold nanoparticles, *Soft Matter*, **3**, 71–74, 2007.
22. J. C. Garcia-Martinez and R. M. Crooks, Extraction of Au nanoparticles having narrow size distributions from within dendrimer templates, *J. Am. Chem. Soc.,* **126**, 16170–16178, 2004.
23. M. M. Alvarez, J. T. Khoury, T. G. Schaaff, M. N. Shafigullin, I. Vezmar, and R. L. Whetten, Optical absorption spectra of nanocrystal gold molecules, *J. Phys. Chem. B,* **101**, 3706–3712, 1997.

24. Y. Choi, T. Thomas, A. Kotlyar, M. T. Islam, and J. R. Baker Jr., Synthesis and functional evaluation of DNA-assembled polyamidoamine dendrimer clusters for cancer cell-specific targeting, *Chem. Biol.,* **12**, 35–43, 2005.

25. X. Shi, S. Wang, S. Meshinchi, M. Van Antwerp, X. Bi, and J. R. Baker Jr., Dendrimer-encapsulated gold nanoparticles as a platform for cancer cell targeting and imaging, *Small*, **3**, 1245–1252, 2007.

26. B. L. Cushing, V. L. Kolesnichenko, and C. J. O'Connor, Recent advances in the liquid-phase syntheses of inorganic nanoparticles, *Chem. Rev.,* **104**, 3893–3946, 2004.

27. J. R. Baker Jr., A. Quintana, L. T. Piehler, M. Banazak-Holl, D. Tomalia, and E. Raczka, The synthesis and testing of anti-cancer therapeutic nanodevices, *Biomed. Microdevices,* **3**, 61–69, 2001.

28. I. G. Campbell, T. A. Jones, W. D. Foulkes, and J. Trowsdale, Folate-binding protein is a marker for ovarian cancer, *Cancer Res.,* **51**, 5329–5338, 1991.

29. P. Garin-Chesa, I. Campbell, P. E. Saigo, J. L. Lewis Jr., L. J. Old, and W. J. Rettig, Trophoblast and ovarian cancer antigen LK26. Sensitivity and specificity in immunopathology and molecular identification as a folate-binding protein, *Am. J. Pathol.,* **142**, 557–567, 1993.

30. D. Weitman, R. H. Lark, L. R. Coney, D. W. Fort, V. Frasca, V. R. Surawski, and B. A. Kamen, Distribution of the folate receptor GP38 in normal and malignant cell lines and tissues, *Cancer Res.,* **52**, 3396–3401, 1992.

31. J. F. Ross, P. K. Chaudhauri, and M. Ratnam, Differential regulation of folate receptor isoforms in normal and malignant tissues *in vivo*

and in established cell lines. Physiologic and clinical implications, *Cancer*, **73**, 2432–2443, 1994.

32. K. Sooklal, L. H. Hanus, H. J. Ploehn, and C. J. Murphy, A blue-emitting CdS/dendrimer nanocomposite, *Adv. Mater.,* **10**, 1083–1087, 1998.
33. J. Huang, K. Sooklal, C. J. Murphy, and H. J. Ploehn, Polyamine-quantum dot nanocomposites: Linear versus starburst stabilizer architectures, *Chem. Mater.*, **11**, 3595–3601, 1999.
34. X. Shi, K. Sun, L. Balogh, and J. R. Baker Jr., Synthesis, characterization, and manipulation of dendrimer-stabilized iron sulfide nanoparticles, *Nanotechnology*, **17**, 4554–4560, 2003.
35. N. C. Beck Tan, L. Balogh, S. F. Trevino, D. A. Tomalia, and J. S. Lin, A small angle scattering study of dendrimer-copper sulfide nanocomposites, *Polymer*, **40**, 2537–2545, 1999.
36. K. Esumi, A. Suzuki, N. Aihara, K. Usui, and K. Torigoe, Preparation of Au colloids with UV irradiation using dendrimer as stabilizer, *Langmuir,* **14**, 3157–3159, 1998.
37. L. Balogh, R. Valluzzi, K. S. Laverdure, S. P. Gido, G. L. Hagnauer, and D. A. Tomalia, Formation of silver and gold dendrimer nanocomposites, *J. Nanoparticle Res.,* **1**, 353–368, 1999.
38. M. E. Garcia, L. A. Baker, and R. M. Crooks, Preparation and characterization of dendrimer-gold colloid nanocomposites, *Anal. Chem.,* **71**, 256–258, 1999.
39. X. Sun, S. Dong, and E. Wang, One-step preparation and characterization of poly(propyleneimine) dendrimer-protected silver nanoclusters, *Macromolecules*, **37**, 7105–7108, 2004.

40. X. Sun, X. Jiang, S. Dong, and E. Wang, One-step synthesis and size control of dendrimer-protected gold nanoparticles: A heat-treatment-based strategy, *Macromolecular Rapid Communications,* **24**, 1024–1028, 2003.

41. W. Lesniak, A. U. Bielinska, K. Sun, K. W. Janczak, X. Shi, J. R. Baker Jr., and L. P. Balogh, Silver/dendrimer nanocomposites as biomarkers: Fabrication, characterization, *in vitro* toxicity, and intracellular detection, *Nano Lett.,* **5**, 2123–2130, 2005.

42. K. Hayakawa, T. Yoshimura, and K. Esumi, Preparation of Gold-dendrimer nanocomposites by laser irradiation and their catalytic reduction of 4-nitrophenol, *Langmuir*, **19**, 5517–5521, 2003.

43. X. Shi, T. R. Ganser, K. Sun, L. P. Balogh, and J. R. Baker Jr., Characteization of crystalline dendrimer-stabilized gold nanoparticles, *Nanotechnology*, **17**, 1072–1078, 2006.

44. J. Zheng, J. T. Petty, and R. M. Dickson, High quantum yield blue emission from water-soluble Au_8 nanodots, *J. Am. Chem. Soc.,* **125**, 7780–7781, 2003.

45. D. Wang, and T. Imae, Fluroscence emission from dendrimers and its pH dependence, *J. Am Chem. Soc.*, **126**, 13204–13205, 2004.

46. K. Esumi, A. Suzuki, A. Yamahira, and K. Torigoe, Role of Poly(amidoamine) dendrimers for preparing nanoparticles of gold, platinum, and silver, *Langmuir,* **16**, 2604–2608, 2000.

47. J. A. Dean, *Lange's Handbook of Chemistry*, *14th Edition*, MaGraw-Hill, Inc, New York, 1992.

48. D. R. Lide, *CRC Handbook of Chemistry and Physics*, *83rd Edition* 2002–2003, CRC Press LLC, New York, 2002.

49. L. Balogh, D. R. Swanson, D. A. Tomalia, G. L. Hagnauer, and A. T. McManus, Dendrimer silver complexes and nanocomposites as antimicrobial agents, *Nano Lett.,* **1**, 18–21, 2001.

50. M. K. Khan, S. S. Nigavekar, D. L. Minc, M. S. T. Kariapper, B. M. Nair, W. G. Lesniak, and L. P. Balogh, *In vivo* biodistribution of dendrimers and dendrimer nanocomposites — Implications for cancer imaging and therapy, *Technology in Cancer Research & Treatment,* **4**, 603–613, 2005.

51. A. Bielinska, J. D. Eichman, I. Lee, J. R. Baker Jr., and L. Balogh, Imaging {Au0-PAMAM} gold-dendrimer nanocomposites in cells, *J. Nanoparticle Res.,* **4**, 395–403, 2002.

52. W. I. Lee, Y. Bae, and A. J. Bard, *J. Am. Chem. Soc.*, **126**, 8358–8359, 2004.

Index